THE DYNAMICS OF TWO-PHASE FLOW IN VAPOUR GENERATORS

by

Constantine Rakopoulos

Dipl. Ing. Mech./Elect. Eng., N.T.U.A.

D.I.C., M.Sc. (London)

Thesis submitted for the degree of

Doctor of Philosophy

of the

University of London

November 1976

Thermal Power Section
Department of Mechanical Engineering
Imperial College of Science and Technology
London SW7 2BX

A B S T R A C T

A theoretical and experimental study has been carried out to investigate the dynamics of two-phase flow in vapour generators, with special reference to density wave oscillations in a forced flow once-through design. A review of two-phase flow instability in straight and helical geometry vapour generators is presented.

A distributed parameter time-varying theoretical analysis of the conservation equations together with the constitutive laws of two-phase flow has been derived by including slip between the phases, variable friction factors, as well as variable heat flux by taking into account the dynamics of the heater wall. The equations have been linearised and Laplace transformed and standard linear-control theory stability criteria has been used to assess the stability of vapour generators. A digital computer program has been written and developed to implement the theoretical analysis. The program has been tested against available data and the effect of the various parameters on instability examined and discussed.

An "Arcton-113"* closed loop comprising a helical, electrically heated, once-through tube in a parallel channel design has been designed, manufactured, erected, commissioned and operated by the present author. A complete description of the experimental facility is given.

The inherent noise of the flowrate signal with the hidden periodicities present in the vapour generator have been recorded and

---

* "Arcton-113" is the Trade Name used by ICI for 1,1,2 Trichloro 1,2,2 Trifluoroethane ($C Cl_2 F . C Cl F_2$). This fluid is more commonly called Freon-113.

analysed using statistical techniques in order to determine the dynamic behaviour of the system concerned.

To facilitate the statistical study of the dynamic behaviour of the vapour generator, a new fast data acquisition and recording system has been designed and developed which is fully described. Computer programs calculating power spectral density and correlation functions using fast Fourier transforms have been written, developed and used to process the experimental data.

Due to unexpected delays in construction of this equipment and consequent pressure on the author's time, preliminary experiments only were carried out, over a limited range of the governing parameters. Analytical results are used to aid the interpretation of the observed dynamic behaviour of the experimental vapour generator.

A C K N O W L E D G E M E N T S

I wish to express my sincere gratitude to my supervisor, Professor W. Murgatroyd, for proposing the topic of this work and for his continuous encouragement, guidance, advice and interest in the work, and also to Dr A.A. El-Shirbini, who gave so generously of his time, assistance and advice at all stages of the work.

I wish to thank Mr D. Bloxham for building the Control Interface Unit and for his useful suggestions and remarks.

Thanks are also due to Messrs J. Knight, N. Wood and J. Martin of the Steam Laboratory for their interest and efforts in installing the test facility.

Acknowledgements are also made to the Imperial Chemical Industries Limited (ICI) for supplying the Imperial College, Mechanical Engineering Department, with 1.5 tons of Arcton-113 free of charge.

My thanks are extended to Miss D. Day, Miss E. Archer and Mrs S. Boote of the Mechanical Engineering Department.

I am also very much grateful to Miss E.A. Quin for her conscientious typing of the manuscript.

I wish to express my gratitude and my deep respect to my parents, who supported me and encouraged me in all aspects during the period of my studies.

Thanks are also due to my wife, Sophie, whose patience and understanding helped me in devoting all my time to my work.

CONTENTS

NOTE: All computer programs are available at the Imperial College of Science and Technology (Thermal Power Section), London University

LIST OF SYMBOLS

A : cross-sectional area (m^2)

a : thermal diffusivity (m^2/s)

B_e : resolution bandwidth (Hz)

B : parameter defined in Chapter 4

b : exponent in heat transfer correlation

C : constant of integration

c : specific heat (J/kg^oC)

D : helix diameter (m)

d : tube diameter (m)

E : specific internal energy (J/kg)

e : 2.718281 ...

F : force (N)

f : friction factor

f : frequency (Hz)

G : mass velocity (kg/m^2s)

G_x : power spectral density function (v^2/Hz)

g : acceleration of gravity (m/s^2)

h : specific enthalpy (J/kg)

h_{cn} : convective heat transfer coefficient ($W/m^2{}^oC$)

h : sampling interval (sec)

h_{fg} : heat of evaporation (J/kg)

J : volumetric average velocity (m/s)

j : imaginary unit = $\sqrt{-1}$

k : thermal conductivity (W/m^oC)

k : experimental orifice coefficient

L : parameter defined in Chapter 4

l : number of frequency components to be smoothed

M : function defined in Chapter 4

$\dot{m}$: mass flowrate (experimental) (kg/s)

N : parameter defined in Chapter 4

N : number of data

n : frequency (Hz)

P : pressure (N/m^2)

p_d : probability density function

Q : heating power (W)

Q' : heating power per unit length (W/m)

Q'' : heating power per unit surface (W/m^2)

Q_v : heating power per unit volume (W/m^3)

q : parameter defined in Chapter 4 (s^{-1})

R : coil radius (m)

R_x : auto-correlation function (v^2)

r : tube radius (m)

S : slip ratio

S_d : slip difference (m/s)

s : Laplace variable: $\sigma + j\,\omega$

T : temperature (^oC)

t : time (s)

U : velocity (m/s)

u : time record values (v)

u : velocity (m/s)

V_j : vapour drift velocity (m/s)

v : specific volume (m^3/kg)

W : mass flowrate (kg/s)

X : Lockhart-Martinelli parameter

x : quality (vapour quality)

y : distance (m)

Z : complex variable (Chapter 4)

z : axial coordinate (m)

Greek Symbols

α : void fraction

β : exponent in pressure drop correlation

Γ : function defined in Appendix A

γ : slip coefficient

Δ : difference

δ : perturbation in a variable

ε_r : normalised standard error

η : number of velocity heads

θ : angle to horizontal plane (degrees)

λ : parameter defined in Appendix A (m^{-1})

μ : dynamic viscosity (Ns/m^2)

ν : kinematic viscosity (m^2/s)

ξ : heated perimeter (m)

ρ : density (kg/m^3)

σ : surface tension (N/m)

τ : time constant (s)

ϕ : two-phase friction multiplier

ω : circular or angular frequency (rad/s)

Δh_s : inlet subcooling (J/kg)

Π : product of terms

Σ : sum of terms

φ^2 : measure of signal to noise ratio

σ_x : standard deviation (v)

ψ^2 : power content (statistical) (v^2)

Subscripts

o : steady-state

up : upstream adiabatic length

d : downstream adiabatic length

1 : subcooled single-phase region

3 : superheat single-phase region

2 : two-phase region

f,l : liquid phase

g,v : vapour phase

fg : liquid-vapour phase

w,m : wall (metal)

b : boiling boundary

s : superheat boundary

g : gravity component

m : momentum component (acceleration)

f : friction component

i : inlet

e : exit

nr : normalised

MP : maximum peak

c : coil

s : straight

Superscripts

0 : steady-state

$\bar{}$: Laplace transform of perturbed quantity

$\tilde{}$: mean value (statistical)

$\hat{}$: estimate (statistical)

$\approx$: raw estimate (statistical)

Dimensionless Groups

Fr : Froude number ($U^2/g.d$)

Nu : Nusselt number ($h.d/k$)

Pr : Prandtl number ($c.\mu/k$)

Re : Reynolds number ($\rho.U.d/\mu$)

N_{De} : Dean number ($Re\ \sqrt{d/D}$)

Abbreviations

ADC : analogue-to-digital converter

DNB : departure from nucleate boiling

DVM : digital voltmeter

FFT : fast Fourier transform

fso : full scale output

LSB : least significant bit

MSB : most significant bit

rms : root mean square

v.h. : velocity heads

CHAPTER 1

INTRODUCTION, BACKGROUND AND OBJECTIVES

The present work is concerned with a study of the dynamics of two-phase flow in vapour generators, with special reference to density wave instability.

Two-phase flow dynamics is a relatively new subject and during the last decade it has received special attention because of its importance in the design of modern once-through steam generators (some in helical form) used largely in advanced nuclear power stations (Taylor et al (1973)).

Dynamic models are required to study the vapour generators behaviour during normal operation, fault operation, start up and shut down, and to assess the extent of the thermal cycling of the tube walls. A knowledge of the dynamic behaviour is essential for both the safe and satisfactory operation of the vapour generator concerned.

As pointed out by Potter (1973) in "a critical review of two-phase flow instability aspects of boiler dynamics", many aspects of the instability mechanisms are still insufficiently understood in order to enable anyone to make predictions or design assessments with a degree of confidence. Due to the inherent complexities of the two-phase flow dynamics, there are very few programmes (especially experimental ones) around the world covering this subject in any depth.

In 1972, a research investigation programme of two-phase flow dynamics started at the Mechanical Engineering Department of Imperial College under the supervision of Professor W. Murgatroyd in collaboration with Dr A.A. El-Shirbini of the same Department.

At this initial stage, the research programme was undertaken by two

postgraduate students, one of whom was the present author.

The task of the present author was to investigate techniques for the stability analysis of once-through vapour generators, particularly those with helical coils, with the ultimate aim of studying the modelling of steam generators of this kind by the use of Freon circuits, thus paving the way for future work of developing simulation laws for the stability study of once-through vapour generators.

The techniques to be investigated included a linear (small signal) analysis of the system and the use of inherent noise in this system for stability predictions.

The intention was to verify the analysis on a special Freon circuit which was designed, constructed and commissioned by the author. However, because of unexpected delays in equipment delivery, the experimental time available was very short. Moreover, changing financial circumstances and a new College safety procedure necessitated the use of a different kind of heater and the operation at a lower pressure than that originally planned, and it was therefore not possible to cover as wide a range of variables as had been envisaged.

In planning the noise and other stochastic experiments, careful attention was given to the problems of data sampling, acquisition and processing. These aspects of experimentation, including the use of fast Fourier transforms, have not, to the author's knowledge, been previously applied to two-phase flow problems.

CHAPTER 2

REVIEW OF TWO-PHASE FLOW INSTABILITY

2.1 RELEVANCE OF THE PROBLEM

Flow instabilities in boiling, condensing and other two-phase flow processes are highly undesirable.

Such instabilities can produce one or more of the following troubles in the system (Tong (1965); Potter (1973)):

i) Sustained flow oscillations cause forced mechanical vibrations of the system components.

ii) Flow oscillations cause system control problems.

iii) Flow oscillations affect the local heat transfer characteristics and may induce premature boiling crises.

iv) Flow instability may cause "carry-over" of water into the superheater and turbine or other circuit components where it has a detrimental effect.

v) Flow instability in water-cooled and water moderated nuclear reactors causes changes of the moderation characteristics introducing fuel control problems.

vi) Flow instability causes thermal cycling of tube walls.

Two-phase flow systems in which these oscillations may become critical include nuclear reactors, conventional power plants, space propulsion systems, cryogenic equipment and other apparatus of the chemical process industry.

The two-phase flow instabilities not only degrade the performance of certain type of reactor cycles but can also result in malfunctions which can

become destructive.

Therefore, understanding by the designer of the conditions that lead to the onset of flow instabilities in two-phase mixtures and their avoidance by suitable control devices can be important for optimum equipment design and for safe operation, especially in PWRs.

2.2 CLASSIFICATION OF FLOW INSTABILITIES

The literature on "two-phase flow instabilities" is generally quite difficult to follow since the blanket term "two-phase flow instabilities" has been used for dissimilar mechanisms. Recent publications (Boure´ et al (1973); Neal et al (1967)) have brought some order, clarity and classification.

The classification is based on the following definitions:

(a) Steady flow: It is one in which the system parameters are functions of the space variables only. Small fluctuations due to turbulence or nucleation are not considered important, although their presence plays a rôle in triggering several instability phenomena. A stable flow, when momentarily disturbed, will tend asymptotically towards its initial operating conditions.

(b) Static instability: A flow is subject to a static instability if, when the flow conditions change by a small step, then another steady-state is not possible in the vicinity of the original steady-state. A static instability leads either to a different steady-state condition or to a periodic behaviour. The cause of the phenomenon lies in the steady-state laws.

(c) Dynamic instability: A flow is subject to a dynamic instability when the inertia and other feedback effects play an essential rôle in the process. The system behaves like a servomechanism and the steady-state laws are not sufficient even for threshold predictions.

(d) Secondary-primary phenomena: A secondary phenomenon is a phenomenon which occurs after a primary one (see "pressure drop

oscillations" in section 2.4.2.5 below).

(e) Fundamental-compound instability: An instability is said to be compound when several elementary mechanisms interact in the process and cannot be studied separately. It is said to be fundamental (pure) in the opposite sense.

The various flow instabilities are shown in Figure 2.1 in diagrammatic form.

2.3 PARAMETERS AFFECTING FLOW INSTABILITY

The following parameters affect the two-phase flow instabilities:

i) Geometry: Length, diameter, slope, inlet-exit restrictions, single or multiple channels, relative roughness.

ii) Operational conditions: Pressure, subcooling, thermodynamic properties of the fluid, mass velocity, power input, forced or natural circulation, surface condition.

iii) Boundary conditions: Axial heat flux distribution, imposed pressure drop across channel(s).

2.4 DESCRIPTION OF FLOW INSTABILITIES

This section describes the characteristics, parametric effects and physical mechanisms of the various types of flow instability as classified in section 2.2.

2.4.1.1 Fundamental static instability

(a) Flow excursion (Ledinegg instability)

This is the type of instability considered by Ledinegg in 1938. This is the first publication dealing with instability of two-phase flow. It is unfortunate that in the past it had become the most widely known, and generally the only one to be considered.

This instability occurs when the slope of the "internal characteristic" of the channel (channel demand pressure drop-flow rate curve) becomes algebraically smaller than the slope of the "external characteristic" of the channel (loop supply pressure drop-flow rate curve).

The criterion for this type of instability is therefore given by the relation (see Figure 2.2):

$$\partial \Delta P/\partial G\Big)_{INT} < \partial \Delta P/\partial G\Big)_{EXT}$$

For a closed channel with an imposed constant pressure drop, this behaviour would require that the channel internal characteristic exhibits a region where the pressure drop decreases with increasing flow.

A physical situation where the sum of the component terms (friction, momentum and gravity) increase with decreasing flow was, for example, experimentally demonstrated by Weiss as reported

by Tong (1965) (see Figure 2.3).

From Figure 2.3, it can be seen that as the inlet velocity (flow) is reduced, with other conditions held the same, the pressure drop increases rapidly once subcooled boiling is initiated, mainly due to the acceleration and friction caused by non-equilibrium voids. This phenomenon is more pronounced at higher heat fluxes.

Depending upon the shapes of the internal and external characteristics, there may be one intersection (point A on Figure 2.2a) or three intersections (points B, C, D on Figure 2.2b) between them. At point C there is a "static" instability; at points A, B, D the flow may be stable or there may be a "dynamic instability". Operation at point C is impossible since a slight increase in flow will cause a shift to point D. If the flow becomes slightly less than at point C, then there will be a spontaneous shift to point B. The new equilibrium point corresponds to such a low flow rate that in most cases burn-out occurs. Thus, with a relatively flat pump characteristic, operation at the negative portion of the internal characteristic is impossible. It can be done possibly by installing a throttling valve upstream, in which case the effective pump characteristic can be steepened enough (broken line, point C′ in Figure 2.2b).

Margetts (1972) reported flow instability failures in several feedwater coiled tube economisers. Calculations of heat transfer and pressure drop behaviour suggested that the severely overheated tube had the highest heat load and was operating at the minimum in the pressure drop-flow rate curve, which was essentially flat and set by the remaining parallel unheated tubes in the bank.

The solution adopted was to eliminate one-third of the unheated tubes to increase the driving pressure drop of the heated

tubes and lagging of the tubes. In other cases, the solution was to install throttling valves at the inlet to each of the tubes.

A "static" instability occurs when a small disturbance in flow rate produces a response which tends to increase the disturbance still further. Time, rates of change, etc., do not play a significant part in causing this instability; it is essentially the steady-state which is unstable, hence the term "static".

(b) Boiling crisis

Very simply stated, boiling crisis is caused by a change of heat transfer mechanism and is characterised by a sudden rise of wall temperature. There are numerous investigators who have dealt with this phenomenon, as reported by Tong (1965), Hewitt and Taylor (1970), Collier (1972).

Mathisen (1967) observed that boiling crisis occurred simultaneously with flow oscillations in a boiling water channel at pressures above 870 psi.

2.4.1.2 Fundamental relaxation instability

(a) Flow pattern transition instability

This type of instability occurs when the flow conditions are close to the point of transition between bubbly and annular flow. It is a purely hydrodynamic instability, and thus it can happen in an adiabatic two-phase flow system (Tong (1965)).

A temporary reduction in flow rate will increase the bubble population in a bubbly-slug flow, which may, in turn, change the flow pattern to annular flow with its characteristically lower pressure drop. Therefore, the excess driving pressure drop will speed

up the flow rate momentarily. This increase in flow rate, however, will decrease the amount of vapour generated which may become insufficient to maintain the annular flow, and the flow pattern then reverts to that of bubbly-slug flow. This cycle can be repeated.

This type of oscillation is partly due to the delay time between acceleration and deceleration of the flow. The mechanism of this instability is a typical relaxation one and is characterised by finite amplitudes at the threshold.

Bergles et al (1967) suggested that their low pressure CHF data might be strongly influenced by the presence of an unstable flow pattern of the bubbly-annular flow regime transition. The CHF would then be described as a secondary phenomenon.

2.4.1.3 Compound relaxation instability

This type of instability involves static phenomena which are coupled so as to produce a repetitive behaviour, which is not necessarily periodic. They are classified as bumping, geysering and chugging. For all these phenomena, the cycle consists of incubation, nucleation, expulsion and re-entry of the fluid in the heated section. The primary interest in those instabilities is currently in connection with liquid metal cooled fast reactors safety. An expansion into these types of instabilities is outside the scope of this work. For details, one can be referred to Boure et al (1973). Chexal and Bergles (1973) reported observations of static expulsion instabilities in a small natural circulation loop resembling a thermosiphon reboiler.

2.4.2 Dynamic Instabilities

2.4.2.1 Fundamental dynamic instability

The mechanism involves the propagation of disturbances which are transported by two kinds of waves:

i) Pressure or acoustic waves

ii) Void or density waves

In any real system, both these kinds of waves may be present and interact. Fortunately, their velocities differ by one or two orders of magnitude, thus allowing an easy discrimination.

2.4.2.2 Acoustic instability (or pressure wave)

Acoustic oscillations have been observed in subcooled boiling, bulk boiling and film boiling. They are characterised by a high frequency (20 - 10000 Hz), the period being of the same order of magnitude as the time required for a pressure wave to travel through the system.

Typical investigations of acoustic oscillations have been reported by Bergles et al (1967) and by Edeskuty and Thurston (1967).

This type of instability is governed by the speed of sound (pressure waves) in the two-phase flow mixture, being considered as a compressible fluid.

2.4.2.3 Density wave instability

For boiling systems, the density wave instabilities are due to multiple regenerative feedbacks between flow rate, vapour generation rate and pressure drop; hence, the name "flow-void feedback"

has been used (Neal et al (1967)). This feedback process includes the complete system, as opposed to a local process such as poor nucleation.

A density wave instability occurs when a small temporary disturbance of flow rate in a heated channel changes the rate of enthalpy rise, thereby changing the density (and voidage). This disturbance affects the pressure drop as well as the heat transfer characteristics. Under certain geometrical arrangements, operating and boundary conditions, the exit pressure fluctuation (restoring force) may be delayed by half a cycle (out-of-phase) relative to the initial flow disturbance so that it reinforces the next (opposite) half cycle of the disturbance. In this case, the oscillations become self-sustained (Neal et al (1967); Davies and Potter (1967)).

In describing the density wave instability, the alternate phrase "time delay oscillations" has been also used (Boure et al (1966,1967)).

The density wave instabilities are low frequency oscillations (0.1 - 5 Hz), whose period is approximately equal to the time required for a fluid particle to travel through the channel. This is where their name "density wave (or kinematic) instability" originates.

Density wave instability is the most common type of two-phase flow instability and has been extensively studied for the last 15 years. Its parametric effects have been often observed and are listed below:

i) Channel length: Crowley et al (1967), experimenting with a constant heat flux Freon-113 loop, found that the reduction of the heated length increased the flow stability under forced circulation.

Mathisen (1967) found the same effect in a natural circulation loop (see Figure 2.4).

ii) Inlet and exit restrictions: The effect of frictional distribution on stability is understandable from simple physical concepts. Since friction is by definition dissipative, it generally damps oscillations. In a boiling channel, a restriction in the single-phase region of the channel (inlet) increases the single-phase flow friction, which is in-phase with the change of inlet flow, and thus it increases the stability limit of the channel (Neal et al (1967)).

The friction in the two-phase flow region or exit, although dissipative, interacts with the flow in a way that in most cases increases the feedback interaction between flow and void (two-phase friction out-of-phase with the change of inlet flow), and this is destabilising. Several investigators have observed these trends (Wallis and Heasley (1961); Davies and Potter (1967)).

iii) By-pass ratio of parallel channels: Collins and Gaseca (1969) studied the by-pass ratio effect on the parallel channel flow arrangement. They experimented in a 19 rod bundle with a heated length of 195" by changing the by-pass ratio from 2 to 18. They found that an increase in by-pass ratio destabilised the flow (see Figure 2.8). Their results agree with the analysis of Carver (1969).

Veziroglu and Lee (1971) have studied density wave instabilities in a cross-connected, parallel channel system. They found that this system was more stable than either a single channel or parallel channels without cross-connections.

iv) Pressure: Experiments have shown that as the pressure is increased, holding other variables constant, the stability limit of the system is increased (i.e. the power at which the channel becomes unstable).

The stabilising effect of increasing pressure, at a given power input, arises from the associated increasing steam density and so the decreasing volumetric rate of steam production. The reduction in void fraction causes a reduction in two-phase flow frictional and momentum pressure drops and also reduces the exit quality because of the increased flow rate. All of these factors have a stabilising effect.

Mathisen (1967) has studied experimentally the effect of pressure on flow stability (see Figures 2.5, 2.6 and 2.7). The investigation was made with a natural circulation loop at low subcoolings.

In Figure 2.5, the threshold of instability and the burn-out heat flux contours are shown on the power-flow curves. As it can be seen, with increasing pressure, the power threshold of instability approaches the burn-out curve. At 71 atm, the boiling crisis occurred simultaneously with flow oscillations.

v) Inlet subcooling: The effect of subcooling on the flow stability limit is not straightforward. The experiments indicate that an increase in subcooling can either delay or precipitate oscillations depending upon the initial degree of subcooling. Thus, the effect of inlet subcooling exhibits a minimum on the power-subcooling curves as it was found by Mathisen (1967) (see Figure 2.6). Crowley et al (1967) observed similar effects in a forced circulation Freon-113 loop and they also noticed that starting a system with high subcoolings

can lead to large amplitude oscillations.

The shape of the curves in Figure 2.6 suggests that there are two competing processes involved when the subcooling is varied, one being stabilising and the other destabilising.

The stabilising process is the decreasing of void fraction and the increasing of the non-boiling length with increasing subcooling.

The destabilising process, with increasing subcooling, is the increasing of the subcooled length and thus the increasing enthalpy transportation time in the non-boiling region.

At small subcoolings, this incremental change of transit time is significant in the response delay of void generation from the inlet flow and so the destabilising mechanism dominates.

At higher subcoolings, the stabilising mechanism dominates.

vi) Mass velocity-power: The mass velocity effect on the threshold power of flow instability was reported by Mathisen (1967) (see Figure 2.5).

Collins and Gaseca (1969) tested the effects of mass velocity and power on the flow oscillation frequency in a 19 rod bundle with steam-water flow at 800 psia. Their experimental investigation (see Figure 2.9) showed that the oscillation frequency increased with mass velocity as well as power input to the channel.

vii) Cosine heat flux: The effect of cosine heat flux distribution was tested by Dijkman (1969). He found its effect stabilising. The reason may be the decrease in local pressure drop at

the exit due to the lower than average heat flux at this region.

viii) Channel wall heat capacity: Most of the flow instability tests have been conducted with electric heaters of small thermal capacitance of which the effects are negligible in evaluating the density wave instability.

The heat capacity of the coolant channel wall sometimes can be an important factor in the energy storage and transfer processes. Energy storage in the channel walls occurs as a result of three phenomena (Neal et al (1967)):

(a) In the non-boiling region, subcooled liquid temperatures respond to flow oscillations, and hence there is a dynamic interchange of heat between the walls and the flowing subcooled liquid.

(b) In the boiling region, the heat transfer coefficient varies because of variations in void fraction and/or mass flow rate induced by flow instability, and hence there is a varying energy storage in the wall.

(c) In the boiling region, dynamic variations in pressure introduce corresponding variations in the temperature of the two-phase flow and consequently there are energy exchanges between the channel wall and the two-phase fluid.

Of these three phenomena, the first (a) is well understood and can be important in affecting the flow stability.

The second phenomenon (b) does not appear to be very

important and generally cannot be accounted for because of incomplete knowledge of boiling heat transfer coefficients.

The third one (c) is thought to be unimportant. Only at very low system pressures, where small changes in pressure correspond to significant changes in saturation temperatures, it could be important.

The effect of wall heat capacity is to increase the phase lag (transportation time delay) of the flow-void transfer function and in this respect the wall heat capacity is destabilising. On the other hand, the wall heat capacity reduces the amplitude of the flow-void transfer function, which is a stabilising effect. The frequency of the disturbance, relative to the heat transfer time constants, determines whether the phase or amplitude effect is greater.

A rigorous analysis of the wall dynamics, for the case of a time-varying heat generation, has been reported by Verheugen et al (1967).

Yadigaroglu and Bergles (1972) explained the higher order oscillations (density wave) observed in a Freon-113 loop, by considering the dynamics of the heater wall in the liquid phase region.

2.4.2.4 Compound dynamic instability

(a) Thermal oscillations

These oscillations appear to be associated with the thermal response of the heating wall after dry-out has occurred (Stenning et al (1965)). It was suggested that the flow could oscillate between film boiling and transition boiling at a certain point; this gives rise to large temperature oscillations in the channel wall subject to constant heat flux. In this type of instability (compound), the higher frequency density wave oscillations act as a disturbance to

destabilise the film boiling. The Freon-11 loop of Stenning et al (1965) used an electrically heated nichrome heater (0.08" wall) and the period of the thermal oscillations observed was around 80 seconds.

Thermal oscillations are considered a regular feature of dry-out of steam-water mixtures at high pressures.

Quin (1966) recorded wall temperature oscillations of several hundred degrees downstream of the dry-out point, with periods ranging from 2 - 20 seconds.

(b) Boiling water reactor instability

In a boiling water nuclear reactor, the thermo-hydrodynamic instability becomes more complicated due to the feedback through a void-reactivity-power link. This feedback effect can be dominant when the time constant of the hydraulic oscillation is comparable with the time constant of the fuel element (Bouré et al (1973)).

A typical theoretical treatment of this type of instability has been presented by Solverg and Bakstad (1967).

(c) Parallel channel instability

As mentioned by Crowley et al (1967), Gouse and Andrysiak observed parallel channel interactions for a two-channel Freon-113 system, where the flow oscillations were generally 180^{o} out-of-phase. Within the unstable region, the two test section flows began to oscillate in-phase with large amplitude oscillations.

Crowley et al (1967) experimented on the same loop with three heated channels operating in parallel with a large by-pass so as to maintain a constant pressure drop. The stability boundaries and periods of oscillations observed were identical for one,

two or three channels. The avoidance of channel interactions in this case was due to the constant pressure drop maintained by the big by-pass.

An interesting experimental investigation was reported by D'Arcy (1967). His test section comprised three internally heated annular flow water channels (at 500 - 1500 psia in forced circulation) connected to inlet and outlet headers. Various modes of flow oscillations were observed. The most common ones were:

i) All three channels oscillating at about the same amplitude in 120^{o} phase difference.

ii) Two channels out-of-phase with the third, and the amplitude in the ratio 2:1.

iii) Two channels oscillating at about the same amplitude and about out-of-phase, the third channel oscillating at much reduced amplitude.

In all cases, the three channels oscillated in such a mode as to maintain the external circuit flow constant and therefore the pressure drop imposed across the channels.

2.4.2.5 Secondary compound dynamic instability

(a) Pressure drop oscillations

For this type of instability, a static instability phenomenon triggers a dynamic instability (secondary phenomenon).

Pressure drop oscillations occur in systems having a compressible volume upstream or within the test section.

A typical investigation by Maulbetch et al

(1967) revealed that this type of oscillation was associated with operation on the negative slope portion of the pressure drop-flow rate curve and caused by small amounts of upstream compressibility. The remedy for this type of instability is a throttling between test section and compressible volume.

Stenning et al (1967) found the same phenomenon in a Freon-11 system with an upstream gas-loaded surge tank. The operating point was again on the negative slope portion of the channel internal characteristic.

Generally speaking, the frequency of pressure drop oscillations is lower than that of density wave oscillations and is governed by the volume and compressibility of the system rather than by transportation and inertia delays. Pressure drop oscillations appear in the low exit quality region while density wave oscillations occur at higher exit qualities.

2.5 ANALYSIS OF FLOW INSTABILITIES

In this section, we will be considering the analysis of the "flow excursion" or "Ledinegg instability" and of the dynamic instabilities with special reference to "density wave instability".

2.5.1 Analysis of Flow Excursion Static Instability

The threshold of flow excursion can be predicted by evaluating the Ledinegg instability criterion:

$$\left.\frac{\partial\ \Delta P}{\partial G}\right|_{INT.DEM.} < \left.\frac{\partial\ \Delta P}{\partial G}\right|_{EXT.SUP.}$$

The pressure drop ΔP is supplied by the pump or by the natural circulation head. G is the hot channel mass velocity.

Margetts (1972), using accurate pressure drop correlations provided by Thom and Chisholm (Collier (1972)), evaluated each channel's demand pressure drop-flow rate curve according to its heat load. He was then able to discover that some of the tubes were working under Ledinegg instability conditions and take some corrective action.

Hands (1974) presented the Ledinegg instability criterion in an interesting way assuming a simple pressure drop model with constant friction factor, in terms of a Jacob number, the friction factor and the length over the diameter of the heated tube.

2.5.2 Analysis of Dynamic Instabilities

A model of the dynamics of a boiling system is a statement and solution of the mass, energy and momentum conservation equations for the single-phase and two-phase fluids together with the so-called constitutive laws and boundary conditions. The constitutive laws define

the properties of the system with a certain degree of simplification or empiricism, e.g. equation of state, steam tables, slip between the phases, two-phase friction correlations and boiling heat transfer behaviour.

The flow is assumed one-dimensional (mean values across each section). Turbulence and boiling noise are neglected so that both the void fraction and phase velocities are smooth functions of time and space. The potential energy term is neglected in the treatment of the energy conservation equation.

The conservation equations can be derived using the usual method of writing a mass, energy or momentum balance over a thin volume element $A\ \Delta z$ of the fluid stream. Then, taking the limit as the volume approaches zero ($\Delta z \to 0$), the definition of the first partial derivatives is applied to yield the partial differential equations.

Generally speaking, the conservation principles yield three equations for each phase, plus three interface relationships (Bird et al (1960)). Using a six conservation equation model is a very rigorous way, since we must take into account interfacial phenomena, such as slip and lack of thermal equilibrium. Since the more numerous the conservation equations are, the more detailed the constitutive laws have to be, most of the existing models use three or four conservation equations.

In the present case, a typical set of six conservation equations as discussed by Bouré et al (1973) is presented. These equations can be written for a one-dimensional flow of constant cross-section without injection nor suction at the wall, as follows:

(a) Mass conservation equation

$$\frac{\partial(A_k\ \rho_k)}{\partial t} + \frac{\partial(A_k\ \rho_k\ u_k)}{\partial z} = M_k \tag{2.1}$$

with interface relationship:

$$\sum M_k = 0 \tag{2.2}$$

(b) Momentum conservation equation

$$A_k \frac{\partial P}{\partial z} + \frac{\partial(A_k\ \rho_k\ u_k)}{\partial t} + \frac{\partial(A_k\ \rho_k\ u_k^2)}{\partial z} = -A_k\ \rho_k\ g\ \sin\theta - F_{ki} - F_{kw} \tag{2.3}$$

with interface relationships:

$$\sum F_{ki} = 0 \tag{2.4}$$

$$\sum F_{kw} = F_{TP} \tag{2.5}$$

(c) Energy conservation equation

$$\frac{\partial(A_k\ \rho_k\ h_k)}{\partial t} + \frac{\partial(A_k\ \rho_k\ u_k\ h_k)}{\partial z} = A_k \frac{\partial P}{\partial t} + A_k\ u_k \frac{\partial P}{\partial z} + Q_{ki} + Q_{kw} \tag{2.6}$$

with interface relationships:

$$\sum Q_{ki} = 0 \tag{2.7}$$

$$\sum Q_{kw} = Q_v \tag{2.8}$$

The above equations hold with $k = l$ for liquid and $k = v$ for vapour.

A_k is the cross-section fraction of phase k, $A_v = \alpha$, $A_l = 1 - \alpha$.

M_k is the mass transferred per unit time and volume to phase k.

Q_{ki}, Q_{kw} is the heat transferred per unit time and volume to phase k (subscript i stands for the interface and w for the wall).

θ is the angle of the channel axis to the horizontal plane.

Many assumptions can be made to further simplify the above written equations:

i) The terms $\partial P/\partial t$ and $\partial P/\partial z$ are usually neglected in the energy equations.

ii) The physical properties (ρ_k, h_k) are considered to be independent of pressure. This assumption is valid only for density wave instability of relatively high pressure systems, where the pressure drop is very small compared to the system pressure. This assumption is not valid for acoustic instability where the two-phase flow is considered compressible, i.e. $\rho_k = f(h_k, P)$.

iii) $h_k = h_{k,sat}$ for both phases. With assumptions (i) and (iii), the phase energy equation (2.6) becomes equivalent to the phase mass conservation equation (2.1), thus reducing the order of the set.

iv) Usually the two momentum equations (2.3) are replaced by their sum (equation (2.11) hereunder) and the "slip equation", result of the elimination of $\partial P/\partial z$ between them and taking into account equation (2.1):

Slip equation:

$$\rho_l \left(\frac{\partial u_l}{\partial t} + u_l \frac{\partial u_l}{\partial z}\right) - \rho_v \left(\frac{\partial u_v}{\partial t} + u_v \frac{\partial u_v}{\partial z}\right) =$$

$$= -(\rho_l - \rho_v)\, g \cos\theta - \left(\frac{F_{li} + M_l u_l}{1-\alpha} - \frac{F_{vi} + M_v u_v}{\alpha}\right) - \left(\frac{F_{lw}}{1-\alpha} - \frac{F_{vw}}{\alpha}\right) \qquad (2.9)$$

In turn, slip equation (2.9) is replaced by a finite correlation.

The above assumptions should be investigated further, especially when fast transients or large pressure drop flows are involved.

By using assumptions (i), (ii), (iii) and (iv), the above set is reduced to a set of three partial differential equations together with two general functional relationships for the slip ratio $S = u_l/u_v$ and the two-phase friction pressure drop gradient F_{TP} (Neal et al (1967)). The heat input Q_v per unit volume of coolant is assumed known.

Mass conservation

$$\frac{\partial\left(\alpha \rho_v + (1-\alpha)\rho_l\right)}{\partial t} + \frac{\partial\left(\alpha \rho_v u_v + (1-\alpha)\rho_l u_l\right)}{\partial z} = 0 \qquad (2.10)$$

Momentum conservation

$$\frac{\partial\left((1-\alpha)\,\rho_l\,u_l + \alpha\,\rho_v\,u_v\right)}{\partial t} + \frac{\partial\left((1-\alpha)\,\rho_l\,u_l^2 + \alpha\,\rho_v\,u_v^2\right)}{\partial z} =$$

$$= -\frac{\partial P}{\partial z} - F_{TP} - \left[(1-\alpha)\,\rho_l + \alpha\,\rho_v\right] g\,\sin\theta \qquad (2.11)$$

Energy conservation

$$\frac{\partial\left((1-\alpha)\,\rho_l\,h_l + \alpha\,\rho_v\,h_v\right)}{\partial t} + \frac{\partial\left((1-\alpha)\,\rho_l\,u_l\,h_l + \alpha\,\rho_v\,u_v\,h_v\right)}{\partial z} = Q_v \qquad (2.12)$$

Slip ratio

$$S = S(\alpha) \qquad (2.13)$$

Two-phase friction pressure gradient

$$F_{TP} = F_{TP}(\alpha, W) \qquad (2.14)$$

where $W = \alpha\,\rho_v\,u_v + (1-\alpha)\,\rho_l\,u_l \;\hat{=}$ mass flow rate

The above set of five equations (2.10) to (2.14) is consistent. There are five equations and five unknowns, namely: u_l, u_v, P, α, and F_{TP}. The saturation enthalpies h_l, h_v and the phase densities ρ_l, ρ_v are constant according to the assumptions (ii) and (iii).

The above equations can be expressed in terms of W and quality x, bearing in mind that $x/1 - x = \alpha/1 - \alpha\,(\rho_v/\rho_l)\,S$.

By using the theory of Zuber and Findlay (1965), equation (2.13) is replaced by an expression involving the vapour phase velocity,

in terms of the average volumetric velocity J and two empirical constants γ and V_j:

$$u_g = \gamma J + V_j \qquad (2.13a)$$

where γ = a constant allowing for the non-uniform distribution of void fraction and volumetric velocity in a cross-section

V_j = vapour drift velocity (slip of vapour phase with respect to the centre of the volume)

2.5.3 Analysis of Density Wave Instability

Two basic approaches have been used for the analysis of density wave instability:

(a) Numerical integration of the conservation equations in the time domain (non-linear analysis) following some initial perturbation.

(b) Linearised study of dynamic response in the frequency domain, followed by classical control theory stability considerations.

During the first years of two-phase flow dynamics, lumped parameter models have been used to predict flow instability and provide some direct physical insight into the mechanism of instability.

However, the use and further development of more refined lumped parameter models like the one by Shotkin (1967) was soon abandoned since they could not treat the distribution and transportation effects adequately.

Therefore, the more complicated (space) distributed parameter models, usually in the form of computer codes, were developed and are

today extensively used.

Since the computer codes can handle the complicated mathematics involved in the equations described in section 2.5.2 above, most of the compounded and feedback effects can be built into the computer codes for analysing the dynamic instabilities.

A typical treatment of the non-linear thermo-hydrodynamic equations, using finite-difference techniques, is given by Meyer and Rose (1963). The computer programs "HYDNA" (Tong (1965)) and "SLIP" (Moxon (1968)) are typical cases of treatment of the non-linear thermo-hydrodynamic equations (time domain) using numerical techniques.

A review of the available models and comparison to data indicates that linearised calculations in the frequency domain predict adequately the threshold and frequency of instability (Neal et al (1967); Blumenkrantz et al (1972)), and they are free from numerical instability pitfalls often encountered in non-linear time domain analysis.

Many simplified models have been used for flow stability analysis as, for example, the ones reported by Davies and Potter (1967), Bouré (1966), Wallis and Heasley (1961), Quandt (1961), Anderson (1970), Ishii and Zuber (1970), Zuber (1967), and Shotkin (1967). The threshold and frequency at instability point are derived in complex closed analytical forms which, in most cases, need to be evaluated by a computer. These "fast-running" models give a good physical understanding of the phenomena involved and what is more important, they give predictions which are in good agreement with experimental data.

Bjorlo et al (1967) reported a comparative study of the mathematical hydrodynamic models applied to selected boiling channel experiments (Scandinavian Group Programmes).

2.6 DIMENSIONAL ANALYSIS AND FLUID-TO-FLUID MODELLING OF TWO-PHASE FLOW INSTABILITIES

Present day science and technology make extensive use of dimensional analysis in both theory and experiment, and in a number of widely differing branches of physics and engineering. Dimensionless groups are useful to reduce the number of independent parameters and to serve as a tool for developing scaling laws. They are developed from a rather simplified mathematical model in which the number of dimensional parameters has already been reduced.

Because of the multitude of parameters affecting a two-phase flow dynamics problem, one is very much inclined to use dimensional analysis. As a word of caution for the dimensional analysis, dynamic similitude can be achieved only for the same type of flow instability, with similar geometry and similar boundary conditions.

Several authors, such as Ishii and Zuber (1970) and Bouré and Mihaila (1967), have used dimensionless groups for two-phase flow instabilities, which are more or less similar.

For a given geometry with a uniform power density along the heated section, the main effects of the fluid properties, the interactions between the phases (such as slip and thermal non-equilibrium), the gravity, the pressure, inlet velocity, inlet enthalpy, and heat flux are taken into account.

A comparison of the principal dimensionless groups used by Bouré et al (1967) and Ishii and Zuber (1970) is given by Bouré et al (1973).

Zuber (1967) introduces explicitly a drift velocity V_j and the corresponding terms in the conservation equations. His system comprises two continuity equations (one for the vapour phase and one for the mixture), one energy equation and one momentum equation. He specifies

Γ_v, the vapour generation rate per unit volume, by a constitutive equation. The "characteristic frequency of evaporation" is then defined as:

$$\Omega = \left[\left(\frac{\rho_f - \rho_g}{\rho_f}\right)\right] \frac{\Gamma_v}{\rho_g} \tag{2.15}$$

The partial differential equations were linearised, Laplace transformed and integrated along the channel. The the steady-state values were subtracted to give a perturbed characteristic equation, which is a fifth order exponential polynomial with two time delays. Assuming equilibrium flow in circular tubes, the above mentioned equation was used to obtain the following dimensionless groups:

$\frac{\rho_f}{\rho_g}$: liquid to vapour density ratio (2.16)

$\frac{L}{D}$: heated length to diameter ratio (2.17)

$Re = \frac{\rho_f u_{fi} D}{\mu_f}$: Reynolds number based on saturated single-phase liquid (2.18)

$Fr = \frac{gL}{u_{fi}^2}$: Froude number (2.19)

$\frac{V_j}{u_{fi}}$: drift number (2.20)

$N_{sub} = \left(\frac{\rho_f}{\rho_g} - 1\right)\left(\frac{h_f - h_i}{h_{fg}}\right)$: subcooling number (2.21)

$N_{pch} = \frac{v_{fg} Q'' 4 L}{h_{fg} u_{fi} D}$: phase change number (2.22)

K_i, K_e : number of inlet velocity heads expressing inlet (outlet) pressure drops

The dimensionless harmonic frequency:

$$\omega^* = \frac{\omega}{\Omega} \tag{2.23}$$

is an auxilary variable at the stability boundary (ω is the frequency with which the system oscillates).

Parametric charts in terms of these groups were developed from solutions to the characteristic equation. In keeping with the assumption that the pressure is essentially constant along the heated channel ($\rho = \rho(h)$ only), the charts were evaluated for high pressure conditions.

The dimensionless groups of Bouré (1967) have been used successfully to scale the data obtained at different pressures (20, 40 and 80 atm) on the same loop with water.

Blumenkrantz and Taborek (1972) have applied the "density effect" model of Bouré (1966) to the prediction of instability in natural circulation systems used in the petrochemical industry, the thermosiphon reboilers. They concluded that similarity analysis in terms of the model's dimensionless groups can be used to extrapolate threshold stability data from one fluid to another.

Generally speaking, dealing with the problems of flow instabilities in boiling channels, the expense of high pressure prototypes makes the alternative of modelling using low pressure fluorocarbon systems attractive.

The very comprehensive set of experimental data for the critical heat flux of Freons by Stevens and Macbeth (1970) have shown that these fluids behave qualitatively in an identical way to water.

For example, the use of Freon-113 (which has a high boiling

point relatively to the other grades of Freon (11, 12, 22)) to scale high pressure water data seems to be attractive.

The modelling procedure is rather straightforward once the prototype geometry and conditions and model fluid have been solved. The pressure is scaled via the density ratio ρ_f/ρ_g. In Figure 2.10, the density ratio versus pressure for various fluids is represented. It can be noticed that the curves representing water and Freon-113 remain essentially equidistant on the logarithmic scale. The water pressures are approximately eight times the corresponding pressures of Freon-113. Once the pressure is fixed, the thermodynamic and transport properties are established.

From the subcooling number, h_i can then be determined. By simultaneously solving L/D, Re, Fr, the geometry and inlet velocity u_{fi} are established. Finally, the phase change number is used to obtain the model heat flux. Figure 2.11 giving u_{fg}/h_{fg} is useful for this part of the calculation.

By referring to formulae (2.21) and (2.22), we obtain:

$$N_{sub} = N_{pch} - x_e \left(\frac{\rho_f}{\rho_g} - 1\right) \tag{2.24}$$

$$\bar{\lambda} = \frac{N_{sub}}{N_{pch}} \qquad \text{(dimensionless non-boiling length)} \tag{2.25}$$

It can easily be seen that the model has already been scaled so that the inlet "negative quality", the relative position of the boiling boundary, and the exit quality x_e are the same as in the prototype.

The drift number V_j/u_{fi} is characteristic of the flow regime and varies along the channel. It is zero for single-phase or homogeneous two-phase flow. Approximate expressions are available only

for low void bubble flow and slug flow (Collier (1972)). The general effect of a finite drift velocity or relative velocity between the two phases is to enhance the stability of the system. In view of the present uncertainty in calculating V_j for every flow regime in the boiling channel, it is probably adequate to ensure that the flow regimes are similar.

By rearranging the groups L/D, Re, Fr, one is led to the relation:

$$D_M = D_p \, (\nu_M/\nu_D)^2$$

Since, for Freon-113, the kinematic viscosity is at most about 50% greater than that for water, the model dimensions for perfect scaling are only slightly larger than the prototype and a function of pressure. In this case, the usual decision is to test a full size model, and scale on the basis of equal Froude numbers to keep the power requirements low. Therefore, the Reynolds number will not be the same (fortunately, this will have a very small effect on the friction factor). Also, the main advantage will be that, by keeping the model geometrically similar to the prototype, the flow regimes and therefore V_j/u_{fi} can be kept similar.

Recently, Harvie (1974) conducted parallel channel flow instability experiments using Freon-12 in a three channel section, which had previously been tested in a water loop (D'Arcy (1967)), in order to examine the feasibility of using Freon-12 as a modelling fluid for stability studies. He reported that the dynamic behaviour in the Freon-12 experiments were similar to that observed in the water experiments, except at very low qualities and he derived a set of empirical laws for scaling the instability threshold.

2.6.1 Modelling or Analysing Low Pressure Systems

(a) The influence of flashing and vapour expansion

Major problems in modelling and in the evaluation of model results arise not only because it is impossible to model all of the important thermal and hydrodynamic features of the high pressure systems, but also because very important steady-state and dynamic phenomena, totally negligible in high pressure systems, may dominate the behaviour of the low pressure systems.

The phase change number is a very important parameter since it is indicative of the amount of vapour generated, and hence the velocity distribution along the test section.

By referring to the original definition of N_{pch}:

$$N_{pch} = \frac{\Omega L}{u_{fi}} \tag{2.26}$$

where Ω is the characteristic frequency of evaporation or velocity gradient, defined in equation (2.15).

The velocity gradient can be written for homogeneous equilibrium flow as (Crowley and Bergles (1970)):

$$\Omega = \frac{dV}{dz} = \frac{4\,Q''\,v_{fg}}{D\,h_{fg}} - G\,c_p\,\left(\frac{v_{fg}}{h_{fg}}\right)\left(\frac{dT}{dP}\right)_s\left(\frac{dP}{dz}\right) + \\ + G\,x\left\{\left(\frac{dv_{fg}}{dT}\right)_s - \frac{v_{fg}}{h_{fg}}\left(\frac{dh_{fg}}{dT}\right)_s\right\}\left(\frac{dT}{dP}\right)_s\left(\frac{dP}{dz}\right) \tag{2.27}$$

The first term represents the increase in velocity due to vaporisation arising from local heat input, while the additional terms represent the flashing and expansion terms as the flow encounters a decreasing pressure.

If the pressure gradient is small compared to the

pressure level, only the vaporisation term is necessary in evaluating the Ω, i.e.

$$\Omega = \frac{dV}{dz} = \frac{4\, Q''\, v_{fg}}{D\, h_{fg}} \tag{2.28}$$

Subsequently, the phase change number N_{pch} assumes the form given in equation (2.22).

When the pressure drop is a significant fraction of the pressure level, which occurs in the case of a low pressure model, or more generally when a high pressure analysis is applied to a very low pressure system, the flashing and vapour expansion terms are significant and the problem becomes seriously difficult. In the scaling case, it would appear at first glance that it would be adequate to have N_{pch} equal for the model and prototype. The model would have a reduced heat flux to compensate for the contribution of flashing and vapour expansion to the velocity gradient. Some averaging procedure would then have to be devised to account for the axial variation of these terms, or the heat flux could be varied axially. This procedure would not necessarily be valid for the dynamic case, and hence the stability prediction would not be accurate, as it was discovered in some M.I.T. low pressure Freon experiments, as discussed by Crowley and Bergles (1970).

The dimensionless analysis, described in section 2.6, seems to be very promising for high pressure systems, where it is assumed that the pressure is constant along the heated section. This assumption is not valid for low pressure systems. At the present time, the distributed parameter approach seems to be the best way to attempt analytical predictions of stability for low pressure systems.

With regard to the modelling of low pressure systems, it is suggested (Crowley and Bergles (1970)) that a pertinent

dimensionless group of the form $\Delta P/P$, where ΔP is the channel pressure drop and P is a characteristic system pressure, could take into account the flashing and vapour expansion terms appearing in equation (2.27).

2.6.2 Additional Considerations When Modelling

The conclusion, from the previous two sections thus far, is that scaling should be rather straightforward, and that refrigerants such as Freon-113 (which has a relatively high boiling point) are well-suited for modelling of high pressure water conditions. However, it is appropriate to mention a few additional factors which may cause the model behaviour to be considerably different than anticipated.

(a) Wall heat storage

Since the model pressure is rather low, there is a temptation to use visual sections since pressure and heat flux may be within the range of electrically conducting glass tubing. Since the glass test section has different properties from the prototype boiler tube, it is necessary to reassess the effect of the wall heat storage on the test section dynamics.

(b) Air solubility

The air solubility of the fluorocarbons is generally an order of magnitude greater than that of water. This high air solubility will increase the void generation rate, which is a stabilising effect since it reduces the pure delay. Recent experiments with fluorocarbons (Murphy and Bergles (1972)) have shown that:

i) Subcooled void fractions are very large when

Freon-113 is not degassed and available correlations are inadequate for predicting subcooled voids with air.

ii) Collapse of subcooled voids containing air is extremely slow.

iii) Long periods of degassing are necessary to reduce the dissolved air to a minimal value (8 hours for a small Freon-113 loop).

It is evident that the dynamics of the subcooled region will be affected by the dissolved air and that this effect is very pronounced with fluorochemicals.

(c) Wettability

The Freons have extremely good wetting characteristics, with the contact angle being only about 3^{0} on Teflon. This suggests a poor nucleation, especially on glass surfaces. There are many examples of nucleate pool boiling curve hysteresis with Freons (Murphy and Bergles (1972)). This kind of hysteresis introduces uncertainty into the steady-state loop characteristics which are a vital input to the dynamic formulation.

(d) Thermal conductivity

Little vapour formation is observed in the bulk boiling region with Freon-113 and there is a storage of energy in the superheated annular film. The throughput velocity is thus low and the delay is increased. This is due in part to the relatively slow diffusion through the low conductivity Freon film which results in a time lag in

vaporisation near the channel exit, an effect which is destabilising.

(e) Fluorocarbon degradation

One advantage of using fluorochemicals for modelling is that the heater wall temperatures are well below the melting point of the usual heater materials, even for subcooled boiling crisis. Unfortunately, these compounds degrade rapidly, even at modest temperatures. For example, at a temperature of 572^{o}F, Freon-113 in contact with steel is estimated to decompose completely in one year. This necessitates avoiding operation at extremely high pressures and heat fluxes, not only because of the degradation but also because of the eventual fouling of the heated surfaces.

As it is pointed out by Crowley and Bergles (1970), all the additional characteristics described in this section appear to have some compensating effect as far as stability is concerned.

2.7 DISCUSSION

Today it is generally believed that the instability mechanisms are understood in broad terms but it is clear that many aspects are insufficiently understood for anyone to make predictions with a high degree of confidence (Potter (1973)), and in that sense the subject is still developing.

The present limitations on predicting the onset of flow oscillations appears to be more closely associated with our inability to predict the steady-state operating conditions with the necessary accuracy than it is with uncertainties in systems dynamics (Neal et al (1967)).

Even for the steady-state, the information of such important factors, such as subcooled boiling, friction factors, slip between the phases (void fraction), heat transfer mechanisms and thermodynamic equilibrium, is based on empirical laws and tends to be specific to the particular boiler design or demonstration test rig. It appears that if significant improvement is to be achieved over existing models, a much stronger emphasis must be placed on the mechanism of mass, momentum and heat transfer transport between the phases for the different flow regimes. Although there is no reason to doubt that all these physical processes involved are amenable to analysis, it is believed that there is still a lot of work to be done before it will be possible to demonstrate a reliable predictive method for all the situations which arise in the study of boiler dynamics (Potter (1973)).

For the present, it is thought that fast-running relatively simple codes will in many cases suffice, provided that the key features are recognised and represented (Moxon (1973); Redfield and Murphy (1971)).

This, of course, does not disregard the merits of the elaborate long-running computer codes (based on a rigorous non-linear analysis of

the conservation equations) in assessing the stability of a system, but the problem is that with these over-comprehensive computer models, the analyst may well be little wiser as regards the basic mechanism affecting the stability of the system concerned (Davies and Potter (1967); Moxon (1973)).

Redfield and Murphy (1971) reported a comparison of the FLASH-4 (compressible, sectionalised) numerical solution of channel hydrodynamics with a simpler momentum integral solution (no density variations due to pressure changes). The result was that the speed advantage of the simpler code (momentum integral solution) was typically in the range 1 - 100 (depending on the average velocities), while the threshold power levels and frequencies ($\simeq$ 1 Hz) agreed to within 2%.

As reported by Potter (1973), a big reason why little scientific progress has been made on boilers dynamics is that there are very few carefully conducted experimental programmes covering this subject. Furthermore, such important aspects, such as implications, practical problems, etc., which arise in boiler design and demonstration test rigs, are not always published. Inevitably, more experimental programmes with emphasis on the analysis and interpretation of the data are needed before a real advance into the subject is achieved. Recently, an interesting experimental investigation of the oscillatory behaviour of a once-through boiler rig has been reported by Fallows et al (1973). Abi-Zadeh (1976) examined theoretically the dynamic behaviour of a once-through boiler rig.

As far as modelling is concerned, the stability data with modelling fluids are still too limited to verify the adequacy of the scaling parameters which have been suggested. A lot of experiments on dynamically similar systems (or the same system) using both water and the

modelling fluid (for example, fluorocarbons) need to be performed before a real improvement is achieved for the fluid-to-fluid modelling of two-phase flow instabilities (Crowley and Bergles (1970)).

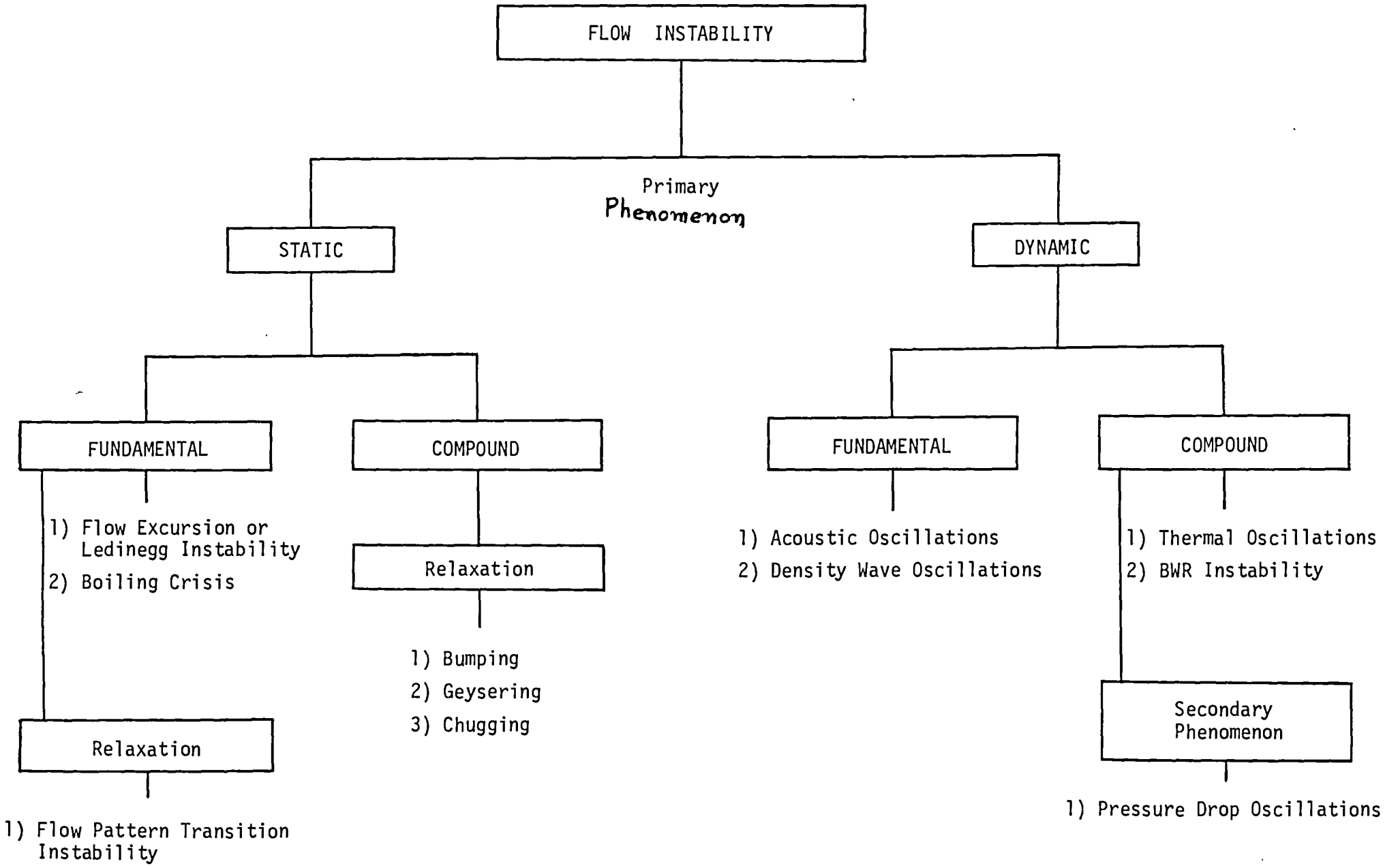

Figure 2.1: Types of flow instability

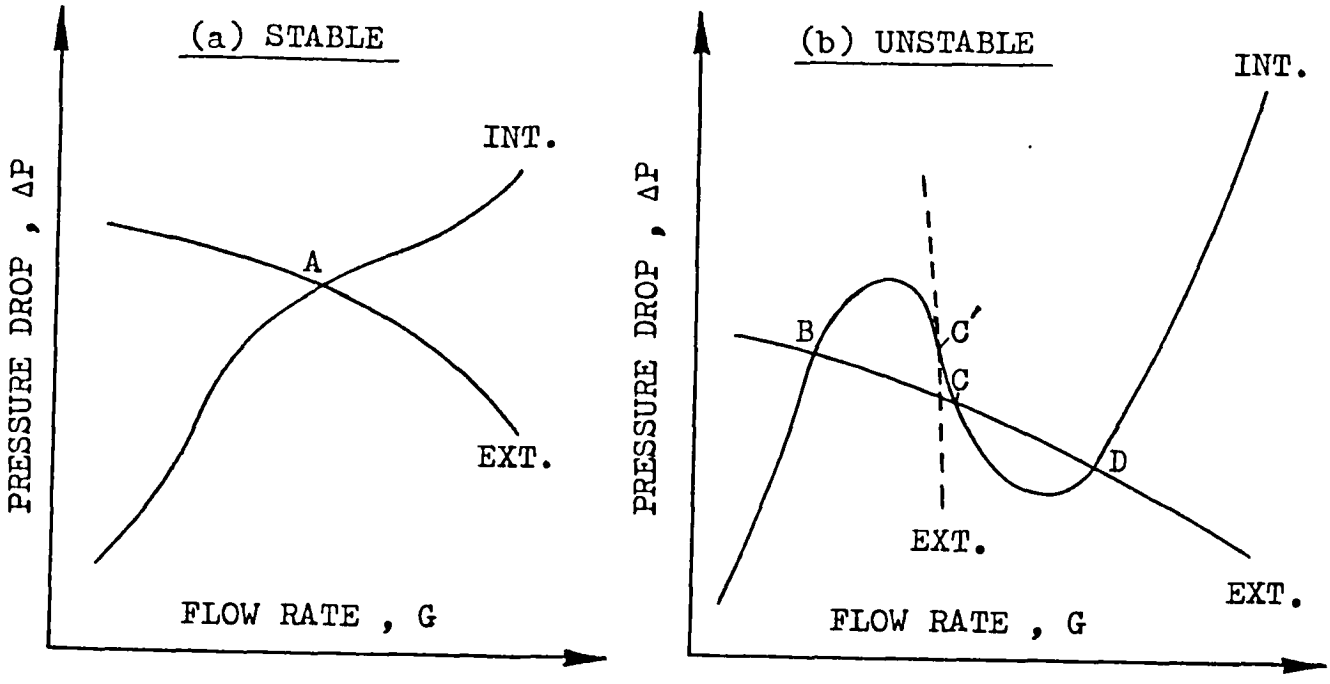

Figure 2.2: Pressure drop-mass flow rate curves for two-phase flow

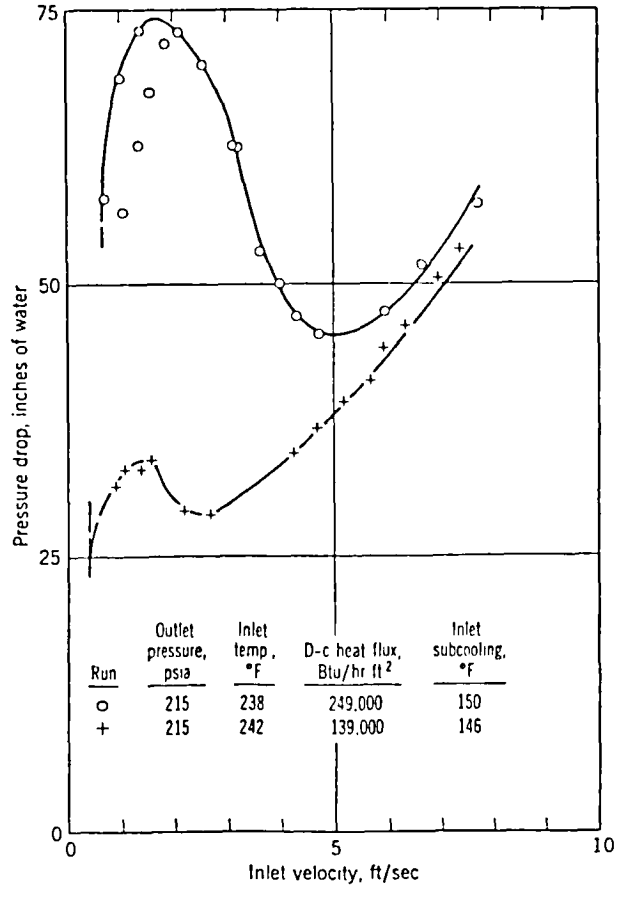

Figure 2.3: Static pressure drop through a 0.174" ID stainless steel heated single tube. From (W13). (Tong (1965))

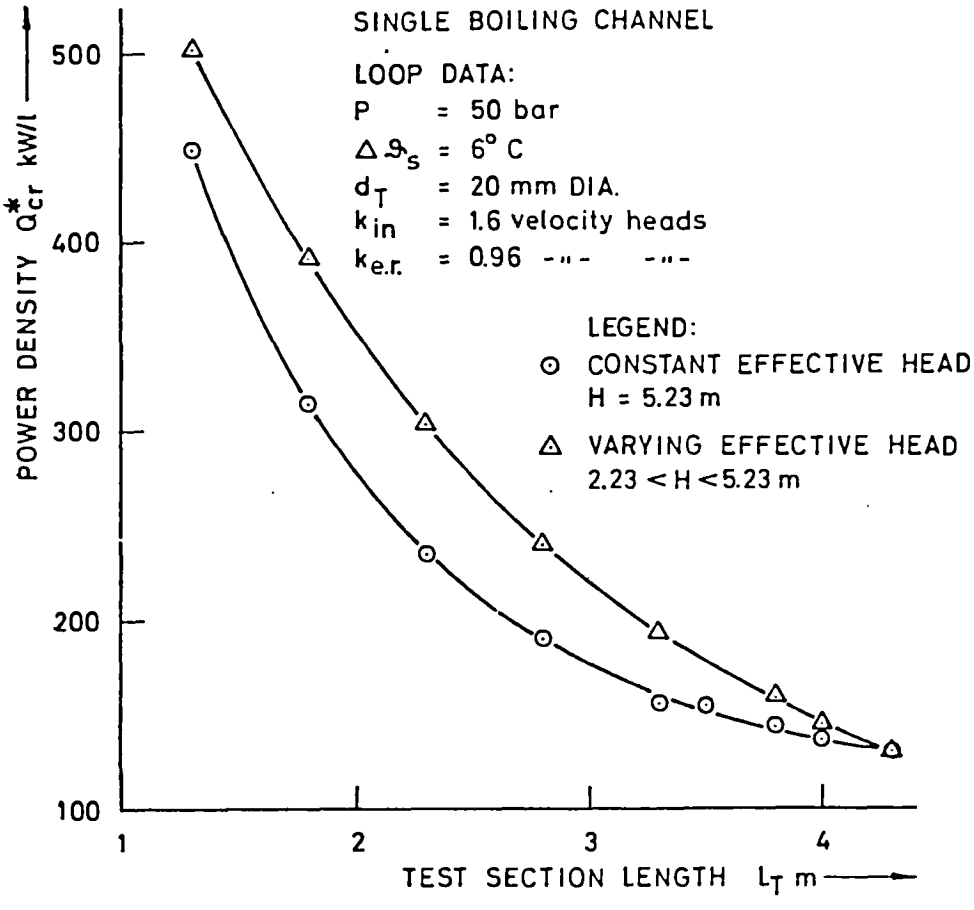

Figure 2.4: Power density at hydrodynamic instability with varying test section lengths (Mathisen (1967))

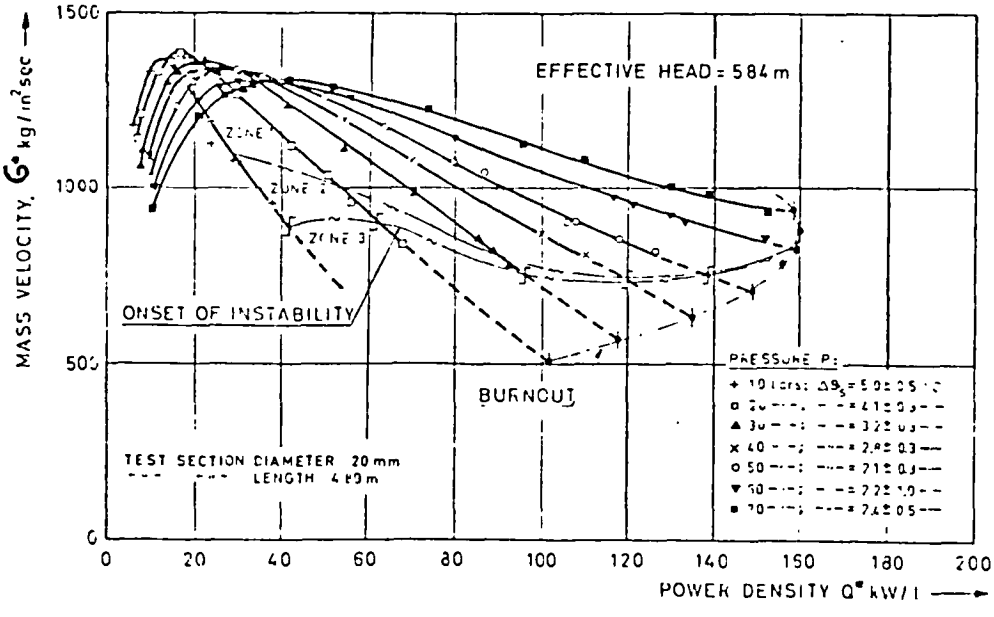

Figure 2.5: Effect of pressure on the flow in single boiling channel (Mathisen (1967))

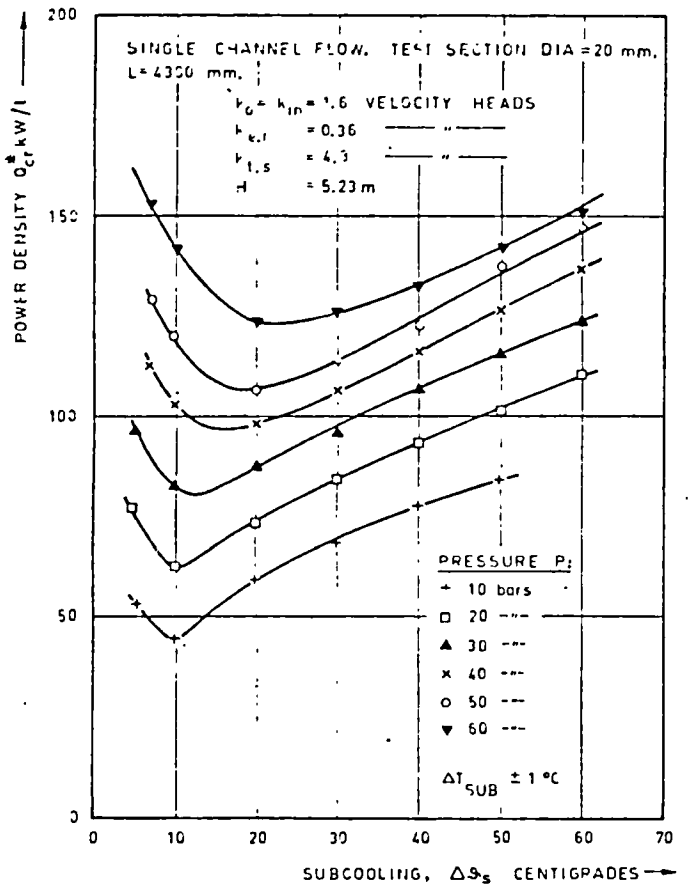

Figure 2.6: Effects of subcooling and pressure in single boiling channel flow (Mathisen (1967))

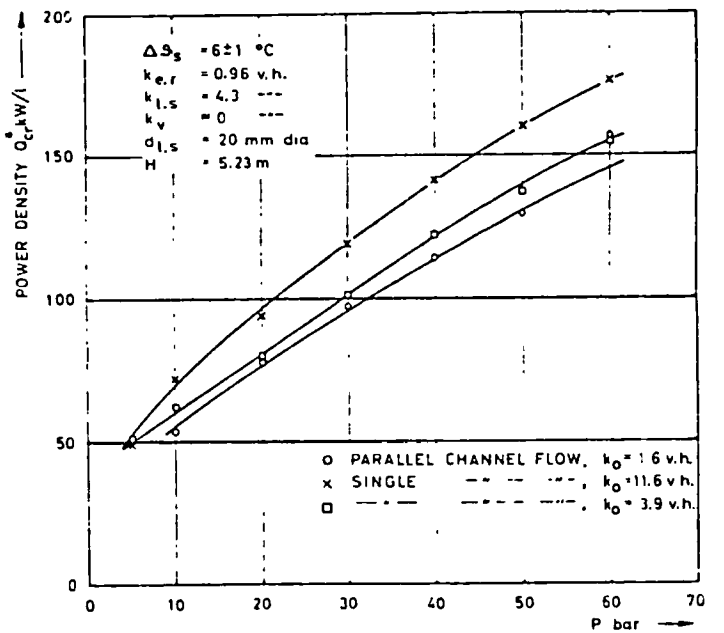

Figure 2.7: Effect of pressure on the power density at hydrodynamic instability (Mathisen (1967))

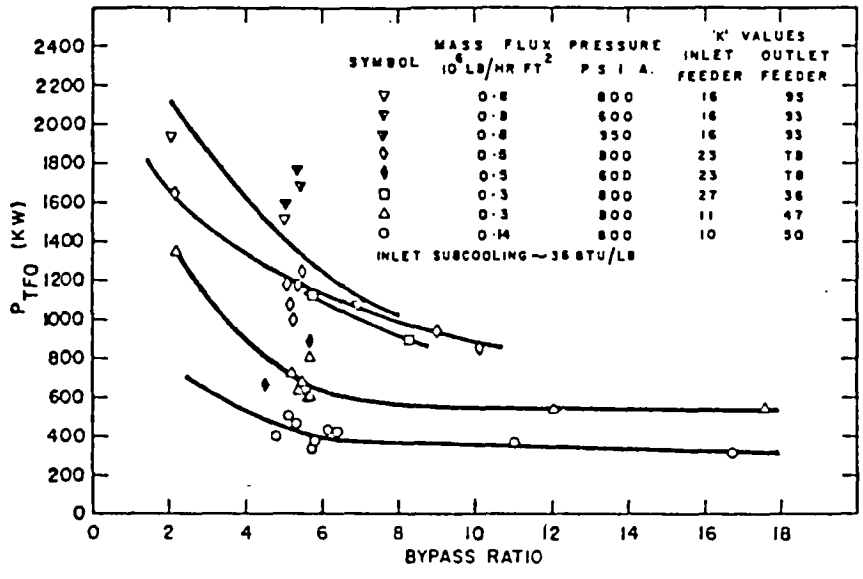

Figure 2.8: Effect of by-pass ratio on the power at the instability threshold (Collins and Gaseca (1969))

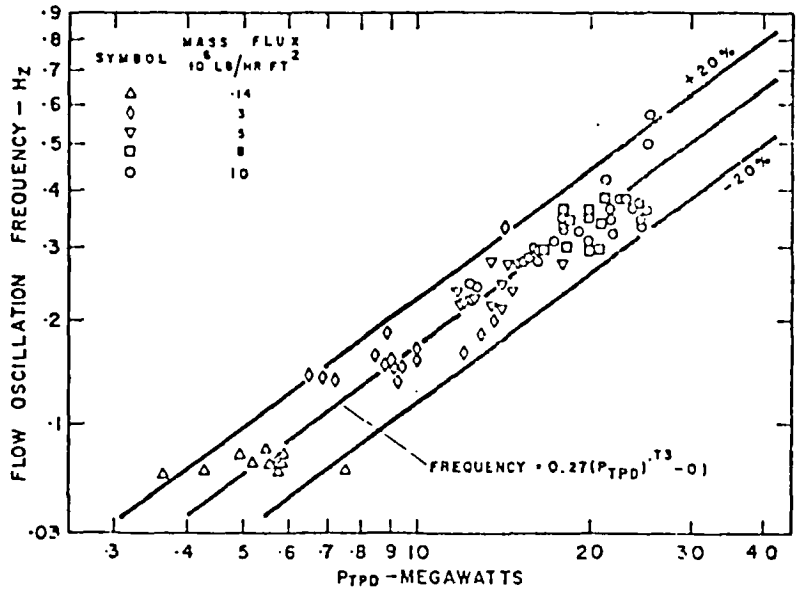

Figure 2.9: Variation of flow oscillation frequency with dryout power (Collins and Gaseca (1969))

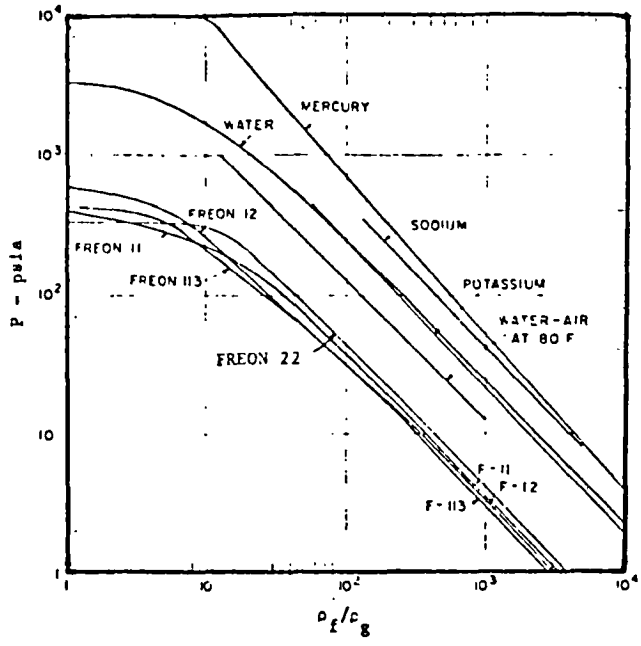

Figure 2.10: Density ratio versus pressure for various fluids (Crowley and Bergles (1970))

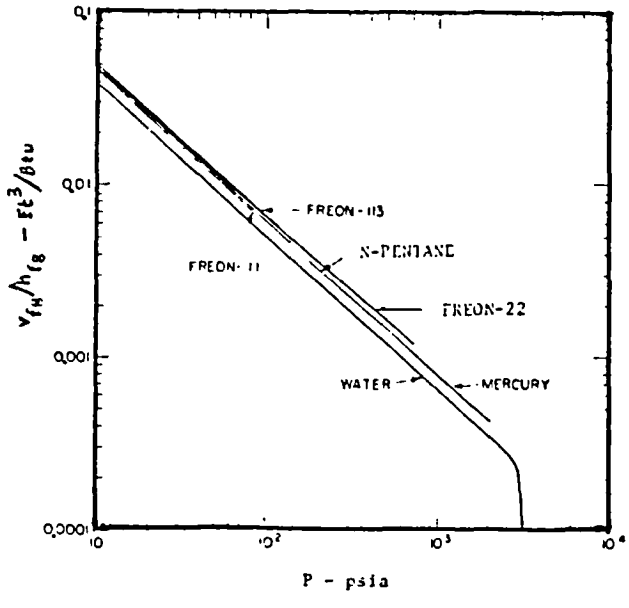

Figure 2.11: Fluid property ratio v_{fg}/h_{fg} versus pressure for various fluids (Crowley and Bergles (1970))

CHAPTER 3

REVIEW OF TWO-PHASE FLOW IN CURVED CHANNELS

3.1 RELEVANCE OF THE PROBLEM

Coil heat exchangers are used for heating and cooling fluids in a wide variety of industries. They are commonly used in chemical reactors, agitated vessels, and storage tanks to heat and cool materials ranging from inorganic and organic chemicals to dairy products, vegetables, etc. The coiled type heat exchangers have been used extensively because their heat transfer coefficients are higher than those of straight tubes and because they can be packed into a given space more economically than straight tubes.

In the case of Gas Cooled Reactors (AGR or HTGR), the cost of the steam generating units depends not only on their heat transfer surface but also on their overall size, since the pressure vessel volume is rather expensive. Therefore, the power density in the steam generator tube bundle - that is, the amount of heat transferred per unit volume of the tube bundle - is an important parameter for judging the merits of a particular design (Gilli (1967)). Apparently, a steam generating unit consisting of helically wound tubes in a multistart arrangement will take a very small volume which is very desirable especially in the case where the units are placed in holes in the prestressed concrete pressure vessel itself ("wormhole" design). Further advantages of the helical type are: no sharp bends; almost cross-flow; good heat transfer coefficients; and increased critical heat fluxes.

A typical example of the above type of steam generating units are the boilers of the Dragon Experimental Reactor, a 20 mW (th) graphite-moderated, helium cooled, high temperature reactor located at Winfrith,

Dorset, England (Franco et al (1964)). There are six heat exchanger/ circulator units placed inside the prestressed concrete pressure vessel.

The evaporator tube bundle consists of seven multistart helicoils fitting into each other concentrically. The outer diameter of the tubes is 18 mm, thickness 2 mm, and the material is carbon steel. By increasing the number of starts with helix diameter, the angles of inclination and the heated tube lengths are equal, despite the differences in diameter of the coils (Franco et al (1964); Gilli (1965)).

Because of the many advantages encountered in the helicoils, during the last few years interest has been growing in the use of helical tubes in once-through high pressure boilers for nuclear and conventional power plants, where the rate of heat transfer is being pushed closer to the limiting heat flux condition.

Therefore, the understanding and analysis of the thermo-hydrodynamic behaviour of single/two-phase flow through bends or coils is of paramount importance for optimum design and safe operation.

3.2 SINGLE-PHASE FLOW PATTERN IN CURVED CHANNELS

When a single-phase fluid flows through a stationary curved pipe, a pressure gradient across the pipe is required to balance the centrifugal force arising from the curvature. The pressure near the wall further from the centre of curvature of the pipe is greater than in the portion which is nearer to it. Considering the pipe lying on a horizontal plane, the fluid near the top and bottom of the pipe is moving more slowly than the fluid in the central portion, and henceforth requires a smaller pressure gradient to balance its centrifugal force.

In consequence, a flow is set up in which the fluid near the top and bottom moves inwards while the fluid in the middle moves outwards. This flow is known as "secondary flow" and it is of the pattern indicated in Figure 3.1. This secondary flow is superimposed on the main stream flow, giving an outward component to the fluid in the mid-plane of the bend, and consequently an inward return flow round the sides leading to the twin-helix motion (Lacey (1970)) shown in Figure 3.2.

As a result of this secondary flow, the region of maximum velocity in the main stream is shifted towards the outside part of the bend (see Figures 3.3 and 3.4).

Because of this displacement in the velocity profile, the total frictional loss near the wall of the pipe increases, and the flow experiences more resistance in passing through the curved pipe than in the case of an identical straight tube under the same operating conditions.

3.2.1 Single-Phase Flow Pressure Drop in Curved Channels

The first theoretical study of the subject was made by Dean (1927) who was able to reduce the equations of continuity and motion to

forms having exact analytical solutions by assuming small curvature r/R, small Reynolds numbers (Re << 100) and therefore a small value (<< 38) of the parameter:

$$N_{De} = Re \cdot \sqrt{\frac{r}{R}} \tag{3.1}$$

called the Dean number, which is a dimensionless group characterising the dynamic similarity of fluid flow in curved channels.

White (1929), and very recently Barua (1963) and Mori and Nakayama (1965), have improved Dean's theoretical analysis for higher values of N_{De} in the laminar region. Their theoretical results agree with experimental velocity measurements at large values of N_{De}.

Mori and Nakayama (1965) found theoretically the following equation for the first approximation of the friction factor in coiled tubes (laminar region):

$$(f_c/f_s)_I = 0.1080 \cdot N_{De}^{0.5} \tag{3.2}$$

which is in good agreement with the various pressure drop correlations such as the empirical equation of Ito (1959):

$$f_c/f_s = 21.5\, N_{De}/(1.56 + \log_{10} N_{De})^{5.73} \tag{3.3}$$

Transition from laminar to turbulent flow in coils occurs at higher values of Re than in straight tubes.

Ito (1959) has proposed the following empirical equation for the prediction of Re_{cr} in a coil:

$$Re_{cr} = 20000 \left(\frac{r}{R}\right)^{0.32} \tag{3.4}$$

which is valid for $0.00116 < r/R < 0.0667$.

For values of r/R smaller than 0.00116, the Re_{cr} is taken to be the same as that for a straight tube (2300).

Mori and Nakayama (1967) have made a theoretical analysis of flow in coils and have given expressions for the friction factor in coils in the turbulent region.

Their theoretical equation agrees well with the empirical equation of Ito (1959) which was derived assuming a one-seventh power velocity distribution law:

$$f_c \left(\frac{r}{R}\right)^{-0.5} = 0.029 + 0.304 \left[Re \left(\frac{r}{R}\right)^2\right]^{-0.25} \qquad (3.5)$$

which is valid for $0.034 < Re\ (r/R)^2 < 300$.

When $N_{De}{}^2 < 0.034$, the friction factor of the curved pipes can be taken as equal to the friction factor for turbulent flow in straight tubes.

For values of $Re\ (r/R)^2 > 6$, Ito (1959) recommends the following empirical equation:

$$f_c \left(\frac{r}{R}\right)^{-0.5} = \frac{0.316}{\left(Re \left(\frac{r}{R}\right)^2\right)^{0.2}} \qquad (3.6)$$

Using the Blasius formula $f_s = 0.316\ Re^{-0.25}$, equation (3.6) can be written as:

$$f_c/f_s = 1.00 \left[Re \left(\frac{r}{R}\right)^2\right]^{1/20} \qquad (3.7)$$

Ito also proposed (1959) some more empirical equations for the friction factor f_c assuming a logarithmic velocity distribution law.

3.2.2 Single-Phase Flow Heat Transfer in Curved Channels

Mori and Nakayama (1965,1967) have theoretically determined the temperature distributions over a cross-section of fluid in a coil for both laminar and turbulent flow. They proceeded in their analysis by assuming constant heat flux, and thermal boundary layer temperature profiles which gave realistic matches with the core temperatures. They also carried out experiments verifying their theoretical temperature and velocity profiles. The velocity and temperature profiles are shown in Figures 3.3 and 3.4 for the laminar and turbulent case, respectively. As it can be seen, the temperature profiles are asymmetric as are the velocity profiles. Sharp changes in temperature were recorded near the wall in both the horizontal and vertical directions. Over the bulk of the cross-section of the fluid, the temperature changes approximately linearly in the horizontal direction and remains almost constant in the vertical direction.

From their theoretical analysis of laminar flow heat transfer inside coils, Mori et al (1965) obtained the following equation for the first approximation of the prevailing Nusselt number Nu:

$$\left[(Nu)_c/(Nu)_s\right]_I = \frac{0.1979}{z} N_{De}^{0.5} \qquad (3.8)$$

where z is the ratio of the thermal and the velocity boundary layer thicknesses, given by:

$$z = \frac{2}{11}\left\{1 + \left[1 + \frac{77}{4\ Pr^2}\right]^{0.5}\right\} \qquad \text{for } Pr > 1$$

and

$$z = \frac{1}{5}\left\{2 + \left[\left(\frac{10}{Pr^2}\right) - 1\right]^{0.5}\right\} \qquad \text{for } Pr < 1$$

From the theoretical analysis of turbulent flow inside coils, by the same authors (1967), the following equation resulted:

$$(Nu)_c = \frac{Pr}{26.2\ (Pr^{0.66} - 0.074)}\ Re^{0.8}\ (\frac{r}{R})^{0.1} \left\{1 + \frac{0.098}{\left(Re\ (\frac{r}{R})^2\right)^{0.2}}\right\} \quad (3.9)$$

This formula agreed well with experimental results for gases.

Seban and McLaughlin (1963) have empirically correlated their heat transfer data for turbulent water flow through coils (under constant heat flux) with the following equation:

$$(Nu)_f\ Pr^{-0.4} = 0.023\ (\frac{r}{R})^{0.1}\ Re_f^{0.85} \quad (3.10)$$

According to Rogers and Mayhew (1964), the constant in the previous equation should be 0.021.

Gilli (1965) reduced analytically the heat transfer and pressure drop characteristics for the flow across banks consisting of plain helical tubes in a multistart arrangement to the well known ones for the flow across banks of straight tubes with in-line and regularly staggered tube patterns (Eckert et al (1950)). For this purpose, correction factors for the effect of tube inclination and of the number of tube rows are introduced. The effective average values of the free flow area (which determines the effective *Re*) and the effective arrangement factors are obtained by integration of the local values.

3.3 TWO-PHASE FLOW PATTERNS IN CURVED CHANNELS

The terminology and the description used for the patterns of two-phase flow in straight vertical or horizontal tubes, somewhat confused in the early years, is today well standardised (Collier (1972); Hewitt and Taylor (1970)).

For the case of curved tubes one might expect that centrifugal forces would keep the phases separate and hence suppress the development of the two-phase flow regimes as these are encountered in straight tubes. However, all these regimes have been observed in flow visualisation studies on air and water mixtures in curved tubes as reported by Owhadi et al (1968), Banerjee et al (1969) and Akagawa et al (1971). Akagawa et al reported that the measured void fractions in a helical coil were found equal to the ones in a horizontal tube in the range of this experiment.

Available information on the flow phenomena in coiled tubes is very limited for two-phase flows. However, a simple discussion of the major factors affecting two-phase flow in coils is given below in an effort to better understand this phenomenon.

A two-phase flow in a coil is subjected to two forces that tend to separate the two-phases because of the difference in their densities. These forces are the centrifugal and gravitational body forces. Besides these separating forces there is also a spiraling secondary flow which is superimposed on the primary flow as generally described in section 3.2. Different combinations of the effects of centrifugal force, gravity, and secondary flow will produce different two-phase flow phenomena in coils.

The velocity (mixture quality) and density (system pressure) of each phase and the radius of curvature must be considered for the particular situation since the balance between separating and secondary flow forces

very much depends on these quantities. Sometimes a simple force balance can give a good insight into observed two-phase flow phenomena.

In high speed flow at high mixture quality flowing in coils, a form of film flow appears to be established (Carver et al (1964); Owhadi et al (1968)), with a characteristic symmetrically striated structure which is strongly reminiscent of the two helices formed in single-phase flow inside coils. These observations led the investigators to postulate the following mechanism. A secondary flow exists in the vapour core of the two-phase flow which exerts a helically disposed shear stress (drag) on the liquid film and causes it to flow along the wall from the outer to the inner wall of the tube, replenishing the losses due to evaporation and entrainment. The liquid on the wall is subject to small radial acceleration effects because of its small axial velocity.

Banerjee et al (1967,1969), experimenting with a horizontal tube coiled about a vertical axis, and at such small velocities that gravitational forces were important, suggested that the previously postulated mechanism was an insignificant factor. They observed that at constant (fairly low) water rate and low gas rates the liquid film was located mainly on the outside of the tube wall, but as the gas velocity was increased the liquid film moved from this position, first into the neutral position and then into the inside of the tube wall ("inverted" position). They explained this phenomenon on the basis that the momentum of the gas phase is higher than that of the liquid phase due to the considerably higher gas velocity outweighing the much lower density.

Banerjee et al (1967,1969) showed that this behaviour could be quantitatively accounted for by a simple force balance, neglecting the secondary flow effect. The difference in the centrifugal force per unit volume in the gas and liquid can be added vectorially to the net

gravitational force on the liquid to give a wall reaction which must pass through the centre-line of the tube, i.e.

$$\frac{1}{R}\left(\rho_g u_g^2 - \rho_f u_f^2\right) = \left(\rho_f - \rho_g\right) g \tan\varphi \qquad (3.11)$$

This relationship involving a Froude number u^2/Rg correlated well the lower and medium velocity data. At higher velocities, this correlation failed because then the liquid was entrained from the film and thrown onto the outer part of the wall and whence flowed back to the inside along helical paths according to the mechanism described by Lacey (1970) and Owhadi et al (1968) (significance of secondary flow).

Recent visualisation studies using high-speed ciné photography looking down the axis of a horizontal tube coiled about a vertical axis have been employed by Hewitt as mentioned by Collier (1972). In the annular flow pattern, liquid was seen to transfer to the inside of the tube as the gas velocity was raised, as found by Banerjee et al (1967) (film inversion), but the film was always highly distorted and ready to disintegrate. At high gas velocities, the strong secondary flow in the gas core induced a corresponding circulation in the liquid film in a mechanism as described by Lacey (1970). Liquid was entrained from a violently disturbed film near the inside tube wall and was carried away by the gas flow (in a spray or rivulet form) across the tube diameter to be deposited on the further wall some distance downstream. The liquid was then returned to the inside surface of the coil still further downstream via the imposed circulation on the film.

This intense peripheral circulation of the liquid film and the efficient separation of the entrained droplets ensures that the likelihood of dry patches is considerably reduced in coils.

Gardner et al (1969) measured the local void fraction using an electrical probe across a diameter at various positions around a 90^{o} bend mounted at the top of a long riser tube. In this case, the competing mechanisms were the momentum of the up-flowing liquid attempting to carry it to the outside of the bend and the gravitational forces tending to make it fall to the inside of the bend. This force balance was expressed again by a Froude number:

$$(Fr)_{\theta} = \frac{j^2}{g\ R\ sin\ \theta} \tag{3.12}$$

where j = total volumetric flux

R = radius of curvature

θ = angle to the horizontal

This simple approach is probably valid only for bubbly and slug flow and at low flow velocities so that there is sufficient time for the gravity to have a significant effect. Since, in this case, the gas velocity involved is small, the previously mentioned phenomena did not occur.

Lacey (1970) examined by a simple mathematical procedure the stability of an inverted film, considering a small sinusoidal perturbation in the flat gas-liquid interface under conditions of negligible gravitational forces.

3.3.1 Two-Phase Flow Pressure Drop in Curved Channels

Pressure drop and void fraction measurements for two-phase flow in helical coils have been reported by Rippel et al (1966), Banerjee et al (1969) by Boyce et al (as mentioned by Collier (1972)), Owhadi et al (1968), Akagawa et al (1971), and Anglesea et al (1974).

Generally speaking, it has been found that for estimating the frictional pressure drop component, the two-phase multiplier to be used should be that for straight tube flow. The influence of coiling on two-phase frictional pressure drops is therefore correctly allowed for by evaluating the single-phase pressure gradients taking into account the increased friction factors resulting from coiling.

As reported by Boyce et al and Akagawa et al (1971), the values of void fraction measured during two-phase flow in coils appeared to remain unchanged from those in a straight pipe. Therefore, it was recommended that the frictional and accelerational components of the pressure drop be evaluated using straight pipe values for the void fraction.

Rippel et al (1966) experimented with a two-phase flow section consisting of a ½" diameter 18 gauge tubing coil wound on a vertical cylinder 8" in centre diameter. The total length was 88.3". The flow was downwards and the two-phase flow combinations used were: air-water, helium-water, Freon-12-water, and air-2-propanol. The flow patterns observed were classified as one of the following types: bubble, slug, stratified, wavy, semi-annular, and annular. These investigators correlated the two-phase frictional pressure drop using the Lockhart-Martinelli analysis. The analysis is made in terms of the dimensionless parameters X, ϕ_g and R_l which have the following definitions:

$$X = \sqrt{\frac{(dP/dL)_l}{(dP/dL)_g}} \triangleq \text{Martinelli parameter}$$

where $(dP/dL)_l$, $(dP/dL)_g$ are the pressure gradients for liquid and gas flowing alone, respectively, and:

$$\phi_l = \sqrt{\frac{(dP/dL)_{TP}}{(dP/dL)_l}} \quad , \quad \phi_g = \sqrt{\frac{(dP/dL)_{TP}}{(dP/dL)_g}}$$

where $(dP/dL)_{TP}$ is the two-phase frictional pressure drop gradient, and R_l is the fraction volume of liquid per unit volume of pipe (hold-up). The value of X depends on whether the single-phase flows would have been laminar or turbulent.

For turbulent-turbulent flow, we have:

$$X_{tt} = \left(\frac{1-x}{x}\right)^{0.9} \left(\frac{\rho_g}{\rho_l}\right)^{0.5} \left(\frac{\mu_l}{\mu_g}\right)^{0.1} \tag{3.13}$$

Figure 3.5 shows the pressure drop for all of the fluid systems studied. The agreement with the Lockhart-Martinelli analysis is fairly good. In Figure 3.6, the limitation of the Lockhart-Martinelli method (for neglecting the mass flow effect) is illustrated, where liquid rates are identified as parameters resulting in separate lines crossing the overall correlation. Liquid hold-up data are presented in Figure 3.7 compared with data for horizontal flow. The large discrepancy at the low liquid to gas rate (small X) is due to errors in the experimental method. The hold-up data for the different two-phase flow systems used is shown in Figure 3.8.

Owhadi et al (1968) studied forced convection water boiling at atmospheric pressure inside coils. They correlated their experimental two-phase flow frictional pressure drop using the Martinelli-Nelson analysis. As shown in Figure 3.9, the agreement is fairly good.

Anglesea et al (1974) conducted measurements of water-steam pressure drop in helical coils at 179 bars. The test coils were made from precision-bore tubes, nominally 12.7 mm internal diameter, 3.18 mm

wall thickness. Heat generation in the test coil was by resistance heating with direct current electricity passing along the tube wall. Tests were performed with three coils having diameters of 0.58 m, 1.32 m, and 2.36 m. The test sections were wound in a helix angle of $5^{o}57'$ and were the same in all respects except for the coil diameter. The two-phase flow test conditions were selected in a way to find the effect of coil diameter on two-phase pressure drop over the following range of conditions at which a coiled-tube AGR boiler would normally operate:

(a) Static pressure = 179 bars.

(b) Flow rate (per tube) = 0.21 to 0.06 kg/s.

(c) Heat flux $\hat{=}$ the heat flux was varied from a maximum of 380 kW/m^2 for a (maximum) flowrate of 0.21 kg/s, the variation with flowrate being about linear.

(d) Thermodynamic qualities = between -0.1 and 1.5.

The experimental results were reduced to give the graphical correlation between the local friction multiplier, quality, mass velocity and coil diameter. A typical graph is shown in Figure 3.10. The "best fit" lines have been drawn in by eye.

The results were compared with various correlations (Baroczy, Chisholm, Martinelli-Nelson, Owens (Collier (1972))). The results of the Baroczy and Owens (homogeneous model) are included in Figure 3.10. It was found that the results of the Baroczy correlation were generally nearest to the experimental data although the predictions based on a simple homogeneous flow model (Owens) were reasonably close.

3.3.2 Two-Phase Flow Heat Transfer in Curved Channels

The two-phase flow heat transfer mechanisms for convective boiling of one component flows are well classified by Collier (1972). Figure 3.11 shows the various flow patterns and corresponding heat transfer regions encountered over the length of a straight tube, where the fluid enters in subcooled conditions and exits as superheated vapour.

One of the first investigations of two-phase flow heat transfer in curved channels was the experimental study of Hendricks et al (as reported by Crain and Bell (1973)). These authors found heat transfer coefficients experimentally for forced convection heat transfer to subcritical (two-phase), supercritical and gaseous hydrogen flowing through tube bends having an angle ranged from 26^{o} to 75^{o} and a radius of curvature ranged from 2 to 7.5". The authors found that for near critical hydrogen, the heat transfer coefficients on the concave surface (outside of curve as seen by fluid) could be as much as three times greater than those on the convex side.

Carver et al (1964) investigated the effect of curvature of a tube on the departure from nucleate boiling. Experiments were performed on two electrically heated helical coil tubes where boiling water at 2600 psia was flowing. The coils were 16 and 65" in radius and had a nominal inside diameter of 0.42" and an angle of inclination with the horizontal of $6^{o}15'$. These authors reached the following results and conclusions:

i) DNB in coiled tubes occurs at different steam qualities for different positions around the circumference of the tube, whereas, for a straight vertical tube, DNB occurs around the complete circumference of the tube at one

steam quality.

ii) Coiled tubes have higher average DNB steam qualities (or more percentage surface under nucleate boiling) than do straight vertical tubes. Also, the small radius (16") coil maintains nucleate boiling to higher steam qualities than does the large radius (65") coil under comparable conditions. Figure 3.12 shows clearly these effects.

iii) Surface temperature fluctuations at the DNB transition point are much lower than those in a straight vertical tube. Surface temperatures under film boiling also are very low compared to those of a straight vertical tube under similar operating conditions. Figure 3.13 shows clearly these effects.

iv) An increase in mass velocity, in general, resulted in an increase in average DNB steam quality.

Owhadi et al (1968) investigated forced convection boiling inside helically coiled tubes. They measured two-phase heat transfer coefficients for water flowing at near atmospheric pressures in two helical coils 9.86 and 20.5" in diameter. The tubing inside diameter was 0.492" and the length 10 feet. The heat was generated by direct current resistance heating in the tubing wall. The water feed rate and heat flux could be varied so that the exit quality could be adjusted between 1.4% vapour to 50^{o}F superheated steam. These authors reached the following results and conclusions:

i) At vapour qualities below 80%, the heat transfer

coefficient was high all round the circumference, although it was usually highest on the side furthest from the helix angle.

ii) The top and bottom portions of the tube surface became dry at about 95% vapour quality, while the points nearest and farthest from the helix axis became dry at over 99% quality. Figures 3.14 and 3.15 show these effects.

Apparently, there was a complete wetting of the tube wall at the higher qualities attributed to the secondary flow in the vapour core. At higher qualities, when the continuous liquid film finally breaks, the remaining liquid is concentrated at the stagnation points of the secondary flow (the 90^{o} and 270^{o} positions) and the heat transfer coefficient at the other points (top-bottom) decreases to the pure vapour coefficient.

The circumferential average heat transfer coefficients were correlated successfully using the Lockhart-Martinelli parameter over the entire range except at low vapour flowrates where a nucleate boiling contribution was apparent as can be seen from Figure 3.16.

Bell and Owhadi (1969) in a later publication recorrelated their experimental results on a local basis rather than on a circumferential average basis.

Crain and Bell (1973), experimenting on the same facility, examined in more detail the heat transfer behaviour in the very high quality region (above 70%).

De La Harpe (1968) performed an experimental study of boiling heat transfer and pressure drop of liquid helium-I under forced

circulation in a helically coiled tube at atmospheric pressure, having a helix diameter of 4.33" and formed from a piece of 0.118" ID, 0.138" OD monel tubing 16 feet long. These authors successfully correlated the heat transfer data with the Lockhart-Martinelli correlating parameter X_{tt} although their pressure drop data were best described by the homogeneous model.

Miropolskiy et al (1966) reported wall temperature distributions and heat fluxes at DNB for single-phase water and steam, and two-phase water-steam mixtures in 90^{o} and 360^{o} pipe bends. The pressure range was 305 to 4300 psia and the flowrate was varied from 7.37×10^{4} to 1.47×10^{6} lb/hr.ft^2. The authors found that, while the heat flux at DNB in bends is less than in straight tubes at low qualities, the reverse phenomenon is true at high qualities. In all cases, the boiling crisis developed near the inside part of the bend.

Miropolskiy and Pikus (1969) reported critical heat fluxes and heat transfer coefficients for film boiling (liquid deficient region) of water in electrically heated pipe bends. The range of pressures investigated was 1420 to 3120 psia and the flow was varied from 7.37×10^{4} to 1.47×10^{6} lb/hr.ft^2. It was found that the heat transfer coefficients for the pipe bends were higher than the ones for straight tubes under similar conditions, apparently due to the effect of secondary flow in transferring liquid droplets to the tube wall.

3.4 CONCLUSIONS

From the previous sections, it can be concluded that results of two-phase frictional pressure drop in curved channels of two component systems are in reasonable agreement with the Lockhart-Martinelli-Nelson technique, where this technique is modified to take into account the curvature of the channel (by modifying the single-phase friction factor). Also, void fraction results for curved channels appear to be in fair agreement with straight tube results.

The extension of these aspects to one component systems, however, is open to question because of the differences of the two systems and the inadequacy of experimental data concerning two-phase one component pressure drop in curved channels.

Concerning two-phase heat transfer correlations in curved channels, it can be concluded that the correlations are empirically deduced from experimental results. Therefore, their application to situations (conditions) outside those of their derivation should be treated with care.

Generally speaking, the pressure drop and heat transfer correlations mentioned could be adequate in most cases for design purposes. However, a more intimate knowledge of the fine structure and properties of flows in curved channels is needed before a real advance can be achieved (Lacey (1970)). Further experimental evidence on the velocity structure in single-phase flow (importance of secondary flow) and in two-phase flow (on a local basis) is needed to permit predictive theories to emerge.

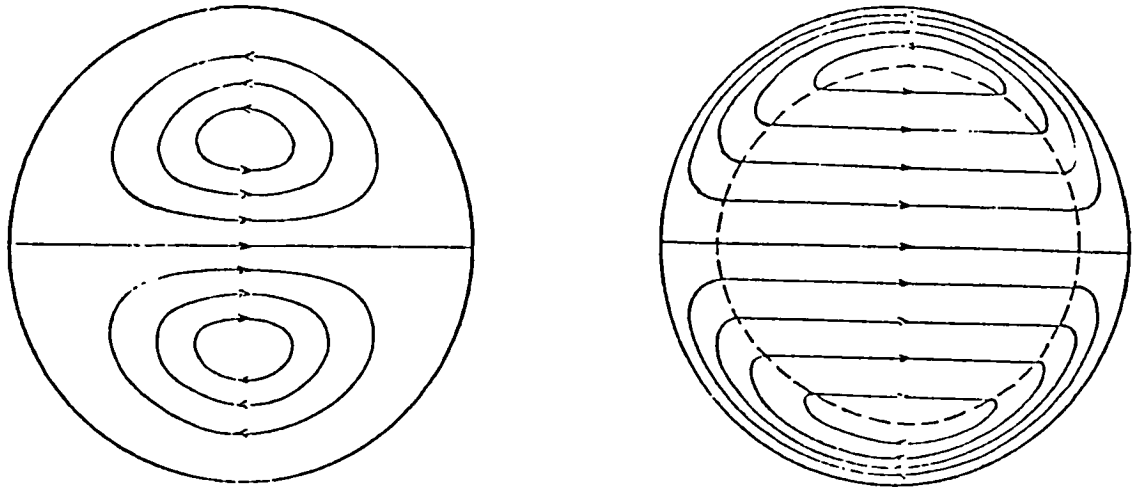

Small Dean number

Large Dean number

Figure 3.1: Flow patterns of secondary flow in curved channels (Mori and Nakayama (1965))

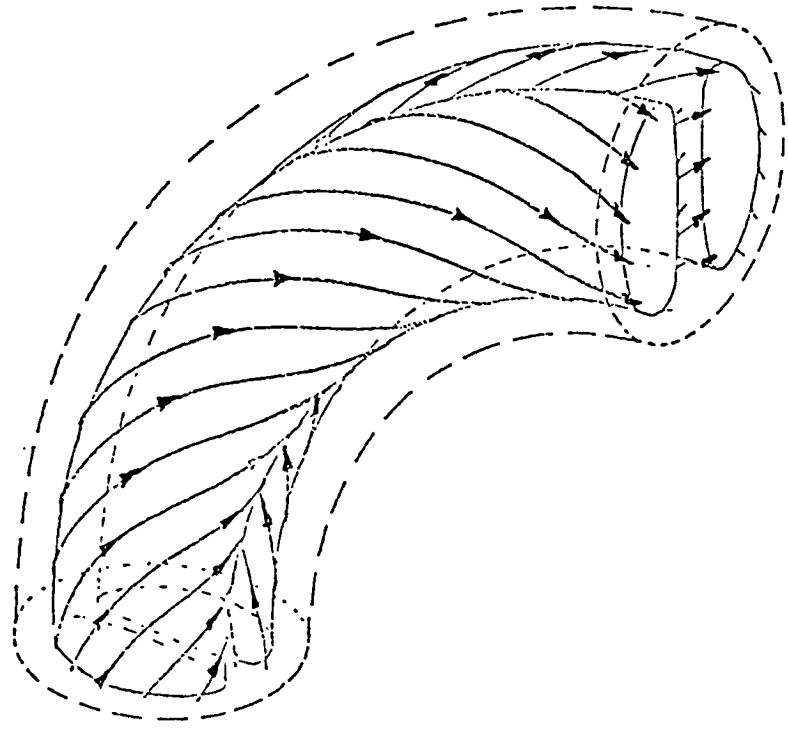

Figure 3.2: Twin-helix flow paths of fluid particles in a curved pipe (Lacey (1970))

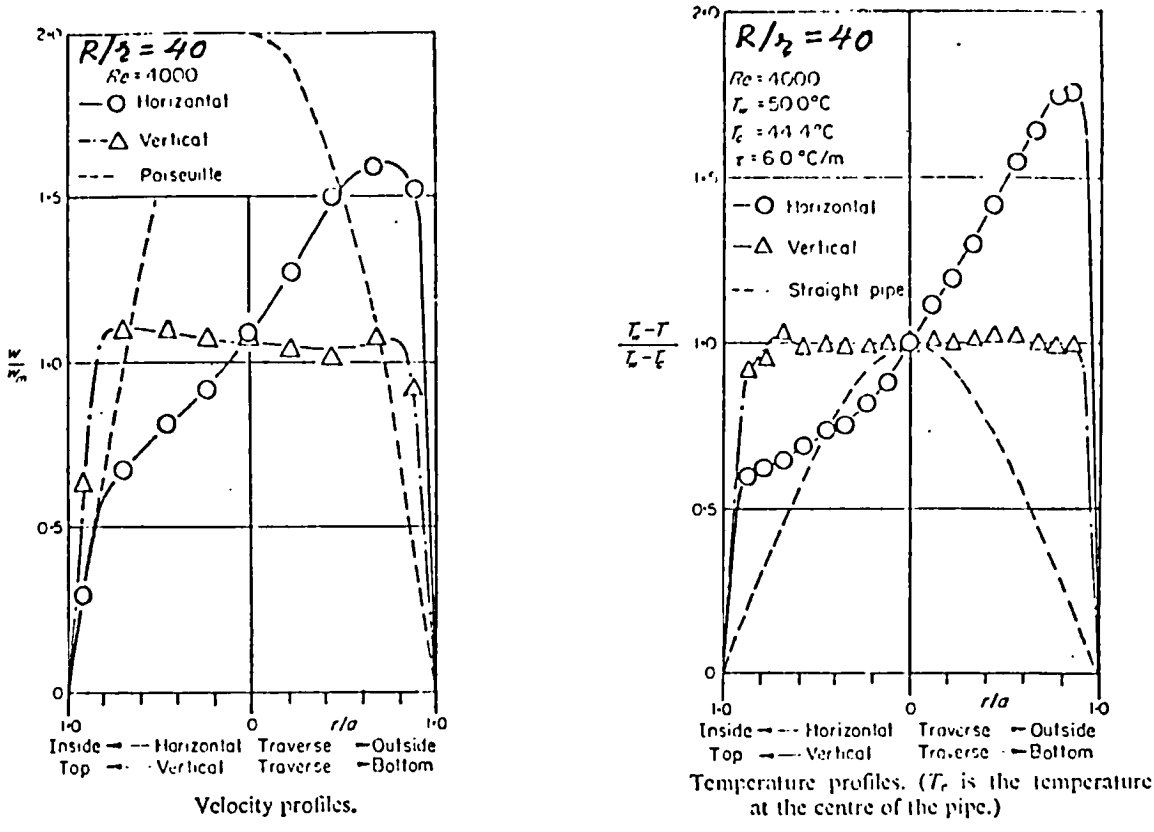

Velocity profiles.

Temperature profiles. (T_c is the temperature at the centre of the pipe.)

The velocity and temperature distributions (R/a = 40, Re = 2·5 × 10^4).

Figure 3.3: Fully-developed laminar air flow in a curved pipe (Mori and Nakayama (1965))

Figure 3.4: Fully-developed turbulent air flow in a curved pipe (Mori and Nakayama (1967))

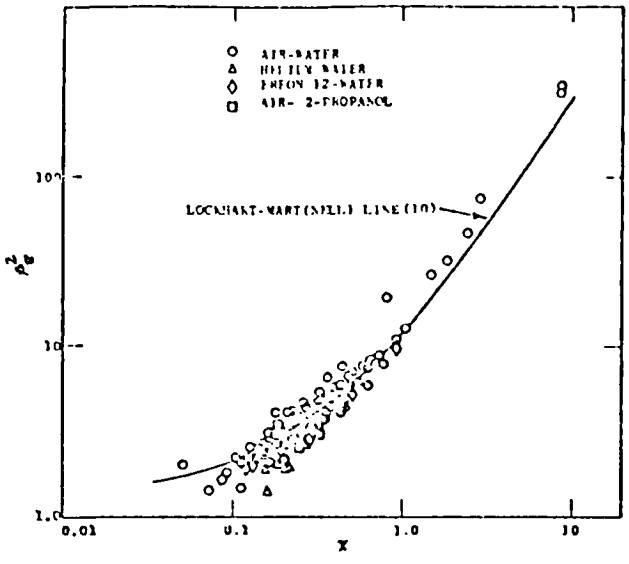

Figure 3.5: Pressure drop in two-phase flow (Rippel et al (1966))

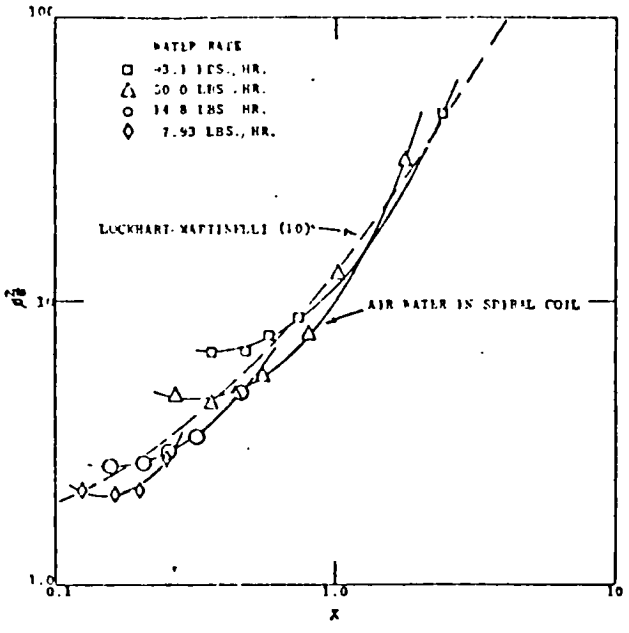

Figure 3.6: Liquid rate parameters in X versus ϕ_g^2 type pressure drop correlation (Rippel et al (1966))

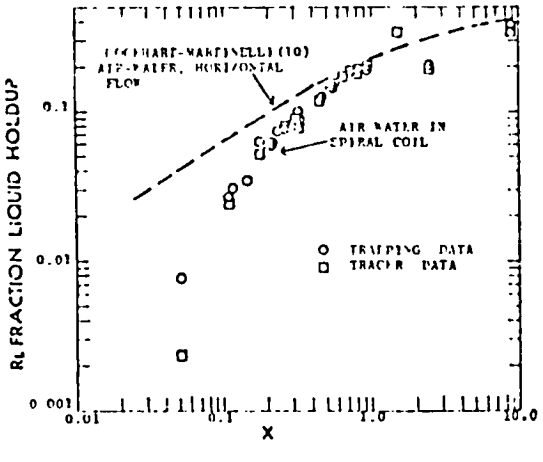

Figure 3.7: Hold-up in spiral coil compared with data from horizontal flow (Rippel et al (1966))

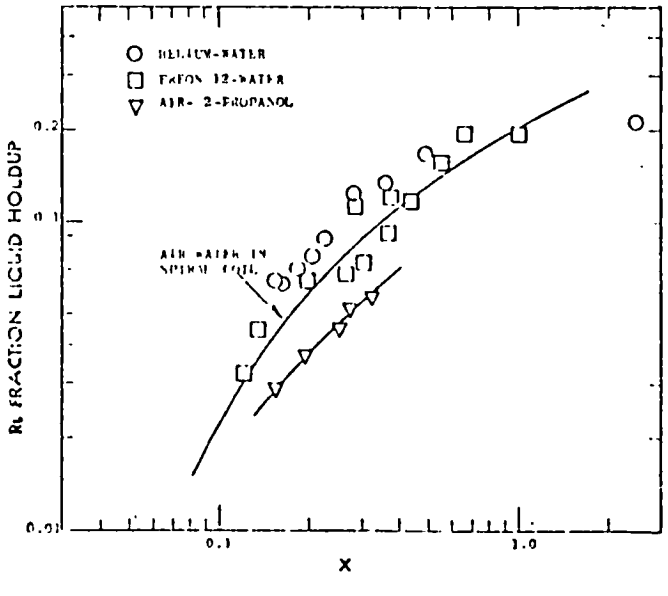

Figure 3.8: Hold-up data for various fluid systems (Rippel et al (1966))

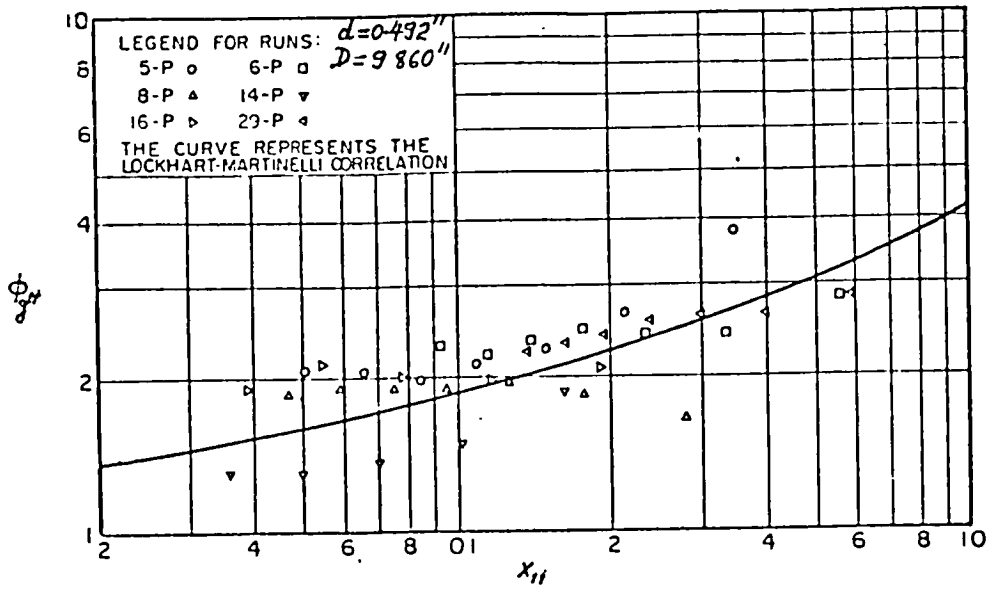

Figure 3.9: Pressure drop correlation for coil (Owhadi et al (1968))

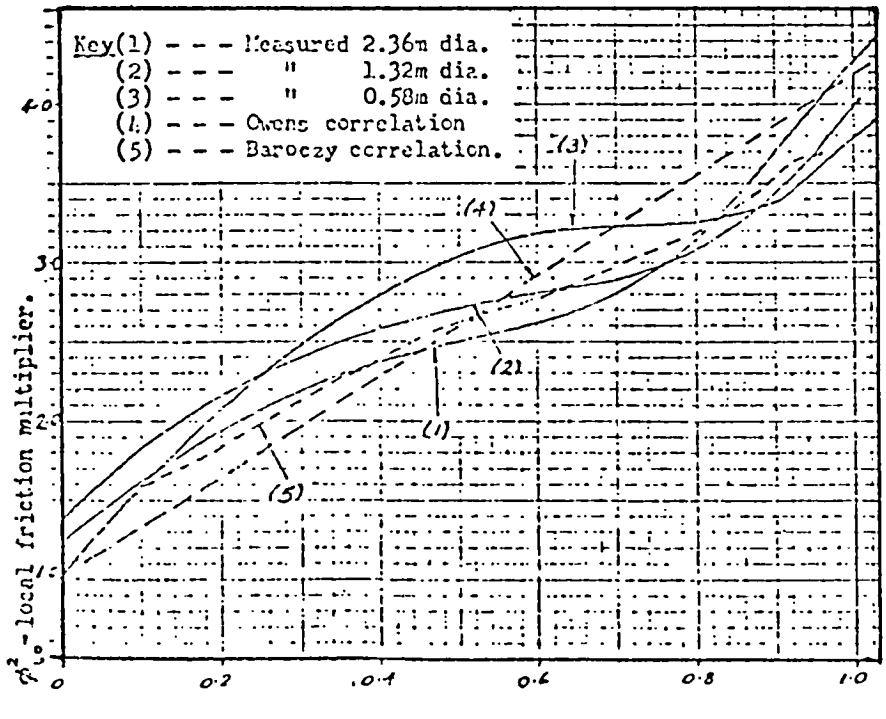

Figure 3.10: Effect of coil diameter on the local friction multiplier and comparison with predictions (P = 179 bars, $\dot{m}$ = 1700 - 1800 kg/m^{2}s) (Anglesea et al (1974))

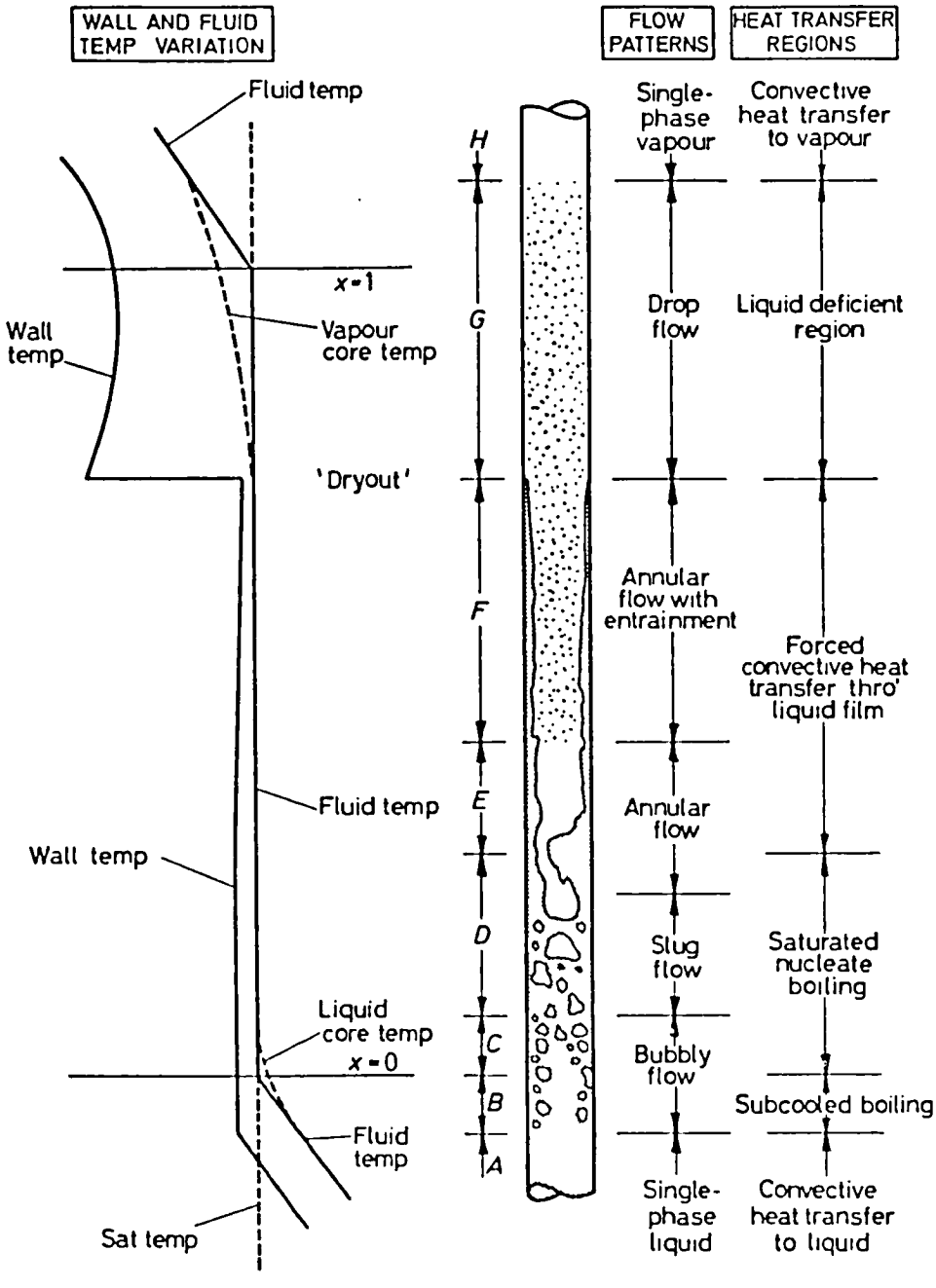

Figure 3.11: Regions of heat transfer in convective boiling (Collier (1972))

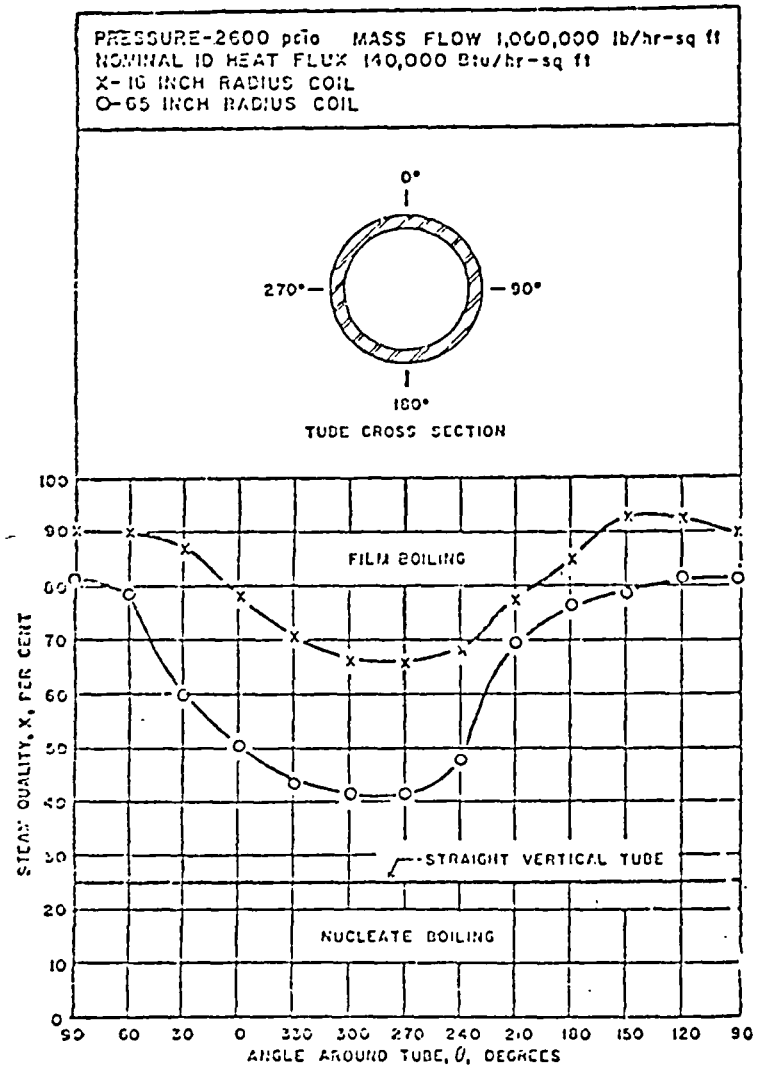

Figure 3.12: Departure of nucleate boiling (DNB)

(Carver et al (1964))

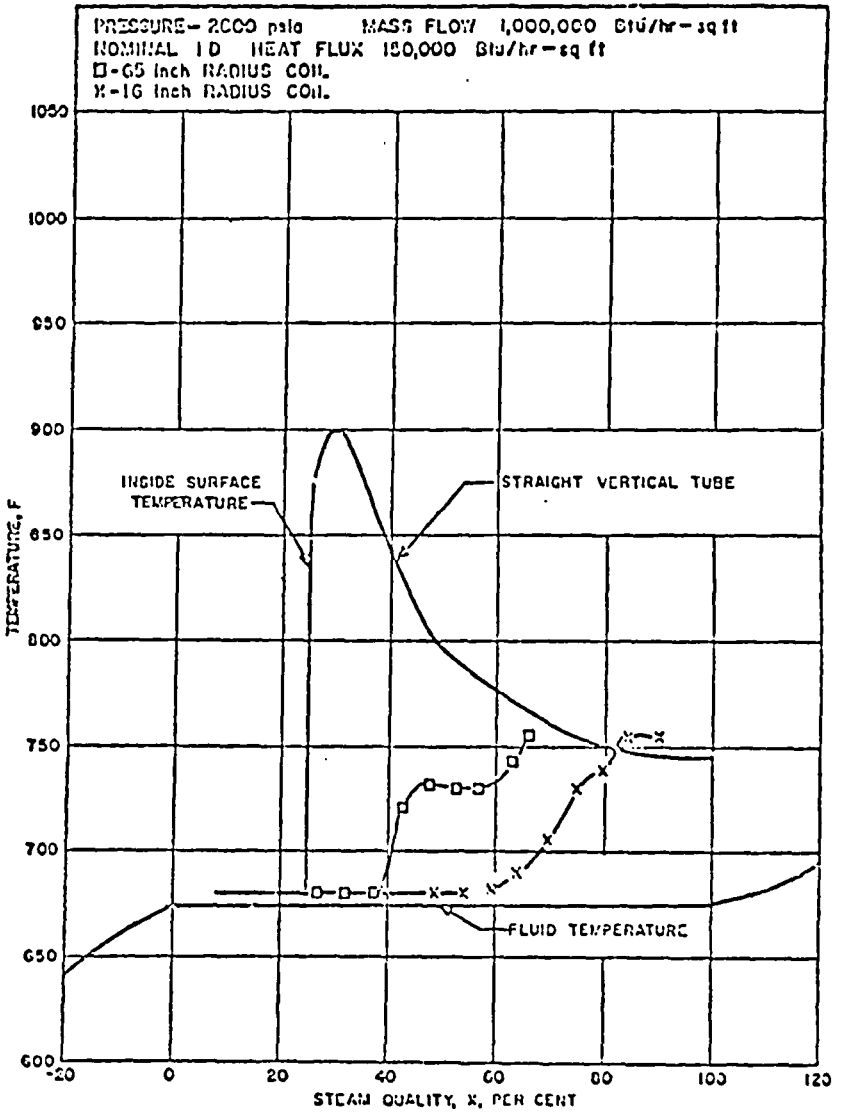

Figure 3.13: Comparison of inside temperature profiles

(Carver et al (1964))

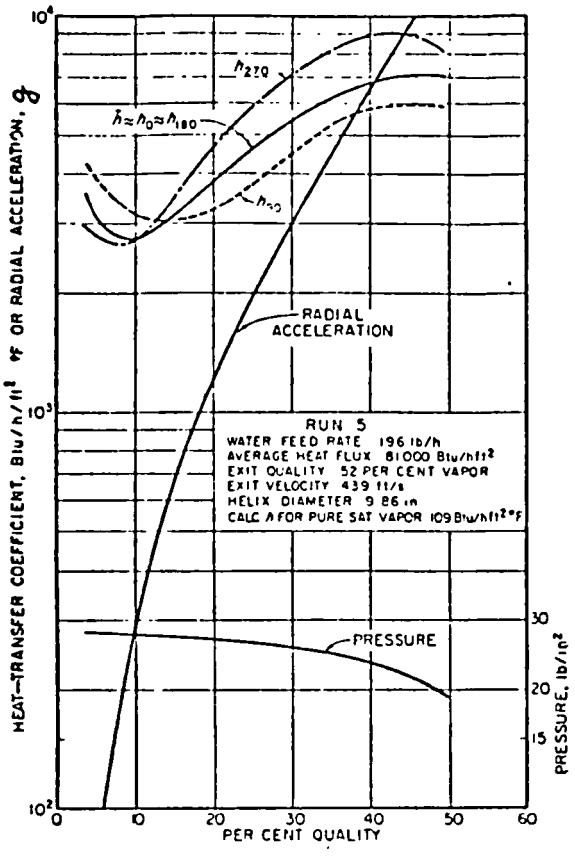

Figure 3.14: Typical experimental results with two-phase exit conditions (Owhadi et al (1968))

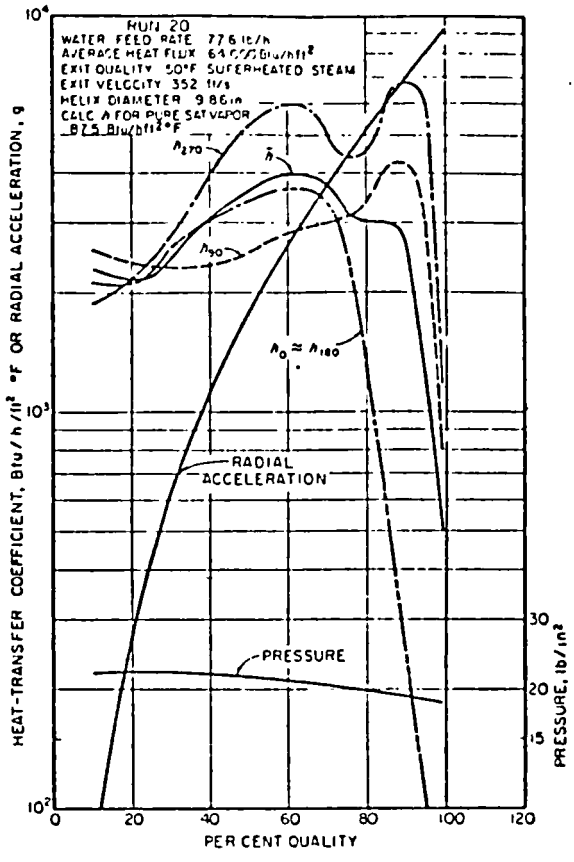

Figure 3.15: Typical experimental results with superheated vapour at exit (Owhadi et al (1968))

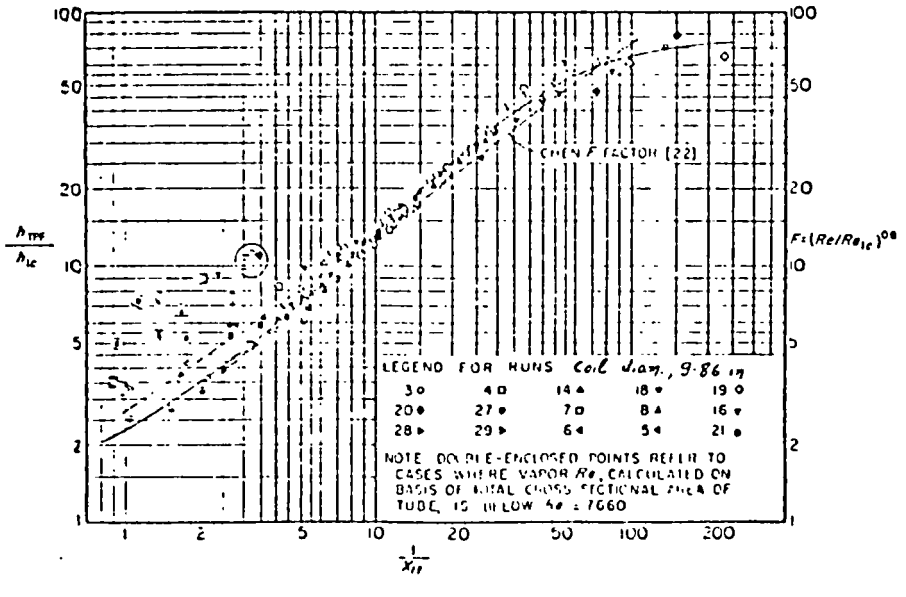

Figure 3.16: Correlation of data of heat transfer in two-phase flow (Owhadi et al (1968))

CHAPTER 4

THE THEORETICAL MODEL

4.1 INTRODUCTION

The subject of the present work is the investigation of the density wave oscillations in once-through helical or straight tubes in a parallel channel arrangement. Macroscopic channel instabilities, like the density wave oscillations, involve the entire two-phase flow system, in contrast to local or microscopic instabilities, and are characteristically associated with time constants of the order of the residence time of the fluid particles in the channel. The distinction between instabilities of flow distribution among several parallel channels or flow instabilities in a single channel stems basically from the formulation of the boundary conditions. Therefore, the problem can be reduced to a single channel instability as long as the conditions at the boundaries are sufficiently specified. Parallel channel instability is the term used to describe unstable flow in a group of channels between the same headers, the pressure difference between the headers being the same for all the channels of the group. Parallel channel instability is important both in "recirculating" and "once-through" designs of boilers, although it is recognised that in a "recirculating" design there is no dry-out region and thus the stability is normally more readily achieved because of the absence of a high quality and superheat region of high pressure drop (Potter (1973)).

The development of a computer model to predict the stability performance of an once-through boiler and its validation by carefully conducted series of experiments presents many major difficulties (Moxon (1973); Potter (1973)), due to the many complex features associated with

two-phase flow in a fully evaporating channel, the situation being aggravated by the presence of the "time" variable in addition to the "distance" variable (distributed parameter model varying in time).

It is possible for someone to use over-elaborate long-running computer codes trying to include all the features associated with the problem. However, such codes are quite expensive and there is no guarantee that some details have still not been omitted, which play an important rôle in the instability (Moxon (1973)).

It is then desirable to use fast-running, relatively simple codes provided that the key features are recognised and represented in the model.

The model used for the present work follows basically the procedure of the work of Davies and Potter (1967) which we have extended by including some additional features associated with our problem.

The additional features are:

Slip between the liquid and vapour phases.

Variable friction factors.

Variable heat flux by taking into account the dynamics of the heater wall in the single-phase region.

Extension to include non-uniform (spatial) heat flux.

Considerable algebra has been carried out on the integration of the momentum equation (Appendix A) in order to bring the various pressure drop components in a transfer function form (of a control feedback system) which is easily amenable to standard linear-control theory stability criteria.

The model incorporates correlations to cope with both helical and straight geometry tubes.

4.2 DESCRIPTION - ASSUMPTIONS

As mentioned in Chapter 2, a model of the dynamics of a boiling system is a statement and solution of the conservation equations for the single and two-phase fluids together with the constitutive laws and boundary conditions.

In our once-through channel, we distinguish five regions which will be treated separately.

The fluid from inlet to exit encounters the following five regions:

Upstream adiabatic length;
Subcooled region (heated);
Two-phase region;
Superheat region; and
Downstream adiabatic length.

The boundary conditions for the channel are:

(a) A constant pressure drop with respect to time is imposed on the channel (parallel channel design). This can be achieved in an experimental study by running a large unheated by-pass in parallel with the channel (Carver (1969); Potter (1973)).

(b) The inlet conditions of pressure and temperature of the fluid are specified and kept constant ($\overline{h}_{in} = 0$).

The following simplifying assumptions are made:

i) The flow is considered to be one-dimensional by taking mean

values across each section. A three-dimensional treatment of the problem is at the present time impossible, not only because of the complexity of the mathematics involved but also because of the lack of information concerning the variation of the dependent variables in the three dimensions.

ii) The lack of information about two-phase flow correlations under transient conditions necessitates the use of static correlations for the dynamic case.

iii) Turbulence and boiling noise are neglected, so that void fraction (or quality) and phase velocities are smooth functions of time and space.

iv) The linearised forms of the equations are assumed adequate to predict the frequency and threshold of instability. It is recognised that the system possesses the property of linearity only over a certain range of operation. Our model will not be able to study the behaviour of the channel inside the unstable region where the non-linearity effects are strong (Blumenkrantz (1972)). For example, the non-linearities will tend to cause "limit cycle oscillations" of the system, well within the unstable region.

v) The densities and saturation enthalpies of both phases are assumed to remain constant with time. These properties are also assumed constant all along the channel, assuming a small pressure gradient or a small pressure drop with respect to the mean pressure level.

vi) The densities in the single-phase regions are assumed constant.

vii) Kinetic and potential energy terms are assumed very small with respect to thermal energy terms, so that they can be ignored in the energy conservation equation (Eckert-Drake (1950)). Also, $\partial/\partial t\ (\rho E)$ is set equal to $\partial/\partial t\ (\rho h)$, i.e. we neglect $\partial/\partial t\ (P)$ compared with $\partial/\partial t\ (\rho h)$, which is a good approximation for small rates of change.

viii) The heat flux is assumed uniform along the channel and not varying with time. Especially for experimental heat transfer rigs, where a power source supplies the heat, this assumption is good. In the case where a big mass of wall material is present (high thermal capacitance), the heat flux-flow interaction is taken into account in the single-phase region assuming a pure convective heat transfer coefficient.

ix) A sharp division is assumed between the subcooled region and the two-phase region. Therefore, the notion of the (bulk) boiling boundary, i.e. the point where the mixed-mean enthalpy reaches saturation, is rather artificially introduced. The effect of subcooled boiling upstream of the boiling boundary is ignored by assuming complete thermodynamic equilibrium. This is a reasonable approximation since it has been reported (Neal et al (1967); Yadigaroglu et al (1972)) that the resulting changes in frictional and gravitational components of the pressure drop, due to subcooled boiling, tend to cancel. The omission of subcooled boiling is especially justifiable when there is a large degree of bulk boiling (high exit qualities) with a high degree of subcooling (importance of one-phase convective region). On the other hand, computational methods capable of dealing with subcooled boiling

conditions, under static or dynamic conditions, are still inadequate (Potter (1973)). However arbitrary the notion of the boiling boundary may be, it has been shown that the effect of its movement on the density distribution in the channel, as manifested by the mathematical analysis, can explain a lot of experimental observations (Crowley et al (1967); Yadigaroglu et al (1972); Moxon (1973); Potter (1973)).

x) Similarly, a sharp division is assumed between the two-phase region and the superheat region, termed the superheat boundary. For coiled tubes, the dry-out point is likely to occur at very high qualities (above 95%) and a small quantity of "carry-over" liquid droplets will enter the superheat region. Since the mathematical details of this region cannot be represented satisfactorily and since it is small in length, we can ignore it, assuming thermodynamic equilibrium and thus introduce the notion of the superheat boundary whose movements, as introduced by the mathematical analysis, effect the velocity perturbations in the superheat region.

xi) The fluid flow is assumed to be turbulent rather than laminar. Although the treatment of laminar flow would be easy by introducing the appropriate correlations, its practical application is limited.

xii) Slip between the phases is allowed for by using the correlation of Zuber and Findlay (1965):

$$U_g = \gamma J + V_j \qquad (4.1)$$

where U_g = vapour phase velocity

γ = slip coefficient which allows for the non-uniform velocity and void fraction distributions over a cross-section.
($\gamma = 1/K_B = 1.13$, reciprocal of Baukoff's constant at low pressures)

J = volume average velocity

V_j = constant vapour drift velocity (slip of the vapour phase with respect to the centre of the volume)

The value of V_j is dependent upon the particular two-phase flow regime. However, in this simplified analysis, the value of V_j is taken as constant throughout the two-phase region:

$$V_j = 1.41 \left[\frac{\sigma g (\rho_f - \rho_g)}{\rho_f^2}\right]^{1/4} \tag{4.2}$$

$$\gamma = \text{constant} \tag{4.3}$$

($\gamma = 1.13$ at low pressures and it is a decreasing function of pressure (Collier (1972)))

Therefore, we consider γ and V_j constant, while γ should go to unity and V_j to zero at unit void fraction. Eventually, with γ and V_j constant, the slip is overestimated at high void fractions, an effect which is stabilising. Therefore, an analysis using values of γ and V_j from intermediate quality data will tend to give an optimistic estimate of the threshold power. On the other hand, by removing slip and assuming an homogeneous model (set $\gamma = 1$, $V_j = 0$), a pessimistic (conservative) estimate of the threshold power is obtained (Neal et al (1967)).

In the boundary of two-phase and superheat regions, a void

fraction of unity will not necessarily correspond to a quality of unity because of the slip correlation used. For mathematical consistency, the void fraction at the exit of the two-phase region will be allowed to depart from unity although the quality will be taken as unity as dictated by the steady-state energy equation for the two-phase region.

The previous deficiency does not exist in the homogeneous model assumption (zero slip between the phases throughout the two-phase region).

xiii) For single-phase flow (heated or unheated), the frictional pressure drop gradient is taken from:

$$\frac{dP}{dz} = - f_i \frac{1}{d} \frac{\rho_i U_i^2}{2} \qquad i = \begin{cases} f \text{ for liquid} \\ g \text{ for vapour} \end{cases} \tag{4.4}$$

where f_i is the single-phase friction factor which is a weak function of Reynold's number in the turbulent region

In the two-phase region, the frictional pressure drop is accounted for by using the Martinelli-Nelson (1948) analysis, i.e.

$$\frac{dP}{dz} = - X(x,P) \frac{f_f}{d} \frac{G^2}{2\rho_f} \tag{4.5}$$

The multiplier $X(x,P)$, if approximated by a higher order polynomial (i.e. $X = B_o + B_1 x + B_2 x^2 + \ldots$) by fitting, for example, the experimental data in the full quality range, is amenable to an analytical treatment such as the present one (see expressions for the quality distribution in the two-phase region in section 4.4.3.3). However, since the mathematical expressions become quite cumbersome and the parameters B_o, B_1, B_2, ..., etc., are not generally available, we have

chosen for the present investigation a first order polynomial of the form $X = 1 + Bx$. The value of the constant B is determined in Appendix A.

xiv) Geometry changes in the flow path (such as restrictions due to valves or other fittings, changes in cross-sections or slope of the channel, etc.), are limited to the upstream and downstream adiabatic lengths only. These (localised) frictional pressure drops are represented simply by the expression:

$$\Delta P = \eta \rho_i U_i^2 \qquad i = \begin{cases} f \text{ for liquid} \\ g \text{ for vapour} \end{cases} \tag{4.6}$$

where η is a constant.

xv) According to assumption (viii), the heat flux is assumed uniform and not varying in time. However, a non-uniform heat flux can easily be approximated by subdividing the element length until the power density is effectively constant in each subdivision. The fluid condition at the inlet to each subdivision is determined by the fluid condition at the exit from the upstream subdivision considering the conservation of mass and energy equations.

4.3 METHOD OF MATHEMATICAL ANALYSIS

4.3.1 Analytical Procedure

The fundamental conservation equations describing the motion of the fluid, as generally presented in Chapter 2, will be linearised and Laplace transformed for each region separately, after taking into account the simplifying assumptions mentioned in the previous section. It can be seen that the mass and energy equations are decoupled from the momentum equation, so that they can be solved separately with respect to void fraction (or density) and phase velocities and enthalpy (or quality) by also taking into account the correlation for slip and the equation of state ($\rho = \rho(h)$), according to our assumptions.

The assumptions made are such that closed analytical solutions can be found for the dependent variables (Laplace transformed perturbations).

Consequently, the linearised conservation of momentum equation can be integrated analytically to bring the perturbation in the overall pressure drop, as made up of the frictional, accelerational and gravitational components in each region.

Although the final expressions for the dependent variables will be obtained by purely analytical methods, their complicated forms necessitate the use of a digital computer for evaluation.

The integrations of the momentum equation is presented in an Appendix form (Appendix A) at the end of this thesis.

It must be noticed that the treatment of the upstream adiabatic length need not be considered separately, since it is a special case ($Q = 0$) of the subcooled region, provided that we introduce the pertinent "equivalent lengths" when we integrate the momentum equation. An exactly similar argument applies for the case of the downstream

adiabatic length as being a special case (Q = 0) of the superheat (or exit condition) region.

4.3.2 Linearisation

In a quasi-linear system, where the deviation from linearity is not too great, linear approximations permit the extension of ordinary linear concepts. This approach acknowledges that the system characteristics change from operating point to operating point, but it assumes linearity in the neighbourhood of a specific operating point. The technique of linearising approximations is more often found under the names "small-signal theory" or "theory of small perturbations" (Shinners (1972)).

The effects of a small amount of non-linearity can be studied analytically by considering small perturbations in the dependent variable about some average value.

Analytically, this can be expressed as:

$$A_n \frac{d^n y}{dt^n} + A_{n-1} \frac{d^{n-1} y}{dt^n} + \ldots + A_1 \frac{dy}{dt} + A_o\, y +$$

$$+ \varepsilon\, f\left(y\,,\ \frac{dy}{dt}\,,\ \ldots\ \frac{d^{n-1} y}{dt^{n-1}}\right) = x(t) \qquad (4.7)$$

where A_i (i = 1, 2, ..., n) are not functions of the dependent variable y or its derivatives

For small non-linearities, the expansion of the solution to this differential equation can be written in power series in ε as:

$$y(t) = y_o(t) + \varepsilon\, y_1(t) + \varepsilon^2\, y_2(t) + \ldots \qquad (4.8)$$

where y_o is the linear component and the rest $\varepsilon\, y_1(t) + \varepsilon^2\, y_2(t) + \ldots$ is the deviation from linearity

Assuming ε to be very small, the non-linear components may be neglected without seriously affecting the system's behaviour.

Linearisation techniques are often applied to those problems where it is desired to linearise non-linear equations by limiting the attention to small perturbations around a reference state (average value). In this context, they will be used in the present analysis.

If, for example, the non-linear equation of the system is:

$$\frac{dx}{dt} = f(x,u) \tag{4.9}$$

(where x,u may be functions of the independent variable t), then the dependent variables can be written as:

$$x = x^0 + \delta x$$
$$u = u^0 + \delta u$$

where the actual variable x is perturbed around the reference state x^0 by δx ($\delta x << x_o$) and similarly for u.

Equation (4.9) holds true for both the reference and the perturbed state, i.e.

$$\frac{dx^0}{dt} = f(x^0,u^0) \tag{4.10}$$

$$\frac{d}{dt}(x^0 + \delta x) = \frac{d}{dt}x^0 + \delta\left(\frac{d}{dt}x\right) = f(x^0 + \delta x, u^0 + \delta u) \tag{4.11}$$

Since the actual perturbation of the system is small, we can

expand equation (4.11) in Taylor series as follows:

$$\frac{dx}{dt} + \delta \frac{dx}{dt} = f(x^0,u^0) + \left(\frac{\partial f}{\partial x}\right)_o \delta x + \left(\frac{\partial f}{\partial u}\right)_o \delta u \qquad (4.12)$$

By subtracting equation (4.10) from equation (4.12), we find:

$$\delta \frac{dx}{dt} = \left(\frac{\partial f}{\partial x}\right)_o \delta x + \left(\frac{\partial f}{\partial u}\right)_o \delta u \qquad (4.13)$$

The resulting equation is very important since it states that the differential equation describing the perturbation around the reference state is linear.

4.3.3 Laplace Transformation

By using the previously-mentioned perturbation technique, our system of non-linear partial differential equations will be reduced to a linear partial one (because of the presence of the two variables, time t and space coordinate z). This set can now be converted into a set of (linear) ordinary differential equations by using the Laplace transformation technique, therefore transforming all the dependent variables and their derivatives from the time domain into the frequency domain by use of the Laplace transform variable $s = \sigma + j\omega$ ($\sigma,\omega = 2\pi\,\eta$, real numbers).

4.4 ANALYSIS

4.4.1 Dynamics of the Heat Source

According to the assumptions, the dynamics of the heat source will be considered, in the subcooled region, assuming a constant heat generation rate and a pure convective heat transfer coefficient in coils as given by Seban and McLaughlin (1963) or in straight tubes as given by Dittus-Boelter (Kay (1968)):

$$(Nu)_f \, Pr^{-0.4} = 0.023 \left(\frac{r_i}{R}\right)^{0.1} Re_f^{0.85} \tag{4.14a}$$

or

$$(Nu)_f \, Pr^{-0.4} = 0.023 \, Re_f^{0.80} \tag{4.14b}$$

The surface of the channel on the other side of the coolant at $r = r_{nc}$ is assumed insulated and the heat transfer to the coolant occurs at the other surface of the channel at $r = r_c$.

A rigorous mathematical solution in the case of time-dependent temperature distribution in the heater, with variable heat generation rate, is given by Verheugen et al (1967).

Our analysis is simplified by assuming constant heat generation rate in time and uniform in space.

As mentioned before, the steady-state heat transfer coefficient h_{cn} is proportional to the bth power (b = 0.85 or 0.80) of the mass flow rate W. Therefore, by taking small perturbations around the mean values of h_{cn} and W, we find:

$$\frac{\delta h_{cn}}{h_{cn}^{0}} = b \, \frac{\delta W}{W^0} \tag{4.15}$$

The heat conduction equation of the heater (in cylindrical coordinates), ignoring axial heat conduction, can be written as (Eckert

and Drake (1950)):

$$Q_v + K_m \frac{\partial^2 T}{\partial r^2} + \frac{K_m}{r} \frac{\partial T}{\partial r} = \rho_m c_m \frac{\partial T}{\partial t} \tag{4.16}$$

By taking small perturbations around mean values and considering Q_v = constant, we find:

$$K_m \frac{\partial^2 (\delta T)}{\partial r^2} + \frac{K_m}{r} \frac{\partial (\delta T)}{\partial r} = \rho_m c_m \frac{\partial (\delta T)}{\partial t} \tag{4.17}$$

By taking the Laplace transformation and introducing the metal (wall) thermal diffusivity $a_m = K_m/\rho_m c_m$, we have:

$$\frac{d^2\overline{T}}{dr^2} + \frac{1}{r} \frac{d\overline{T}}{dr} - \frac{s}{a_m} \overline{T} = 0$$

Introducing the transformation $Z = r \sqrt{s/a_m}$, we obtain the following differential equation:

$$Z^2 \frac{d^2\overline{T}}{dZ^2} + Z \frac{d\overline{T}}{dZ} - Z^2 \overline{T} = 0 \tag{4.18}$$

where Z is, in general, complex

This is a modified Bessel equation (McLachlan (1961)). Its general solution is given by (Spiegel (1968)):

$$\overline{T}_r = C_1 I_o (r \sqrt{s/a_m}) + C_2 K_o (r \sqrt{s/a_m}) \tag{4.19}$$

where I_o, I_1 and K_o, K_1 are the modified Bessel functions of the first and second kind, respectively (subscripts o and 1 denote zero and first

order, respectively).

The constants of integration C_1, C_2 will be evaluated from the boundary conditions. The value of C_2 can be directly calculated from the condition of insulation at the wall surface lying on the other side of the coolant:

$$K_m \left.\frac{\partial \overline{T}_r}{\partial r}\right]_{r=r_{nc}} = 0 \qquad (4.20)$$

therefore:

$$C_1 \sqrt{s/a_m}\, I_1 (r_{nc} \sqrt{s/a_m}) - C_2 \sqrt{s/a_m}\, K_1 (r_{nc} \sqrt{s/a_m}) = 0 \qquad (4.21)$$

Consequently, equation (4.19) becomes:

$$\overline{T}_r = C_1 M (r \sqrt{s/a_m}) = C_1 \left[I_o (r \sqrt{s/a_m}) + \frac{I_1 (r_{nc} \sqrt{s/a_m})}{K_1 (r_{nc} \sqrt{s/a_m})} K_o (r \sqrt{s/a_m}) \right] \qquad (4.22)$$

It can be observed that no source term appears in the time-dependent part of the conduction equation (4.17). Therefore, the transient solution will be independent of the radial heat source distribution and so the inclusion of the boundary condition at $r = r_{nc}$ allows the treatment of the case of a wall without internal heat generation. The physical meaning of that is that the transient heat flux to the coolant springs entirely from the heat stored in the heater (thermal capacity).

The transient heat flow into the coolant at $r = r_c$ can now be evaluated by taking into account the variations of heat transfer coefficient and fluid enthalpy due to the mass flow rate oscillations and performing Laplace transformation:

$$\overline{Q}''_{r=r_c} = \pm K_m \left.\frac{\partial \overline{T}_r}{\partial r}\right)_{r=r_c} = h_{cn}^{\,0} \left(\overline{T}_{r=r_c} - \overline{T}_b\right) + \overline{h}_{cn} \left(T^{\,0}_{r=r_c} - T_b^{\,0}\right) \qquad (4.23)$$

where the + sign applies for the internally cooled pipe, and the

- sign applies for the externally cooled pipe.

By substitution from equations (4.22) and (4.15), we have:

$$\pm K_m C_1 \sqrt{s/a_m}\, M'\left(r_c\sqrt{s/a_m}\right) = h_{cn}^{\,0}\left[C_1 M\left(r_c\sqrt{s/a}\right) - \overline{T}_b\right] + b\,\frac{\overline{W}}{W^0}\, h_{cn}^{\,0}\,\frac{Q'}{\xi h_{cn}^{\,0}} \qquad (4.24)$$

where $M'(x)$ denotes the first derivative of $M(x)$, i.e.

$$M'\left(r\sqrt{s/a_m}\right) = I_1\left(r\sqrt{s/a_m}\right) - \frac{I_1\left(r_{nc}\sqrt{s/a_m}\right)}{K_1\left(r_{nc}\sqrt{s/a_m}\right)} K_1\left(r\sqrt{s/a_m}\right) \qquad (4.25)$$

We put:

$$\psi = \frac{h_{cn}^{\,0}\, r_c}{K_m} \qquad (4.26a)$$

$$E(z) = \frac{b}{K_m}\,\frac{Q'(z)}{W^0} \qquad (4.26b)$$

$$\tau_k = \frac{r_c^{\,2}}{a_m} \qquad (4.26c)$$

Then, equation (4.24) becomes:

$$\pm \sqrt{\tau_k\, s}\; C_1\, M'\left(\sqrt{\tau_k\, s}\right) = \psi\left[C_1\, M\left(\sqrt{\tau_k\, s}\right) - \overline{T}_b\right] + E\,\frac{r_c}{\xi}\,\overline{W} \qquad (4.27)$$

Defining:

$$F(s) = \mp \sqrt{\tau_k\, s}\,\frac{M'\left(\sqrt{\tau_k\, s}\right)}{M\left(\sqrt{\tau_k\, s}\right)} \qquad (4.28)$$

equation (4.27) takes the form:

$$\overline{T}_w = \overline{T}_{r=r_c} = C_1 M(\sqrt{\tau_k s}) = \frac{\psi \overline{T}_b - E(r_c/\xi)\overline{W}}{\psi + F(s)} \qquad (4.29)$$

Therefore, the transient part of the temperature at the wall on the coolant side is evaluated from equation (4.29) without the need to know the value of C_1.

It must be emphasised that, even if we assume $Q'(z) = Q' =$ constant, $\overline{T}_w$ is a function of s and the spatial coordinate z, since the bulk fluid enthalpy perturbation is a function of s and z, i.e.

$$\overline{h}_f(z,s) = c_f \overline{T}_b(z,s) \qquad (4.30)$$

Equations (4.29) and (4.30) will be used later in the derivation of flow-to-enthalpy transfer function in the subcooled region.

In equation (4.28), the negative sign applies for the internally cooled pipe and the positive sign for the externally cooled pipe.

The previous analysis can easily be extended to include the case of a solid cylinder heater (annular geometry channel). In this case, r_c equals the radius of the cylindrical rod and $r_{nc} = 0$.

The distribution of the perturbed Laplace transformed temperatures inside the rod is given again by equation (4.19). The constant of integration C_2 in equation (4.19) must be zero, otherwise the temperature perturbation on the axis of the rod would be infinite, i.e.

$$\overline{T}_{r=r_{nc}=0} = C_1 I_o(0) + C_2 K_o(0)$$

where:

$$K_o(0) = +\infty \qquad \text{(McLachlan (1961))}$$

Therefore:

$$C_2 = 0$$

and thus:

$$\overline{T}_r = C_1 I_o (r\sqrt{s/a_m}) = C_1 M (r\sqrt{s/a_m}) \tag{4.31}$$

The previous analysis now applies with the new value for $M(r\sqrt{s/a_m})$ taken from equation (4.31) and $M'(r\sqrt{s/a_m})$ evaluated as:

$$M'(r\sqrt{s/a_m}) = I_1 (r\sqrt{s/a_m}) \tag{4.32}$$

The transient part of the temperature at the wall on the coolant side ($r = r_c$) is evaluated again from equation (4.29), where the value of $F(s)$ from equation (4.28) is taken with the positive sign (externally cooled surface).

The modulation of the heat (flux) input to the fluid, $\delta Q''(z,s)$, is given by the flow-to-heat flux transfer function defined as (Laplace transform variables):

$$(TF)_Q = \frac{\overline{Q}''}{\overline{W}} \tag{4.33}$$

The transient part of the heat flux into the coolant at $r = r_c$ is found from equations (4.23), (4.24) and (4.29) as:

$$\overline{Q}'' = h_{cn}{}^0 \left(\frac{\psi\, \overline{T}_b - E\,(r_c/\xi)\, \overline{W}}{\psi + F(s)} - \overline{T}_b \right) + b\, \frac{\overline{W}}{W^0}\, \frac{Q'}{\xi}$$

Dividing through by $\overline{W}$, we find:

$$\frac{\overline{Q}''}{\overline{W}} = h_{cn}{}^{0} \left[\frac{\psi \ (\overline{T}_b/\overline{W}) - E \ (r_c/\xi)}{\psi + F(s)} - \frac{\overline{T}_b}{\overline{W}} \right] + b \frac{Q'}{W^0 \ \xi} \tag{4.34}$$

According to equation (4.30), the term:

$$\frac{\overline{T}_b}{\overline{W}} = \frac{1}{c_f} \frac{\overline{h}_f}{\overline{W}} = \frac{1}{c_f} (TF)_h$$

where $(TF)_h$ is the flow-to-enthalpy transfer function and is evaluated in the next section (equation (4.49) or (4.51))

By also taking into account the definitions (4.26a) and (4.26b), equation (4.34) becomes:

$$\frac{\overline{Q}''}{\overline{W}} = \frac{h_{cn}{}^{0} \ \psi \ ((TF)_h/c_f) - E \ (\psi \ K_m/\xi)}{\psi + F(s)} - \frac{h_{cn}{}^{0}}{c_f} (TF)_h + \frac{K_m \ E}{\xi}$$

or:

$$(TF)_Q = \frac{\overline{Q}''}{\overline{W}} = \left(- \frac{h_{cn}{}^{0}}{c_f} (TF)_h + \frac{K_m}{\xi} E \right) \frac{F(s)}{F(s) + \psi} \tag{4.35}$$

Some limiting cases for the flow-to-enthalpy $(TF)_h$ and flow-to-heat flux $(TF)_Q$ transfer functions for the case of a uniform heat flux distribution are given by Yadigaroglu and Bergles (1972).

4.4.2 Subcooled Region

According to our assumptions, the density in this region does not vary either in space or in time.

The conservation of mass and energy equations, for this single-phase region, are:

Mass: $$\frac{\partial}{\partial z}(\rho_f U_1) + \frac{\partial}{\partial t}\rho_f = 0$$

Energy: $$\frac{\partial}{\partial z}(\rho_f U_1 h_f) + \frac{\partial}{\partial t}(\rho_f h_f) = Q_\nu$$

For incompressible flow, ρ_f = constant, therefore:

$$\overline{\rho}_f = 0 \tag{4.36}$$

Therefore, the conservation equations become:

$$\frac{\partial}{\partial z} U_1 = 0 \quad \text{and thus} \quad U_f^0 = U_1^0 = \text{constant} \tag{4.37}$$

$$\frac{\partial}{\partial z}(U_1 h_f) + \frac{\partial}{\partial t} h_f = \frac{Q_\nu}{\rho_f} \tag{4.38}$$

For each of the dependent variables, we consider small perturbations around the steady-state, i.e.

$$U_1(z,t) = U_1^0(z) + \delta U_1(z,t)$$

$$h_f(z,t) = h_f^0(z) + \delta h_f(z,t)$$

$$\frac{A}{\xi} Q_\nu = \frac{A}{\xi} Q_\nu^0 + h_{cn}^0 (\delta T_{r=r_c} - \delta T_b) + \delta h_{cn} (T_{r=r_c} - T_b)$$

The last two terms on the RHS of the last equation stem from the transient heat flow into the coolant at $r = r_c$, as expressed by equation (4.23) of the previous section, due to the thermal capacity of the heater wall.

By also taking the Laplace transforms, equations (4.37) and (4.38) become:

$$\frac{\partial}{\partial z}\,\overline{U}_1 = 0 \qquad \text{or} \qquad \overline{U}_f = \overline{U}_1 = \text{constant for any } z \tag{4.39}$$

$$U_1^{\,0}\,\frac{d\overline{h}_f}{dz} + \overline{U}_1\,\frac{dh_f^{\,0}}{dz} + s\,\overline{h}_f = \frac{\xi}{A\,\rho_f}\left[h_{cn}^{\,0}\,(\overline{T}_{r=r_c} - \overline{T}_b) + \overline{h}_{cn}\,(T_{r=r_c} - T_b)\right] \tag{4.40}$$

From equation (4.38) for steady-state, we find:

$$\frac{\partial}{\partial z}\,h_f^{\,0} = \frac{Q_v}{\rho_f\,U_1^{\,0}}$$

therefore:

$$h_f^{\,0} = \frac{Q_v}{\rho_f\,U_1^{\,0}}\,z + h_{fi}^{0} \tag{4.41}$$

where h_{fi}^{0} is the fluid enthalpy at the inlet to this region.

Substituting the values of $\partial h_f^{\,0}/\partial z$, $\overline{T}_{r=r_c}$, $\overline{T}_b$ and $\overline{h}_{cn}$ from equations (4.41), (4.29), (4.30) and (4.15), respectively, into equation (4.40) and noting that $T_{r=r_c} - T_b = Q'/(\xi\,h_{cn}^{\,0})$ and using equation (4.26b), we obtain:

$$U_1^{\,0}\,\frac{d\overline{h}_f}{dz} + \overline{U}_1\,\frac{Q_v}{\rho_f\,U_1^{\,0}} + s\,\overline{h}_f = \frac{\xi}{A\rho_f}\left\{h_{cn}^{\,0}\left[\frac{\psi\,(\overline{h}_f/c_f) - E\,(r_c/\xi)\,\overline{W}}{\psi + F(s)} - \frac{\overline{h}_f}{c_f}\right] + b\,\frac{h_{cn}^{\,0}}{W^0}\,\overline{W}\,\frac{Q'}{\xi\,h_{cn}^{\,0}}\right\} =$$

$$= \frac{\xi}{A\,\rho_f}\left[-\frac{h_{cn}^{\,0}\,(b/K_m)\,(Q'/W^0)\,(r_c/\xi)\,\overline{W}}{\psi + F(s)} - \frac{h_{cn}^{\,0}\,F(s)\,(\overline{h}_f/c_f)}{\psi + F(s)} + b\,\frac{Q'}{\xi}\,\frac{\overline{W}}{W^0}\right] \tag{4.42}$$

After some rearrangement and separation of the terms and

taking into account equation (4.26a) and the relation $W^0 = A\ \rho_f\ U_1{}^0$, we find:

$$\frac{d\overline{h}_f}{dz} + \frac{1}{U_1{}^0}\left[s + \frac{h_{cn}{}^0\ \xi}{A\ \rho_f\ c_f}\frac{F(s)}{\psi + F(s)}\right]\overline{h}_f =$$

$$= -\frac{Q'}{W_o{}^2}\left[(1-b) + b\,\frac{\psi}{\psi + F(s)}\right]\overline{W} \qquad (4.43)$$

We put:

$$\tau_f = \frac{A\ \rho_f\ c_f}{h_{cn}{}^0\ \xi} \qquad (4.44)$$

$$N(s) = \frac{1}{U_1{}^0}\left[s + \frac{1}{\tau_f}\frac{F(s)}{\psi + F(s)}\right] \qquad (4.45)$$

$$L(s) = \frac{Q'}{W_o{}^2}\left[(1-b) + b\,\frac{\psi}{\psi + F(s)}\right] \qquad (4.46)$$

Then equation (4.43) becomes:

$$\frac{d\overline{h}_f}{dz} + N(s)\ \overline{h}_f = -L(s)\ \overline{W} \qquad (4.47)$$

This is a linear ordinary differential equation where the Laplace transformed variable $\overline{h}_f$ is the dependent variable and z is the independent variable.

The integrating factor is $e^{N(s)z}$, therefore:

$$\frac{d}{dz}\left[\overline{h}_f\ e^{N(s)z}\right] = -L(s)\ e^{N(s)z}\ \overline{W} \qquad (4.48)$$

Equation (4.48) can now be integrated along the subcooled region with the boundary condition $\overline{h}_f(z=0,s) = \overline{h}_{fi} = 0$, to bring the flow-to-enthalpy transfer function:

$$\overline{h}_f \, e^{N(s)z} - \overline{h}_{fi} = - L(s) \, \overline{W} \int_0^z e^{N(s)z} \, dz$$

$$\frac{\overline{h}_f}{\overline{W}} = - \frac{L(s)}{N(s)} \left(1 - e^{-N(s)z} \right) \tag{4.49}$$

The time dependence of the enthalpy perturbations is characterised by three time constants:

The wall time constant τ_k, defined in equation (4.26c)

The fluid heat capacity time constant τ_f, defined in equation (4.44)

The film conductance time constant defined as:

$$\tau_h = \frac{\tau_k}{\psi} = \frac{r_c \, K_m}{a_m \, h_{cn}^{\,0}} \tag{4.50}$$

By completely neglecting the heat storage at the wall, we find from equation (4.28), $F(s) = 0$.

Consequently, from equations (4.45) and (4.46), we get:

$$N(s) = \frac{s}{U_1^{\,0}} \quad , \quad L(s) = \frac{Q'}{W_o^{\,2}}$$

Substituting these values into equation (4.49) and noting that $Q' = Q_v \, A$, $W^0 = A \, \rho_f \, U_1^{\,0}$ and $\overline{W} = A \, \rho_f \, \overline{U}_1$, we find, after rearrangement:

$$\frac{\overline{h}_f}{\overline{U}_1} = - \frac{Q_v}{\rho_f \, U_1^{\,0}} \left(\frac{1 - e^{-s(z/U_1^{\,0})}}{s} \right) \tag{4.51}$$

It can be seen that $z/U_1^{\,0} = \tau_z$ is the fluid transit time through this region, up to a distance z.

The time varying position of the boiling boundary is determined by the enthalpy variations of the coolant. In a very low pressure system, the movements of the boiling boundary are also affected by pressure variations.

By taking small perturbations at any point z inside this region, we get (see Figure 4.1.a):

$$\delta h_f(z,t) = - \delta y(z,t) \frac{dh_f^0}{dz} \tag{4.52}$$

where the value of dh_f^0/dz is given by equation (4.41).

Taking the Laplace transform of equation (4.52) and substituting into equations (4.49) and (4.51), we get:

$$\overline{y}_b = \overline{U}_1 \frac{A \rho_f^2 U_1^0}{Q_\nu} \frac{L(s)}{N(s)} \left[1 - e^{-N(s)y_1}\right] \tag{4.53}$$

and

$$\overline{y}_b = \overline{U}_1 \left[\frac{1 - e^{-s\tau_1}}{s}\right] \tag{4.54}$$

where $\overline{y}_b$ is the time varying position of the boiling boundary. We define:

$$\tau_1 = \frac{y_b}{U_1^0} \tag{4.55}$$

where y_b is the length of the subcooled (heated) region and τ_1 as defined by equation (4.55) is the fluid transit time through the whole subcooled (heated) region.

The important findings of equations (4.36), (4.39) and (4.53) or (4.54) can now be used to integrate the perturbed Laplace transformed

momentum equation between the inlet and the boiling boundary in order to bring the overall perturbation in pressure drop through this region as made up by the three components of friction, acceleration and gravity. The integration is executed in Appendix A.

For the case of frictional pressure drop, it must be noticed that the single-phase friction factor has the general form:

$$\lambda^0 = \frac{C^{0\prime}}{Re^{\beta}} \quad \text{and thus} \quad \lambda^0 = \frac{C^0}{(U_1{}^0)^{\beta}} \tag{4.56}$$

Therefore:
$$\delta\lambda = -\beta\, C^0\, (U_1{}^0)^{-\beta-1}\, \delta U_1{}^0 \tag{4.57}$$

Dividing equation (4.57) by equation (4.56) and taking Laplace transforms, we obtain:

$$\frac{\overline{\lambda}}{\lambda^0} = -\beta\, \frac{\overline{U}_1}{U_1{}^0}$$

Therefore:
$$\overline{\lambda} = -\lambda^0\, \beta\, \frac{\overline{U}_1}{U_1{}^0} = -\lambda^0\, \beta\, \frac{\overline{W}}{W^0} \tag{4.58}$$

4.4.3 Two-Phase Region

4.4.3.1 Velocity and void-fraction distributions

The conservation of mass and energy equations for the two-phase region, as stated in Chapter 2, are:

Mass:

$$\frac{\partial}{\partial z}\left[\rho_f\,(1-\alpha)\,U_f + \rho_g\,\alpha\,U_g\right] + \frac{\partial}{\partial t}\left[\rho_f\,(1-\alpha) + \rho_g\,\alpha\right] = 0 \tag{4.59}$$

Energy:

$$\frac{\partial}{\partial z}\left[\rho_f\,(1-\alpha)\,h_f\,U_f + \rho_g\,\alpha\,h_g\,U_g\right] + \frac{\partial}{\partial t}\left[\rho_f\,(1-\alpha)\,h_f + \rho_g\,\alpha\,h_g\right] = Q_v \qquad (4.60)$$

If we make the homogeneous model assumption:

$$S = \frac{U_g}{U_f} = 1 \qquad (4.61)$$

Therefore:

$$\frac{x}{(1-x)} = \frac{\alpha}{(1-\alpha)}\frac{\rho_g}{\rho_f}S = \frac{\alpha}{(1-\alpha)}\frac{\rho_g}{\rho_f} \qquad (4.62)$$

Let: $\rho_2 = \rho_f\,(1-\alpha) + \rho_g\,\alpha$ (mixture density) (4.63)

By using equation (4.62), we find:

$$\rho_f\,(1-\alpha)\,h_f + \rho_g\,\alpha\,h_g = \left[\rho_f\,(1-\alpha) + \rho_g\,\alpha\right]\left[(1-x)\,h_f + x\,h_g\right] = \rho_2\,h_2 \qquad (4.64)$$

where: $h_2 = (1-x)\,h_f + x\,h_g$ (mixture enthalpy) (4.65)

and the mixture density can be expressed as follows, in terms of the vapour quality x:

$$\rho_2^{-1} = (1-x)\,v_f + x\,v_g \qquad (4.66)$$

Now the mass and energy conservation equations can be written according to equations (4.63), (4.64) and (4.61), where we set:

$$U_g = U_f = U_2 \quad \text{(mixture velocity)} \qquad (4.67)$$

Mass: $$\frac{\partial}{\partial z}(\rho_2 U_2) + \frac{\partial}{\partial t}\rho_2 = 0 \qquad (4.59a)$$

Energy: $$\frac{\partial}{\partial z}(\rho_2 U_2 h_2) + \frac{\partial}{\partial t}(\rho_2 h_2) = Q_v \qquad (4.60a)$$

However, if we take into account the slip between the phases (using the correlation described in assumption (xii) of section 4.2), we must start from the form of mass and energy conservation equations given by equations (4.59) and (4.60). The non-slip case ($S = 1$) will then be a special case (set $\gamma = 1$, $V_j = 0$).

The velocity and void fraction distributions for the static and dynamic case will be found by solving simultaneously the equations of mass and energy (4.59) and (4.60).

Multiplying the mass equation by h_f and subtracting it from the energy equation yields:

$$\frac{\partial}{\partial z}(\alpha U_g) + \frac{\partial}{\partial t}(\alpha) = q\frac{\rho_f}{\rho_f - \rho_g} \qquad (4.68)$$

Similarly, multiplying the mass equation by h_g and subtracting it from the energy equation yields:

$$\frac{\partial}{\partial z}\left[(1-\alpha) U_f\right] + \frac{\partial}{\partial t}(1-\alpha) = -q\frac{\rho_g}{\rho_f - \rho_g} \qquad (4.69)$$

where we define:

$$q = \frac{\rho_f - \rho_g}{\rho_f \rho_g}\frac{Q_v}{h_g - h_f} \qquad (4.70)$$

The volume average velocity is by definition (Collier (1972)):

$$J = (1 - \alpha)\, U_f + \alpha\, U_g \tag{4.71}$$

By adding together equations (4.68) and (4.69), we obtain:

$$\frac{\partial J}{\partial z} = q \tag{4.72}$$

Therefore: $$J = J_{in} + q\, z \tag{4.73}$$

and thus: $$J^0 = J^0_{in} + q\, z \tag{4.74}$$

and: $$\overline{J} = \overline{J}_{in} = \text{constant for every } z \tag{4.75}$$

From mass conservation considerations at the boiling boundary interface, we obtain:

$$J^0_{in} = U_1{}^0 = U_f{}^0 \tag{4.76}$$

By taking small perturbations of the steady-state velocities at the boiling boundary, we obtain (see Figure 4.1.b):

$$\overline{J}_{in} = \overline{U}_1 - \overline{y}_b \left(\frac{dJ}{dz}\right)_{y=y_b} \tag{4.77}$$

and taking into account equation (4.72):

$$\overline{J}_{in} = \overline{U}_1 - q\, \overline{y}_b \tag{4.78a}$$

Therefore: $$\overline{J} = \overline{J}_{in} = \overline{U}_1 - q\, \overline{y}_b = \text{constant} \tag{4.78b}$$

for every point z in the two-phase region.

The vapour velocity is given by the correlation of Zuber and Findlay (assumption (xii) in section 4.2):

$$U_g = \gamma J + V_j \tag{4.79}$$

By using equation (4.73), we obtain:

$$U_g = \gamma J_{in} + \gamma q z + V_j \tag{4.80}$$

Therefore:

$$U_g^0 = \gamma J_{in}^0 + V_j + \gamma q z = U_{g_{in}}^0 + \gamma q z \tag{4.81}$$

and:
$$\overline{U}_g = \gamma \overline{J}_{in} = \gamma (\overline{U}_1 - q \overline{y}_b) = \text{constant for any } z \tag{4.82}$$

where we have defined:

$$U_{g_{in}}^0 = \gamma J_{in}^0 + V_j \tag{4.83}$$

The liquid velocity is found from equation (4.71) taking into consideration equation (4.79):

$$U_f = \frac{J - \alpha (\gamma J + V_j)}{1 - \alpha} = \frac{(J_{in} + q z)(1 - \alpha \gamma) - \alpha V_j}{1 - \alpha} \tag{4.84}$$

Therefore, for the steady-state:

$$U_f^0 = \frac{(J_{in}^0 + q z)(1 - \alpha^0 \gamma) - \alpha^0 V_j}{1 - \alpha^0} \tag{4.85}$$

By dividing equation (4.82) by equation (4.85), we

obtain the expression for the slip ratio:

$$S = \frac{U_g^0}{U_f^0} \tag{4.85a}$$

It can be noticed that the assumption of a constant drift velocity V_j throughout the channel does not imply either a constant relative velocity, or a constant slip ratio S.

In Appendix B, the expression for the slip ratio S as a function of void fraction (α) and input velocity (U_1^0) is found.

By perturbing and Laplace transforming equation (4.71), we get:

$$\bar{J} = (1 - \alpha^0)\,\bar{U}_f - \bar{\alpha}\,U_f^0 + \alpha^0\,\bar{U}_g + \bar{\alpha}\,U_g^0$$

Solving for $\bar{U}_f$ and using equation (4.82), we get:

$$\bar{U}_f = \frac{1}{1 - \alpha^0}\left[\bar{J}_{in}\,(1 - \gamma\,\alpha^0) + \bar{\alpha}\,(U_f^0 - U_g^0)\right] \tag{4.86}$$

The distributions for the steady-state void fraction α^0 and its perturbation (Laplace transformed) $\bar{\alpha}$ are determined below.

From equation (4.68) for steady-state (we set $\Delta\rho = \rho_f - \rho_g$):

$$\frac{\partial}{\partial z}\,(\alpha^0\,U_g^0) = q\,\frac{\rho_f}{\Delta\rho} \tag{4.87}$$

We integrate equation (4.87), taking into account equation (4.81):

$$\alpha^0 = \frac{\alpha_{in}^0\,U_{g_{in}}^0 + q\,\rho_f\,z/\Delta\rho}{U_{g_{in}}^0 + \gamma\,q\,z} \tag{4.88}$$

At this moment, it is appropriate to change the independent variable from z to τ_2 (transit time) defined as follows:

$$\tau_2 = \int_o^z \frac{dz}{U_g^0} \tag{4.89}$$

which is the transit time of the vapour phase in the two-phase region up to a distance z.

By using equation (4.81), we find from equation (4.89):

$$\tau_2 = \int_o^z \frac{dz}{U_{g_{in}}^0 + \gamma q z} = \frac{1}{\gamma q} ln \frac{U_g^0}{U_{g_{in}}^0} \tag{4.90}$$

Therefore:

$$U_g^0 = U_{g_{in}}^0 e^{\gamma q \tau_2} \tag{4.91}$$

By using τ_2 instead of z, equation (4.87) becomes:

$$\frac{1}{U_g^0} \frac{d}{d\tau_2} (\alpha^0 U_g^0) = q \frac{\rho_f}{\Delta\rho} \tag{4.92}$$

By using equation (4.91), we integrate equation (4.92):

$$\alpha^0 U_{g_{in}}^0 e^{\gamma q \tau_2} - \alpha_{in}^0 U_{g_{in}}^0 = q \frac{\rho_f}{\Delta\rho} U_{g_{in}}^0 \frac{1}{\gamma q} (e^{\gamma q \tau_2} - 1)$$

or $$\alpha^0 e^{\gamma q \tau_2} - \alpha_{in}^0 = \frac{\rho_f}{\Delta\rho \gamma} (e^{\gamma q \tau_2} - 1)$$

or $$\alpha^0 = \frac{1}{\gamma \Delta\rho} \left[\rho_f - (\rho_f - \gamma \Delta\rho \alpha_{in}^0) e^{-\gamma q \tau_2} \right] \tag{4.93}$$

At the boiling boundary ($x_{in}^0 = 0$), we have:

$$\alpha^0_{in} = 0 \tag{4.94}$$

and therefore equation (4.93) becomes:

$$\alpha^0 = \frac{\rho_f}{\gamma\ \Delta\rho}\ (1 - e^{-\gamma q \tau_2}) \tag{4.95}$$

We perturb and Laplace transform equation (4.68):

$$\frac{d}{dz}\ (U_g^{\ 0}\ \bar{\alpha}) + s\ \bar{\alpha} = -\ \bar{U}_g\ \frac{d\alpha^0}{dz} \tag{4.96}$$

and in terms of the variable τ_2 defined in equation (4.90):

$$\frac{d}{d\tau_2}\ (U_g^{\ 0}\ \bar{\alpha}) + U_g^{\ 0}\ s\ \bar{\alpha} = -\ \bar{U}_g\ \frac{d\alpha^0}{d\tau_2} \tag{4.97}$$

The integrating factor for equation (4.97) is $e^{s\tau_2}$. Therefore:

$$\frac{d}{d\tau_2}\ (U_g^{\ 0}\ \bar{\alpha}\ e^{s\tau_2}) = -\ \bar{U}_g\ \frac{d\alpha^0}{d\tau_2}\ e^{s\tau_2} \tag{4.98}$$

By differentiating equation (4.95), we obtain:

$$\frac{d\alpha^0}{d\tau_2} = \frac{q\ \rho_f}{\Delta\rho}\ e^{-\gamma q \tau_2} \tag{4.99}$$

Substituting equation (4.99) into equation (4.98) and integrating, we take:

$$U_g^{\ 0}\ \bar{\alpha} = U_{g_{in}}^{\ 0}\ \bar{\alpha}_{in}\ e^{-s\tau_2} - \frac{\gamma\ q\ \rho_f}{\Delta\rho}\ \bar{J}_{in}\ \frac{e^{-\gamma q \tau_2} - e^{-s\tau_2}}{s - \gamma\ q} \tag{4.100}$$

By taking small perturbations around the steady-state void fraction at the boiling boundary, we obtain, according to Figure 4.1.c:

$$\bar{\alpha}_{in} = -\bar{y}_b \left(\frac{d\alpha^0}{dz}\right)_{y=y_b} = -\bar{y}_b \frac{1}{U_{g_{in}}^0} \left(\frac{d\alpha^0}{d\tau_2}\right)_{in} \tag{4.101}$$

By using equation (4.99) for $\tau_2 = 0$, we obtain:

$$\bar{\alpha}_{in} = -\frac{\bar{y}_b}{U_{g_{in}}^0} \frac{q\,\rho_f}{\Delta\rho} \tag{4.102}$$

Therefore, equation (4.100) takes the form:

$$U_g^0\,\bar{\alpha} = -\frac{q\,\rho_f}{\Delta\rho}\bar{y}_b\, e^{-s\tau_2} - \frac{\rho_f}{\Delta\rho}\bar{J}_{in}\frac{e^{-\gamma q\tau_2} - e^{-s\tau_2}}{s/\gamma\, q - 1} \tag{4.103}$$

4.4.3.2 Mass flow rate distribution

By definition, the liquid, vapour and total mass flow rates are given by (Collier (1972)):

$$G_f = \rho_f (1 - \alpha)\, U_f \tag{4.104}$$

$$G_g = \rho_g\, \alpha\, U_g \tag{4.105}$$

$$G = \rho_f (1 - \alpha)\, U_f + \rho_g\, \alpha\, U_g \tag{4.106}$$

By using equations (4.71) and (4.79), equation (4.106) becomes:

$$G = \frac{\rho_f}{\gamma}(U_g - V_j) - \Delta\rho\, \alpha\, U_g \tag{4.107}$$

For the steady-state:

$$G_f^0 = \rho_f (1 - \alpha^0) U_f^0 \tag{4.104a}$$

$$G_g^0 = \rho_g \alpha^0 U_g^0 \tag{4.105a}$$

$$G^0 = \frac{\rho_f}{\gamma} (U_g^0 - V_j) - \Delta\rho \alpha^0 U_g^0 \tag{4.107a}$$

For the perturbations (Laplace transformed):

$$\overline{G}_f = \rho_f (1 - \alpha^0) \overline{U}_f - \rho_f \overline{\alpha} U_f^0 \tag{4.104b}$$

$$\overline{G}_g = \rho_g \alpha^0 \overline{U}_g + \rho_g \overline{\alpha} U_g^0 \tag{4.105b}$$

$$\overline{G} = \frac{\rho_f}{\gamma} \overline{U}_g - \Delta\rho \alpha^0 \overline{U}_g - \Delta\rho \overline{\alpha} U_g^0 \tag{4.107b}$$

By substituting from equations (4.82) and (4.103) for $\overline{U}_g$ and $U_g^0 \overline{\alpha}$, respectively, equation (4.107b) takes the form:

$$\overline{G} = (\rho_f - \Delta\rho \alpha^0 \gamma) \overline{J}_{in} + q \rho_f \overline{y}_b e^{-s\tau_2} + \rho_f \overline{J}_{in} \frac{e^{-\gamma q \tau_2} - e^{-s\tau_2}}{s/\gamma\, q - 1}$$

From equation (4.95):

$$\rho_f - \Delta\rho \alpha^0 \gamma = \rho_f e^{-\gamma q \tau_2} \tag{4.95a}$$

Therefore:

$$\overline{G} = \rho_f \overline{J}_{in} e^{-\gamma q \tau_2} + q \rho_f \overline{y}_b e^{-s\tau_2} + \rho_f \overline{J}_{in} \frac{e^{-\gamma q \tau_2} - e^{-s\tau_2}}{s/\gamma\, q - 1}$$

or

$$\overline{G} = \rho_f \overline{J}_{in} e^{-\gamma q \tau_2} \frac{s}{s - \gamma q} - e^{-s\tau_2} \frac{\rho_f \gamma q}{s - \gamma q} \overline{J}_{in} + q \rho_f \overline{y}_b e^{-s\tau_2} \quad (4.108)$$

4.4.3.3 Quality distribution

By definition:

$$x = \frac{G_g}{G} = \frac{\rho_g \alpha U_g}{G} \quad (4.109)$$

For the steady-state:

$$x^0 = \frac{\rho_g \alpha^0 U_g^0}{G^0} \quad (4.110a)$$

or, using equations (4.95) and (4.91):

$$x^0 = \frac{\rho_g \rho_f U_{g_{in}}^0}{G^0 \gamma \Delta\rho} (e^{\gamma q \tau_2} - 1) \quad (4.110)$$

By perturbing and Laplace transforming equation (4.109):

$$\overline{x} = \frac{\rho_g}{(G^0)^2} \left(G^0 \alpha^0 \overline{U}_g + G^0 \overline{\alpha} U_g^0 - \alpha^0 U_g^0 \overline{G} \right) \quad (4.111)$$

Substituting for α^0, $\overline{U}_g$, $\overline{\alpha} U_g^0$, U_g^0 and $\overline{G}$ from equations (4.95), (4.82), (4.103), (4.91) and (4.108), respectively, we have:

$$\overline{x} = \frac{\rho_g \rho_f}{(G^0)^2} \left\{ \frac{G^0 \overline{J}_{in}}{\Delta\rho} (1 - e^{-\gamma q \tau_2}) + G^0 \left(- \frac{q}{\Delta\rho} \overline{y}_b e^{-s\tau_2} - \right. \right.$$

$$\left. - \frac{\gamma q \overline{J}_{in}}{\Delta\rho} \frac{e^{-s\tau_2} - e^{-\gamma q \tau_2}}{\gamma q - s} \right) - \frac{U_{g_{in}}^0 \rho_f}{\gamma \Delta\rho} \left(\left(\frac{\gamma q}{\gamma q - s} \overline{J}_{in} + q \overline{y}_b \right) \cdot \right.$$

$$\cdot\left(e^{(\gamma q-s)\tau_2} - e^{-s\tau_2}\right) - \bar{J}_{in}\frac{s}{\gamma q - s}\left(1 - e^{-\gamma q\tau_2}\right)\Bigg]\Bigg\} \tag{4.112}$$

The steady-state position of the superheat boundary is found from the energy equation ($x^0_{out} = 1$):

$$y_s = \frac{h_g - h_f}{Q_v} G \tag{4.113}$$

Therefore, from equations (4.81), (4.90) and (4.95):

$$U^0_{g_{out}} = U^0_{g_{in}} + \gamma q y_s \tag{4.114}$$

$$\tau_{2_{out}} = \frac{1}{\gamma q} ln \frac{U^0_{g_{out}}}{U^0_{g_{in}}} \tag{4.115}$$

$$\alpha^0_{out} = \frac{\rho_f}{\gamma \Delta\rho}\left(1 - e^{-\gamma q\tau_{2_{out}}}\right) \tag{4.116}$$

According to the discussion in assumption (xii) of section 4.2, with the slip correlation used, the void fraction given by equation (4.116) will be allowed to depart from unity although the quality (x^0_{out}) is unity.

The perturbation in the position of the superheat boundary is taken by considering small perturbations of the steady-state void fraction α^0_{out} at this position (see also Figure 4.1.d):

$$\bar{\alpha}_{out} = -\bar{y}_s \left(\frac{d\alpha^0}{dz}\right)_{y=y_s} = -\frac{\bar{y}_s}{U^0_{g_{out}}}\left(\frac{d\alpha^0}{d\tau_2}\right)_{out} \tag{4.117}$$

or, using equation (4.99):

$$\bar{y}_s = -\bar{\alpha}_{out} \frac{U_{g_{out}}^{0} \Delta\rho}{q\, \rho_f} e^{\gamma q \tau_2} \tag{4.118a}$$

or, using equation (4.101) for $\tau_2 = \tau_{2_{out}}$:

$$\bar{y}_s = \bar{y}_b\, e^{(\gamma q - s)\tau_{2_{out}}} + \frac{\bar{J}_{in}}{q} \frac{1 - e^{(\gamma q - s)\tau_{2_{out}}}}{s/\gamma\, q - 1} \tag{4.118}$$

We are now in a position to integrate the perturbed Laplace transformed momentum equation between the boiling and the superheat boundary in order to bring the overall pressure drop perturbation in the two-phase region. The integration is performed in Appendix A.

4.4.4 Superheat Region

The treatment of this region is exactly the same as that of the subcooled region.

For incompressible flow:

$$\rho_g = \text{constant}$$

Therefore:
$$\bar{\rho}_g = 0 \tag{4.119}$$

From the conservation of mass equation, we obtain:

$$\frac{\partial}{\partial z} U_3 = 0$$

Therefore:
$$\frac{\partial}{\partial z} \bar{U}_3 = 0 \tag{4.120}$$

For the steady-state using equation (4.74), we get:

$$U_3^0 = \text{constant} = J_{out}^0 = J_{in}^0 + q\, y_s = U_1^0 + q\, y_s \qquad (4.121)$$

The constant value of the velocity perturbation in this region can be found by taking small perturbations of the steady-state velocity at the superheat boundary position as according to Figure 4.1.e:

$$\overline{U}_3 = \text{constant} = \overline{J}_{out} + \overline{y}_s \left(\frac{\partial J^0}{\partial z}\right)_{y=y_s} \qquad (4.122a)$$

or, using equations (4.72) and (4.78), we obtain:

$$\overline{U}_3 = \overline{U}_1 - q\, \overline{y}_b + q\, \overline{y}_s = \text{constant} \qquad (4.122)$$

In a similar way (see also Figure 4.1.f), we find:

$$\overline{h}_{in_3} = -\overline{y}_s \left(\frac{dh_g^0}{dz}\right)_{y=y_s} = -\frac{Q_v}{\rho_g U_3^0}\, \overline{y}_s \qquad (4.123)$$

The integration of the momentum equation in this region is executed in Appendix A.

4.4.5 Coupling Between Successive Elements

4.4.5.1 Single-phase flow

According to assumption (xiv) of section 4.2, geometry changes are limited to the upstream and downstream adiabatic lengths only.

Between elements i and $i-1$, conservation of mass and energy gives, for the steady and the perturbed state, respectively:

$$(A\ U^0_{in})_i = (A\ U^0_{out})_{i-1} \tag{4.124}$$

$$(h^0_{in})_i = (h^0_{out})_{i-1} \tag{4.125}$$

and

$$(A\ \overline{U}_{in})_i = (A\ \overline{U}_{out})_{i-1} \tag{4.126}$$

$$(\overline{h}_{in})_i = (\overline{h}_{out})_{i-1} \tag{4.127}$$

4.4.5.2 Two-phase flow

According to assumption (xv), in the case of non-uniform heat flux, we need to know the relations between the mass flow rates and qualities (enthalpies) for two successive elements, each one assumed as having a uniform heat flux.

Between elements i and $i-1$, the principle of conservation of mass and energy yields (here changes in cross-sectional area are not permitted according to assumption (xiv) of section 4.2):

$$(G^0_{in})_i = (G^0_{out})_{i-1} \tag{4.128}$$

$$(x^0_{in})_i = (x^0_{out})_{i-1} \tag{4.129}$$

Then the mass-flow rates of the individual phases and average volumetric velocity follow from the relation:

$$J^0 = \frac{G_f{}^0}{\rho_f} + \frac{G_g{}^0}{\rho_g} = \frac{(1 - x^0)\ G^0}{\rho_f} + \frac{x^0\ G^0}{\rho_g} \tag{4.130}$$

Therefore, the vapour phase velocity and void fraction are calculated from the relations:

$$U_g^0 = \gamma J^0 + V_j \tag{4.131}$$

$$\alpha^0 = G_g^0/(\rho_g U_g^0) \tag{4.132}$$

Similarly, the relations for the perturbations follow from the relations:

$$(\overline{G}_{in})_i = (\overline{G}_{out})_{i-1} \tag{4.133}$$

$$(\overline{x}_{in})_i = (\overline{x}_{out})_{i-1} \tag{4.134}$$

Therefore:

$$\overline{G}_g = x^0 \overline{G} + \overline{x} G^0 \tag{4.135}$$

$$\overline{G}_f = (1 - x^0) \overline{G} - \overline{x} G^0 \tag{4.136}$$

$$\overline{J} = \frac{\overline{G}_f}{\rho_f} + \frac{\overline{G}_g}{\rho_g} \tag{4.137}$$

$$\overline{U}_g = \gamma \overline{J} \tag{4.138}$$

$$\frac{\overline{\alpha}}{\alpha^0} = \frac{\overline{G}_g}{G_g^0} - \frac{\overline{G}_f}{G_f^0} \tag{4.139}$$

4.5 BOUNDARY CONDITIONS

In a "parallel channel" design, the pressure difference between the headers is assumed to be the same for all the channels involved.

The sum of all the perturbations in pressure drop in a channel must be equal to the perturbation in pressure difference between the headers $\delta\ (-\Delta P_{TOT})$, i.e.

$$\delta\ (-\Delta P_{TOT}) = \delta\ (-\Delta P_1) + \delta\ (-\Delta P_2) + \delta\ (-\Delta P_3) \qquad (4.140)$$

where $\delta\ (-\Delta P_1)$ is the subcooled region pressure drop perturbation, as made up from the gravity, momentum and friction component, including the contribution of the upstream adiabatic length

$\delta\ (-\Delta P_2)$ is the corresponding quantity for the two-phase region

$\delta\ (-\Delta P_3)$ is the corresponding quantity for the superheat region, including the contribution of the downstream adiabatic length

The stability problem is to investigate the behaviour of an inlet velocity perturbation $\delta U_{in} = \delta U_1$ for the boundary condition imposed.

In our case, $\delta\ (-\Delta P_{TOT}) = 0$, i.e. the pressure difference between the headers is constant (not varying in time).

4.6 STABILITY ASSESSMENT

4.6.1 Feedback Analysis

The methods of linearisation and Laplace transformation used to manipulate the non-linear partial differential equations describing our physical system permits, at this stage, the application of conventional linear control theory methods to assess the absolute and relative stability of the system concerned (Shinners (1972); Sensicle (1968); Di Stefano et al (1967)).

Proceeding through the entire system, one can build up a block diagram in which each block represents a mathematical relationship between the dependent variables. As described in standard textbooks, the block diagram is a shorthand, graphical representation of a physical system, illustrating the functional relationships among its components. This latter feature permits evaluation of the contribution of the individual elements to the overall performance (stability) of the system. Using standard reduction techniques, any linear feedback control system can take its canonical form (see Figure 4.2) which gives the ratio of output/input for the total system. Having taken the Laplace transformation and set all the initial conditions for the perturbed variables to zero, the ratio of output/input for the total system gives its transfer function $F(s)$ or its unit impulse response in the time domain by taking the inverse Laplace transformation of the $F(s)$, where s is the Laplace transform variable which is generally a complex number:

$$s = \sigma + j\,\omega$$

where σ = rate of divergence (+) or convergence (-)

ω = circular frequency (rad/sec)

By setting $\sigma = 0$, therefore $s = j\omega$, and substituting into the transfer function $F(s)$, we obtain the frequency response function $F(j\omega)$ which represents the steady response of the system to a sinusoidal input of frequency (circular) ω.

The following definitions refer to the canonical form of a feedback control system as illustrated in Figure 4.2.

G = forward transfer function

H = feedback transfer function

GH = open loop transfer function

$\frac{C}{R}$ = closed loop transfer function or control ratio

$\frac{E}{R}$ = error ratio or actuating signal ratio

$\frac{B}{R}$ = primary feedback ratio

$\otimes$ = summing point where the feedback is combined with the input

It is shown in standard textbooks that for positive feedback control systems (- sign at the summing point), the following relations hold:

$$\frac{C}{R} = \frac{G}{1 + GH} \tag{4.141}$$

$$\frac{E}{R} = \frac{1}{1 + GH} \tag{4.142}$$

$$\frac{B}{R} = \frac{GH}{1 + GH} \tag{4.143}$$

It must be emphasised that G and H are not necessarily unique for a particular system.

The characteristic equation of the system is determined by

setting the denominator of the closed loop transfer function equal to zero, i.e.

$$1 + GH = 0 \tag{4.144}$$

As is well known, instability is indicated by poles of the closed loop transfer function (or zeros of the characteristic equation) in the right half of the complex (Laplace variable) s plane. We thus seek roots of the characteristic equation $1 + GH = 0$ for positive values of the real part σ.

Stability can be investigated in several ways. One way is to scan the complex s plane and locate the poles of the closed loop transfer function (or alternatively zeros of the characteristic equation) which have a positive real part. The number of these poles is equal to the number of the unstable modes, and their real and imaginary s coordinates are the divergence rate and circular frequency, respectively. An alternative way to determine the absolute and relative (how close the system is to being unstable) stability is to apply Nyquist's criterion. This is a plot of the open loop GH frequency response on an Argand diagram. If the system studied is unstable, the number of unstable frequencies is given by the number of times this frequency response encircles the (-1,0) point in a clockwise direction. From a Nyquist analysis, the determination of the relative stability of the system is possible by means of gain and phase margins, and also the evaluation of the closed loop frequency response.

4.6.2 Feedback Form Representation of Our Physical System

The thermohydrodynamic equations describing our physical system can be represented by a feedback system such as that described in

section 4.6.1.

We set:

$$R = \text{input signal} = -\overline{\Delta P}_{TOT} \tag{4.145}$$

$$C = \text{output signal} = \overline{U}_{in} \tag{4.146}$$

As mentioned before, the choice of the transfer functions for the forward $G(s)$ and feedback path $H(s)$ is arbitrary. It is customary to use:

$$G = \frac{\overline{U}_{in}}{-\overline{\Delta P}_1} \tag{4.147}$$

$$H = \frac{-\overline{\Delta P}_2 + (-\overline{\Delta P}_3)}{\overline{U}_{in}} \tag{4.148}$$

Therefore, the actuating signal $E = R - B$ represents the condition:

$$-\overline{\Delta P}_1 = -\overline{\Delta P}_{TOT} - \{-\overline{\Delta P}_2 + (-\overline{\Delta P}_3)\} \tag{4.149}$$

Instability of this feedback system arises when the output signal C becomes self-sustained without any input signal R and therefore represents the hydraulic instability in which the inlet velocity U_{in} varies although the total pressure difference $-\Delta P_{TOT}$ between the common headers remains constant.

The canonical feedback control block diagram is shown in Figure 4.3.

For this system we have:

$G(s)\,H(s)$ = open loop transfer function =

$$= \frac{(-\overline{\Delta P}_2) + (-\overline{\Delta P}_3)}{(-\overline{\Delta P}_1)} \tag{4.150}$$

$1 + G(s)\,H(s)$ = characteristic equation =

$$= \frac{(-\overline{\Delta P}_1) + (-\overline{\Delta P}_2) + (-\overline{\Delta P}_3)}{(-\overline{\Delta P}_1)} \tag{4.151}$$

This approach to instability is equivalent to an examination of the inlet flow-to-pressure drop transfer function, frequently called dynamic hydraulic impedance (Dorsch (1967); Anderson (1970); Neal et al (1967); Paul and Riedle (1972)). Other investigators have used power-to-inlet flow or power-to-void transfer functions (Dijkman (1969)). The flow-to-pressure drop transfer function, however, seems to provide the most representative and valuable analytical description of a boiling channel, although experimentally it might be easier to oscillate the heat input rather than the flow.

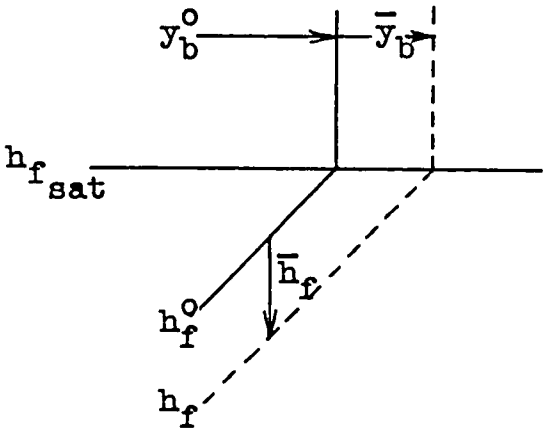

(a) Boiling boundary perturbation induced by enthalpy perturbation

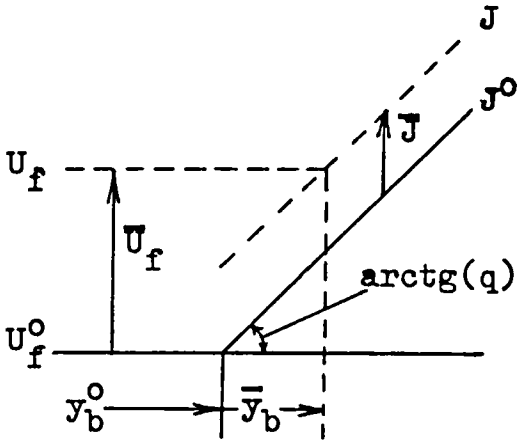

(b) Effect of boiling boundary perturbation on perturbed velocities

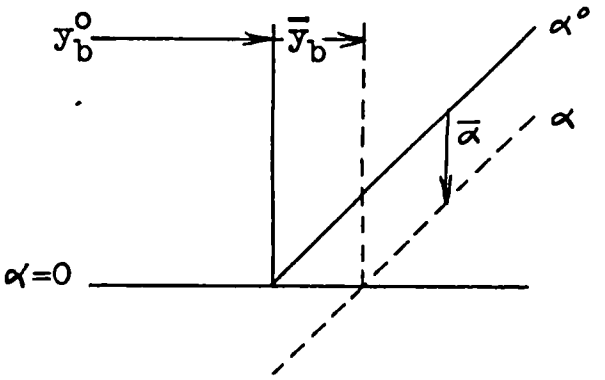

(c) Void fraction perturbation induced by boiling boundary perturbation

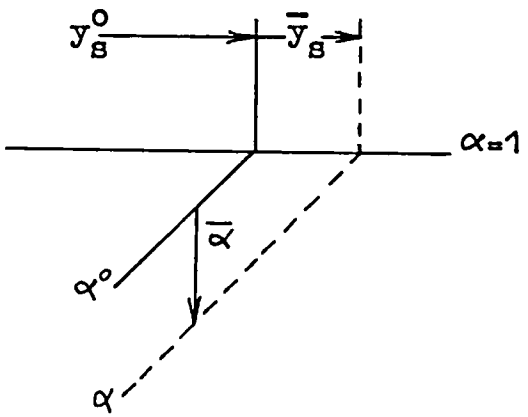

(d) Superheat boundary perturbation induced by void fraction perturbation

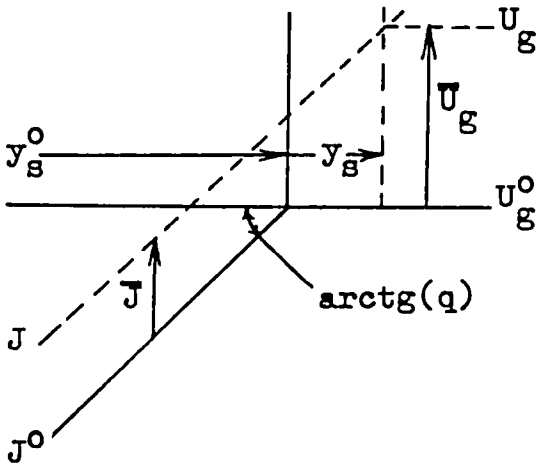

(e) Effect of superheat boundary perturbation on perturbed velocities

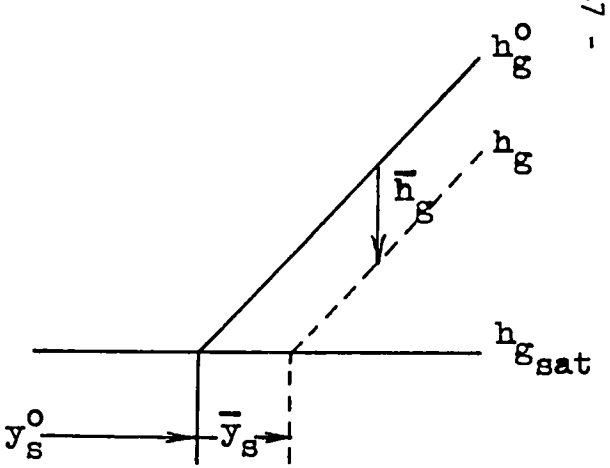

(f) Enthalpy perturbation induced by superheat boundary perturbation

Figure 4.1

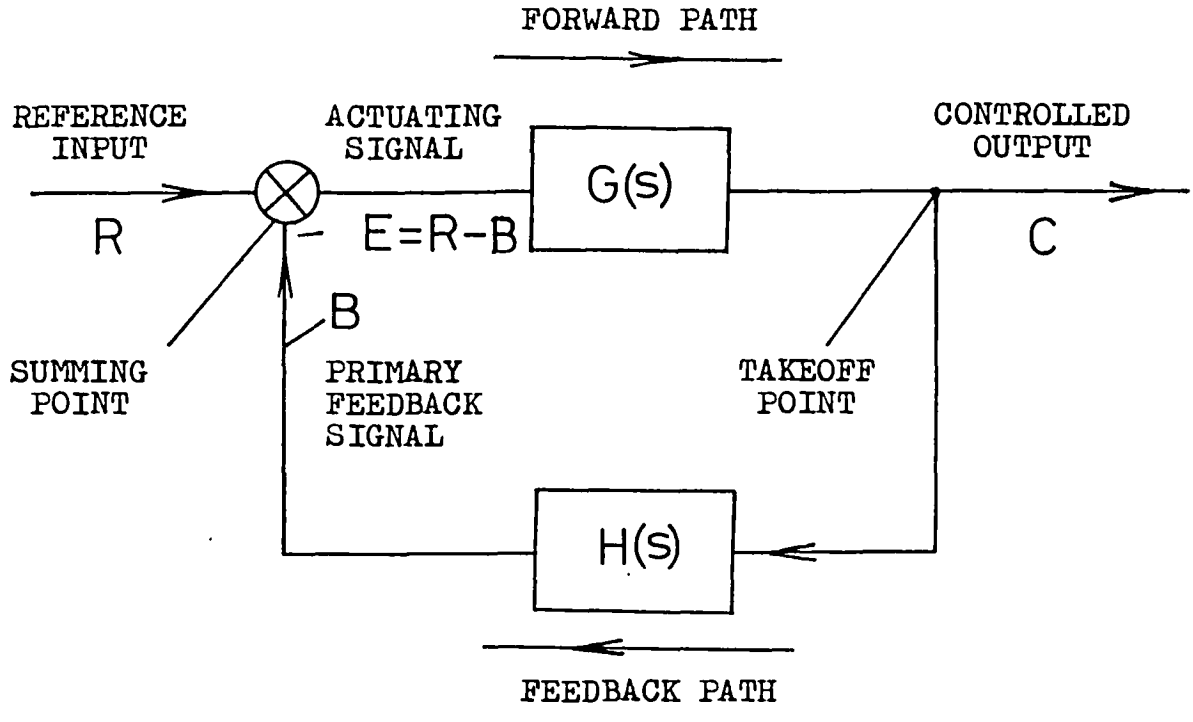

Figure 4.2: Canonical closed loop feedback control system

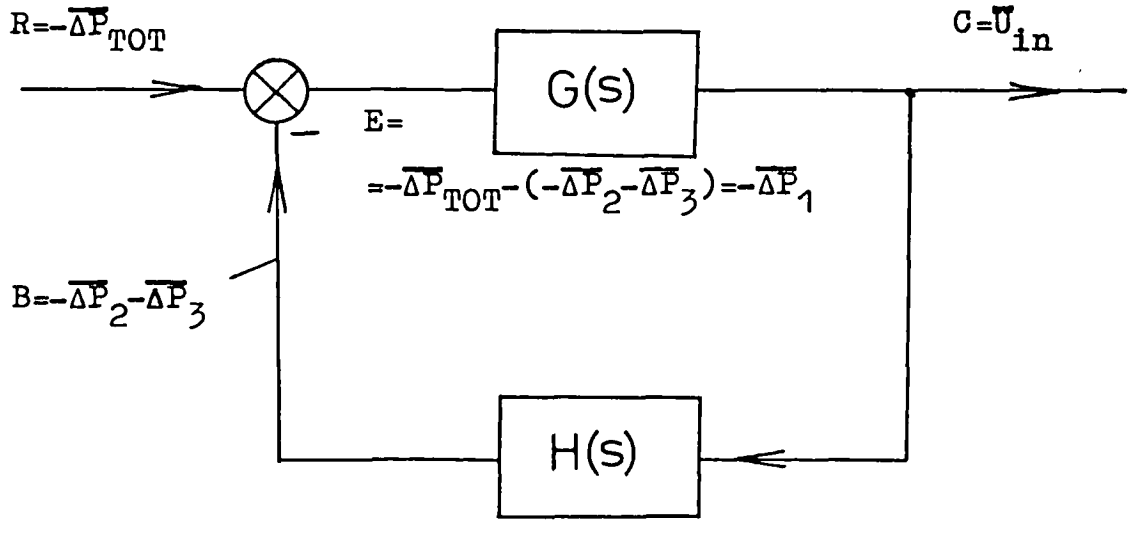

Figure 4.3: Closed loop feedback system representing our physical system

CHAPTER 5

THE COMPUTER PROGRAM

5.1 INTRODUCTION

In order to implement the theory developed in the previous chapter, a computer program has been written and developed to perform the complex number arithmetic required to evaluate the complex transfer functions. This was written in FORTRAN IV language and was run and developed on the CDC 6400 Imperial College computer.

There are two versions of the program. The first one (FLOSIL) computes the open loop frequency response and the inverse of the closed loop frequency response (total dynamic impedance), and the second one (GEFLOS) finds the conditions and the frequency of oscillations at the threshold of instability.

The programs are rather straightforward and easy to follow since no numerical analysis is involved. Sufficient comment cards have also been provided to assist understanding.

5.2 STRATEGY OF THE PROGRAM

5.2.1 Steady-State

The first step in both versions of the program is to enter the input data which describe the geometry of the vapour generator (i.e. straight or helical, and pertinent dimensions) and the conditions of operation (i.e. pressure, subcooling, gags and inlet velocity). From the specified conditions of operation, the thermodynamic and transport properties of the fluid concerned (in our case, Freon-113) are computed by interpolation using subroutine "ABC", from a table of the properties of the fluid given as "data".

The second step is to calculate the friction factors for the conditions of operation specified during the first step.

The third step is to enter the power and then calculate the basic parameters needed for the solution of the steady and dynamic case. The calculated basic parameters include the lengths, the velocities, and the residence times for each region, as well as the exit quality (or superheat), void, slip, etc.

The fourth step calculates the steady-state components of pressure drop for each region separately (frictional, gravitational and accelerational). These values are printed at the beginning of the output together with the basic parameters calculated in the previous steps.

The fifth step calculates (if required) the time constants needed for the calculation of the dynamics of the heater wall.

These five steps conclude the steady-state part of the program.

5.2.2 Dynamic State

As mentioned in section 4.6 of Chapter 4, the hydrodynamic equations can be represented by a feedback system. The forward and feedback path of the system can be analysed to represent each pressure drop perturbation component separately, each one being the product of a transfer function times the perturbation in the position of the boiling boundary or the perturbation of the two-phase velocity or the perturbation in the position of the superheat boundary or the perturbation of the superheat velocity, all these effects resulting from a perturbation of the inlet velocity. This is obvious from the form of each pressure drop perturbation component as derived in Appendix A.

The four effects mentioned above are themselves the product of a transfer function times the perturbation of the inlet velocity. According to the analysis presented in Chapter 4, these particular transfer functions are expressed as follows (the symbol inside <> denotes the FORTRAN name used):

(a) Boiling boundary effect:

$$q\frac{\overline{y}_1}{U_1} = q\frac{\overline{y}_1}{\overline{U}_1}\frac{\overline{U}_1}{U_1} = q\frac{1-e^{-s\tau_1}}{s}\frac{\overline{U}_1}{U_1} = \langle TR1\rangle\frac{\overline{U}_1}{U_1} \qquad (5.1)$$

(b) Two-phase velocity effect:

$$\frac{\overline{U}_2}{U_1} = \frac{\overline{U}_1 - q\,\overline{y}_1}{U_1} = (1-\langle TR1\rangle)\frac{\overline{U}_1}{U_1} = \langle TR2\rangle\frac{\overline{U}_1}{U_1} \qquad (5.2)$$

(c) Superheat boundary effect:

$$q\frac{\overline{y}_2}{U_1} = \frac{r^* e^{-s\tau_2} - 1}{1 - s/\gamma q}\frac{\overline{U}_2}{U_1} + r^* e^{-s\tau_2} q\frac{\overline{y}_1}{U_1} =$$

$$= \frac{r^* e^{-s\tau_2} - 1}{1 - s/\gamma q} \langle TR2\rangle \frac{\overline{U}_1}{U_1} + r^* e^{-s\tau_2} \langle TR1\rangle \frac{\overline{U}_1}{U_1} =$$

$$= \langle TR3\rangle \frac{\overline{U}_1}{U_1} \qquad (5.3)$$

(d) Superheat velocity effect:

$$\frac{\overline{U}_3}{U_1} = \frac{\overline{U}_1 + q\,(\overline{y}_2 - \overline{y}_1)}{U_1} = \langle TR2\rangle \frac{\overline{U}_1}{U_1} + \langle TR3\rangle \frac{\overline{U}_1}{U_1} =$$

$$= \langle TR4\rangle \frac{\overline{U}_1}{U_1} \qquad (5.4)$$

From the form of the expressions in equations (5.1), (5.2), (5.3) and (5.4) and the form of each component of pressure drop perturbation as given in Appendix A, it can be seen that each transfer function (individual pressure drop perturbation (denoted with a general index i) over inlet velocity perturbation) can be made dimensionless by dividing $-\overline{\Delta P}_i$ by $\rho_f U_1^2$ and $\overline{U}_1$ by U_1. Therefore, the overall transfer function ($-\overline{\Delta P}_{TOT}/\overline{U}_1$) can be made dimensionless by this procedure, since it is in fact the sum of all the feedback signals (the process of linearisation permits the act of summation).

Both versions of the program calculate the individual transfer functions:

$$\left(\frac{-\overline{\Delta P}_i}{\rho_f U_1^2} \Big/ \frac{\overline{U}_1}{U_1}\right) \qquad (5.5)$$

for various values of the circular frequency ω ($s = \sigma + j\,\omega$, where $\sigma = 0$). Then, by combining them in the way described in section 4.6.2 of Chapter 4, they calculate the inverse of the closed loop frequency response (otherwise called total dimensionless dynamic impedance):

$$\frac{-\overline{\Delta P}_{TOT}/\rho_f\, U_1^2}{\overline{U}_1/U_1} \tag{5.6}$$

The version "FLOSIL" prints out the frequency response as given by equation (5.6) and also prints out each individual transfer function as given by equation (5.5). This permits consideration of the relative magnitudes and phases of the individual perturbed pressure drop components and assess the dominant ones contributing to the instability. This can, for example, be visualised by drawing a "vector" plot of all the perturbed pressure drop components. Instability occurs only if the magnitude in equation (5.6) equals zero for a certain value of ω (the frequency of oscillation). The version "FLOSIL" produces also a print out of the open loop frequency response (as defined in section 4.6 of Chapter 4), in order to assess the stability of the system concerned by applying Nyquist's criterion.

The version "GEFLOS", after calculating the values of the expression in equation (5.6) for the various values of ω, finds the minimum value of the magnitude in equation (5.6) and the corresponding frequency by calling subroutine "MINIMA". Then it repeats the same procedure for other values of power. The value of power for which the minimum value becomes zero is the threshold point of instability and the corresponding frequency is the frequency of oscillation.

By specifying an appropriate value for a FORTRAN variable <MDYN>, we instruct the program either to neglect or to allow for the

inertia of the heater wall.

Whenever the inertia of the heater wall is allowed for, the form of the perturbations given by equations (5.1), (5.2), (5.3) and (5.4) are modified according to the theoretical analysis in Chapter 4. For that case, subroutine "BESIMG" is called to evaluate the complex Bessel functions (Appendix C).

Similarly, slip may be allowed for or neglected by specifying an appropriate value for a FORTRAN variable <IDSL>.

For the cases of helical or straight geometry heaters, the following FORTRAN variables (supplied as "data") must be specified as indicated below:

		Helical geometry	Straight geometry
<HLDIAM>	$\hat{=}$	Helix diameter	0.0
<TURNS>	$\hat{=}$	Number of helix turns	1.0
<PITCH>	$\hat{=}$	Helix pitch	Total heated length

The way the problem has been formulated mathematically makes it possible to supply the steady-state pressure drop components as "data" without modifying that section of the program which calculates the dynamic (perturbations) part of the pressure drop components. The steady-state pressure drop components may be available from an accurate non-linear analysis of the steady-state or from experimental measurements.

The data for the thermodynamic and transport properties of Arcton-113 were taken from ICI's technical bulletins and the ASHRAE Handbook.

5.3 PROGRAM TESTS

5.3.1 Basis for Comparison and Program Testing

It would have been most useful to examine in the present work the validity of the computer programs FLOSIL and GEFLOS against available experimental instability data for helical geometry once-through steam generators in a parallel channel arrangement besides our experimental data.

Unfortunately, there are very few experimental results covering this subject available in the open literature. Even for results on instability in straight tubes in a recirculating design, insufficient details are available to enable us to make adequate use of them, for example, concerning the upstream and downstream geometrical arrangements (frictional distribution), which play an important rôle in the dynamic behaviour of the vapour generator considered. Furthermore, the threshold of instability is not always defined the same way.

For the present study, the data of Saha et al (1975) are used to form the basis of a comparison and examination of the effect of the different parameters on instability and to demonstrate the use of the program. However, we cannot draw conclusions from the results of Saha et al (1975) because we do not know the geometrical arrangements upstream and downstream of the test section. They lump together all the equipment upstream of the heated test section and assign an experimentally determined orifice coefficient, the same procedure being applied for the part downstream of the heated test section.

We have chosen these experimental data since the boiler they were experimenting on is similar in many respects to the one which was built by the present author.

The test section of Saha et al is a 2.743 m long, straight

vertical round tube made of stainless steel with outside diameter of 12.7 mm and inside diameter of 10.22 mm which is heated electrically. The fluid employed is Freon-113 at high pressures (≃ 10 - 13 bars) and inlet velocities (≃ 1 m/sec). A large by-pass runs parallel to the test section to impose a constant pressure drop. Upstream and downstream of the heated test section, two valves are installed in order to set the desired amount of throttling. A preheating unit is included in the test section part to regulate the subcooling. We believe that in this respect, the design of our experimental rig is superior in the sense that the preheating unit is installed before the inlet header (before the by-pass), therefore decoupling the effect of the preheating unit on the dynamic behaviour of the test section.

5.3.2 Results of Comparison and Effect of Various Parameters

Table 5.1 lists some of Saha et al (1975) experimental runs together with the theoretically predicted results applying our computer programs. The input data for the programs were chosen so as to allow for a comparison between the findings of Saha et al and the corresponding theoretical predictions. We took the same pressure, inlet velocity, inlet and outlet gags, and predicted the frequency and power at the threshold of instability.

Two cases are considered, namely the non-slip case ($S_d = 0$) and the slip case ($S_d \neq 0$). For both cases, we assumed a constant two-phase friction multiplier of 2, i.e. $f_2 = 2.f_1$, as also recommended by Saha et al (an accurate value of the two-phase friction multiplier was not available from steady-state measurements). For the non-slip case, we assumed a value for the slip coefficient $\gamma = 1.05$, lower than the value ($\gamma = 1.13$) recommended by Bankoff because of the relatively high

pressures of the system in question (Collier (1972)). We made some runs assuming γ = 1.13 which gave over-optimistic predictions for the threshold power. This is understandable since a high value of γ underestimates the void fraction at the higher exit qualities, an effect which is stabilising (Neal et al (1967)). On the other hand, by assuming γ = 1 (no slip), we obtain a pessimistic prediction of the threshold power.

For the sake of comparison only, say that the test section of Saha et al (1975) is a tube with a mean helix diameter of 0.28 m, a pitch of 0.25 m and three turns which give the same total length of 2.743 m. (These dimensions are fairly similar to our helical geometry tube test section which has a mean helix diameter of 0.3048 m, a pitch of 0.254 m and 3.5 turns which give a total length of 3.4 m.)

In the same Table, Table 5.1, the predicted conditions at the instability threshold for this fictitious helical geometry case (assuming S_d = 0 and $S_d \neq 0$) are indicated. Also, the case of very small subcooling (5 kJ/kg) is treated theoretically.

From Table 5.1 and Figures 5.1 to 5.10, it can be seen that, in general, the non-slip case gave predictions of the power and frequency at the instability threshold lower than the experimental results. On the other hand, the consideration of slip between the phases gave predictions of power and frequency higher than the experimental results.

Figures 5.1 to 5.6 are the outputs from GEFLOS for different runs. These Figures show the relation between both the minimum dimensionless dynamic impedance and the corresponding frequency versus power. The parameters (e.g. inlet velocity, pressure, subcooling, gags, etc.) are indicated on each Figure.

The threshold power and frequency are found by linear

extrapolation of the minimum dimensionless dynamic impedance against power to zero. For all the cases, it was found that the points near the instability threshold power were approximately on a straight line. It can also be seen that the minimum dynamic impedance starts to increase with power after reaching the zero value.

Figures 5.7 and 5.8 show the Nyquist plots of the open loop frequency response for runs I(a) and IV(a) (both for $s_d = 0$ and $s_d \neq 0$) at the experimentally observed instability threshold power. Figures 5.9 and 5.10 show the associated Bode plots of the inverse closed loop frequency response for run IV(a). All these Figures are the outputs from FLOSIL (the associated parameters are again shown on each Figure).

By comparing Figures 5.3, 5.7, 5.9 and 5.10, all corresponding to the same run, it can be seen that they are in agreement. Figure 5.3 shows that the non-slip case is unstable and the slip case is stable (at the experimental threshold power level). We reached the same results by applying Nyquist's criterion as can be seen from the Nyquist plots of Figure 5.7. The Nyquist curve passes to the left of the (-1,0) point for the non-slip case, while it passes to the right of the (-1,0) point when slip is considered. The same results were reached by applying the Bode plots (magnitude and phase against log frequency) of the dimensionless dynamic impedance as indicated in Figures 5.9 and 5.10. However, care must be taken here since the system is already unstable for the non-slip case (Figure 5.9), which is indicated only by the high jump of the phase-angle curve at the point of the dip of the amplitude curve, while the value of the amplitude at the dip point has started increasing again above zero after exceeding the threshold power level.

In general, the Nyquist plot of the open loop frequency response should precede the Bode plot of the inverse closed loop frequency

response since it will directly reveal the existence of unstable modes and their number. This is indicated by the number of times it encircles the (-1,0) point in a clockwise direction. The existence and the number of unstable modes (if any) from the Bode plot of the inverse closed loop frequency response is indicated by high jumps ($\simeq > 180^{o}$) in the phase-angle curve at the points of dip of the magnitude curve.

From Table 5.1 and Figures 5.1 to 5.10, it can be seen that the computer program predicts correctly the effects of the different parameters on instability as have been reported by numerous investigators as discussed in Chapter 2. These points are discussed in detail below.

Comparing sets IV, I and Figures 5.1, 5.2, 5.3, 5.4, it can be seen that for all the cases, an increase of the inlet orifice coefficient (inlet gagging) strongly stabilises the system. This was always predicted by the computer program.

Comparing sets I, III and Figures 5.2, 5.4, 5.5, it can be seen that a decrease in pressure level destabilises the system. This was always predicted correctly by the computer program. The destabilising effect with the decrease in pressure level is due to the large density variations during boiling at low pressure levels.

Comparing the runs of set IV and the runs of set I, it can be seen that the computer program predicts correctly the effect of the subcooling on instability. At low subcoolings, the increase of subcooling has a destabilising effect, while at higher subcoolings, the increase of subcooling has a stabilising effect. The position of the minimum in the "subcooling-power at instability" curve depends strongly upon the single-phase friction factor selected.

While most of the other investigators have reported that an increase of outlet gagging destabilises the system, this was not found

to be so by the computer program. Sometimes the effect was found to be stabilising and sometimes destabilising. This effect was also reported by Saha et al (1975), who found from their experimental investigation that in most cases the effect of an increase in the outlet orifice coefficient had a stabilising effect. This can be seen by comparing sets I(a) and VII and also Figures 5.4 and 5.6. The complicated effect of the outlet restrictions has been discussed by Neal et al (1967). From a linear analysis point of view (as is the case in our analysis), this can be explained by the fact that the outlet pressure drop component is not always favourable (in terms of its phase) to destabilising the system. For example, the vector plots of Figures 5.11 and 5.12 show that the outlet frictional pressure drop perturbation is not out-of-phase with the inlet velocity perturbation.

From Table 5.1 it can be seen that the computer program predicts correctly the increase of the potential frequency of oscillations with increasing power when keeping the subcooling constant. It can also be observed that the program predicts correctly the decrease of the potential frequency of oscillations with increasing subcooling when keeping the power constant. This is because, as has been reported by many investigators such as Yadigaroglu and Bergles (1972), Dorsch (1967), Neal et al (1967) etc., the period of density wave oscillations is roughly equal to the transit time of the fluid particles in the heater. The total transit time through the subcooled, two-phase and superheat regions can be calculated easily from the theoretical analysis of Chapter 4 for the non-slip case (homogeneous flow) as:

$$t_{TOT} = t_1 + t_2 + t_3 = \frac{\rho_f}{Q_v} \Delta h_{sub} +$$

$$+ \frac{h_{fg}}{Q_v} \frac{\rho_f \rho_g}{\Delta\rho} ln \left(1 + \frac{\Delta\rho}{\rho_g} x_{ex}\right) + \frac{\rho_g}{Q_v} \Delta h_{sup} \qquad (5.7)$$

The computer program can also predict higher order oscillations (for example, by increasing the power), which will be revealed by more than one encirclement of the (-1,0) point of the open loop frequency response or from dips of the magnitude (and jumps of phase-angle) at higher frequencies of the Bode plot of the inverse closed loop frequency response function.

Table 5.1 shows that the helical geometry case is slightly more unstable than the corresponding straight geometry case. The reason for that can be seen from the vector plot of the pressure drop components for the straight and helical geometry configurations. For example (for the run I(a)), from Figures 5.11 and 5.12 it can be seen that the dominant component contributing to instability is the two-phase friction. Therefore, the increased two-phase friction due to the helical shape deteriorates the stability of the system. It must be emphasised that this is not a general conclusion and in other cases, where, for example, the two-phase gravity component is the dominant one, the effect of helical geometry could be stabilising by reducing the magnitude of the two-phase gravity component (see from Figures 5.11 and 5.12 the relatively high phase of the two-phase gravity vector). Generally speaking, any of the feedback components can be the dominant cause for the instability, depending on the design and the operating conditions of the vapour generator in question. The vector plots of Figures 5.11 and 5.12 have been obtained by running FLOSIL for the straight and helical geometry

case, respectively, taking the slip between the phases into account. These Figures show the pressure drop components at almost zero frequency, at the unstable frequency and at the intermediate frequency of 0.355 Hz.

The results so far have been obtained by not taking into account the dynamics of the heat source. When the inertia of the heater wall was taken into account, the predicted power threshold was much higher than the reported experimental one. For the data of Saha et al (1975), which formed the basis for our program testing, the parameters associated with the heater wall were taken as:

$$K_m = 0.032 \text{ kW/m}^{\circ}\text{C} \quad , \quad c_m = 0.460 \text{ kJ/kg}^{\circ}\text{C}$$

$$\rho_m = 7800 \text{ kg/m}^3 \quad \text{therefore,} \quad a_m = 8.92 \times 10^{-6} \text{ m}^2/\text{sec}$$

inside diameter $d_i = 1.02$ cm , outside diameter $d_o = 1.27$ cm

The time constants associated with the heater dynamics, as given in Chapter 4, are found as follows from our computer program (run I(a)):

$$\tau_k = 2.928 \text{ sec} \quad , \quad \tau_f = 2.891 \text{ sec} \quad \text{and} \quad \tau_h = 14.123 \text{ sec}$$

It can be seen that $2\pi\ \tau_k$, $2\pi\ \tau_f$ and $2\pi\ \tau_h$ are much higher than the period of oscillations associated with this work (τ = 1 - 5 sec). Therefore, the high frequency approximation as given by Yadigaroglu and Bergles (1972) can be applied up to a certain frequency, i.e.

$$\frac{\delta Q''}{Q''} = b \frac{\delta U_1}{U_1} \tag{5.8}$$

which gives the modulation of the heat input into the fluid $\delta Q''$

associated with an inlet velocity perturbation δU_1 (see also section 4.4.1). The parameter b (0.80 or 0.85) is defined as the exponent of the Reynolds number in the heat transfer correlation of equations (4.14a) and (4.14b).

In that case, the transfer function due to the boiling boundary movement (equation (5.1)) becomes:

$$\langle TR1 \rangle_{INERTIA} = (1 - b) \langle TR1 \rangle = (1 - b)\, q\, \frac{1 - e^{-s\tau_1}}{s} \qquad (5.9)$$

i.e. the boiling boundary movement perturbation is reduced by a factor of 5, which has a strong stabilising effect.

Equations (5.8) and (5.9) hold up to a particular frequency, since the parameter $b \to 0$ for $\omega \to \infty$. The more important the heat storage mechanism in the wall (high τ_k), the higher the frequency at which equations (5.8) and (5.9) hold to a good approximation. Physically this is related to whether the tube material has sufficient thermal capacity to sustain the heat flux-flow interactions at higher frequencies as explained by Verheugen et al (1967) and Moxon (1973).

Moxon (1973) reported the strong stabilising effect of the heat flux-flow interaction for the case of a helical once-through steam generator heated by a pressurised primary fluid in counter-flow. The worth of the couplings was about a factor of five on the gag size.

All these effects are revealed from a polar plot of the <TR1> transfer function as given by FLOSIL. For the run I(a), where slip is taken into account, Figure 5.14 gives the polar plots of the <TR1> transfer function for the cases where the heater dynamics is taken into account and not. The reduction in the magnitude of <TR1> is quite considerable due to the heat flux-flow coupling.

Figure 5.15 gives the corresponding polar plots for a fictitious case with time constants:

$$\tau_k = 0.100 \text{ sec} \quad , \quad \tau_f = 0.400 \text{ sec} \quad \text{and} \quad \tau_h = 0.200 \text{ sec}$$

In that case, the two <TR1> transfer functions are quite the same, since $2\pi\ \tau_k$, $2\pi\ \tau_f$ and $2\pi\ \tau_h$ are now lower than the period of oscillations and therefore the low frequency approximation, as given by Yadigaroglu and Bergles (1972) applies, i.e. equations (5.8) and (5.9) with $b = 0$, even at low frequencies. Physically this means that the thermal capacity of the heater wall is not sufficient (τ_k low) to sustain the heat flux-flow interactions, therefore the modulation of the heat input into the fluid due to an inlet velocity perturbation is zero and there is not reduction to the value of the boiling boundary movement perturbation.

The effect on instability is clearly shown in Figure 5.13, which is a plot of the open loop frequency response function for run I(a) for the two different heater time constant sets.

5.4 CONCLUSIONS

With reference to the previous section, it can be concluded that the present computer program predicts correctly the effect of the various parameters on instability (i.e. effect of gags, pressure, subcooling, power, etc.), as reported by several investigators, and gives reasonable predictions with reported experimental data.

The results have shown that the selection of slip between the phases (void fraction relationship) and the two-phase friction multiplier are very important factors in assessing quantitatively the stability of the system.

The effect of heat flux-flow interactions has been demonstrated. It is found that the inclusion of heater dynamics in the single-phase region could change considerably the conditions at the threshold point, depending on the values of the heater-wall time constants.

It has been shown that the potential frequency of oscillations is affected by the residence time of the fluid particles in the heater, which mainly depends on the subcooled residence time of the flow. Therefore, the inclusion of a subcooled boiling region would modify this frequency and also the power at the instability point since it would change the values of the "effects" described by equations (5.1), (5.2), (5.3) and (5.4).

The different stability criteria produced by the computer program (Nyquist plots, Bode plots, minimum hydraulic dynamic impedance and vector plots of the various pressure drop perturbation components) are capable of providing detailed information and insight into the mechanism of instability.

It is recognised that a complicated non-linear analysis would possibly give better quantitative agreement (for a specific system) with

experimental results but at the expense of much longer computer time.

The main advantage of the present computer program is that it is fast running and is based on a theoretical model (presented in Chapter 4), which includes important features for the stability of the system concerned.

The author believes that there is need for extensive testing of the program, against experimental data, in order to assess its merits. Unfortunately, such experimental data on stability of vapour generators are scanty, especially those having helically coiled tubes in a once-through design.

TABLE 5.1

Set	P (bar)	K_i (v.h.)	K_e (v.h.)	u_{fi} (m/s)		Δh_s (kJ/kg)	Q (kW)	Predicted Q (kW)				f (Hz)	Predicted f (Hz)			
								Straight Tube		Helical Tube			Straight Tube		Helical Tube	
							Exper.	$S_d = 0$	$S_d \neq 0$	$S_d = 0$	$S_d \neq 0$	Exper.	$S_d = 0$	$S_d \neq 0$	$S_d = 0$	$S_d \neq 0$
IV	12.1	6.55	2.03	0.98		5.0		10.00	11.40+				1.100	–		
					a	13.7	8.50	7.35	11.40	6.90	9.75	0.785	0.550	0.810	0.480	0.680
					b	24.4	7.00	8.40	12.50			0.425	0.360	0.480		
I	12.1	2.85	2.03	0.98		5.0		6.85	9.60				0.850	1.260		
					a	11.4	7.50	5.20	7.75	5.10	6.80	0.835	0.460	0.660	0.420	0.560
					b	24.4	5.00	6.80	9.20			0.420	0.260	0.330		
					c	54.2	9.20	13.60	9.20+			0.335	1.160	–		
VII	12.1	2.85	10.66	0.98		11.4	6.50	6.80	10.60	6.50	9.20	0.645	0.420	0.660	0.390	0.560
III	10.3	2.85	2.03	1.02		9.3	6.50	4.75	6.65	4.70	6.00	0.780	0.500	0.680	0.460	0.580

Data from Saha et al (1975)

$\gamma = 1.05$, $f_2 = 2.f_1$, wall dynamics ignored

+ higher than indicated value

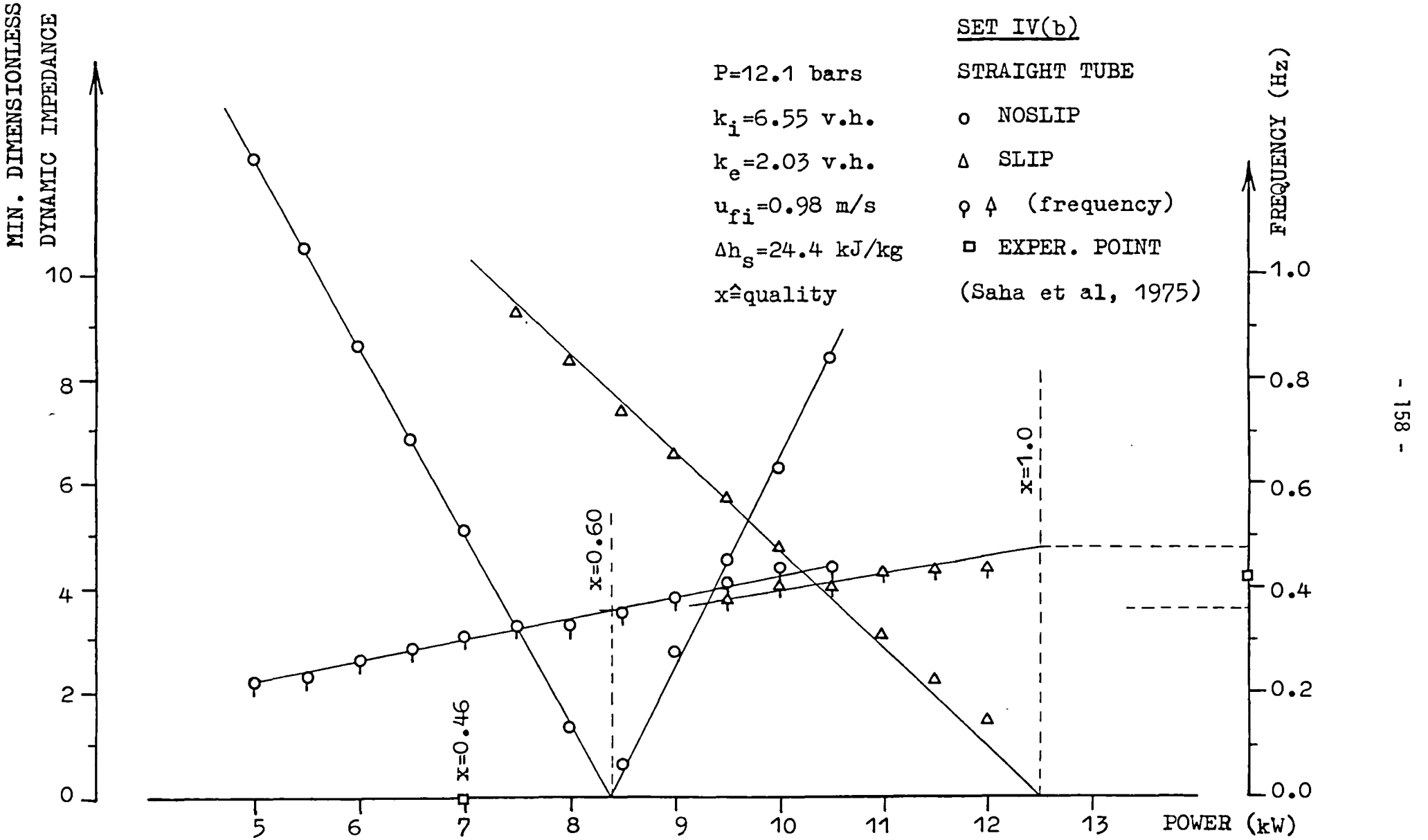

Figure 5.1: Power and frequency at the instability threshold

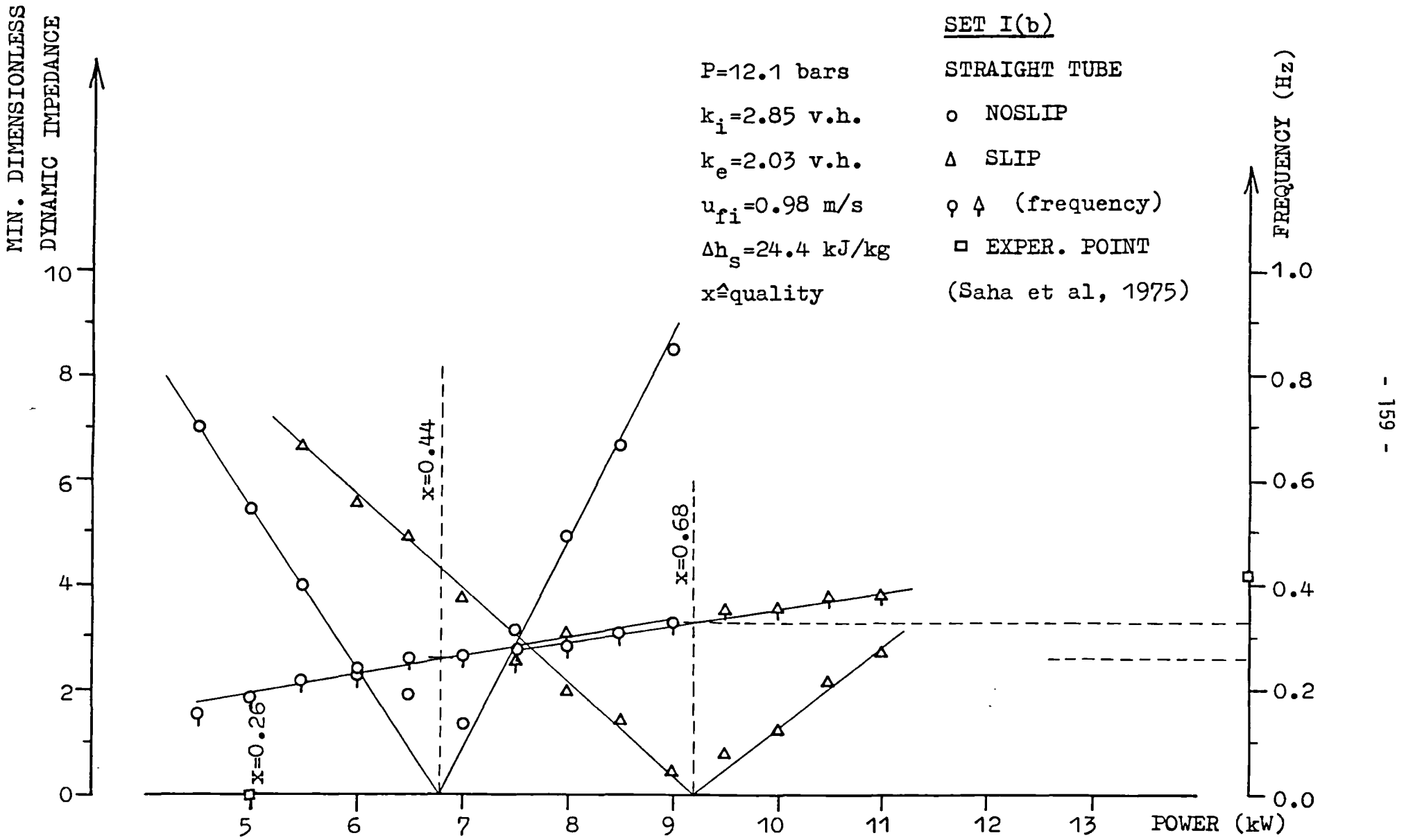

Figure 5.2: Power and frequency at the instability threshold

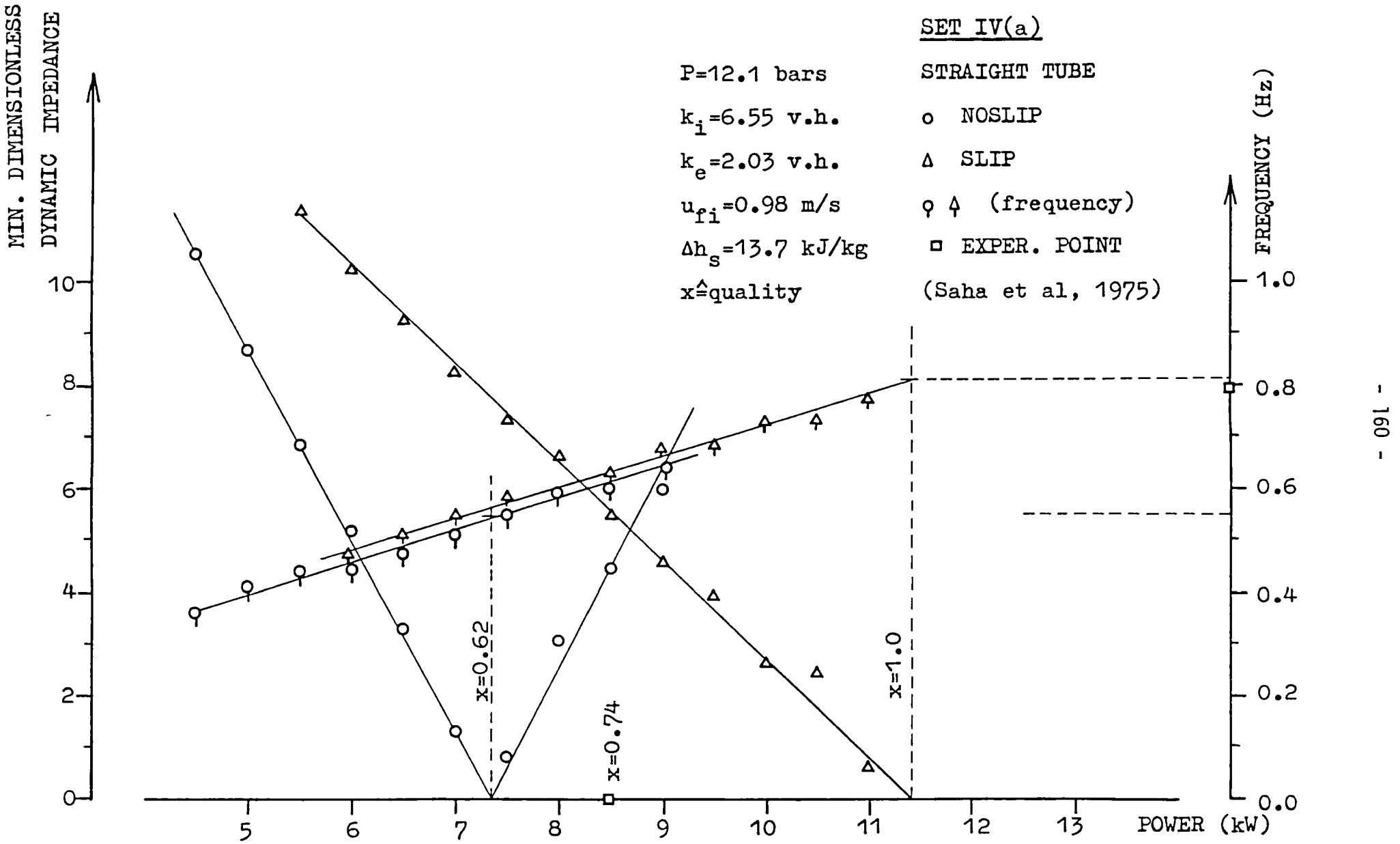

Figure 5.3: Power and frequency at the instability threshold

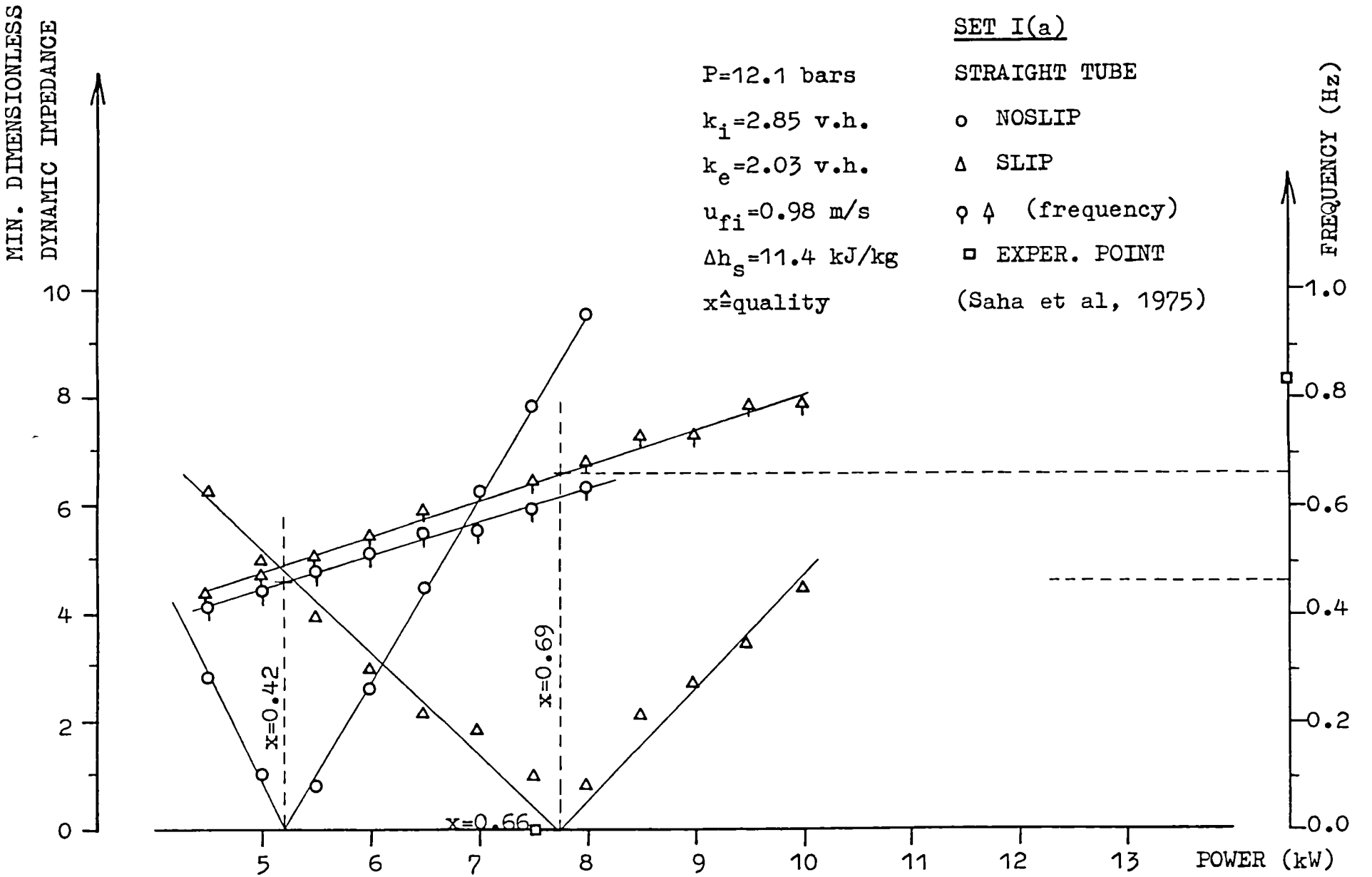

Figure 5.4: Power and frequency at the instability threshold

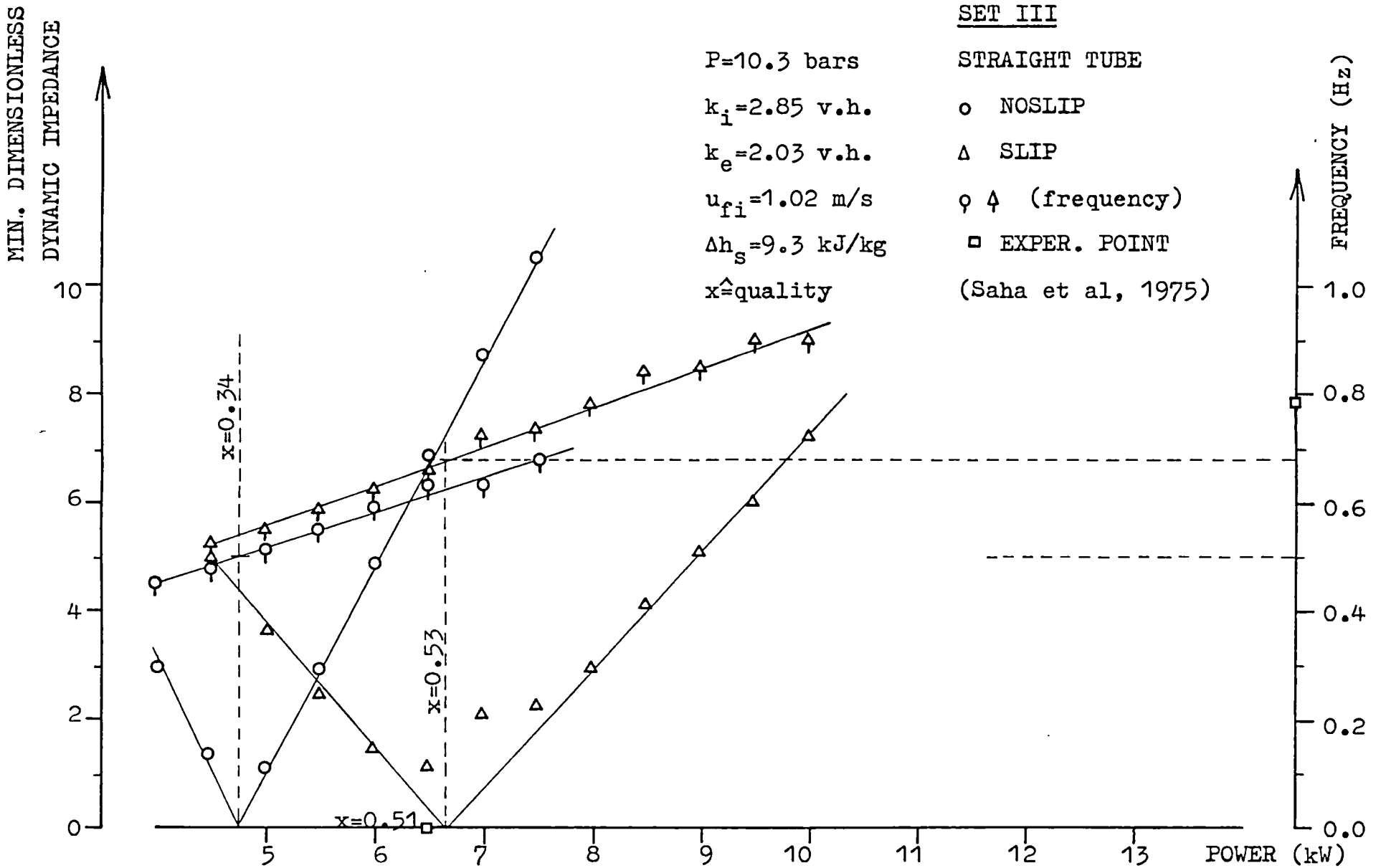

Figure 5.5: Power and frequency at the instability threshold

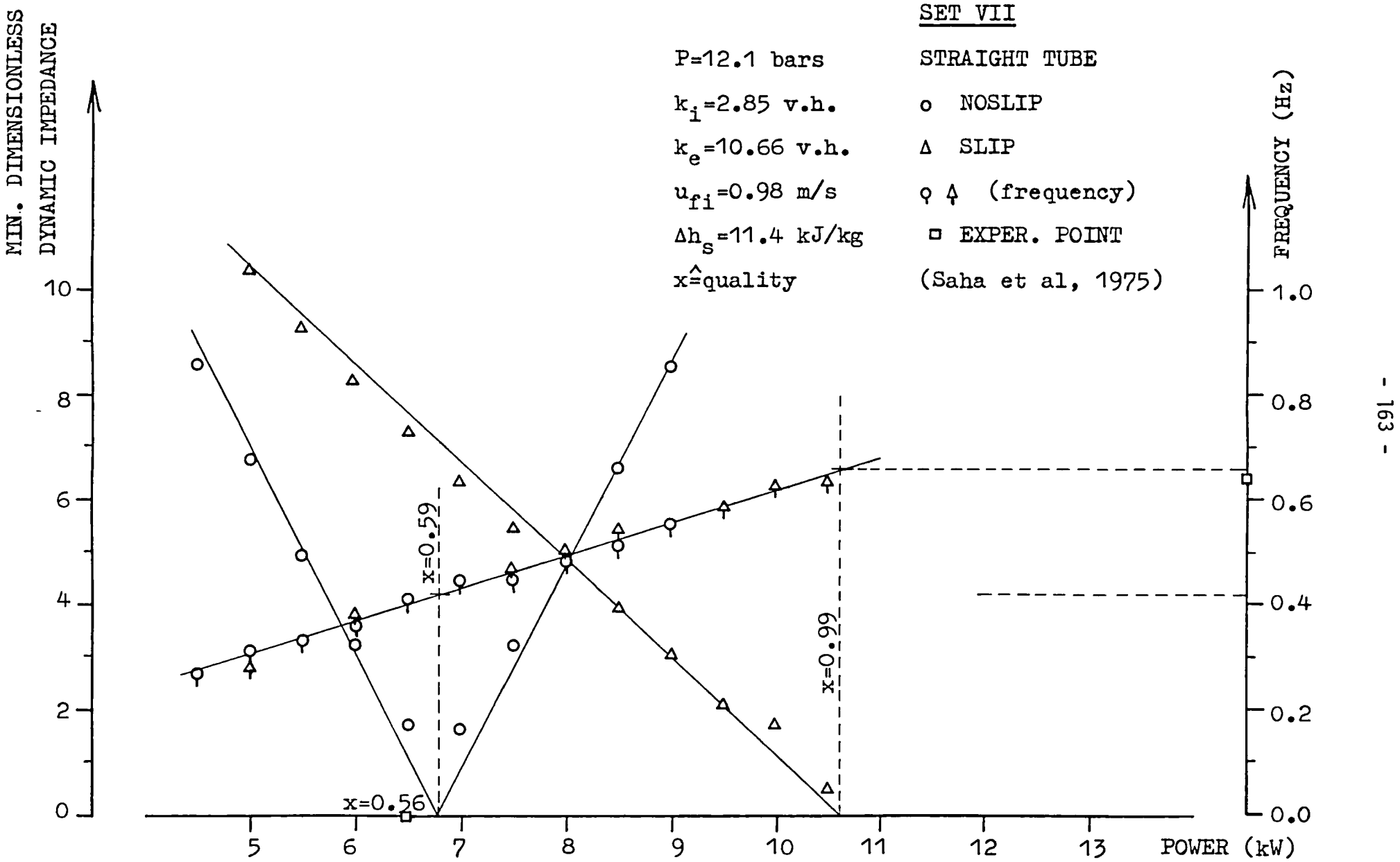

Figure 5.6: Power and frequency at the instability threshold

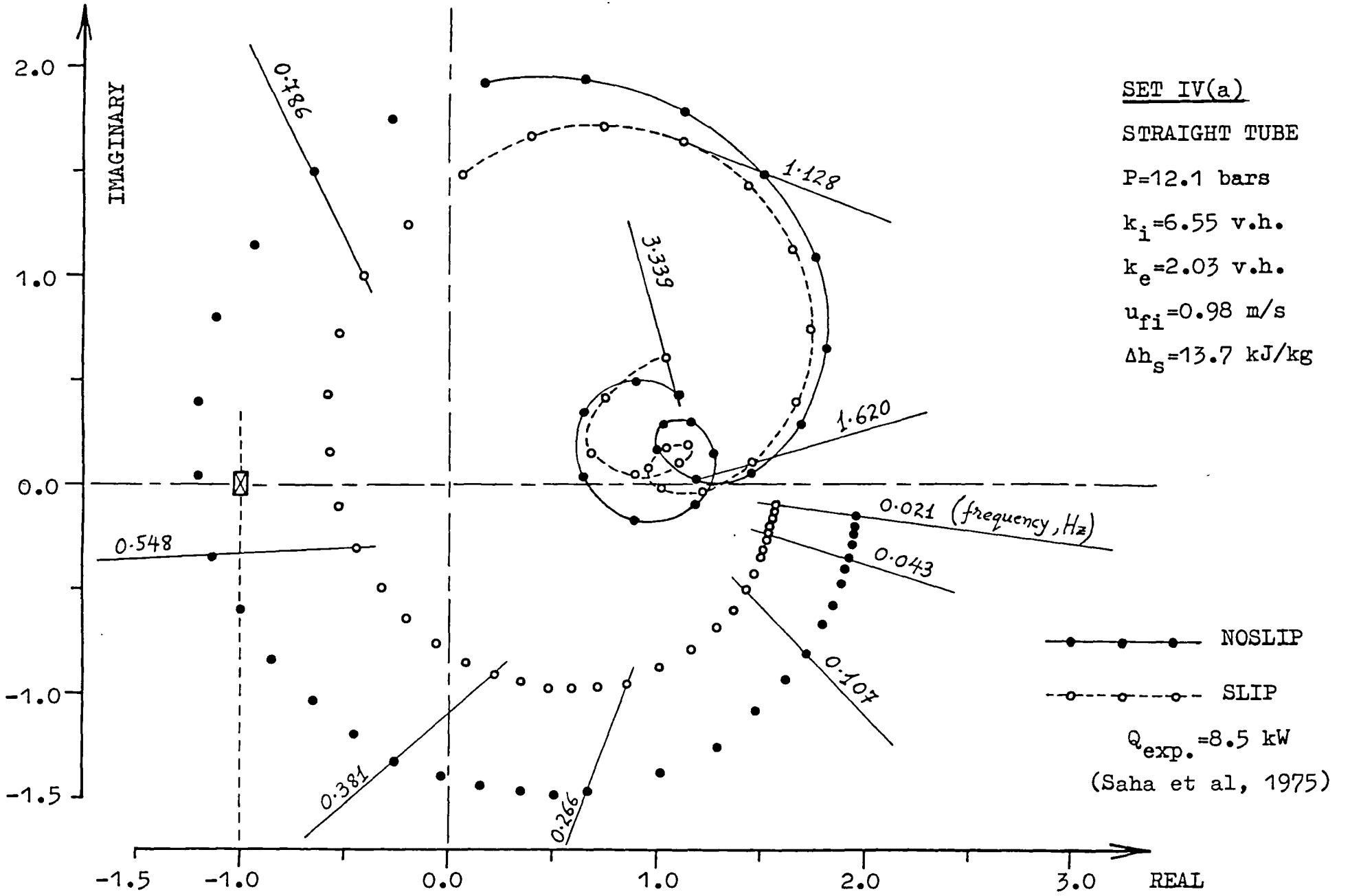

Figure 5.7: Open loop frequency response at the experimental threshold power

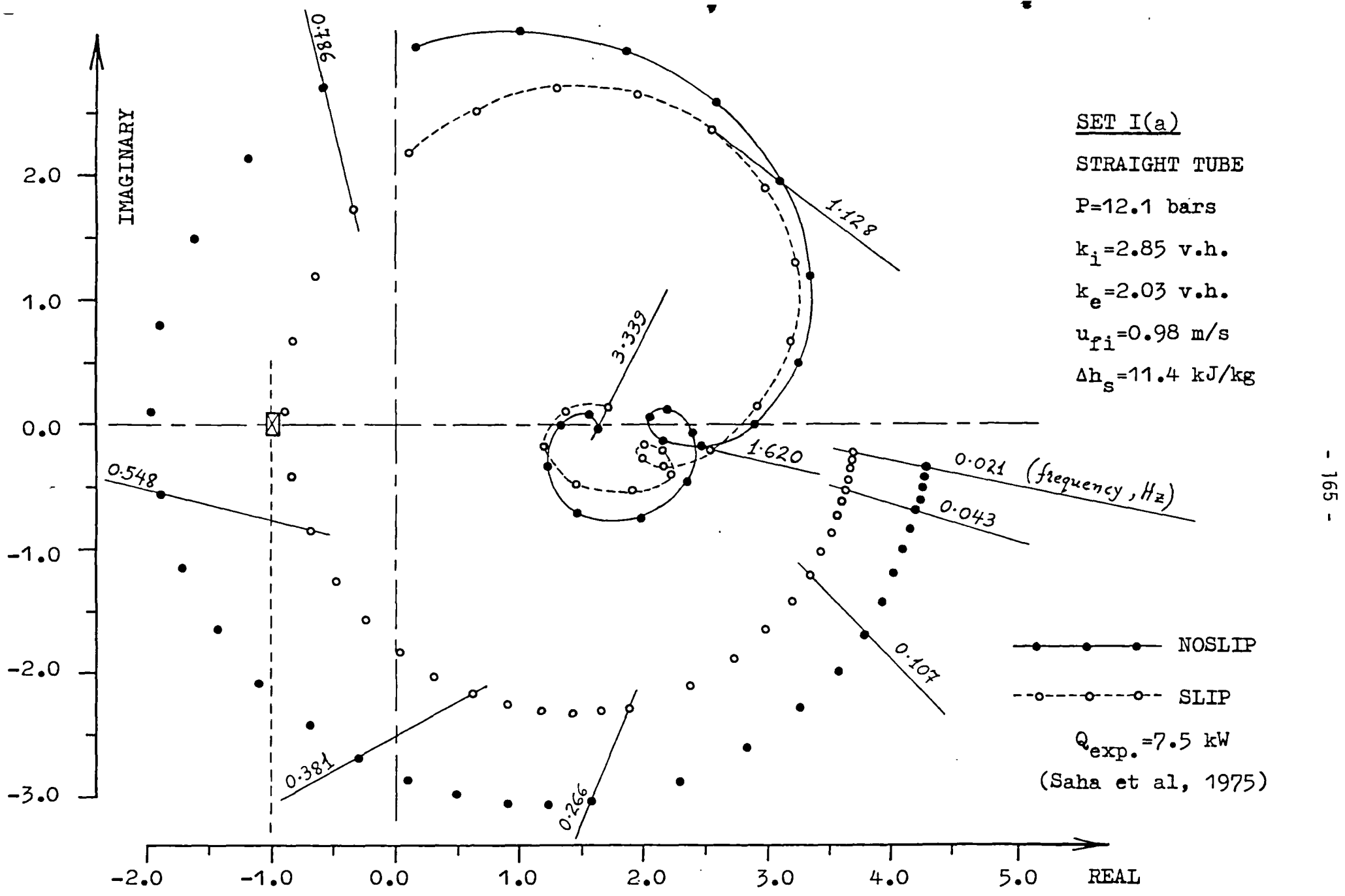

Figure 5.8: Open loop frequency response at the experimental threshold power

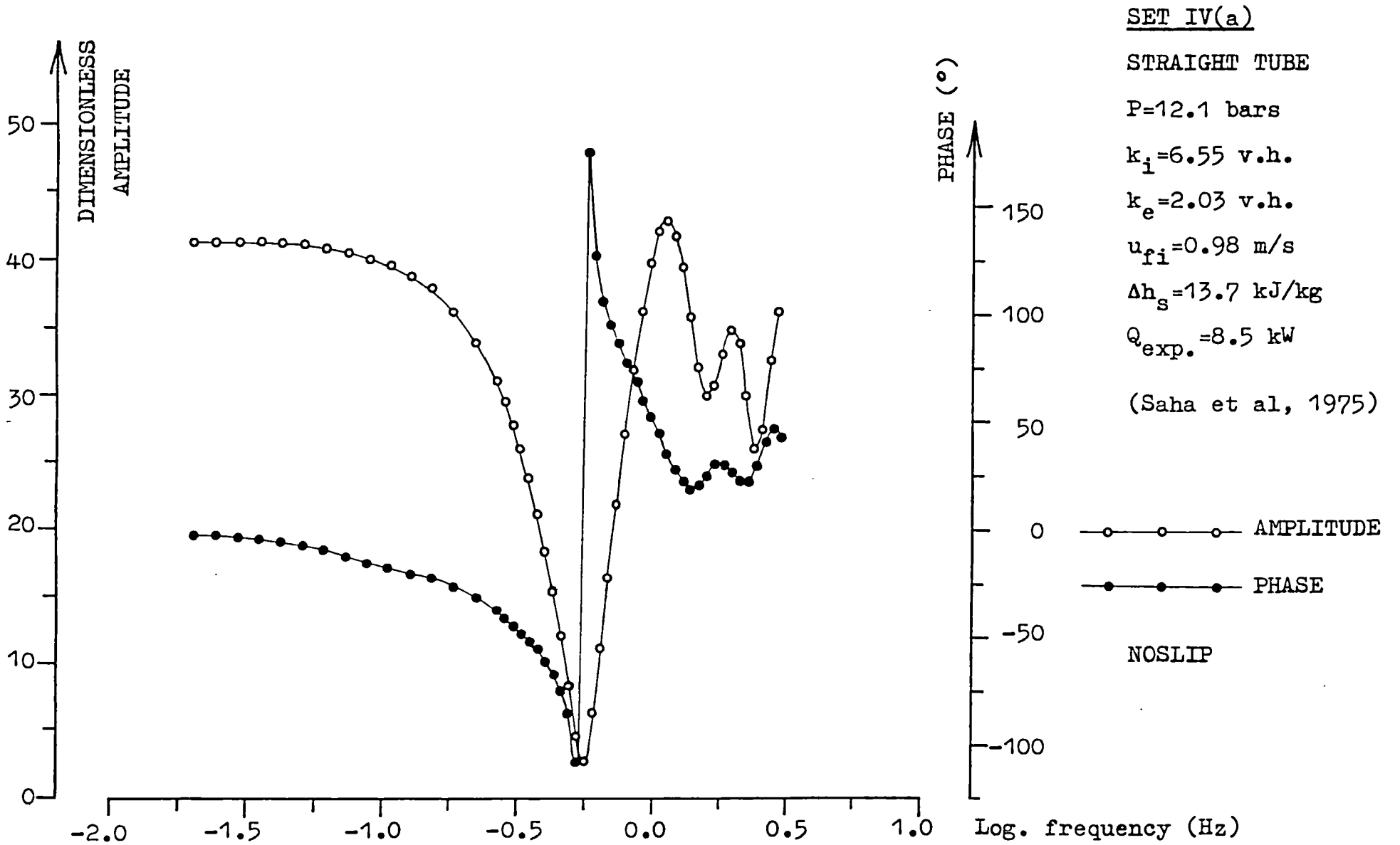

Figure 5.9: Bode plot of the inverse closed loop frequency response at the experimental threshold power

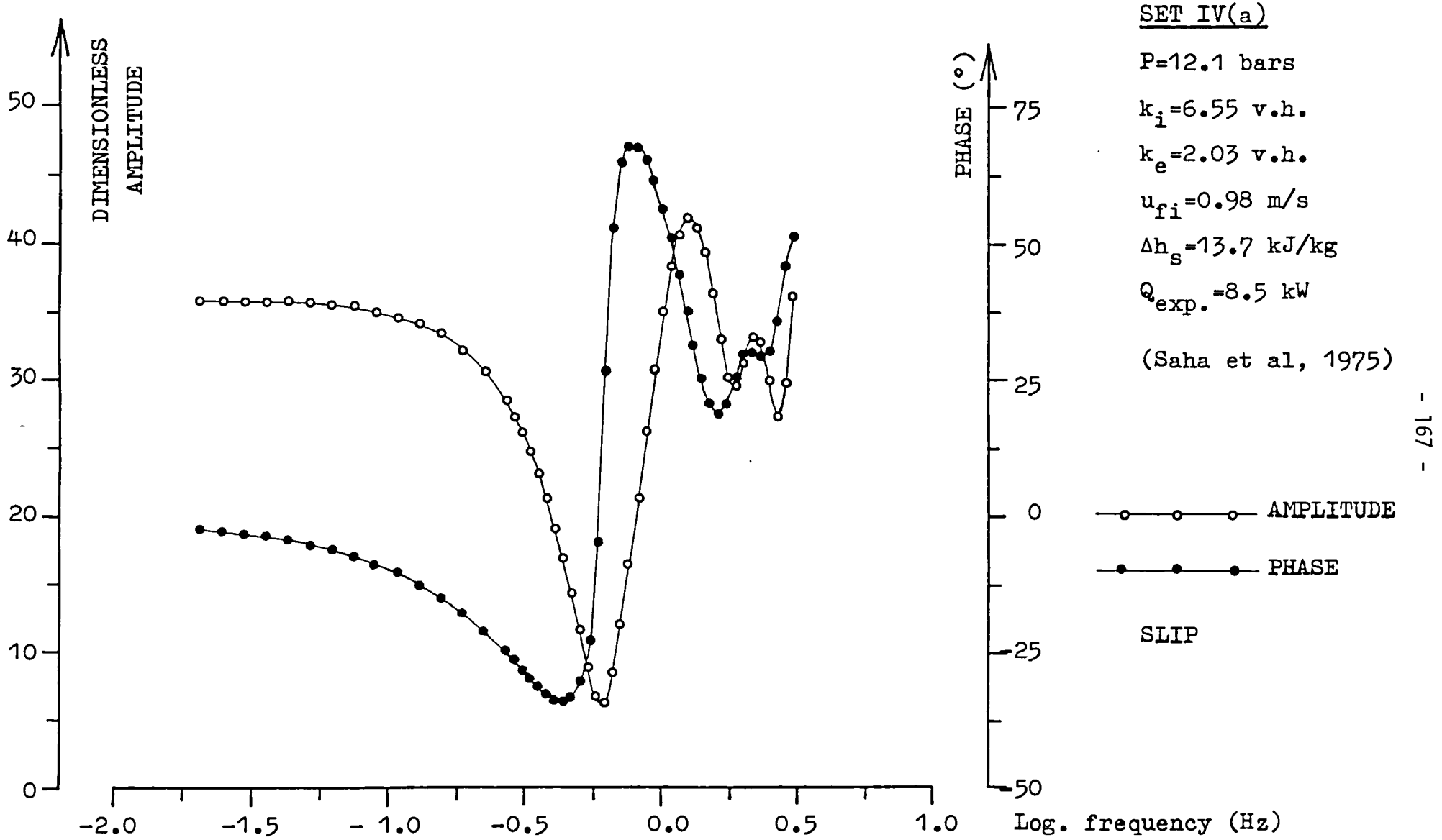

Figure 5.10: Bode plot of the inverse closed loop frequency response at the experimental threshold power

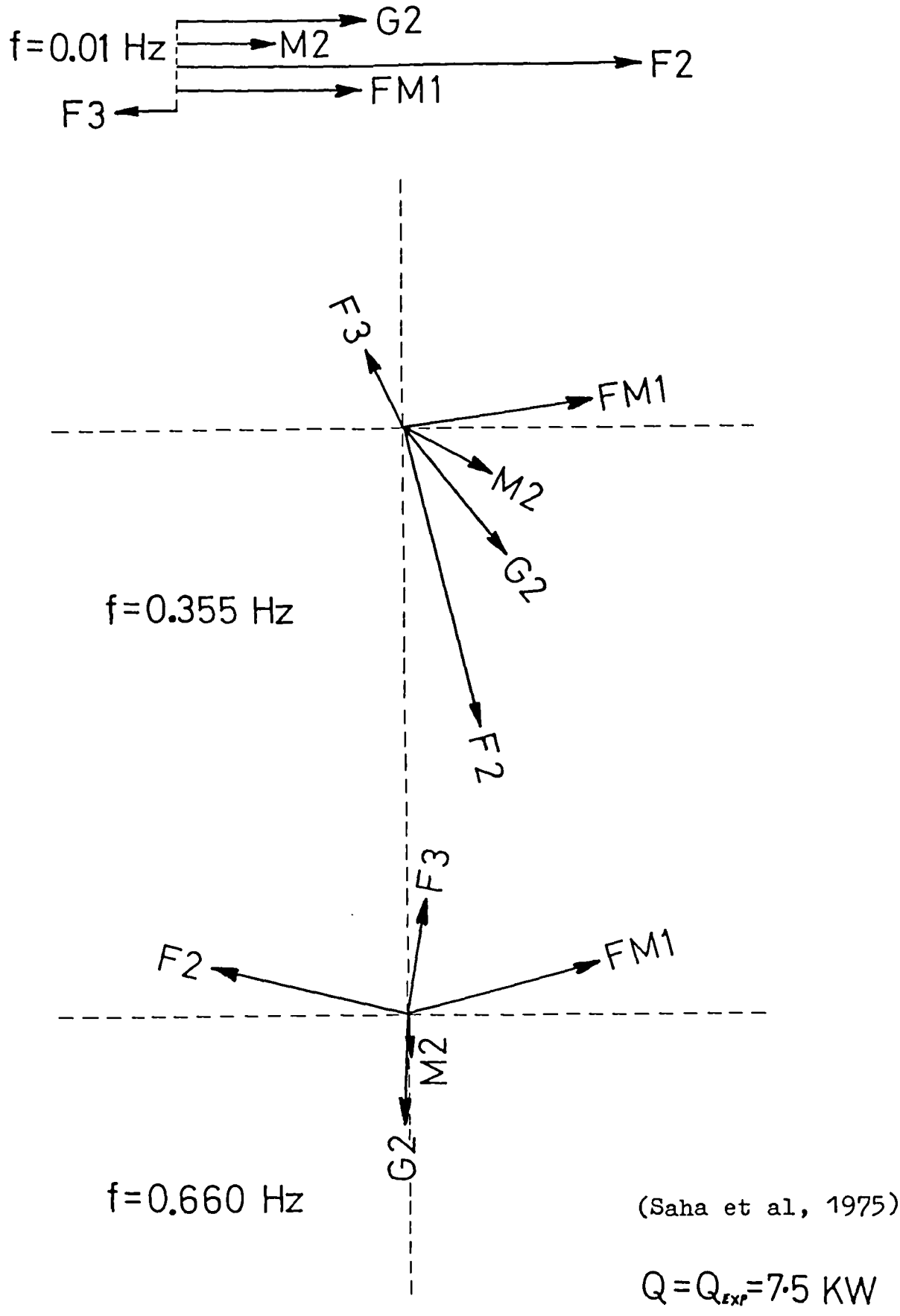

Figure 5.11: Vector plot of pressure drop components
Set I(a). Straight tube. Slip.
(frequency of oscillations 0.660 Hz)

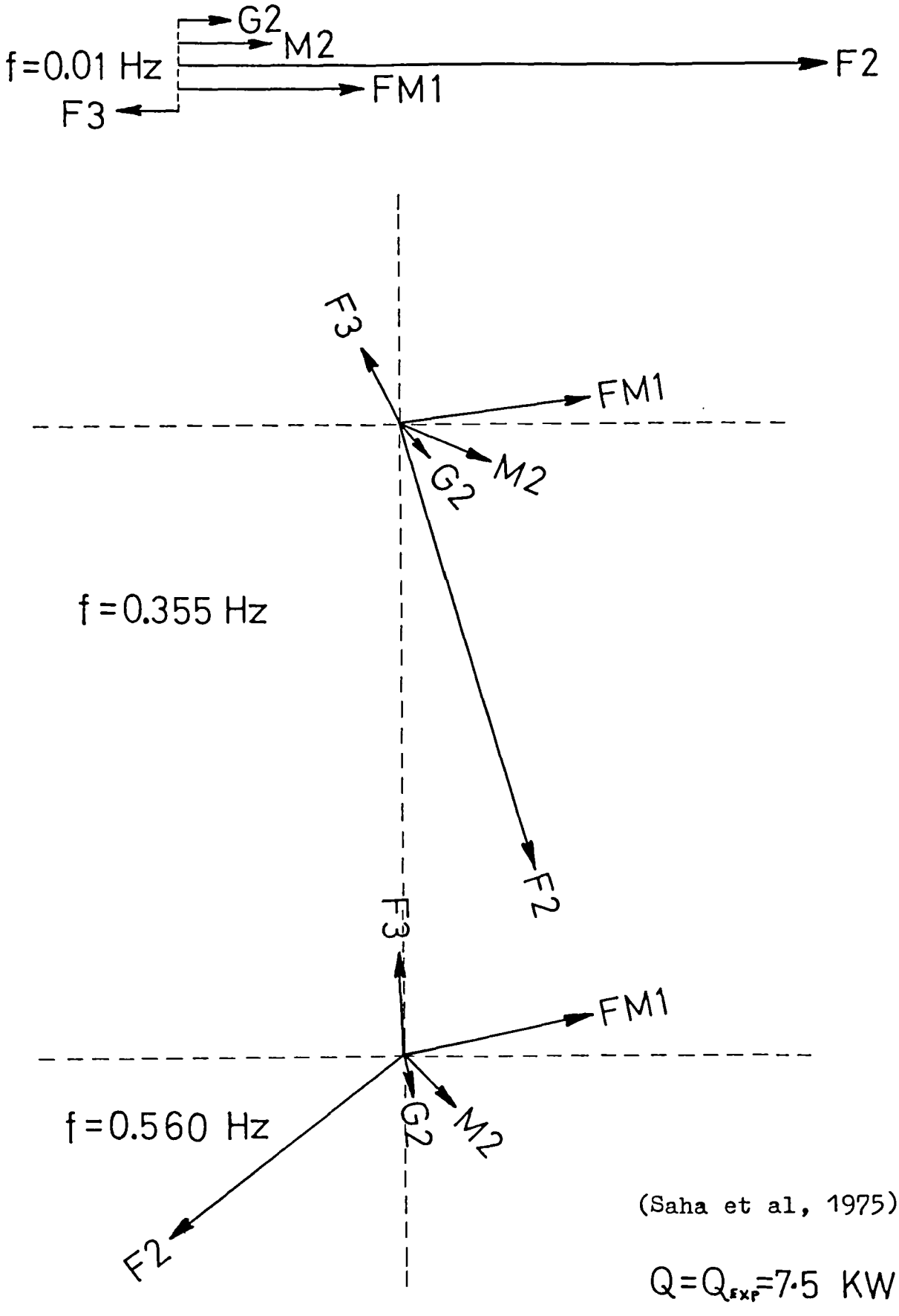

Figure 5.12: Vector plot of pressure drop components

Set I(a). Helical tube. Slip.

(frequency of oscillations 0.560 Hz)

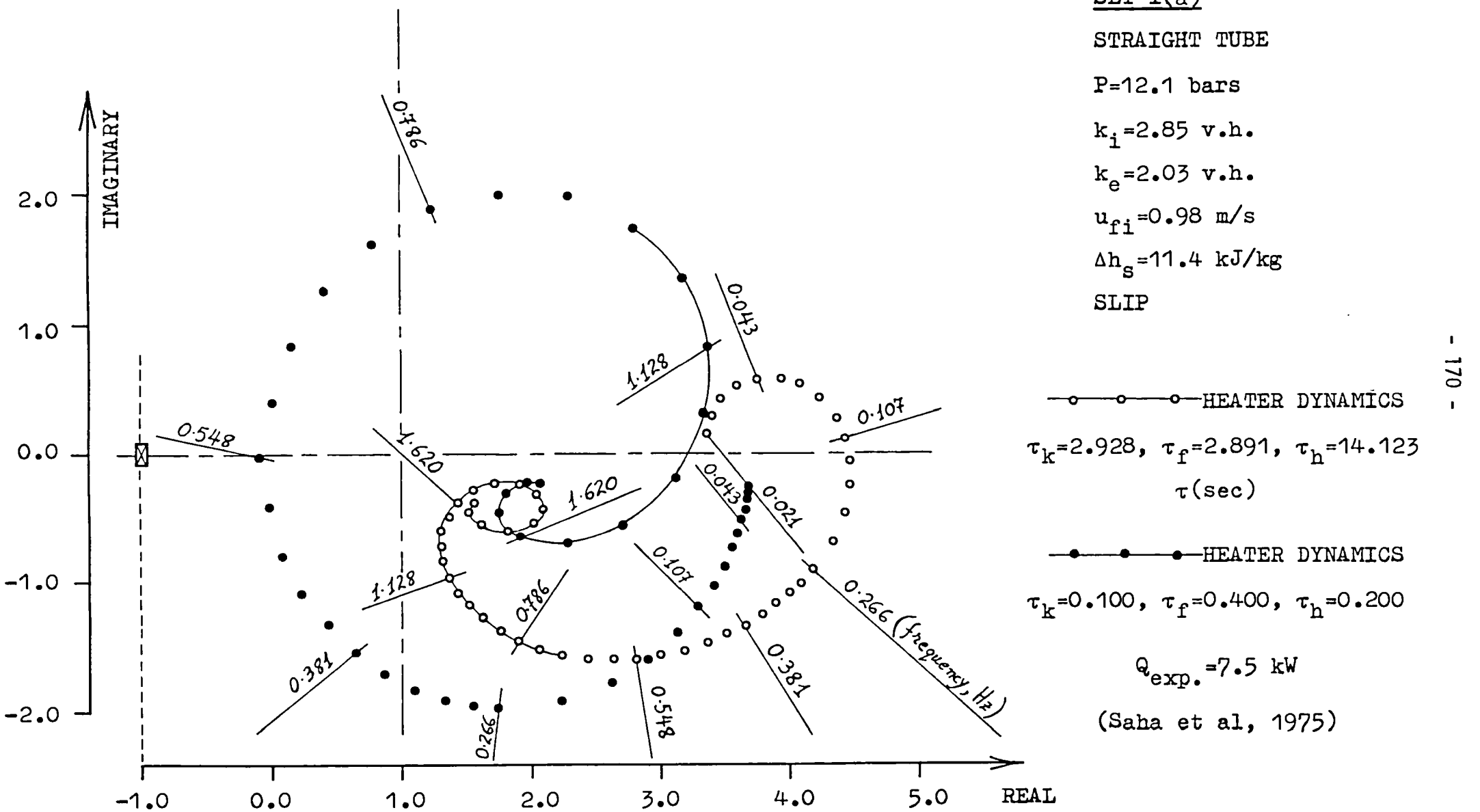

Figure 5.13: Open loop frequency response - Effect of heater dynamics

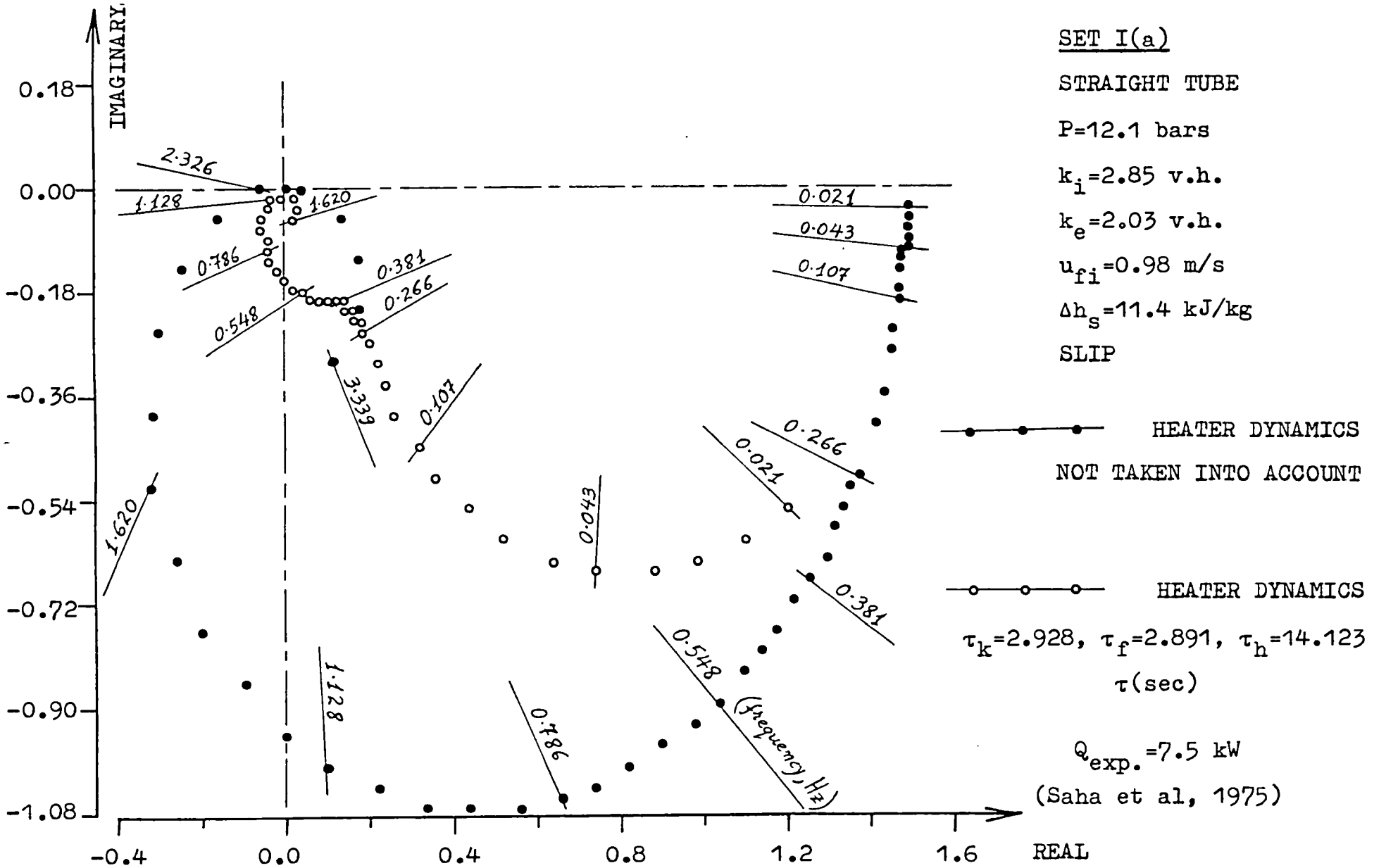

Figure 5.14: Polar plot of <TR1> transfer function - Effect of heater dynamics

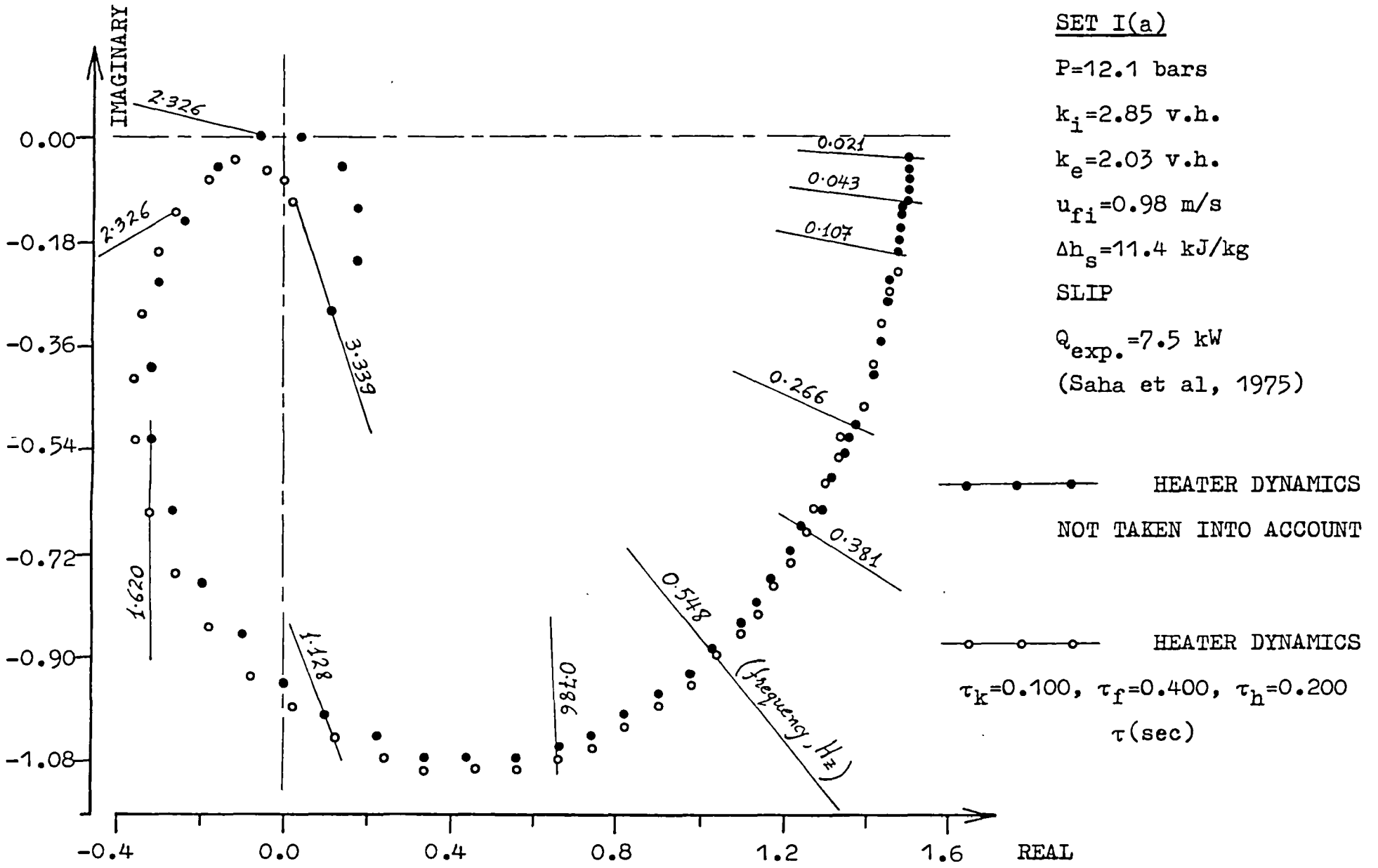

Figure 5.15: Polar plot of <TR1> transfer function - Effect of heater dynamics

CHAPTER 6

DESCRIPTION OF THE EXPERIMENTAL FACILITY

6.1 INTRODUCTION

This chapter describes an experimental facility designed, constructed, commissioned and operated by the present author in order to investigate the dynamic characteristics (with special reference to density wave instabilities) of an once-through helical monotube boiler, employing Freon-113 as the working medium, with a constant pressure drop maintained across it.

As pointed out by Potter (1973), there seems to be very few experimental programmes covering the subject of two-phase flow dynamics. Furthermore, the accumulation of basic knowledge is slow and always tends to be specific to the particular design of the actual boiler or demonstration test rig.

In the present experimental work, instruments of high reliability, and modern methods of data acquisition and processing techniques were used.

In order to achieve our objective within the constraints of operating a rather small system at relatively low pressure and power requirements, we have selected to use Freon-113 as the first test fluid. The design of the rig had to be within the limits of the College budget.

The design, manufacture, erection, commissioning and operation of the two-phase loop facility was not an easy task and it took the present author more than two years to build it.

Since the idea was to make available a tool in which specific single and two-phase flow phenomena could be investigated, an effort was made to build a highly flexible system operating in a wide range of variables by using the appropriate components, control equipment, safety devices and instrumentation.

6.2 CHOICE OF WORKING FLUID

As described in Chapter 2, fluids used for simulation, such as the refrigerant family, are particularly favoured because of their small heats of vapourisation and low critical pressures and temperatures compared with those of water. Therefore, the required experimental rigs are simpler and less expensive, and the test sections could be operated at lower pressures and temperatures requiring only moderate heat fluxes. This also permits operation throughout the unstable region or during oscillatory behaviour even when dry wall conditions exist.

Several of the Freons belonging to the refrigerant family (such as Freon-11, Freon-12, Freon-21, Freon-22, Freon-113, etc.), are commercially available having non-corrosive properties.

Since it has been established that the density ratio of the two phases is one of the important parameters in simulation, as mentioned by Stevens and Macbeth (1970) and Crowley and Bergles (1970), and since Freon-12 and Freon-113 resemble water in their pressure-density characteristics, the selection was decided to be between these two grades of Freon.

The boiling point of Freon-113 at ambient conditions is 117.6^{o}F, which is higher than the ambient temperature, and therefore it is easily stored in liquid form under normal ambient conditions. On the other hand, Freon-12 has a lower saturation temperature than the ambient one. Therefore, the selection of Freon-113 was favoured.

Freon-113 is non-flammable, clean, safe to use and it is easily available in the United Kingdom, being manufactured in large quantities.

6.3 GENERAL DESCRIPTION OF THE EXPERIMENTAL RIG

The main purpose of the experimental investigation was to obtain the steady and non-steady operating characteristics of two-phase one-component flow in forced convection vertical upflow in parallel heated channels of helical geometry with a constant pressure drop boundary condition imposed across the channels.

Figure 6.1 is a drawing of the Freon-113 rig, and Figure 6.2 gives a diagram of the flow path of the loop.

The test facility consists mainly of one fluid loop which supplies the test section (coil) and the parallel by-pass with continuous flow of Freon-113. A circulating centrifugal pump is positioned at a lower level and supplies the pressure and flow. The performance characteristics of the pump allow for substantial throttling prior to the test section to provide a stiff system and decouple the pump, condenser, holding tank and the rest of the components from the test section.

To minimise the possibility of flow oscillations, due to system component interactions, no accumulators or fluid surge chambers are included upstream of the test section, as these component interactions can lead to misleading experimental dynamic behaviour which reflects the behaviour of the loop rather than that of the evaporator.

The fluid discharged from the pump passes through a serpentine-type preheater and then is divided into two streams; one of the streams goes to the test section while the other passes through the by-pass.

The design is such that with all the valves open, about 15% of the fluid leaving the preheater passes through the test section while the rest passes through the by-pass. The presence of the parallel by-pass places the heated test section to be operated under constant pressure drop, hence decoupling the test section from the dynamics of the rest of

the loop. The constant pressure drop imposed by the parallel by-pass approximates the conditions existing in a large tube bundle.

Valves permit the regulation of the division of the flow between the test section and the by-pass.

Vapourisation occurs in the test section and the two-phase flow mixture flows through the riser into a plenum tank where it mixes with the by-pass flow and then flows into the condenser.

The condenser capacity is greatly in excess of that required to decouple the fluid flow downstream of the test section from the remainder of the loop. The condenser is of the vertical type and a high degree of subcooling is achieved by means of an inverted U tube at the exit of the condenser (see Figure 6.1). This is necessary to avoid cavitation in the pump.

The subcooled condensate is returned to the holding tank, which, in turn, supplies the pump.

Since it was difficult to obtain a pump with the exact pressure/discharge characteristics, a throttling and flow regulating valve is fitted at the discharge side of the pump together with a small by-pass line, which returns a certain amount of Freon liquid directly into the holding tank.

The flow through the test section and the main by-pass can be adjusted by varying the flow through the pump by-pass as well as adjusting several valves in the system, located at several strategic points, as generally indicated in Figure 6.1.

All joints in the loop were sealed by welding, brazing or silver-soldering. Fluon (PTFE) tape was also used throughout very successfully on the smaller diameter threaded joints.

The loop construction material was mainly mild steel (black) which

would be compatible with other refrigerants.

6.3.1 Flow, Pressure and Temperature Measuring Stations in the Loop

The pressures around the loop are measured by "Budenberg" Bourdon type pressure gauges, with direct dial reading, with a pressure range of 0 - 160 psig. Owing to calibration against a deadweight tester, the accuracy is better than 1% of full scale output (fso).

The temperatures around the loop are measured by "Pye Ether" Copper-Constantan thermocouples fixed into suitable thermowells, which are fitted into the pipework and tanks. The temperatures are monitored on a "Pye Ether" digital panel meter, having an automatic cold junction compensator, via a 1 - 9 way multi-point switch selector. The temperature range of the instrument is $-200^{o}F$ - $+600^{o}F$ and the estimated accuracy is $\pm 2^{o}F$.

The flow in the loop is measured at the pump discharge side (FM1) and at the by-pass line (FM2) by two "Wallace and Tiernan" Vareameters (Rotameters). Calibration charts are provided and the accuracy is better than 2% of full scale output.

The flow (FM), pressure (P) and temperature (T) measuring stations are indicated in Figure 6.1.

P1, T1 : Liquid Freon at preheater inlet

P2, T2 : Liquid Freon at inlet header

P3, T3 : Liquid Freon at by-pass line

P4 : Vapour Freon in condenser

T4 : Condensate Freon at condenser outlet

P5 : Holding tank pressure

T5 : Liquid Freon at pump inlet

P6, T6 : Condenser cooling water at inlet

P7, T7 : Condenser cooling water at outlet

FM1 : Freon flow through preheater

FM2 : Freon flow through by-pass

FM3 : Condenser cooling water flow

6.3.2 Components, Controls and Safety Devices in the Rig

(a) Holding tank

The holding tank is made of mild steel; N.B. Sch. 20 tubular body and the end plates are 1" thick. All flanged connections are manufactured according to BS 10, Table E (BS 1500).

The holding tank design specifications are (Figure 6.3):

Inner diameter	=	1.5 ft
Length between end plates	=	3.0 ft
Vessel capacity	=	5.3 ft^3
Shell thickness	=	5/16"
Working pressure	=	70 psig
Working temperature	=	220^oF
Design pressure	=	110 psig
Design temperature	=	260^oF
Hydraulic test pressure	=	170 psig
Insulation	=	1" mineral wool

A 2" "Birkett" type spring loaded safety valve is fitted to flange (B) (Figure 6.3). This valve is set to relieve at 110 psig with a discharge rate of 1209 lb/hr of Freon gas with not more than 10%

accumulation.

The liquid Freon level in the holding tank is indicated by means of a "Klinger" reflex type sight-glass gauge, which is connected to flanges (J_1) and (J_2) (Figure 6.3). Valves are fitted to allow for the isolation and removal of the sight-glass without depressurising the vessel. The valves are equipped with a safety ball which instantly shuts off the flow of Freon in the event of a glass breakage.

An automatic "Bayham" control level gauge system is incorporated in the tank and connected to flange (I). This system has a round dial calibrated in inches (0 - 18") to indicate the liquid level in the tank. It also contains 4 micro-switches with the following action:

i) High level alarm switch to make contact 2" from the top of the tank.

ii) Low level alarm switch to make contact 5" from the bottom of the tank.

iii) A switch to start the pump when the liquid level is 10" from the bottom of the tank.

iv) A switch to switch-off the pump when the liquid level reaches 3" from the bottom of the tank.

This device is therefore a safeguard against either liquid flooding or starvation which might have a detrimental effect on the pump or the experimental facility as a whole.

The pressure in the holding tank is maintained at a set value by means of a pneumatic "Taylor" controller, which is connected to flange (D) (Figure 6.3). This instrument measures, indicates and controls the process variable (pressure). This controller has an auto-

manual switch selector facility and a selection of control responses is provided.

A "Taylor" air supply filter regulator maintains a regulated constant supply pressure (20 psig) to the pneumatic controller. The controller produces a 3 - 15 psig output signal proportional to the pressure sensed by the primary element in the holding tank. The output pressure signal is then transferred to a Hi-flow diaphragm valve which accordingly controls the cooling water flow rate to the condenser.

(b) Condenser

The vapour Freon leaving the test section is condensed by a vertical type condenser manufactured by "Holden and Brooke".

This condenser is a fixed tubeplate, four-tube-pass, single-shell-pass heat exchanger, with the test fluid (Freon-113) flowing in the shell and the cooling water in the tubes.

The condenser design specifications are:

Material	=	Mild steel
Design code	=	BS 1500
Flanges	=	BS 10, Table E
Number of tubes	=	40
Tubes outer diameter	=	0.75"
Tubes length	=	60"
Tubes pitch	=	0.945"
Tubes arrangement	=	Triangular
Baffles	=	Segmental 25% cut
Shell outer diameter	=	8.62"
Rated Freon vapour flow	=	3240 lb/hr

Rated cooling water flow	=	6800 lb/hr
Freon working temperature	=	$300^{o}F$
Subcooling	=	$50^{o}F$
Freon operating pressure	=	85 psig
Freon design pressure	=	100 psig
Shell side test pressure	=	150 psig
Water operating pressure	=	30 psig
Water design pressure	=	43 psig
Tube side test pressure	=	65 psig

The condenser pressure is controlled by regulating the cooling water mass flow rate, as described in the holding tank section.

A spring safety valve, similar to that in the holding tank, is fitted to the condenser.

(c) Pump

A glandless canned centrifugal pump manufactured by A.P.V. Osborne-Craig was used.

The pump and motor are integral, the stator windings being sealed off with a corrosion-resistant non-magnetic can, the rotor assembly being similarly sealed. The rotor shaft is carried on PTFE tape bearings.

Figure 6.4.b is a diagram of the cross-section of the pump. Figure 6.4.a gives the pump head-flow characteristic and the minimum net positive suction head required.

The pump specifications are:

Capacity	=	10 gpm

Differential head	=	125 ft
N.P.S.H. (minimum)	=	4 ft
Design temperature	=	350^{o}F
Design pressure	=	300 psig
Test pressure	=	450 psig
Impeller diameter	=	6.25"
Motor power	=	3 HP
Phases	=	3
Voltage	=	380/420 v
Cycles	=	50 c/s
Speed	=	2880 rpm
Full load	=	5.9 amps

Other features:

i) In order to increase the working temperature range, an auxiliary impeller is fitted to the rear of the rotor, and the liquid trapped in the rotor cavity is circulated by this impeller through an external heat exchanger water-jacket fitted around the stator band. A separate supply of cooling water at the rate of about 1.5 gpm is required.

ii) The windings are fitted with thermistors to give them protection from excessive temperature rise whether caused by electrical overload, or inadvertent increase in the temperature of the pumped liquid.

The pump was placed on a lower floor, 7 feet below the

inlet to the test section, in order to provide sufficient positive suction at the pump inlet.

(d) Preheater

The liquid Freon, before entering the test section, is preheated to the desired degree of subcooling by a five branch serpentine type heater (Figure 6.1). This simple preheater was manufactured from standard parts in the College. Each of the five legs (branches) is made from 1" BS mild steel tube with an effective straight length of 22". Every two adjacent straight lengths are connected by a 4.5" radius return bend, which does not provide an effective heat transfer surface.

The heating power to raise the liquid Freon temperature is provided by "Electric Surface Heating" where the heat is applied to the exterior surface of the tube. 15 heating rod elements manufactured by "Hedin" were used for that purpose, three elements being positioned along each straight leg.

The electric heating elements (rods) specifications are:

Outside diameter	=	5/16"
Length	=	37"
Voltage	=	240 v
Power (each)	=	500 W

The heating elements are Incoloy sheathed, fully annealed with 2" cold sections each end and 5 BA terminals.

The whole assembly was placed into a rectangular box being completely packed with heat transfer alumina cement.

The loop preheater permits the automatic regulation of

the test section inlet temperature (subcooling) by means of a "Gulton" temperature controller-thyristor, driver-thyristor system.

The sensing element is an Iron-Constantan thermocouple being fixed onto the preheater exterior surface near the exit end. The signal from the thermocouple is applied to the input of the "Gardian" temperature controller where it is amplified and used to operate a full scale indicator and also to control the level of a 0 - 10 mA output signal, depending on the difference between the sensed signal (surface temperature) and the set point reference voltage (pre-selected temperature). The controller has a proportional + integral + derivative control action. It also has an automatic cold junction compensator.

A "West" single-phase thyristor driver unit accepts the controller's mA output and converts it to a series of modulated pulses in a cycle syncopation mode making possible the control of the thyristor fed loads. The unit provides fine control and rapid response with freedom from mains waveform distortion. There is a linear relationship between the input signal and load power. The driver incorporates such important features as manual maximum power control and an auto-manual switch selector facility which permits manual operation of the driven unit (thyristor) over its full range.

The "West" thyristor unit is a solid state device capable of interrupting the flow of current in a similar manner to a contactor. However, unlike the contactor, it has no moving parts and can operate at much higher speeds. When fed by a driver having cycle syncopation output pulses, it is able to interrupt (or allow to pass) current for exactly one cycle of mains voltage, i.e. 1/50th second.

A second Iron-Constantan thermocouple is fixed onto one of the heating rods and is connected to a "Gulton" trip relay system (on-

off controller), which will cut off the power supply to the preheater if the sensed temperature accidentally exceeds a pre-selected temperature level on the controller dial. This is carried out as a safety precaution against overheating.

6.4 TEST SECTION

The test section consists mainly of a mild steel coiled tube which is heated electrically. There are two straight tube sections upstream and downstream which are not heated (Figure 6.5).

The coil is formed from 1/4" N/B BS 1387 medium wall thickness (0.092") mild steel tube.

The helical coil specifications are:

Outside tube diameter	=	0.0135 m
Inside tube diameter	=	0.0088 m
Mean helix diameter	=	0.3048 m
Pitch length	=	0.2540 m
Number of turns	=	3.5
Height	=	0.8890 m
Length	=	3.5171 m
Angle of inclination	=	16.87^{o}
Straight parts (each end)	=	0.250 m

Due to physical limitations, the valves, venturi, flow and pressure transducers were fitted to 1/2" N/B mild steel straight tubes upstream and downstream of the helical coil.

The helical coil was aluminium sprayed and then an aluminium alloy cylinder was cast around it as shown in Figure 6.5.

The aluminium cylinder specifications are:

Inside diameter	=	0.2540 m
Outside diameter	=	0.3556 m
Height	=	0.9398 m

Melting temperature = $600^{o}C$

The helical tube-aluminium cylinder assembly is heated electrically by two "Isopad" heating isojackets designed to fit around the outside and inside surface area of the aluminium cylinder. These isojacket units comprise heating element, element carrier, thermal insulation and outer metal shell stove enamelled.

The inside heating jacket slides on the inside cylinder surface area and makes a tight contact. The outside heating jacket is made of two halves which are hinged and fastened by toggle clips, thus making a very good contact with the outside surface of the aluminium cylinder.

The heating elements are mineral-insulated stainless steel sheathed and they are fitted to a stainless steel wire mesh which comes in contact with the heated surface. The heating elements can withstand temperatures up to $600^{o}C$.

AC power (at 240 v and 50 Hz) up to a maximum of 3.6 kW is supplied to the inside jacket and up to 4.0 kW to the outside jacket. The terminal boxes with the conduit entries are fitted to the outside metal enclosure.

One NiCr/NiAl thermocouple is attached to the heating element of each of the heating jackets and is connected to a "CSW-Isopad" trip relay system (on-off controller), which will cut off the power supply to the test section if either or both of the sensed temperatures accidentally exceed a pre-selected temperature level on the controllers dial. This is carried out as a safety precaution against element overheating.

An Iron-Constantan thermocouple is fixed into a small hole of the aluminium cylinder very near to the coil outlet point. This thermocouple, in conjunction with a "Gulton" temperature controller-thyristor, driver-

thyristor system, regulates the power supply to the test section in an exactly similar way to the one described in the previous section (there is again an auto-manual switch selector facility).

6.4.1 Test Section Instrumentation

(a) Wattmeter

The measurement of power is accomplished with a "Norma" Wattmeter (electrodynamometer instrument).

The Wattmeter specifications are:

Voltage range	=	24 - 60 - 120 - 240 v
Rating	=	1 - 5 A
Frequency range	=	15 - 65 Hz
Accuracy	=	Class 0.5 (0.5% fso)
Scale	=	Linear, 120 divisions

Because of the higher power requirements, the Wattmeter is connected to a separate precision current transformer.

The current transformer specifications are:

Secondary rating	=	5 A
Primary rating (via terminals)	=	10 - 25 - 50 A
Accuracy	=	Class 0.5 (0.5% fso)
Test voltage	=	2 kv

(b) Thermocouples

The bulk fluid temperature measurements near the entrance

and exit points of the heated test section is accomplished with two "Westmic" mineral-insulated Copper-Constantan thermocouples. They have a 1.0 mm sheath diameter in 18/8/1 stainless steel with grounded junction and they are fitted with a stainless steel taper male stud compression fitting threaded 1/8" BSPT. The thermocouple time constant is 0.15 seconds. The temperatures were monitored on an "Advance" DVM through a selector switch.

(c) Venturi-meter

Upstream of the heated part of the test section, a "Barco" Venturi is fitted for dynamic flow measurements. The Venturi was favoured against a flow orifice firstly because of its lower pressure drop, and secondly because the orifice would form a wake which could introduce unwanted resonnances into the flow signal.

The Venturi specifications are:

Material	=	Bronze
Pipe size (straight)	=	15.5 mm
Beta ratio (throat ID/pipe ID)	=	0.323
Maximum pressure	=	17.5 bars
Maximum temperature	=	$125^{o}C$
Accuracy	=	±1%

Care was taken to leave sufficient length both upstream and downstream of the Venturi in order to ensure maximum accuracy.

An identical Venturi with a beta ratio of 0.251 was available in order to measure lower flow rates. This Venturi was not used in the present work.

(d) Differential pressure transducer

For dynamic flow measurements, a "Bell and Howell" differential pressure transducer is used to sense the pressure difference between the Venturi pressure tappings. This transducer is a bonded strain gauge instrument designed to measure low differential pressures in the presence of high line pressure, up to 207 bars.

The differential pressure transducer specifications are:

Pressure range	= 0 - 20" WG
Rated electrical excitation	= 10 v DC
Output voltage	= 0 - 15 mv
Compensated temperature range	= -54 - +120^{o}C
Resolution	= Infinite
Non-linearity and hysteresis	= ±1% fso

(e) Pressure transducers

For dynamic pressure measurements, two "Bell and Howell" pressure transducers are fitted to the inlet and exit of the test section. These transducers are again of the bonded strain gauge type.

The pressure transducers specifications are:

Pressure range	= 0 - 100 psig
Rated electrical excitation	= 10 v DC
Full range output	= 40 mv
Compensated temperature range	= -10 - +120^{o}C
Resolution	= Infinite
Non-linearity and hysteresis	= ±0.2% fso

6.4.2 Venturi-Meter and Transducers Calibration

(a) Venturi-meter

The Venturi-meter was calibrated with water, using an inclined manometer, a graduated vessel and stopwatch. The calibration curve between differential pressure across the Venturi and volumetric flow is shown in Figure 6.6 and agrees with the manufacturer's calibration curve. The manufacturer gives an accuracy of ±1%.

The flow rate range represented by the solid line in Figure 6.6 (viscosity immune area for high Reynolds numbers ≈ > 5000) may be evaluated from the Venturi theoretical formula as given by Kay (1968):

$$Q = c_v A_p \sqrt{\frac{2 \rho g h}{\rho^* \left[(\frac{A_p}{A_t})^2 - 1 \right]}} \qquad (6.1)$$

with a discharge coefficient c_v = 0.97, where:

A_p = pipe cross-sectional area (d_p = 15.5 mm)

A_t = throat cross-sectional area ($d_t = b.d_p$)

(b = beta ratio = 0.323)

Q = volumetric flow rate

g = acceleration of gravity (= 9.81 m/sec)

h = pressure difference expressed as head of fluid with density ρ

ρ^* = density of fluid

In Figure 6.6, the differential level h is expressed in metres of water at normal conditions and the flow rate corresponds to flow rate of water at the same conditions as well, i.e. in this case,

$\rho^* = \rho$ (specific gravity of fluid (SG) = 1).

If the specific gravity of the fluid to be measured is different from 1, then $\rho^* = \rho$ (SG). The (SG) of the fluid (Freon-113) will depend on the conditions of pressure and temperature.

In Figure 6.6, the velocity inside the coil is also given (assuming again (SG) = 1):

$$u_c = \left(\frac{d_p}{d_c}\right)^2 \frac{Q}{A_p} \tag{6.2}$$

where: u_c = velocity in the coil

d_p = Venturi pipe diameter (= 15.5 mm)

d_c = coil pipe inside diameter (= 8.8 mm)

$Q/A_p = u_p$ as given by equation (6.1)

(b) Differential pressure transducer

The differential pressure transducer was tested and calibrated in the laboratory. In order to generate the small differential pressures required, the level of the water inside an inclined manometer tube above the transducer port centreline was varied and measured, while the other transducer port was left open to the atmosphere. During this procedure, the transducer was vented thoroughly. The voltage output from the transducer was monitored on an accurate digital voltmeter. This calibration procedure was repeated for both the high and low pressure port sides of the differential pressure transducer.

The resulting calibration curve is shown in Figure 6.7. The characteristic is linear with sensitivity of 0.156 volts per cm_{H_2O}.

The combined effects of non-linearity and hysteresis do not exceed ±1% of full scale output from the best straight line through the calibration points.

A dynamic calibration followed the above described static calibration.

The transducer, together with transducer pipework, was pressurised (with air) and the air was released suddenly (via a bursting disc) to impose a negative step change. The transient voltage was recorded and examined on a "memory" oscilloscope.

The response time to 90% of the final value for the imposed full range pressure step input was found to be less than 0.3 seconds. The transient voltage was found to correspond to a highly damped second order system with damping ratio $\zeta \simeq 0.9$ and natural frequency $\omega_n \simeq 12$ rad/sec. Therefore, the transducer frequency response was flat in the range of interest (0.01 - 1.5 Hz or ≃ 0.06 - 9 rad/sec).

(c) Pressure transducers

The pressure transducers were tested and calibrated in the laboratory. They were calibrated against a deadweight tester and an accurate digital voltmeter.

The resulting calibration curves are shown in Figure 6.8. The characteristics are linear with sensitivities of 0.08 volts per psi and 0.084 volts per psi for the 6_{up} (upstream) and 7_{dn} (downstream) transducers, respectively. The combined effects of non-linearity and hysteresis do not exceed ±0.2% of full scale output from the best straight line through the calibration points.

The natural frequency for the transducers was higher than 10 kHz which is vastly in excess of the range of frequencies of interest.

6.4.3 Transducer Signal Conditioning Equipment

A "Bell and Howell" miniature signal conditioning system was provided in order to make the output from the transducers compatible with the data acquisition control interface unit.

Each transducer was provided with one 1 - 190 instrumentation amplifier and one 8 - 125 bridge supply and balance unit mains energised.

These units are of modular design and they provide high flexibility and versatility. These modules, together with a miniature mains control unit, were plugged into a 19" rack assembly.

The 1 - 190 amplifier is a compact general purpose differential DC amplifier with high accuracy, low noise and a very wide gain range of 0.2 - 1000. The output voltage from this amplifier is 0 - 8 v maximum. Therefore, a gain voltage of 500 was selected for the differential pressure transducer and of 200 for the two pressure transducers.

The 8 - 125 is a combined bridge balance and DC supply unit of low noise and high accuracy. It is compatible with the 1 - 190 amplifier both mechanically and electrically. This unit combines a stabilised DC power (voltage) supply with versatile balance facilities to cope with 2, 3 or 4 wire bridge connections (our transducers had a Wheatstone bridge of strain gauge windings in which all four arms were active). The constant voltage output supply could be preset within the range of 3 - 12 v (for our transducers, the preset was 10 v DC).

6.5 DATA ACQUISITION AND RECORDING SYSTEM

Since the experimental investigation was decided to be a statistical one, it was felt that the data acquisition and recording system had to be capable of providing high accuracy and be automated to a high degree.

It was fortunate that at the time it was decided to develop a very sophisticated, rather expensive data acquisition-recording system. In the end, the selection was decided to be between a set of Correlator-Spectrum Analyser combination (modern reliable analogue equipment with ample bandwidth) and a sophisticated digital recording system for off-line operation with the Imperial College computer (CDC 6400). Although the set of analogue equipment would perform the statistical operations very reliably, the digital recording system was favoured mainly because of its high versatility.

The system was based on a Kennedy 8000 Series "Read/Write Buffered Formatter" and "Magnetic Tape Transport Unit" combination. The unique feature of this system is that the recording technique which is employed to record digital information onto the magnetic tape (IBM compatible 2400 series) is rather well standardised, being used by IBM and other big computer manufacturers (including CDC). A "Control Interface Unit" had to be designed and built in the College in order first to make the transducers signals compatible with the system, and second to control the stream of information into the "Kennedy" system. The development of both the hardware and the software side of the system was not an easy task, and took a rather large share of the available time. The present author spent a long time on debugging the software side of the system. The assistance offered at this stage by the Computer Advisory Centre was minimal since this system was a completely new one.

In what follows, a rather detailed description will be given

of the data acquisition and recording system as this might prove useful to future users.

6.5.1 Read/Write Buffered Formatter

The formatter which was used in the present work is a "Kennedy 8232 Series" which provides a simplified interface that can accept or supply data asynchronously at data rates of 0 - 1,000,000 characters per second. Data will be accepted without interruption if the average data rate over the period of one record does not exceed a certain rate which depends on the buffer size, the packing density and the speed of the magnetic tape transport. For our model, the maximum data rate for no loss of data is ≈ 26000 characters/second. When the data rate exceeds this value, a "busy" signal appears at the interface.

The interface contains two independent memories (buffers), each of which is capable of storing a complete record of a length equal to 2048 characters (buffer size). Incoming data are fed into an empty memory and the input data stream is transferred to the other memory when an "end of record" command is received, or when the memory capacity is filled. As soon as a memory is filled, a readout to tape takes place. This readout must be completed before the opposite memory is filled, otherwise there will be an interruption of the continuous data transfer. This is the limit which establishes the maximum continuous data rate of 26000 characters/second.

Our model provides a read-after-write check with automatic backspace, erase and rewrite. Therefore, if a read error occurs and the block must be rewritten, the maximum data rate of 26000 characters/second becomes smaller and the "busy" signal may appear at the interface.

Additional inputs include the "end of record" command which

will terminate a record and which should be applied within the buffer length specified. An "end of file" input is also provided to generate the "end of file" sequence on tape.

All formatting electronics (parity generator, gap control, etc.), are included within the system.

6.5.2 Magnetic Tape Transport Unit

The "Magnetic Tape Transport" used in the present work is a "Kennedy 8107 Series" which is compatible with the "8232 Formatter" both mechanically and electronically. This model is equipped with the necessary electronics and read-after-write head and offers triple-density operation in a 7-track mode. The packing density (200, 556 and 800 characters/inch) is selectable by operation of a push-button on the "Tape Transport Unit".

The tape speed is 45 inches/second on a 10.5 inch reel. All motion control, timing and read/write logic functions, including clock generation, are performed by the "Formatter" which accepts control commands from the "Interface Control Unit" built in the College.

The "Magnetic Tape Transport Unit" is equipped with the necessary electronics to control the tape motion and to read, write, read-after-write, and erase digital data on 0.5 inch magnetic tape. Head specifications and mechanical and electrical tolerances conform to requirements for IBM compatibility in NRZI format (non-return-to-zero change at logic 1), which is the most widely accepted recording technique for recording parallel data onto multitrack recorders.

The parameters which ensure the IBM compatibility relate to track width, number of tracks, position of the tracks on the width of the tape, form of check characters, spacing of check characters from data,

length of interrecord gaps, the characters used to identify a file gap, as well as the mechanical dimensions of reels and hubs.

The gaps between the records (each record contains 2048 characters) and at the beginning and end of the tape are required to allow the tape to start and stop while the computer manipulates the data.

The NRZI format provides for both vertical and horizontal parity checks. The check characters define to a very high level of confidence that a block that is written/read is accurate. Our 7-track machine uses six tracks for recording data and the remaining track carries the vertical parity information. The longitudinal redundancy check character is written at the end of each block on a per track basis. The combined vertical and longitudinal parity test reduces the probability of not detecting an error. The vertical parity for our 7-track machine can be selected (wired) "even" ("binary coded decimal" code) or "odd" (binary). The recorder and the computer can accept any code set applied, the only restriction being that the 000000 character in the 7-track system using "even" parity (BCD) must not be used. For the present case, an "odd" parity was selected (binary code).

6.5.3 Control Interface Unit

The "Control Interface Unit" is a fast analogue data collection and conversion system which also controls the stream of digital information into the "Kennedy 8000 Series" system described in the previous sections.

The console of the "Control Interface Unit" comprises a calculator type push-button array with a line of five 7-segment displays and a cluster of indicating lamps (LED) to reveal the status of the overall system.

The part of the "Control Interface Unit" which copes with the analogue data collection and conversion (to digital), consists mainly of the following components:

(a) An 8-channel multiplexer to couple the output signals from the transducers (8 maximum) into the analogue to digital converter in some sequence, the transducer signals being already conditioned by the "conditioning system" described in section 6.4.3. The interface accepts analogue signals in a voltage form in the range 0 - 10 v DC.

(b) A sample-and-hold amplifier to make a fast "acquisition" of the varying analogue signal and "hold" this signal for a finite period of time, ≃ 1.2 μsec for the ADC used, necessary for the analogue to digital converter to perform the conversion process.

(c) An analogue-to-digital converter to convert the analogue input data into its equivalent digital form. Additional "logic" keeps track of which data source is coupled to the converter at any instance.

The ADC used was a 10-bit one. Therefore, the analogue signal is quantised by partitioning the full span of the analogue continuum (from zero to 1023/1024 of "full scale") into 2^{10} = 1024 discrete ranges. Since the analogue values within a given range are represented by the same digital code, which corresponds to the nominal mid-range value, an inherent "quantisation uncertainty" of ± 1/2 LSB (≃ 1‰) always exists. The conversion time is 1.2 μsec.

Since a 10-bit ADC and a 7-track machine (6 bits for each character in a row, the seventh being the parity bit) were available, the following layout of a "reading" within a "character" was chosen. The 4 MSB of the digitised "reading" were accommodated in the least significant part of the first character and the 6 LSB in the second character. The remaining sixth and fifth bits (in the most significant part) in the first characters were hardwired to "1". The knowledge of the described layout of a "reading" is very important for computer data handling purposes. Possible uses of the two spare bits could be the use of a 12-bit ADC (higher accuracy but slower rate data collection) or sign extension if the ADC were it connected to read negative input levels.

The multiplexer, sample and hold amplifier and ADC 1123 used were of "Analog Devices" make.

The rest of the "Control Interface Unit" consists of logic electronics circuitry to accept the control commands (which are input via the push-buttons fitted to the console) and transfer the information (data) into the "Kennedy" data storage system.

The push-button array consists of 16 push-buttons (PB). Ten of them are numerals (0, 1, 2, ..., 9). The action of the remaining six push-buttons is described briefly below.

"SKIP" PB

Depression of PB "SKIP" allows the selection of the starting channel of the scanner, by depressing an octal digit (i.e. 0, 1, ..., 7). The value entered is displayed on the left-most isolated 7-segment display. By entering a "1", the channel specified by the octal digit will be permanently selected, indicated by the decimal point in the 7-segment display being unilluminated. By entering an "0", channels will

be scanned from the entered octal digit to channel 7. This mode is indicated by the decimal point on the channel select 7-segment display being illuminated.

"PRINT" PB

Depression of PB "PRINT" routes the decimal key depressions to a "records total" register, i.e. we select the total number of records to be written (each record is 2048 characters or 1024 readings, according to the chosen layout of a "reading"). The contents of this register are displayed on the clustered four 7-segment displays.

"*" PB

Depression of PB "*" controls the scan (sampling) rate of the analogue information by an internal oscillator set to scan at low enough rates (≃ 1 s/s) to note individual recordings, whether the "SEND" PB is depressed or not. This allows transducer calibration in conjunction with the feature that allows any channel to be permanently selected.

"SEND" PB

Depression of PB "SEND" starts a recording run. During this phase of operation, the four clustered 7-segment displays show the "octal" value of the digitised analogue information as a value between $0 - 1777_8$. In most cases, the scan rate will be too high to see individual digitised values on the display.

"CLEAR" PB and "#" PB

Depression of PB "CLEAR" clears the channel select and records/runs digits, specifies "zero" records and makes "write status

select" (WSEL) false. Depression of PB "#" rewinds the tape to the "load point" if WSEL is already false. Depression of PB "SEND" will record a BOT (beginning of tape gap) only if "zero" records are to be recorded and the tape is at the "load point" in a "write enable" state. Depression of PB "#" with WSEL true will record an EOF (end of file gap).

6.5.4 Additional Electronic Equipment

A "Venner" square pulse generator was used to dictate the scan rate at which the analogue to digital conversions will take place (external oscillator). For this purpose, a suitable input was provided on the console of the "Control Interface Unit".

A "Marconi" digital counter was used to monitor the exact value of the scan rate since this was very important for the experiments.

A dual beam oscilloscope and a dual strip chart recorder were available in order to give a "visual" indication of the state of the transducers signals.

Figure 6.9 is a block diagram of the electronics set-up for the data collection and recording.

Figure 6.10 shows a photograph of the Freon-113 test facility.

Figure 6.11 shows a photograph of the differential pressure transducer and pressure transducer fitted to the test section inlet.

Figure 6.12 shows a photograph of the electronics set-up for the data acquisition and recording.

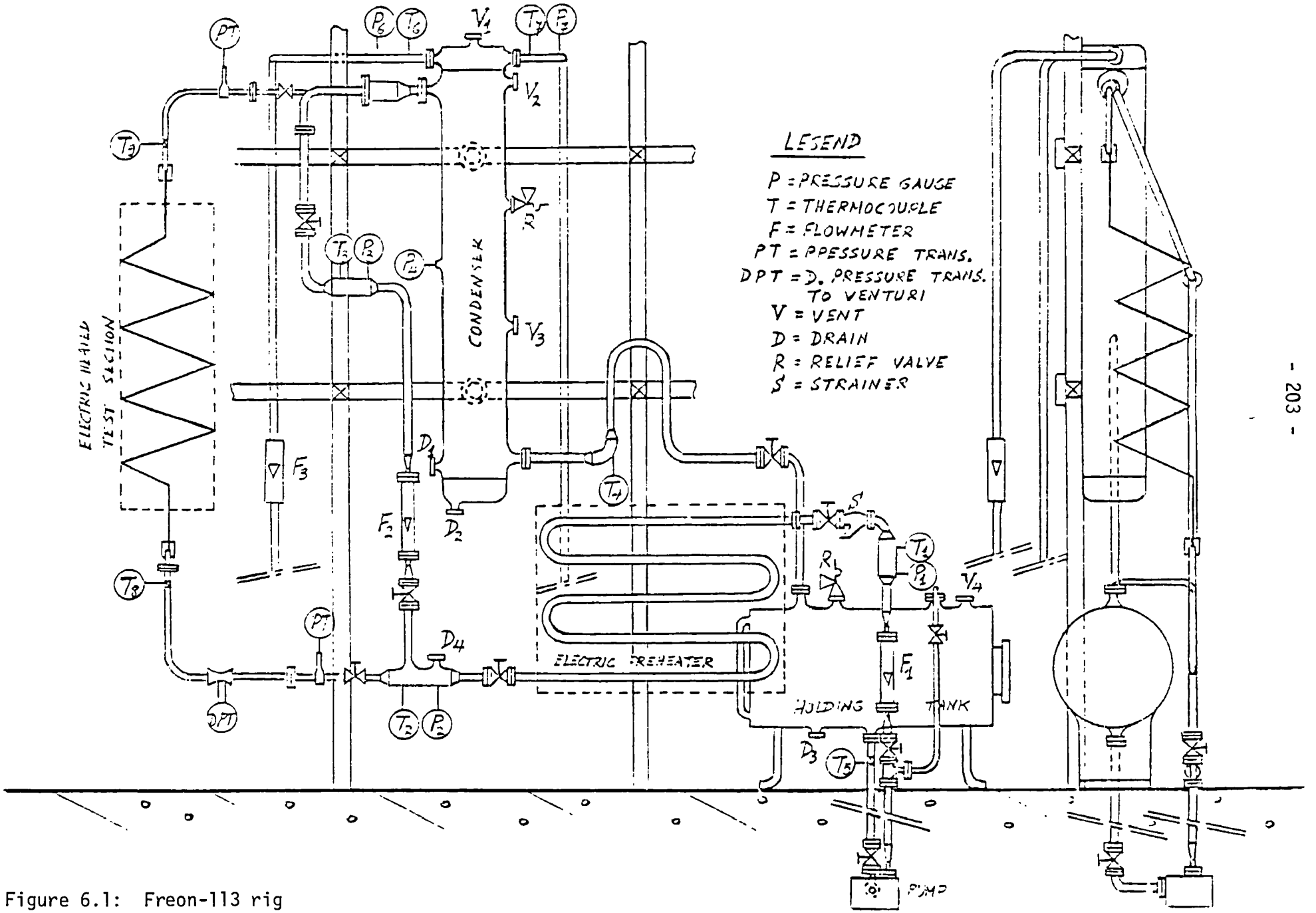

Figure 6.1: Freon-113 rig

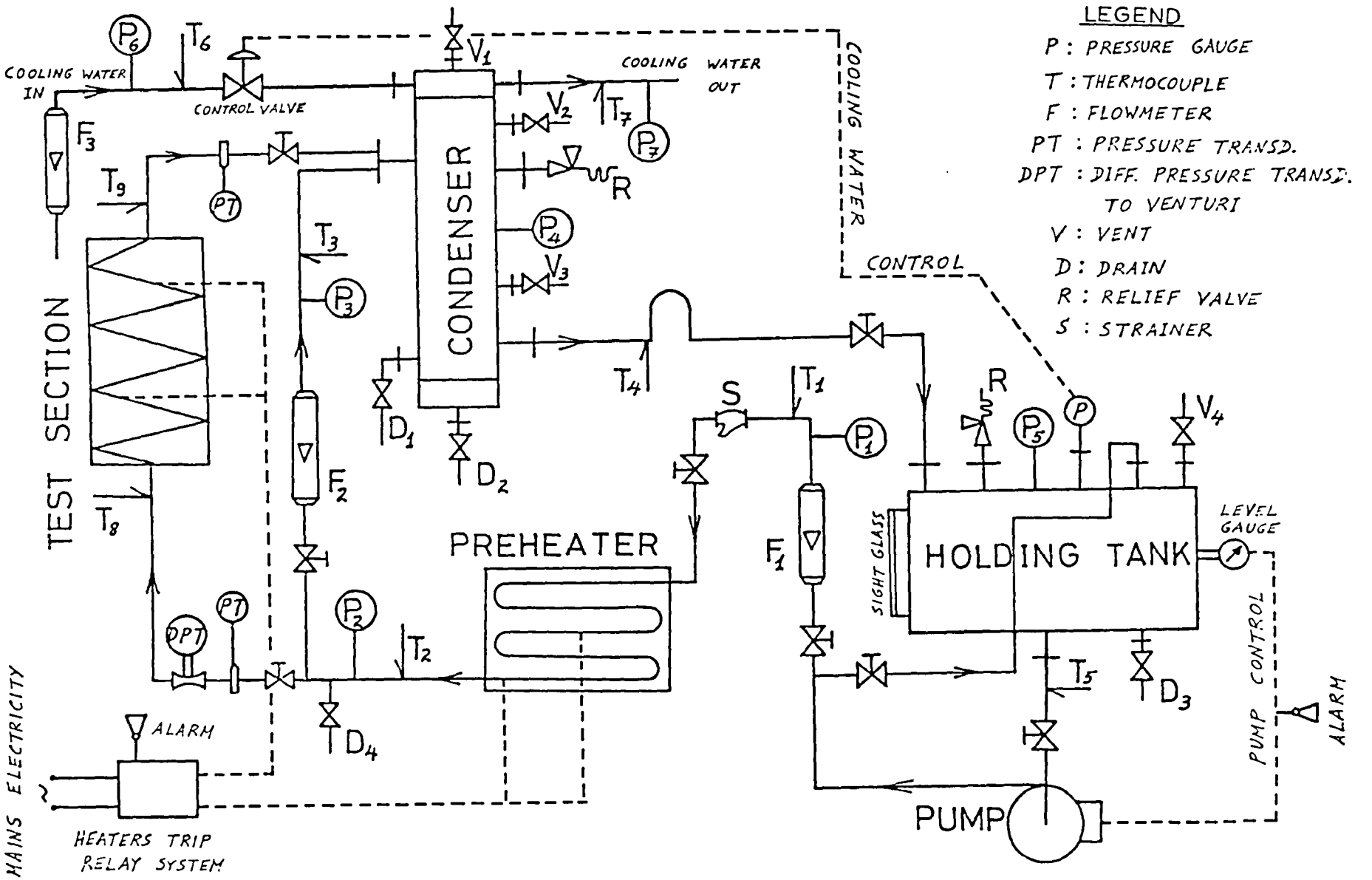

Figure 6.2: Flow diagram for Freon-113 loop

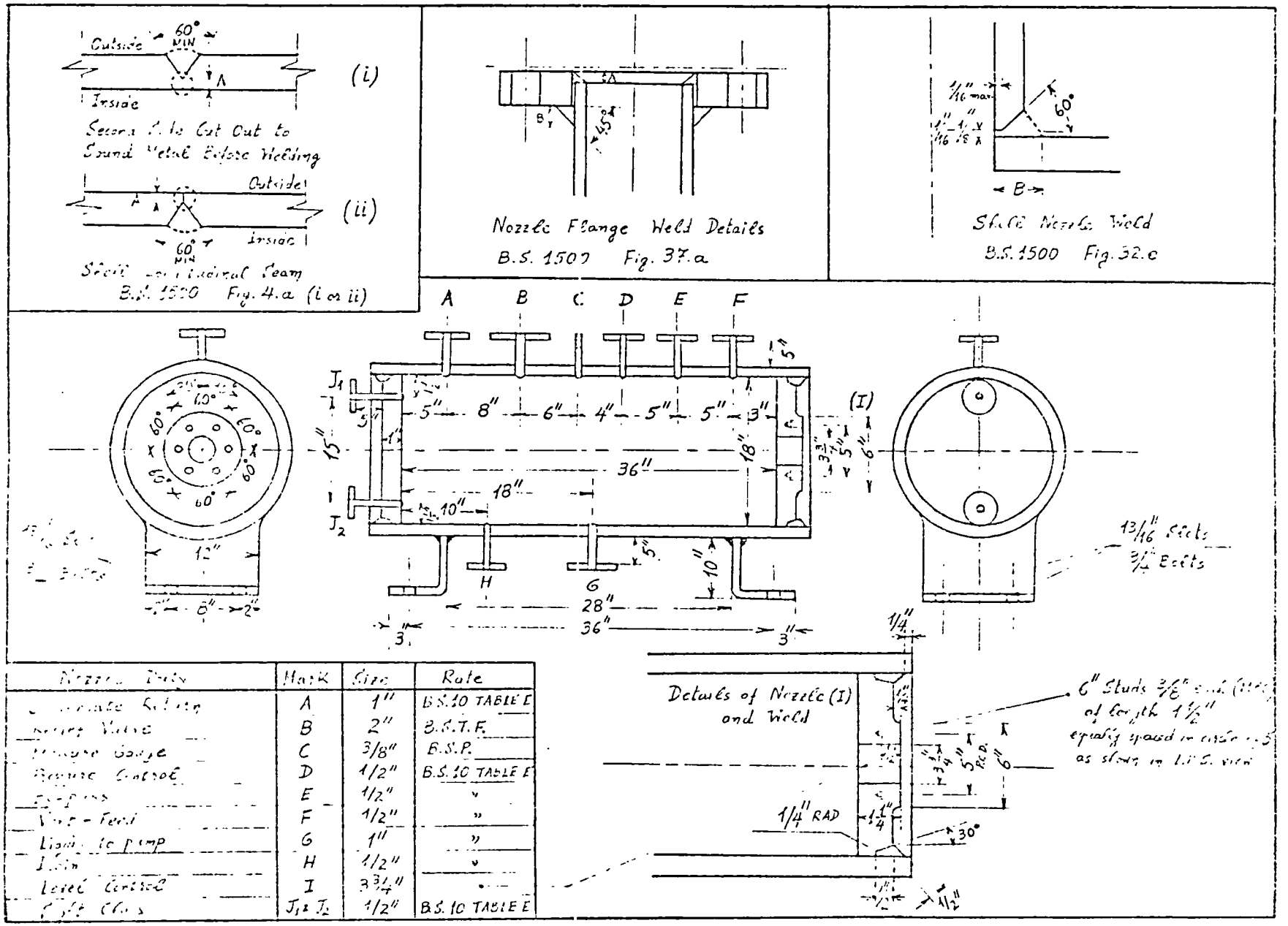

Figure 6.3: Drawing of holding tank

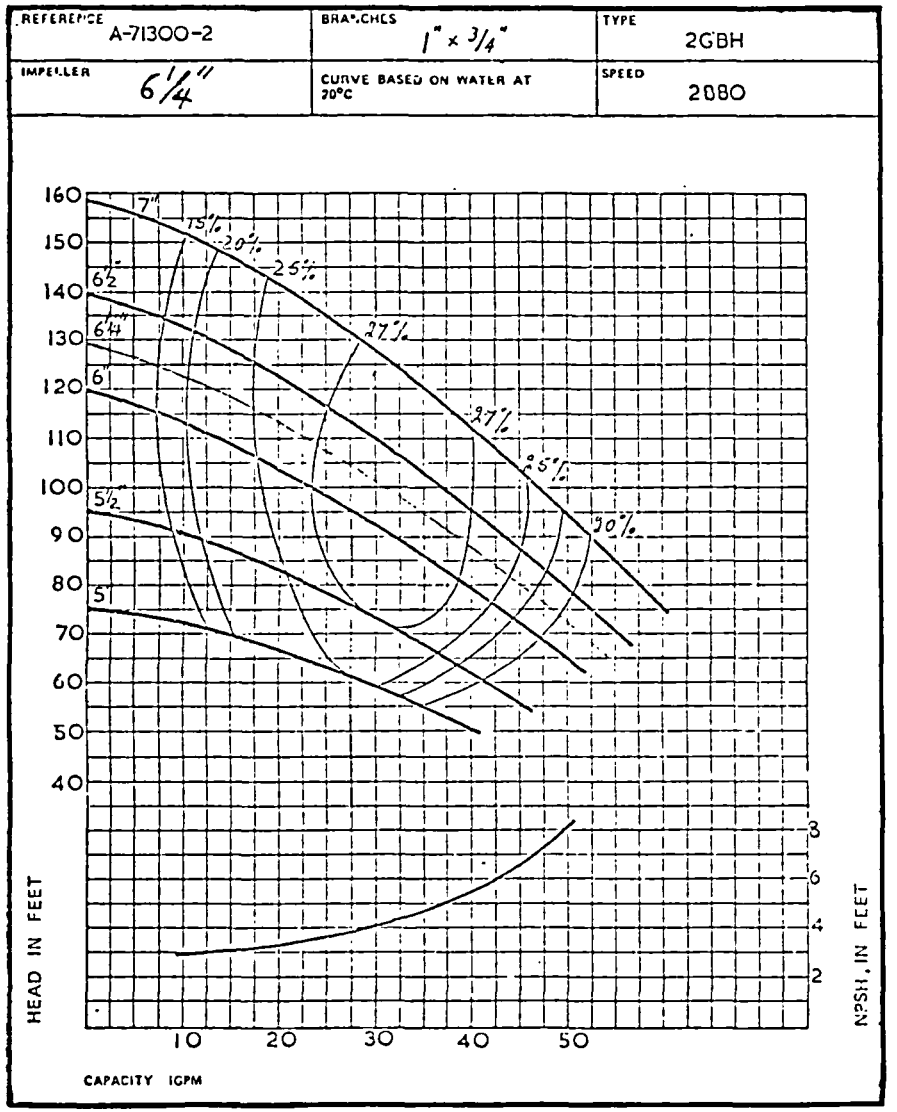

Figure 6.4.a: Pump characteristic (6¼")

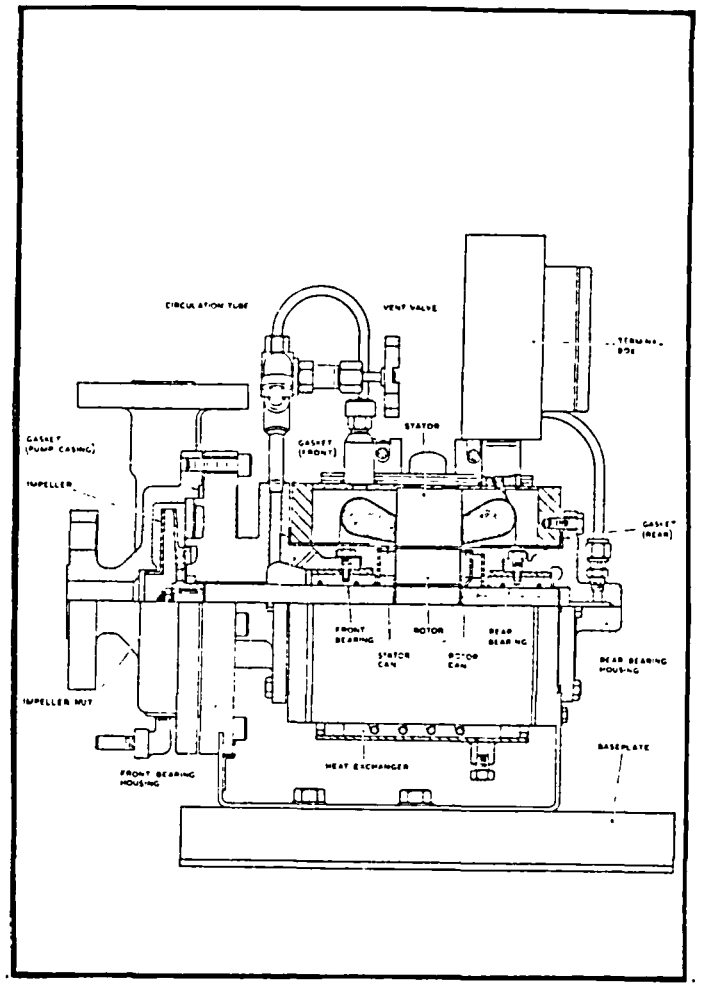

Figure 6.4.b: Pump cross-sectional view

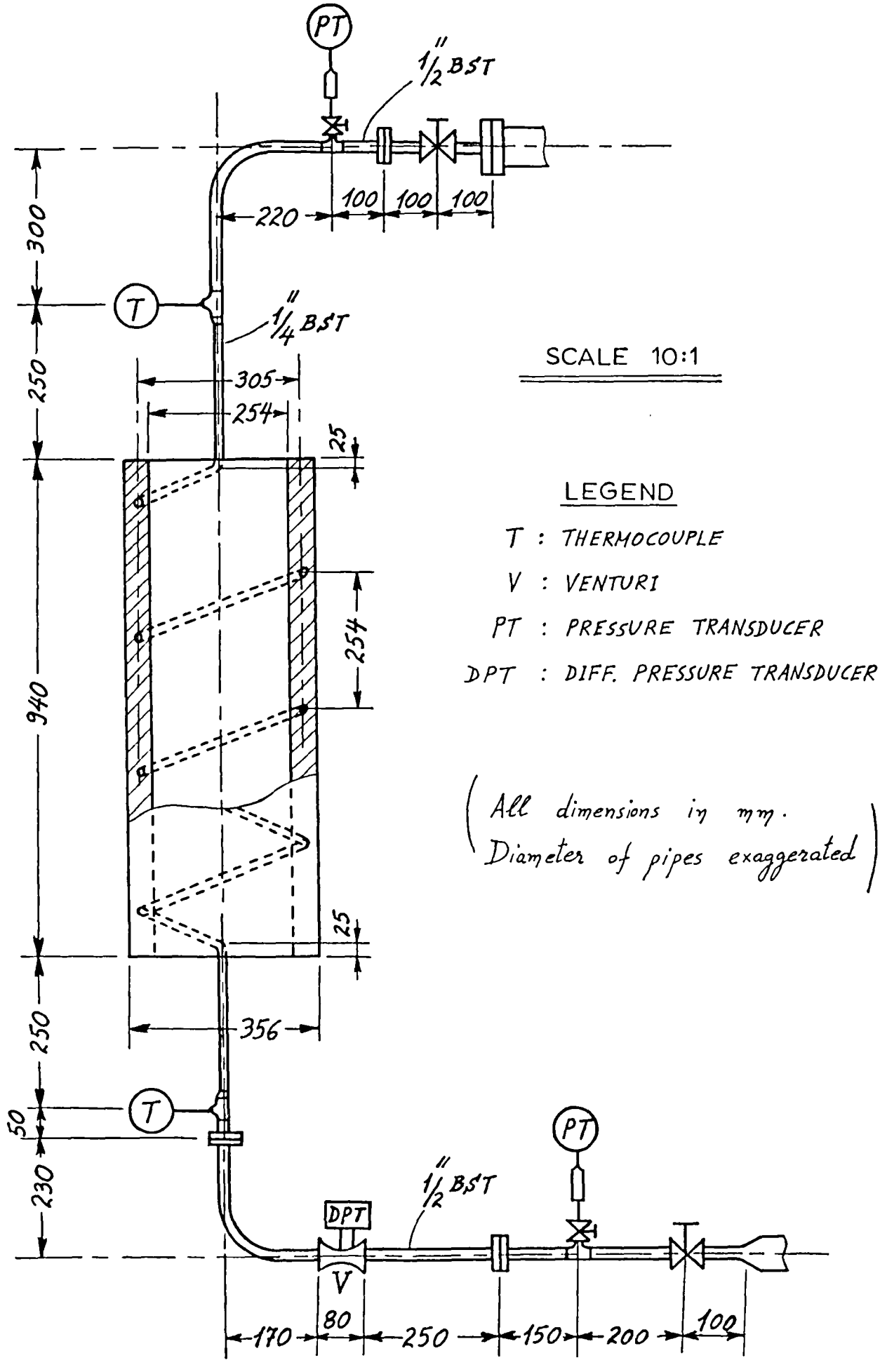

Figure 6.5: Test section

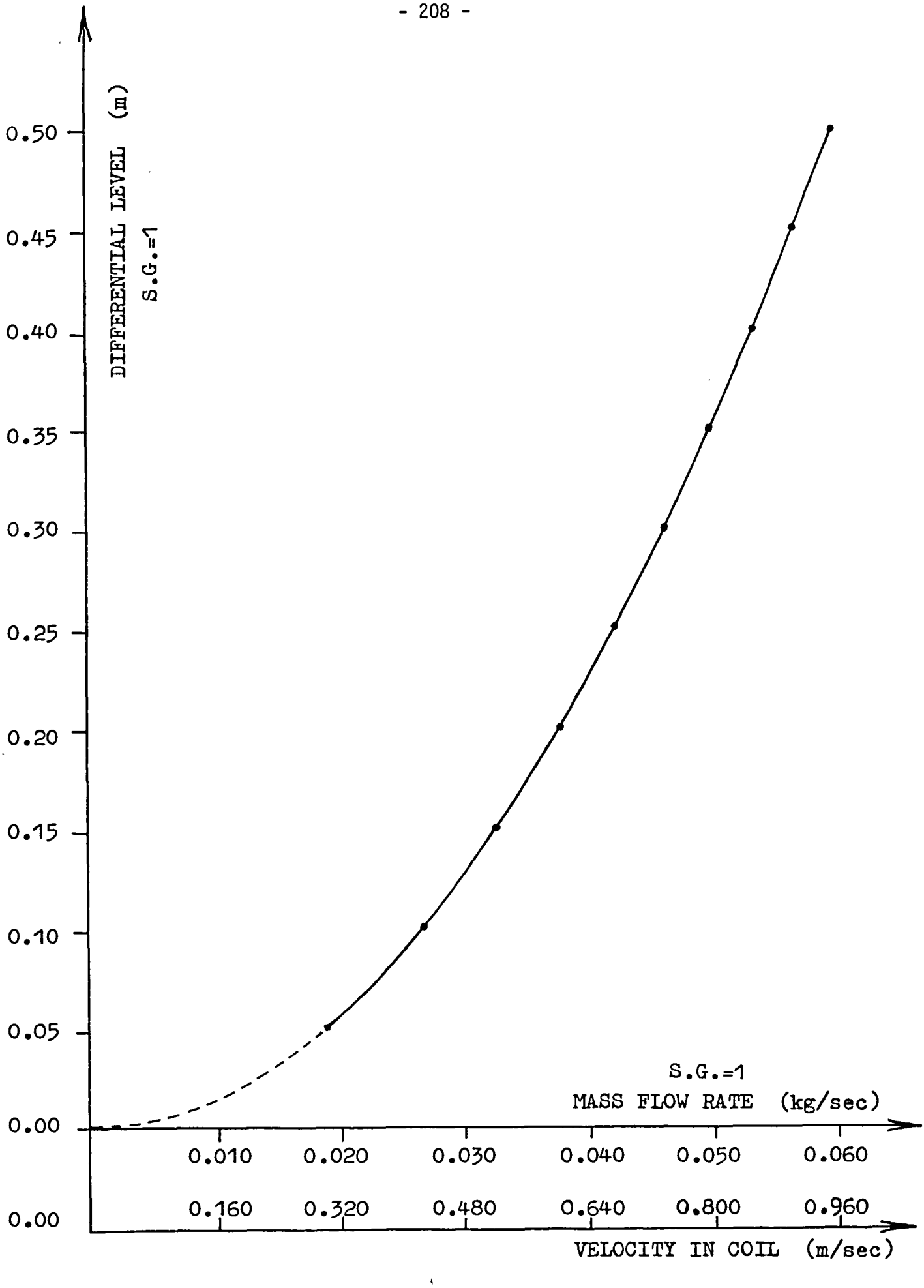

Figure 6.6: Venturi calibration curve

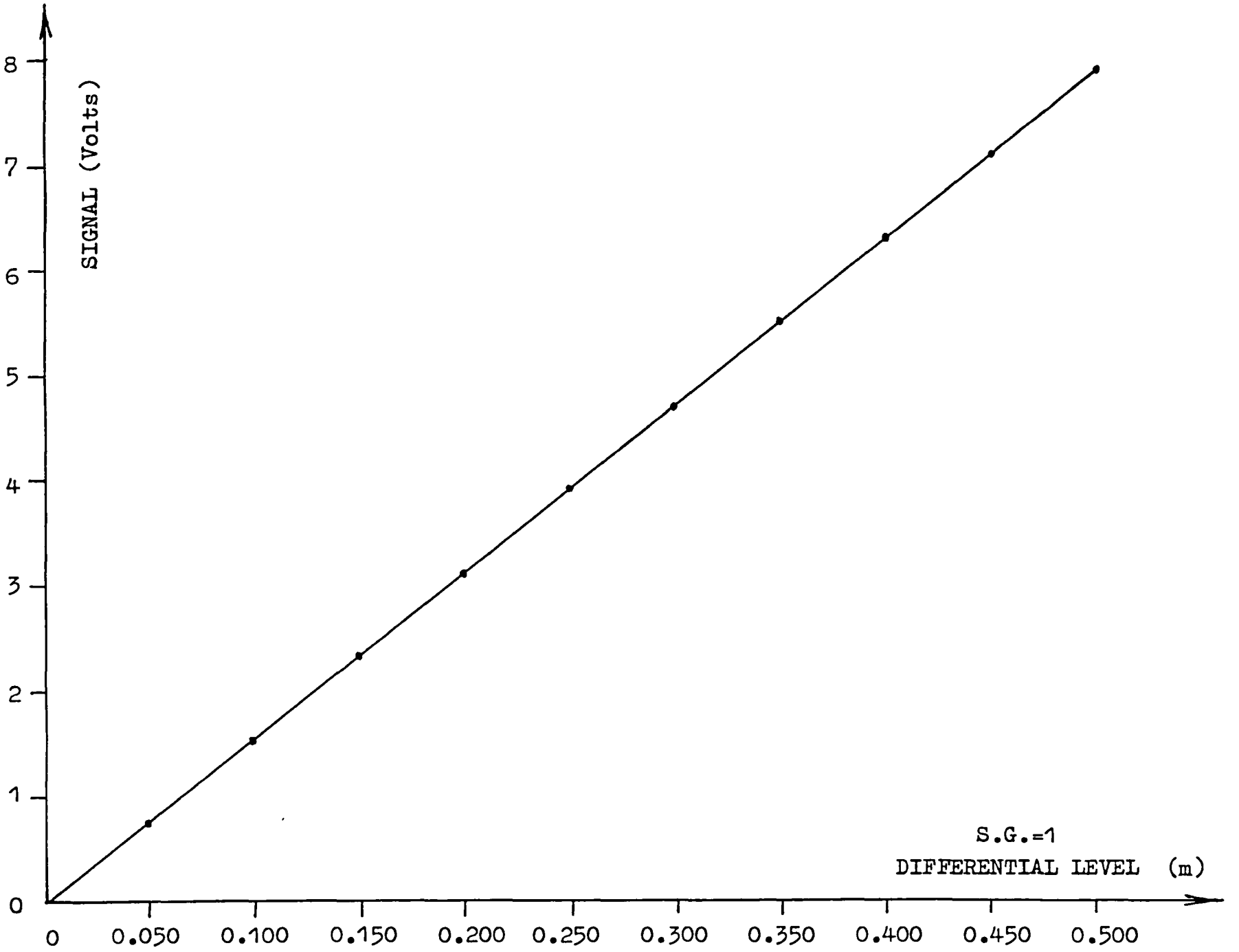

Figure 6.7: Differential pressure transducer calibration curve

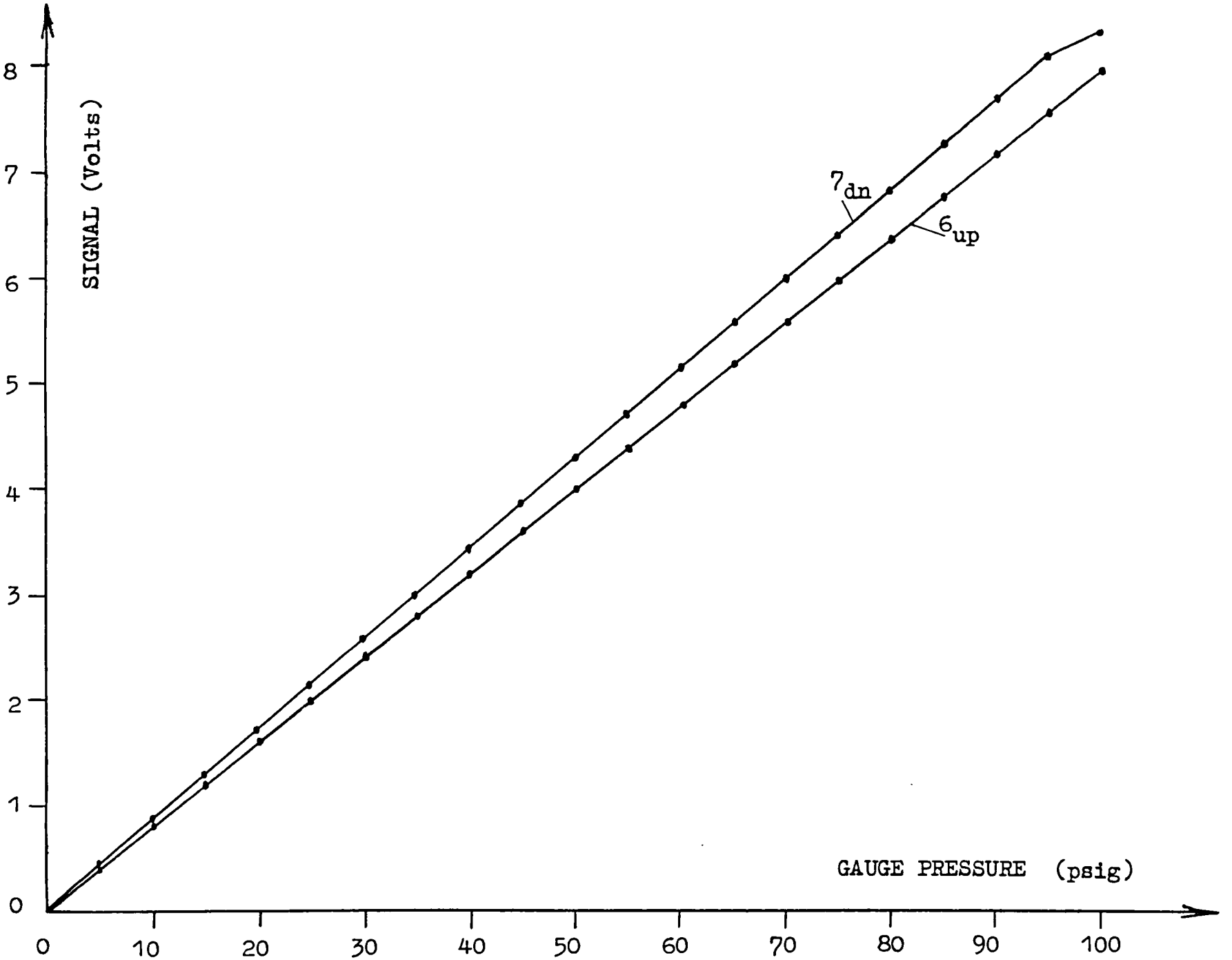

Figure 6.8: Pressure transducers calibration curves

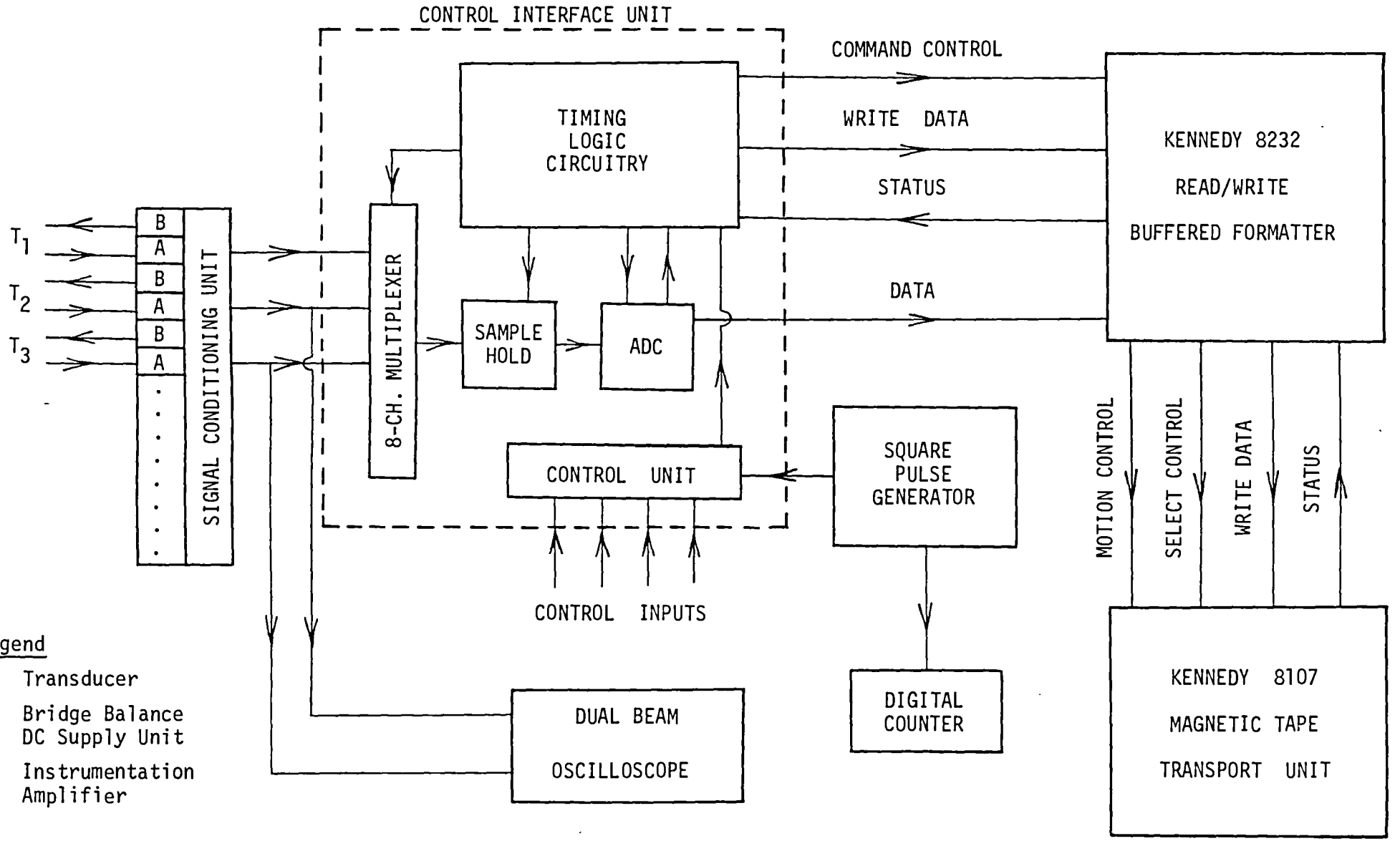

Figure 6.9: Block diagram of electronic set-up for data acquisition and recording

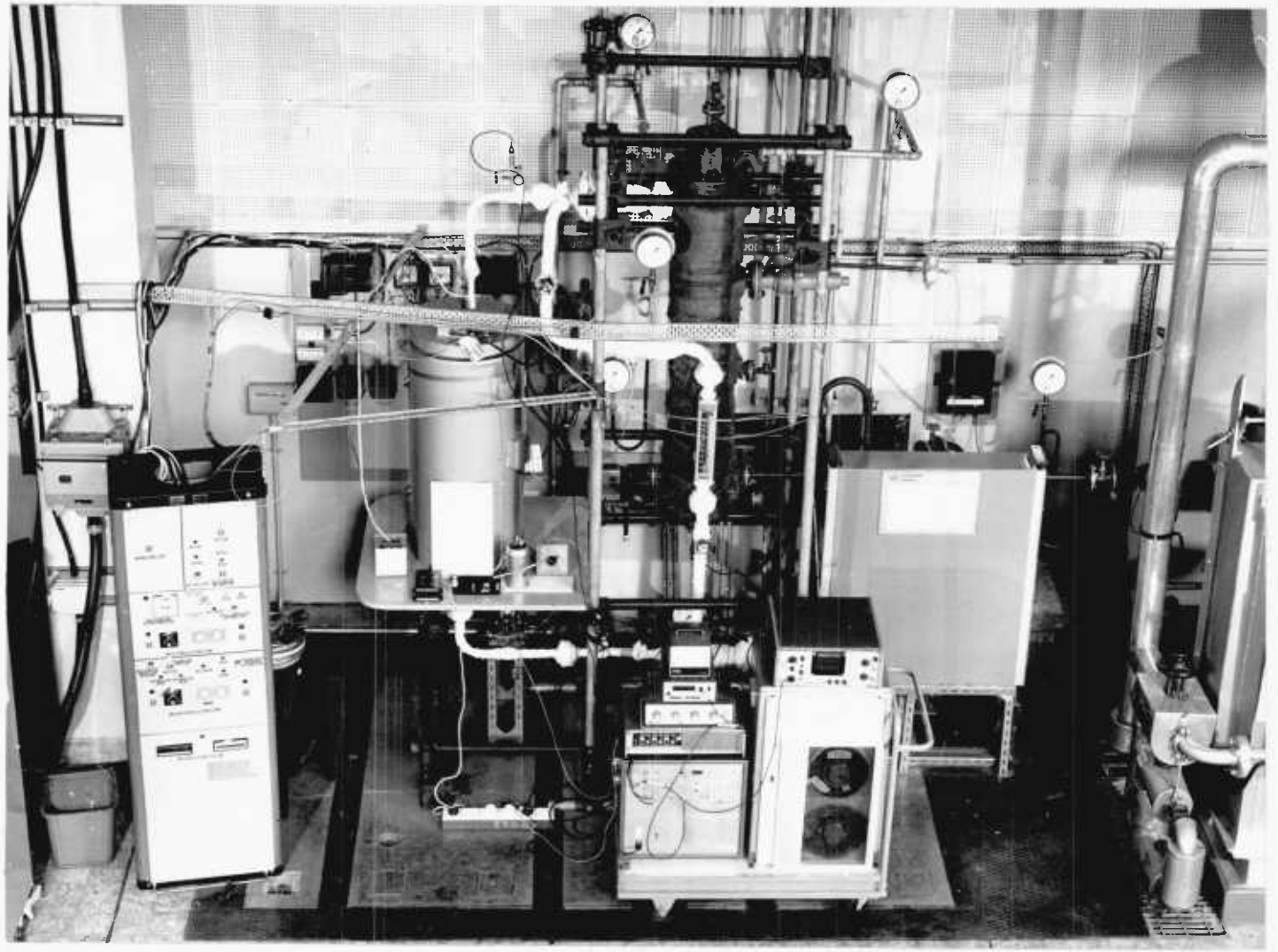

Figure 6.10: Photograph of the Freon-113 test facility

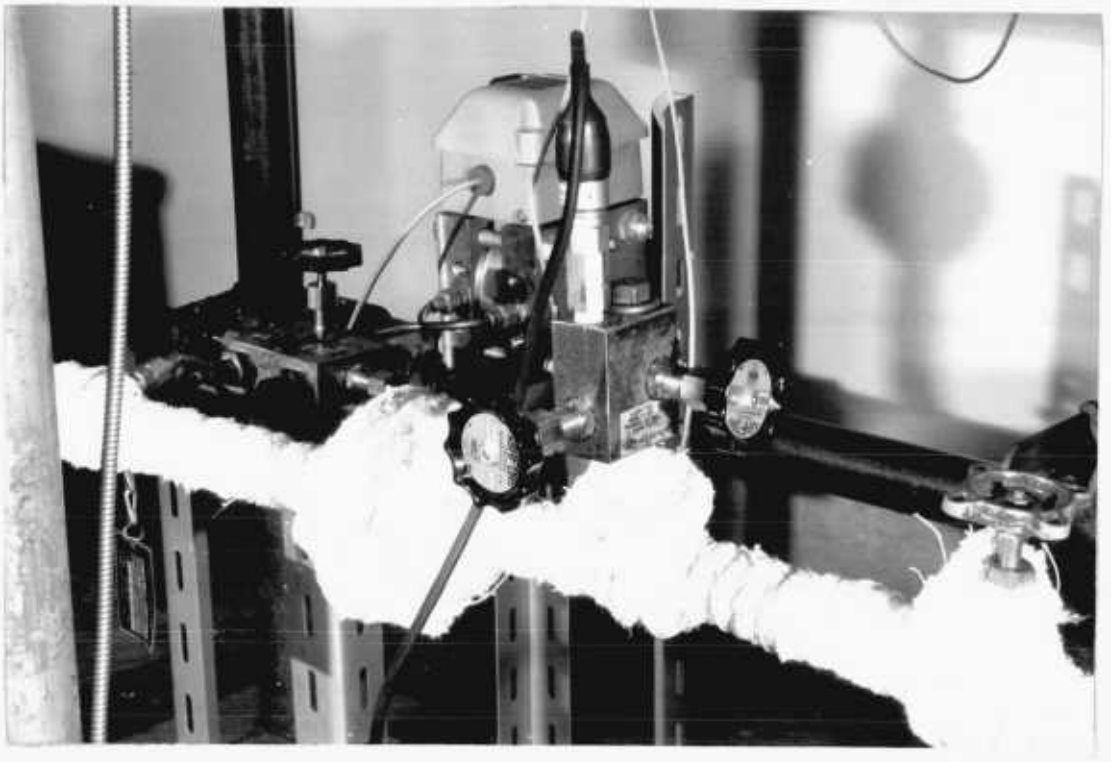

Figure 6.11: Photograph of the differential pressure transducer and pressure transducer at test section inlet

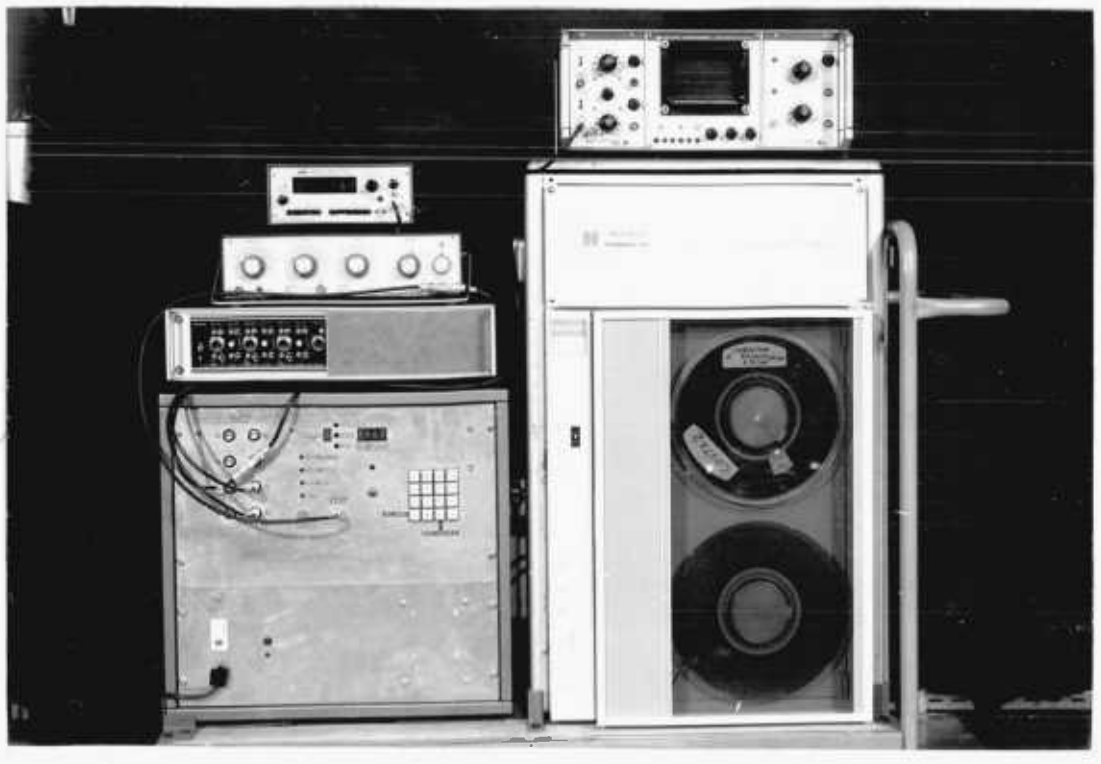

Figure 6.12: Photograph of the electronic set-up for the data acquisition and recording

CHAPTER 7

THE EXPERIMENTS AND DISCUSSION OF THE RESULTS

7.1 THEORY OF THE EXPERIMENT

It is generally accepted that parameters in a stable system operating in a nominally steady-state contain inherent fluctuations (noise) which usually have fairly well defined spectral properties. This observable noise is the result of various inherent noise excitations, the sources of which are often unknown. Any resonant properties of the observed noise are attributable to the characteristic feedbacks and non-linearities constituting the response of the system. In all practical cases, the maintenance of noise or any movement requires an "energy" input. The actual noise source will probably be a combination of noise in the energy input and the result of various random processes in the system (such as boiling in our physical system, which in turn requires "energy" input to be sustained).

For the physical system examined in this work, the feedback mechanism which causes the flowrate oscillation, results from the mass flowrate, vapour generation rate (variation of void fraction or density), and pressure drop interaction in a way similar to that described in the theoretical analysis of Chapter 4.

The system subjected to continuous excitation will selectively amplify the noise at a certain frequency (or frequencies) to produce resonances. The continuous excitation in our case is caused by the increase of power input (heat flux) without the need of external mass flowrate excitation. If the feedback gain (which is a function of power input) is sufficiently large, the damping of one of these resonances may be removed giving a sustained spontaneous oscillation which is taken as

the threshold of instability. Although a linear analysis, like the present one, would predict that a further increase in the feedback gain could lead to a divergent amplitude unstable system, it must be noticed that "non-linearities" in the system become more significant and produce constant amplitude "limit cycle" oscillations. This is revealed from a "non-linear" theoretical treatment of the problem and from experimental measurements (Neal et al (1967); Blumenkrantz and Taborek (1972)).

7.2 REPRESENTATION OF OUR PHYSICAL SYSTEM - ASSUMPTIONS

In order to justify the methods used for the analysis of the experimental measurements, some initial assumptions must be made *a priori*:

(a) We assume the process to be ergodic. This makes possible the description of the properties of the process by computing time averages over specific sample functions in the ensemble, rather by computing ensemble averages at specific instants of time. As pointed out by Bendat and Piersol (1971), the property of ergodicity is generally possessed by random data representing stationary physical processes.

(b) We assume that the system can be adequately described by a linear model. This restricts the measured levels of the signal in question (flowrate) to low levels (typically < 10%).

(c) Since, for the present experimental study, only one "output" of the system is to be recorded and processed (flowrate signal), the various individual noise sources (such as the pump pressure head, the boiling process and small variations in the heat power input or neutron power in the case of a nuclear reactor) are assumed as forming a single combined noise source injected into the system at any chosen point without the need to know the associated transfer functions by which each noise source acts upon the system in question. Furthermore, the single combined noise source is assumed to be a white noise.

(d) We assume that the external noise source into the system is stationary, i.e. independent of the system operating conditions. This is

not always true since, as also reported by Cummins (1968), very small non-stationary trends are present sometimes comparable with the signal noise level. In this case, depending on the non-stationary trend, either we can remove the trend by making a linear regression (or a higher order polynomial one) or interpret accordingly the results of the spectral analysis by applying concepts of non-stationary random processes (Bendat and Piersol (1971)).

7.3 GENERAL CONSIDERATIONS IN THE DATA PROCESSING

Since our physical system was operating at low pressures, temperatures and power levels, it was possible to operate it safely just inside the unstable region making sure that the noise signal level was smaller than the one specified in assumption (b) of the previous section. Therefore, whenever possible, we increased the signal to noise ratio in order to make the requirements in record length as small as possible and save in signal processing time. This treatment is sometimes impossible in the case of an actual nuclear reactor channel or boiler where the signal noise level has to be kept small for safety reasons. In this case, the record length required is rather high. Investigations of this kind have been reported by Gall (1973), Cummins (1969), and Corran and Cummins (1963). Most of the other investigators, where safety considerations permitted it, operate the system well inside the unstable region and make recordings of the time history record on paper chart from which they imply the instability threshold power and frequency of oscillations. We believe that our method is more scientifically based and gives a better insight of the phenomenon, although we recognise that the measured instability thresholds might be on the pessimistic side. Nonetheless, this depends on the definition of the instability point as this may be defined as the point where spontaneous oscillations begin to grow or the point where they have reached an amplitude physically unacceptable by the system in question. This latter definition depends mainly upon the particular application.

Originally, it had been planned to measure the statistical properties of the flowrate signal, sensed across the differential pressure transducer (single output), and then to proceed to the measurements of the statistical cross-properties and transfer function between the above

mentioned signal from the differential pressure transducer (flowrate), and the difference of the signals from the two fast pressure transducers fitted to the inlet and exit of the test section (total pressure drop across the test section). Therefore, the dynamic parts of these two signals would give a measure of the dynamic hydraulic impedance (as this was defined in the theoretical analysis of Chapter 4) of the experimental vapour generator.

Unfortunately, new safety regulations (imposed very recently) have restricted the operation to low pressures. In these conditions, the errors in the pressure transducers rendered such measurements useless and therefore our work to date has been confined to looking at the statistical analysis of a single output (flowrate signal from the differential pressure transducer).

7.4 TECHNIQUES FOR THE DATA ACQUISITION AND PROCESSING

The techniques for the acquisition and processing of the experimental data for the present study can be classified into the following three primary categories:

(a) Data collection, preparation and recording.

(b) Data qualification and translation.

(c) Data analysis.

7.4.1 Data Collection, Preparation and Recording

The primary element in the data collection is the instrumentation transducer which will translate the quantity which measures the physical phenomenon of interest into an analogue signal with a calibrated relationship between the input and output quantities. The transducers used for the present experimental work have already been described in detail in Chapter 6, section 6.4, where their specifications including accuracy and static and dynamic calibration characteristics were given. Also, in the same section, the transducers signal conditioning equipment were described.

The new data collection and recording system has already been described in section 6.5 of Chapter 6. However, we shall elaborate more on the raw data preparation as this constitutes a key phase for the later stage of signal processing. The data preparation stage includes data editing procedure, data digitisation procedure and data preprocessing procedure.

Prior and during the recording period, the transducers signals were visually inspected on an oscilloscope in order to detect

possible spurious or degraded data signals which might have resulted from signal dropout, loss of signal due to transducer malfunctions, etc. This consisted the data editing procedure.

The data digitisation procedure consisted of the sampling and quantisation operations which were performed by the analogue-to-digital converter as described in section 6.5.3 of Chapter 6.

The sampling was performed in equally spaced intervals and was selected such that the sampling rate (or scan rate) would be higher than twice the maximum frequency present in the signal. The sampling interval h was therefore chosen from the relation:

$$f_c = \frac{1}{2h} > f_{max} \tag{7.1}$$

where f_{max} is the maximum frequency component present in the signal, h is the sampling interval (sec), and f_c is the "Nyquist" or "folding" frequency.

Sampling at rates much higher than $1/h$ samples per second will yield correlated and highly redundant data therefore increasing the cost of calculations, while sampling at rates lower than $1/h$ samples per second will lead to confusion between the low and high frequency components, causing the problem of "aliasing" as is explained, for example, by Hsu (1970).

The quantisation operation is performed by the 10-bit ADC. This corresponds to 1024 discrete levels as described in section 6.5.3 of Chapter 6. For ideal conversion, the quantisation error probability density function is defined by:

$$p(x) = 1 \qquad -0.5 < x < 0.5$$
$$= 0 \qquad \text{otherwise}$$

Since $p(x)$ is symmetric around $x = 0$, the mean value μ_x of the error is zero and therefore the variance of the error is given by:

$$\sigma_x^2 = \int_{-\infty}^{+\infty} (x - \mu_x)^2 \, p(x) \, dx = \int_{-0.5}^{0.5} x^2 \, dx = \frac{1}{12} \qquad (7.2)$$

Therefore, the rms value of the quantisation error is:

$$\sigma_x = \sqrt{\frac{1}{12}} \simeq 0.29 \text{ scale units}$$

The peak signal to rms noise ratio for the present case of 1024 scale units is:

$$(1024 \, \Delta x)/(0.29 \, \Delta x) \simeq 4000$$

which is unimportant with respect to other sources of errors (for example, transducers).

A stage which usually follows the recording is the reformating, i.e. change of the format generated by the analogue to digital conversion system into another format accepted by the computer by using machine language programming. Fortunately, in our case the data acquisition and recording system used produces a format which is directly acceptable by the computer without having to go through the trivial and laborious procedure of reformating.

7.4.2 Data Qualification and Translation

The data qualification stage consisted of producing a plot of the time history records which would reveal any apparent non-stationary trends and also the form of the periodicities.

The data translation stage consisted of translating the experimental data recorded in the data recording system into physical units. For this purpose, a computer program was written. As described in section 6.5.3 of Chapter 6, each reading consisted of 10 bits. Each digitised reading was divided into two parts. The 6 LSB were accommodated into the second character and the 4 MSB were accommodated into the least significant part of the first character, the two remaining bits being hardwired to "1". Since each computer word consists of 60 bits, it means that 5 successive readings are placed into a computer word from left to right as the computer reads the tape.

Therefore, when reading the data from the computer, each computer word (starting from the beginning) must be shifted in a left circular fashion by 12 bits and afterwards the 50 first bits must be set to zero (i.e. the 48 first bits plus the next two bits which were hardwired to "1"). This operation can be accomplished by using the computer statement LRSHFT and a masking replacement describing a logical "AND" operation with the masking constant:

$$\text{MASKA} = 0000\ 0000\ 0000\ 0000\ 1777_8 \qquad \text{(in octal form)}$$

The shift and masking operations must be repeated 5 times for each computer word and 1024 times for each record. The last 16 LSB of the 205th computer word before the EOR, contain zeros and therefore they must be omitted as not containing "actual" data.

The same procedure is repeated for all the following records until the EOF is reached.

Appendix D presents the listing of such a computer program where:

<NOREC> = number of records in one file

<NCHAN> = number of channels (maximum of 3 in the present case)

<X,Y,Z> = three arrays which are filled with the data from the three channels (or two, or one only)

The meaning of the rest of the variables is obvious.

7.4.3 Data Analysis

In this section, a brief exposition is presented of those aspects of random functions which are of importance for the present experimental study. The treatment is rather heuristic and the basic two references to the following have been "Digital Signal Processing" by Oppenheim and Schaffer and "Random Data Analysis and Measurement Procedures" by Bendat and Piersol. The symbolism of Bendat and Piersol has been adopted and any differences are self-explanatory.

A brief description of some aspects of the stochastic analysis which are of importance for dealing with two-phase flow phenomena was given by Rakopoulos (1972).

In the following discussion, the formulae assume the experimental data to be processed as discrete time series values representing sample records from stationary ergodic random processes. The experimental data values $\{u_n\}$ are assumed digitised according to the considerations (Nyquist folding frequency) discussed in section 7.4.1.

The discussion includes methods for the computation of arithmetic quantities (mean values - standard deviations - removal of DC component), trend removal, filtering, probability density functions, auto-correlation functions and power spectral density functions using fast Fourier transforms (FFT).

7.4.3.1 Arithmetic quantities

(a) Mean value

The record mean value $\bar{u}$ is given by:

$$\bar{u} = \frac{1}{N} \sum_{n=1}^{N} u_n \tag{7.3}$$

where N is the number of data samples and u_n are the data values.

(b) Removal of DC component

The data values u_n are transformed to have a zero mean value by subtracting the mean value (DC component). This simplifies the analysis and it is also necessary for the computation of spectral properties by using fast Fourier transform algorithms.

Therefore, we define a new time history record:

$$x(t) = x(t_o + n\,h) = u_n - \bar{u} \qquad n = 1, 2, \ldots, N \tag{7.4}$$

The new mean value $\overline{x} = 0$. All subsequent formulae will now be stated in terms of the transformed data values $\{x_n\}$.

(c) Standard deviation

The record standard deviation is given by:

$$\sigma_x = \left[\sum_{n=1}^{N} \frac{(x_n)^2}{N-1} \right]^{\frac{1}{2}} \tag{7.5}$$

7.4.3.2 Trend removal

Sometimes a special correction is needed to remove a trend in the data. Least squares procedures are usually employed for the removal of linear as well as higher order polynomial trends as, for example, reported by Cummins (1968). The existence of trends distorts the low frequency power spectral content.

For the present study, a least square procedure was employed to remove the linear trend (if any). The first degree polynomial is defined by:

$$\hat{u}_n = b_o + b_1 (n\,h) \qquad n = 1, 2, \ldots, N \tag{7.6}$$

Using a least square method fit, the coefficients b_o and b_1 are given as follows:

$$b_o = \frac{2\,(2N+1) \sum_{n=1}^{N} u_n - 6 \sum_{n=1}^{N} n\,u_n}{N\,(N-1)} \tag{7.7}$$

$$b_1 = \frac{12 \sum_{n=1}^{N} n\,u_n - 6\,(N+1) \sum_{n=1}^{N} u_n}{h\,N\,(N-1)\,(N+1)} \tag{7.8}$$

where h is the constant sampling interval (sec).

7.4.3.3 Filtering

For the present experimental study, the frequencies

of interest were in the range 0.02 - 1.5 Hz (density wave oscillations). The differential pressure transducer frequency response was flat in this range and it was steeply decreasing above that range. Therefore, either analogue or digital filtering of the data was not needed. The sampling rates selected were 5 or 10 samples per second (h = 0.2 or 0.1 seconds, respectively) which are higher than twice the maximum frequency of 1.5 Hz (f_c = 2.5 Hz $\hat{=}$ Nyquist folding frequency).

7.4.3.4 Probability density function

The probability density function of the time record $u(t)$ can be estimated by:

$$\hat{p}(u) = \frac{N_u}{N\,W} \tag{7.9}$$

where W is a narrow interval centred at u and N_u is the number of data values which fall within the range $u \pm W/2$. Hence, an estimate $\hat{p}(u)$ is obtained digitally by dividing the full range of u into an appropriate number of equal width class intervals, tabulating the number of data values in each class interval, and dividing by the product of the class interval width W and the sample size N. Obviously, the estimate $\hat{p}(u)$ is not unique since it clearly depends upon the number of class intervals and their width selected for the analysis.

For the present study, a computer program (PROBIL) was written to calculate the estimates of the probability density function as given by equation (7.9). Sixteen class intervals were chosen for the present experimental data. The computer program gives also (for comparison purposes) the values of the Gaussian probability density function with the same mean value and standard deviation computed for the experimental data record:

$$p(u)_{GAUSS} = \frac{1}{\sigma_u \sqrt{2\pi}} exp \left[- \frac{(u - \mu_u)^2}{2\sigma_u^2} \right] \qquad (7.10)$$

where μ_u and σ_u are the mean value and standard deviation of the time record $u(t)$.

7.4.3.5 Fast Fourier transform

Fourier series and Fourier transforms of data differ in their theoretical properties but not in their digital computational details because only a finite range Fourier series or transform can be computed with digitised data, and this finite range can always be considered as the period of an associated Fourier series.

The main reason for the importance of fast Fourier transforms over the conventional methods stems from the fact that they can be used to provide estimates of the spectral density and correlation functions directly from the time history records and much quicker.

In Appendix E, a brief description of the basis for fast Fourier transform calculation procedures is given.

For the present data analysis, a standard subroutine of the NAG (Nottingham Algorithm Group) Library was used to calculate the fast Fourier transform of the complex record $z(n) = x(n) + j\ y(n)$.

7.4.3.6 Power spectral density function

For the calculation of power spectral density function, the "direct Fourier transform" or "Cooley-Tukey" method based on computing the power spectral density function via a finite-range fast Fourier transform (FFT) of the original data was used.

Procedural steps:

1. Truncation of data sequence or addition of zeros so that $N = 2^p$. In our case, this stage was always avoided since the length of each record was $1024 = 2^{10}$ "words" as explained in Chapter 6. Therefore, we always selected a number of records which was an integer multiple of 2.

2. Tapering of time record to reduce the "leakage" because of the finite record length used. A cosine taper data window was used to taper one-tenth of the data record on either side.

3. Computation of the Fourier components defined by:

$$X_k = \frac{X(f_k, T_r)}{h} = \sum_{n=0}^{N-1} x_n \exp\left[-j \frac{2\pi k n}{N}\right] \qquad (7.11)$$

at the usual FFT discrete frequency values:

$$f_k = \frac{k}{T_r} = \frac{k}{N h} \qquad k = 0, 1, \ldots, N-1 \qquad (7.12)$$

using FFT procedures.

4. Computation of the raw estimates of the power spectral density function $\tilde{\tilde{G}}_k$ from:

$$\tilde{\tilde{G}}_k = \tilde{\tilde{G}}_x(f_k) = \frac{2}{N h} |X(f_k, T_r)|^2 = \frac{2h}{N} |X_k|^2$$

for $k = 0, 1, \ldots, N-1 \qquad (7.13)$

where $T_r = N.h$ is the record length.

5. Adjustment of these estimates for the scale factor due to the cosine tapering used in step 2. Therefore, $\tilde{\tilde{G}}_k$ is replaced by $\tilde{\tilde{G}}_k/0.875$.

6. Frequency smoothing by averaging l neighbouring frequency components of the raw spectral estimates, i.e.

$$\hat{G}_k = \frac{1}{l}\left[\tilde{\tilde{G}}_k + \tilde{\tilde{G}}_{k+1} + \ldots + \tilde{\tilde{G}}_{k+l-1}\right] \tag{7.14}$$

The resolution bandwidth for the raw spectral estimates is:

$$B_e = 1/T_r \tag{7.15}$$

For the smooth spectral estimates, the resolution bandwidth becomes:

$$B'_e = l\, B_e = \frac{l}{T_r} \tag{7.16}$$

Therefore, the normalised standard error is given by:

$$\varepsilon_r = \sqrt{\frac{1}{B'_e\, T_r}} = \sqrt{\frac{1}{l}} \tag{7.17}$$

7.4.3.7 Auto-correlation function

The estimated auto-correlation function $\hat{R}_r$ at the displacement rh is defined by:

$$\hat{R}_r = \hat{R}_x(r\,h) = \frac{1}{N-r}\sum_{n=1}^{N-r} x_n\, x_{n+r} \qquad (7.18)$$

for $r = 0, 1, 2, \ldots, m$

where r is the lag number and m is the maximum lag number. The time lag is $\tau = rh$.

The method used for the computation of the auto-correlation function was the roundabout approach of first computing the power spectrum by direct fast Fourier transform procedures and then computing the inverse fast Fourier transform of the power spectrum.

Procedural steps:

1. Augmentation of the N data record ($\{x_n\}$ $n = 0, 1, \ldots, N-1$) with N zeros to obtain a new $\{x_n\}$ sequence of $2N$ terms. This step is required in order to avoid the calculation of another correlation function called "circular" correlation.

2. Computation of the $2N$ point FFT giving X_k for $k = 0, 1, \ldots, 2N-1$.

3. Computation of the raw spectral estimates $\tilde{\tilde{G}}_k$ for $k = 0, 1, \ldots, 2N-1$ using equation (7.13).

4. Computation of the $2N$ point inverse FFT of $\tilde{\tilde{G}}_k$ and multiplication by the scale factor $N/(N-r)$ to obtain $\hat{R}_r$ for $r = 0, 1, \ldots, N-1$. The second half of $\hat{R}_r$ ($r = N, N+1, \ldots, 2N-1$)

is discarded. When taking the inverse FFT of G_k smoothing must not be performed.

Two computer programs (ASPEC and ACORL) have been written and developed to compute the power spectral density and correlation functions using FFT techniques. The programs have been tested against data having known spectral properties. These data were taken either from standard subroutines of the Computer Library or generated by appropriate electronic equipment in the Electronics Laboratory.

7.5.1 Commissioning of the Freon Loop

Prior to loading with Freon-113, the experimental rig was pressurised with Freon-12 vapour at 6 bars to be tested for leakage. Then the system was evacuated and filled slowly with Freon-113 under gravity.

Before circulating the Freon, the following steps were taken:

i) The water supply was checked.

ii) The valves were tested and each valve was ensured to be open except for the first valve downstream of the pump which was kept half closed (for these conditions, the main flow would be ≃ 0.7 kg/sec).

iii) All the automatic controls (including the safety devices) were checked.

After these checks had been completed, the pump was switched on and then the Freon-113 was heated by supplying electric power to both the preheater and the test section for nearly one hour. When the system pressure reached approximately 1.5 bar (in the condenser), the vent at the top of the condenser (highest point in the rig) was opened slowly and the mixture of air and Freon vapour was released through a long polythene tube to an extraction duct. After the air venting had been completed, the vent was secured closed and all the heaters were switched off, and the cooling water through the condenser was set to a maximum (≃ 1.2 kg/sec).

During all the time the safety indicators and alarms were in action.

7.5.2 Test Procedure

For each data run, the flow was adjusted by regulating the valves downstream of the pump so that the main flow was roughly 0.7 kg/sec. The inlet and exit throttlings at the test section were fixed and the subcooling was adjusted by the automatic preheater. The pressure at the test section exit was kept at 1 atm, and the cooling water flow through the condenser, for the heating powers considered, was varying in the range 0.4 - 0.6 kg/sec.

The test section power was increased in three or four steps and sufficient time was allowed so that the system could reach steady running conditions. During the course of a run, the Freon inlet temperature was constant inside $\pm$ 0.5^{o}C. It was observed that the flow through the test section was reduced due to the increased pressure drop characteristics of the two-phase flow mixture. If a certain flowrate was to be maintained, then either the test section upstream valve was opened slightly or a needle valve in the by-pass line was slightly adjusted. This would change the by-pass to the test section flowrate ratio slightly, but still the high by-pass ratio ($\simeq$ 12 - 15) would ensure the constant pressure drop condition maintained across the test section.

We have investigated conditions of uniform and oscillating flows for the following range of variables:

(a) Pressure level at test section inlet: 1.7 - 2.0 bars

(b) Freon inlet temperature constant: 31 - 33^{o}C

(c) Mass flowrate through test section: 0.045 - 0.060 kg/sec
(corresponding Freon velocities through coil: 0.50 - 0.65 m/sec
assuming a density of 1440 kg/m^{3})

(d) Two different valve settings

(e) Three different heating powers of 2, 2.5 and 3 kW

During the course of a run, the mass flowrate signal from the differential pressure transducer (fitted to the test section inlet) was continuously monitored and observed on an oscilloscope at a high sensitivity to reveal the nature of the flow noise level. Meanwhile, all the monitoring equipment was continuously observed.

After reaching the desired conditions of flow noise, recording was made of the mass flowrate signal according to the considerations described in the next section.

After the recording had been completed, all the heaters were switched off and the condenser cooling water was set to a maximum. The system was left for approximately 90 minutes to cool down to ambient temperature and then the pump was switched off and the cooling water stopped. The system was then again tested for leakage.

7.6 SELECTION OF PARAMETERS FOR DATA RECORDING AND REDUCTION

The mass flowrate signal from the differential pressure transducer was recorded into the data acquisition system described in Chapter 6. The sampling interval selected was 0.1 seconds for all the cases but two where it was selected as 0.2 seconds. For the worst case of h = 0.2, the sampling frequency is 5 samples per second, which is twice as high as the maximum frequency component present in the signal. This was proved correct *a posteriori* since all the power spectral density curves have a zero value for f > 2.5 Hz. Therefore, no aliasing occurred.

We accepted a normalised standard error ε_r = 0.25 for the power spectral density functions. Therefore, the value of l (number of neighbouring frequency components to be averaged to perform smoothing), as calculated from equation (7.17), is:

$$l = \frac{1}{\varepsilon_r^2} = \frac{1}{0.25^2} = 16$$

If N is the number of data elements to be recorded, then the record length is $T_r = Nh$ and the resolution bandwidth of the smoothed spectrum is:

$$B'_e = \frac{l}{T_r} = \frac{16}{N \times (0.1)} \text{ Hz}$$

We selected N = 2 × 1024 = 2048 = 2^{11} data for all the cases, which gives a resolution bandwidth of (for the worst case of h = 0.1 seconds):

$$B'_e = \frac{16}{2048 \times 0.1} = \frac{16}{204.8} = 0.078125 \text{ Hz}$$

Therefore, the minimum frequency to be investigated had to be (centred in the middle of the bandwidth):

$$f_{min} = \frac{B'_e}{2} = \frac{0.078125}{2} = 0.0390625 \text{ Hz}$$

Although the accepted normalised standard error (ε_r = 25%) might seem excessive at a first glance, it must be emphasised that it refers to the random portion of the data. As pointed out by Bendat and Piersol (1971), if the purpose of the test is to find hidden periodicities (as in the present case), then B'_e can be made smaller (i.e. l small) against the accuracy of the power spectral density curve (i.e. ε_r high).

Obviously, a higher number of recorded data N would increase the accuracy. We tried some runs with N = 4096 data, but in this case the lower frequency components were distorted due to various trends whose magnitudes were comparable to the noise signal level.

Two parameters of interest for the stability analysis were considered. The first one was the square of the normalised standard deviation, defined by:

$$\sigma_{nr}^2 = \frac{\sigma_x^2}{\tilde{u}^2} \tag{7.19}$$

where σ_x and $\tilde{u}$ are defined by equations (7.3) and (7.5). The standard deviation σ_x is the one found after any linear trend removal, and $\tilde{u}$ is the mean value of the recorded mass flowrate signal.

The second parameter was the ratio of the power content at the highest peak of the power spectral density function (corresponding to a frequency f_{MP}) divided by the overall power content. This ratio φ^2 is a measure of the signal to noise ratio:

$$\varphi^2 = \frac{\psi_x^2(f_{MP}, B'_e)}{\sigma_x^2} \tag{7.20}$$

where, in general, $\psi_x^2(f,B_e)$ is the mean square value of $x(t)$ within the bandwidth B_e centred at f and is estimated by:

$$\hat{\psi}_x^2(f,B_e) = \frac{1}{T}\int_0^T x^2(t,f,B_e)\,dt = \int_{\xi=f-B_e/2}^{\xi=f+B_e/2} G_x(\xi)\,d\xi \qquad (7.21)$$

When the lower and upper limits in the integral of equation (7.21) are 0 and ∞, respectively, (or f_{min} and f_{max}) and the mean value $\tilde{x} = 0$, then the integral of equation (7.21) equals σ_x^2. Therefore, the value of φ^2 represents the fraction of the overall power content of the signal which is occupied by the highest peak (if any). In equation (7.21), G_x is the power spectral density function of $x(t)$.

For the present study, the mean value $\tilde{u}$ of the signal (flowrate) has been subtracted from each value u_n. Therefore, according to equation (7.4), we considered the new time history record :

$$x(t) = x(t_o + n\,h) = u_n - \tilde{u} \qquad n = 1, 2, \ldots, N$$

The value of σ_x^2 (where $\tilde{x} = 0$) can be directly taken from the value of the auto-correlation function $R_x(0)$ at the origin (time lag $\tau = 0$), as given by Lee (1966).

The value of $\psi_x^2(f_{MP},B_e')$ can be approximated (using the power spectral density plot) by the formula:

$$\psi_x^2(f_{MP},B_e') = G_x(f_{MP})\,B_e' \qquad (7.22)$$

according to equation (7.21) and assuming $G_x(f_{MP})$ = constant inside the bandwidth B_e'. In other words, we consider the area of a rectangle with base B_e' and height $G_x(f_{MP})$.

The output from our computer program ASPEC gives actually the normalised power spectral density function with respect to the square of the mean value of the signal, i.e.

$$G_{nr}(f) = \frac{G_x(f)}{\tilde{u}^2} \tag{7.23}$$

Therefore, according to equations (7.19), (7.20) and (7.23), we take for the parameter φ^2:

$$\varphi^2 = \frac{G_{nr}(f_{MP})}{\sigma_{nr}^2} B'_e \tag{7.24}$$

At this stage, we will make a note on the time history record which was actually processed. As mentioned in Chapter 6, the relationship between the pressure drop measured across the Venturi-meter and the output signal from the transducer $\{u'_n\}$ is linear, i.e.

$$u'_n = c_1 \Delta P \tag{7.25}$$

and the relationship between the differential pressure and mass flowrate is of the square law type:

$$\dot{m} = c_2 \sqrt{\Delta P} \tag{7.26}$$

therefore:

$$u'_n = c_3 \dot{m}^2 \tag{7.27}$$

where c_1, c_2, c_3 = constants.

For the present work, we took the square root of the recorded raw signal, so that our time history record (to be further processed) was:

$$u_n = \sqrt{u'_n} = \sqrt{c_3}\, \dot{m} \tag{7.28}$$

Considering the case where the variation of the mass flowrate is sinusoidal of the form:

$$\dot{m} = \tilde{\dot{m}} \, (1 + a \sin \omega t) \tag{7.29}$$

we find from equation (7.27):

$$u_n' = c_3 \, \tilde{\dot{m}}^2 \, (1 + 2a \sin \omega t + a^2 \sin^2 \omega t) \tag{7.30}$$

where a is the dimensionless amplitude of the fluctuation in $\dot{m}$. Now, if a is small (less than 0.10), the last term in equation (7.30) can be ignored, i.e.

$$u_n' = c_3 \, \tilde{\dot{m}}^2 \, (1 + 2a \sin \omega t) \tag{7.31}$$

which has the same frequency as the signal u_n given by equation (7.28), but twice as high dimensionless amplitude fluctuation.

7.7 THE EXPERIMENTAL RESULTS - DISCUSSION

Table 7.1 lists the different experimental runs performed inside the range of parameters stated in section 7.5.

Eighteen successful runs were carried out which are listed in Table 7.1. The first ten runs correspond to an open upstream valve position and a half closed downstream valve position, referred to as the unstable set. The last eight runs correspond to a half closed upstream valve position and an open downstream valve position, referred to as the stable set.

Apart from these eighteen runs, more runs were performed which failed due, for example, to inexperienced operation, electrical interference, etc.

In Table 7.1, the Freon inlet temperature T_{in}, the mass flowrate $\dot{m}$, and the corresponding velocity U_c through the coil are given. For each different value of heating power (2, 2.5 or 3 kW), the mass flowrate is given in a decreasing way in order to demonstrate the approach to the instability point. The mean value $\tilde{u}$ of the time history record u_n, given by equation (7.28), is shown in the same Table. The value $\tilde{u}$ was calculated from the computer program (units in $\sqrt{\text{volts}}$) and then the values of $\dot{m}$ and U_c were calculated taking into account the static calibration characteristics for the differential pressure transducer and the Venturimeter as given in detail in Chapter 6.

The exit quality for each run is also indicated in the same Table. The pressure change through the test section for all the runs is quite considerable ($\simeq$ from 1.8 to 1.0 bar) and so is the change of the Freon thermodynamic and transport properties. For comparison purposes, we considered for all the runs the following values:

$$\Delta h_s = 8 \text{ kJ/kg} \quad , \quad h_{fg} = 140 \text{ kJ/kg}$$

and therefore the exit quality was calculated from the formula:

$$x_{ex} = \frac{\frac{Q \text{ (kW)}}{\dot{m} \text{ (kg/sec)}} - 8}{140} \tag{7.32}$$

The chosen value for the inlet subcooling of 8 kJ/kg, corresponding to $\Delta T_{sub} = 8^{o}C$ ($c_f \simeq 1$ kJ/kg), may seem at a first glance small since the Freon inlet temperature is $\simeq 32^{o}C$ and the saturation temperature at 1 bar is $47^{o}C$. In fact, as reported by Murphy and Bergles (1972), any concentration of dissolved gases in the Freon (as it is air in our case) reduces the boiling point considerably. The higher the concentration of dissolved gases, the higher the reduction on the boiling point. Assuming that the boiling took place at $\simeq 1.3$ bar, we estimated a boiling point of $\simeq 40^{o}C$, from where $\Delta T_{sub} \simeq 40^{o}C - 32^{o}C = 8^{o}C$.

Table 7.1 shows for each run the computed values for the square of the normalised standard deviation σ_{nr}^2, the frequency f_{MP} corresponding to the highest peak of the power spectral density function, the normalised power content $\psi_{nr}^2(f_{MP})$ at the highest peak, and the parameter φ^2 giving a measure of the signal to noise ratio as all these parameters were defined in detail in the previous section. The sampling interval h (sec) is also given.

Figures 7.1 to 7.36 show the power spectral density and auto-correlation plots for all the runs listed in Table 7.1, as they were computed by our digital computer programs ASPEC and ACORL described in section 7.4.3. Figures 7.37 to 7.40 display for four of the runs the probability density plots (before trend and DC component removal) together

with the corresponding Gaussian ones having the same mean value and standard deviation, as they were computed by our computer program PROBIL.

It can be seen that the experimental probability density functions follow quite closely the Gaussian ones with two small bumps around the mean value denoting the existence of possible sinusoidal components (Bendat and Piersol (1971)).

From Table 7.1 and Figures 7.1 to 7.36, it can be seen that the noise (σ_{nr}^2) increases with a decrease in flow for the same power or an increase in power for the same flow, both for the unstable and stable set. This is according to analytical predictions as described in Chapter 5 and it will be demonstrated in the next section.

For the unstable set, it can be seen that as we reduce the flow (for constant heating power), the content of the power spectrum begins to concentrate on a selected frequency (f_{MP}) and eventually $\psi_{nr}^2(f_{MP})$ is clearly distinguished having a high value ($\simeq$ 10 times higher than the rest of the spectrum). Accordingly, by definition, the value of the parameter φ^2 increases considerably with a decrease in flow (for the same heating power).

The same effect can be observed from the auto-correlation plots, where with continuously decreasing flow the signal begins to take the form of a clear, strong sinusoid.

This clearly demonstrates that the damping of one of the resonances is removed giving rise to sustained spontaneous oscillations in a mechanism similar to the one described in section 7.1.

It can also be seen that with increasing power, the resonance moves to higher values (for f_{MP} and $\dot{m}$ kept constant), an effect according to analytical predictions.

The unstable set corresponds to an open upstream valve (low upstream

throttling) which encourages the inception of instability according to analytical predictions. On the other hand, the stable set corresponds to a half closed upstream valve (high upstream throttling) and as it can be observed, the noise (σ_{nr}^2) is much lower compared with the corresponding case of the unstable set (same Δh_s, Q and $\dot{m}$) and what is more important, there is no apparent favour for a certain resonance. The stabilising effect of the upstream throttling is again in agreement with analytical predictions. For the stable set, the higher values of the power spectrum are concentrated in the region 0.25 - 0.40 Hz, sometimes with smaller spikes in the region 1.0 - 1.3 Hz.

Obviously, for the stable set, the parameters $\psi_{nr}^2(f_{MP})$ and φ^2 do not have any significant importance since there are more than one "potential" resonances of about the same value either close together or spread apart. For the completeness of the work, however, their values are given in the same Table 7.1, but no conclusions must be drawn from these values.

From the range of exit qualities and the range of frequencies reported herein, we believe that the observed instabilities are density wave oscillations. Indeed, the period of oscillations for the present experimental work (2 - 2.5 sec) is roughly equal to the transit time of a particle in the heated test section, as is verified by our computer program.

7.8 COMPARISON WITH ANALYTICAL PREDICTIONS

As described in the previous section, the parametric trends (effect of governing variables) of the density wave oscillations were verified by our experimental investigation. In this section, we will compare the observed dynamic behaviour of our boiler with analytical predictions from our computer model described in Chapters 4 and 5.

As a word of caution, we must emphasise from the beginning that a basic assumption of the theoretical model is that the heated channel pressure drop must be small compared to the pressure level (incompressible model), an assumption which is poor in the present case, since the pressure level was changing from ≃ 2.0 bar to 1.0 bar. Therefore, the significant change in the thermodynamic and transport properties could not be taken into account. Also, at low pressures there is substantial flashing which, together with vapour expansion, increases the velocity gradient. The velocity gradients arising from flashing and vapour expansion are very different from the velocity gradients produced by heat input as reported by Crowley and Bergles (1970), and their effect on density wave oscillations tends to be stabilising. Also, the inevitable concentration of air in the Freon could not be taken into account by the theoretical model.

Our computer program was supplied with the geometrical dimensions of the heated coil and the upstream and downstream straight adiabatic sections as these were given in Chapter 6.

The properties were evaluated at a reference upstream pressure of 2 bars.

Two different valve settings were considered, as described in the previous section.

The values of the orifice coefficients, K_i and K_e, for the upstream

and downstream valves, respectively, were determined experimentally for all liquid flow through the test section by the formulae:

$$\Delta P_i = K_i \rho_f U_f^2 \qquad \text{and} \qquad \Delta P_e = K_e \rho_f U_f^2$$

The values for the two positions of each valve are:

Upstream valve :	Open position	K_i	= 140 v.h. (14.6)
	Half closed position ($2\frac{1}{4}$ turns closed)	K_i	= 350 v.h. (36.5)
Downstream valve:	Open position ($1\frac{3}{4}$ turns closed)	K_e	= 8.5 v.h. (0.885)
	Half closed position ($1\frac{7}{8}$ turns closed)	K_e	= 17 v.h. (1.77)

The values inside the parentheses are the orifice coefficients referred to the test section tube inside diameter (d_c = 0.0088 m, $\frac{1}{4}$" BSTE, medium thickness) and the values outside the parentheses are referred to the inside diameter of the upstream or downstream straight tubes ($d_{up} = d_d$ = 0.0155 m, $\frac{1}{2}$" BSTE, heavy). The ratio of each pair is equal to the square of the ratio of the inside cross-sectional areas, i.e.

$$\left(\frac{d_{up}}{d_c}\right)^4 = \left(\frac{0.0155}{0.0088}\right)^4 = 9.6$$

The two-phase friction factor was taken constant and equal to the single phase friction factor, i.e. $f_2 = f_1$.

The inlet subcooling considered was Δh_s = 8 kJ/kg, as explained in the previous section.

The program was run for uniform heating powers of 2, 2.5 and 3 kW and

for Freon velocities through the coil of 0.70, 0.65, 0.60, 0.55 and 0.50 m/sec.

The parameters associated with the heater wall are:

$$k_m = 0.200 \text{ kW/m}^{\circ}\text{C} \quad , \quad c_m = 0.890 \text{ kJ/kg}^{\circ}\text{C}$$

$$\rho_m = 2780 \text{ kg/m}^3, \text{ therefore, } a_m = 80.83 \times 10^{-6} \text{ m}^2/\text{sec}$$

inside diameter $d_i = 0.88$ cm , outside diameter $d_o = 5.0$ cm

The time constants associated with the heater dynamics, as given in Chapter 4, are found as follows from our computer program (for $U_c = 0.60$ m/sec):

$$\tau_k = 0.239 \text{ sec} \quad , \quad \tau_f = 2.969 \text{ sec} \quad \text{and} \quad \tau_h = 9.837 \text{ sec}$$

The last two columns of Table 7.1 (as this was introduced in the previous section) are filled with the approximate phase cross-over frequency f_π and the inverse of the gain margin g_π, as these are determined from the Nyquist stability plots computed by FLOSIL, taking into account the slip between the phases and ignoring the heater dynamics.

The quantities f_π and g_π are a measure of the relative stability (Di Stefano et al (1967)) of a feedback control system and are defined as follows.

The phase cross-over frequency f_π is that frequency at which the Nyquist polar plot crosses the negative real axis and the inverse of the gain margin g_π is the corresponding distance of the intersection point

from the origin (real number). If $g_\pi < -1$, the system is unstable, if $g_\pi > -1$, the system is stable, and if $g_\pi = -1$, the system is just stable. The higher the deviation of g_π from the -1 value on the lower or higher side, the higher the instability or stability, respectively, of the system concerned.

From Table 7.1, it can be seen that the analytical predictions verify the observed experimental behaviour, i.e. the system tends to a more unstable condition by decreasing the flow (keeping the heating power constant), or by increasing the power (keeping the flow constant). It can also be seen that the potential frequency of oscillations f_π moves to higher values with increasing power (for Δh_s and $\dot{m}$ kept constant). The strongly stabilising effect of the increased upstream throttling of the stable set is predicted as well.

In general, the unstable set (ten first runs) is predicted unstable and the stable set (eight last runs) is predicted stable. The agreement from the quantitative point of view is rather reasonable by taking into account that the model is rather simple and that it does not consider some important factors, as these were described at the beginning of this section.

When the inertia of the heater wall was taken into account, we found a high stabilising effect (because of the same reasons stated in section 5.3.2 of Chapter 5). The unstable set was predicted stable and the stable set much more stable.

For comparison purposes, Figures 7.41, 7.42 and 7.43 show the stabilising effect of the heat flux-flow interaction, as was described in section 5.3.2 of Chapter 5. These Figures show the Nyquist plots of the open loop frequency response for the conditions of the unstable set, for U_c = 0.60 m/sec, Δh_s = 8 kJ/kg and for the three different heating powers

of 2, 2.5 and 3 kW. Each Figure contains two Nyquist plots; one when the heater dynamics are ignored and one when they are considered.

Figure 7.44 shows the three Nyquist plots of the open loop frequency response (ignoring the heater dynamics) for the conditions of the stable set, for U_c = 0.60 m/sec, Δh_s = 8 kJ/kg, and for the three different heating powers of 2, 2.5 and 3 kW.

The Freon-113 properties were evaluated at 2 bars.

7.9 CONCLUSIONS

The dynamic behaviour of the present experimental vapour generator verifies the parametric trends of the density wave oscillations as has been reported in experimental and theoretical studies of the subject.

The stochastic analysis developed to study the dynamics of the experimental vapour generator gives meaningful results and insight into the phenomenon. This method is found to be efficient and quick and it has been made possible by the development of a new data acquisition and recording system (described in Chapter 6).

From the discussion of the previous section, it can be concluded that the analytical predictions from our computer model (described in Chapters 4 and 5) are in qualitative agreement with the experimental results. The phase cross-over frequency f_π and the inverse of gain margin g_π are used successfully to compare deterministic quantities with the stochastic quantities (f_{MP}, σ_{nr}^2, ψ_{nr}^2, φ^2) computed from the experimental runs. Such a kind of comparison has not, to the author's knowledge, been applied before to two-phase flow dynamics problems.

The quantitative agreement between analytical predictions and experimental results is reasonably fair.

It appears that modifications of the analytical formulation of the model are required before it can be applied to low pressure systems such as the present one. For these systems, the effect of dissolved air in the Freon, the effect of flashing and vapour expansion, and the wall heat storage need to be investigated further.

We believe that our theoretical model would give better quantitative agreement if higher pressures were permitted to be applied to our experimental facility, since the influence of the previously mentioned factors would then be reduced, and furthermore the data at these higher

pressures would be useful in studying the modelling of dynamically similar high pressure steam generators.

TABLE 7.1

Run No.	K_i, K_e (v.h.)	Q (kW)	T_{in} (^oC)	$\tilde{u}_n$ ($\sqrt{v}$)	U_c (m/s)	$\dot{m}$ (kg/s)	x_{ex}	f_{MP} (Hz)	σ_{nr}^2 (10^{-4})	Maximum ψ_{nr}^2 (10^{-4})	φ^2	h (sec)	U_c (m/s)	f_π (Hz)	g_π
R 1	UNSTABLE SET K_i = 14.6 , K_e = 1.77	2.0	33.0	2.2160	0.639	0.0570	0.19	~0.40	0.6985	0.0781	0.112	0.1	0.60	0.25	-1.08
R 2			32.5	2.0630	0.595	0.0531	0.21	0.44	0.7284	0.0977	0.134	0.1	0.55		-1.30
R 3			32.5	1.7565	0.507	0.0452	0.26	0.56	3.5653	0.0625	0.175	0.2	0.50		-1.50
R 4		2.5	31.5	2.0897	0.603	0.0538	0.27	~0.40	1.0649	0.0937	0.088	0.1	0.65	0.30	-1.40
R 5			31.0	1.9499	0.562	0.0502	0.30	0.48	1.6570	0.3516	0.212	0.1	0.60		-1.60
R 6			32.5	1.7564	0.507	0.0452	0.34	0.58	3.7927	1.2734	0.336	0.1	0.55		-1.80
R 7		3.0	33.0	2.3077	0.666	0.0594	0.30	~0.40	0.9389	0.0937	0.100	0.1	0.70	0.35	-1.60
R 8			32.5	2.1273	0.614	0.0548	0.33	0.48	1.1491	0.1797	0.156	0.1	0.65		-1.82
R 9			31.5	2.0754	0.599	0.0534	0.34	0.56	2.7168	0.6328	0.233	0.1	0.60		-2.05
R10			33.0	1.9099	0.551	0.0492	0.38	0.60	2.8785	0.7617	0.265	0.2	0.55		-2.37
R11	STABLE SET K_i = 36.5 , K_e = 0.88	2.0	32.5	1.9358	0.558	0.0498	0.23	~0.3	0.4483	0.0664	0.148	0.1	0.60	0.27	-0.48
R12			33.0	1.7053	0.492	0.0439	0.27		0.8769	0.0937	0.107	0.1	0.50		-0.65
R13		2.5	33.0	1.9602	0.565	0.0505	0.30	0.2 ~ 0.4	0.4685	0.0664	0.142	0.1	0.65	0.34	-0.60
R14			31.5	1.9207	0.554	0.0494	0.30		0.7590	0.1133	0.149	0.1	0.60		-0.67
R15			32.5	1.8430	0.532	0.0474	0.32		0.8980	0.0898	0.100	0.1	0.55		-0.78
R16		3.0	31.0	2.0541	0.592	0.0529	0.35	0.2 ~ 0.4	0.8769	0.0719	0.082	0.1	0.70	0.40	-0.68
R17			32.5	1.8066	0.521	0.0465	0.40		0.9498	0.0914	0.096	0.1	0.60		-0.88
R18			31.5	1.7856	0.515	0.0460	0.41		1.2859	0.1680	0.131	0.1	0.55		-0.99

Number of data N = 2048; ~ denotes approximate region

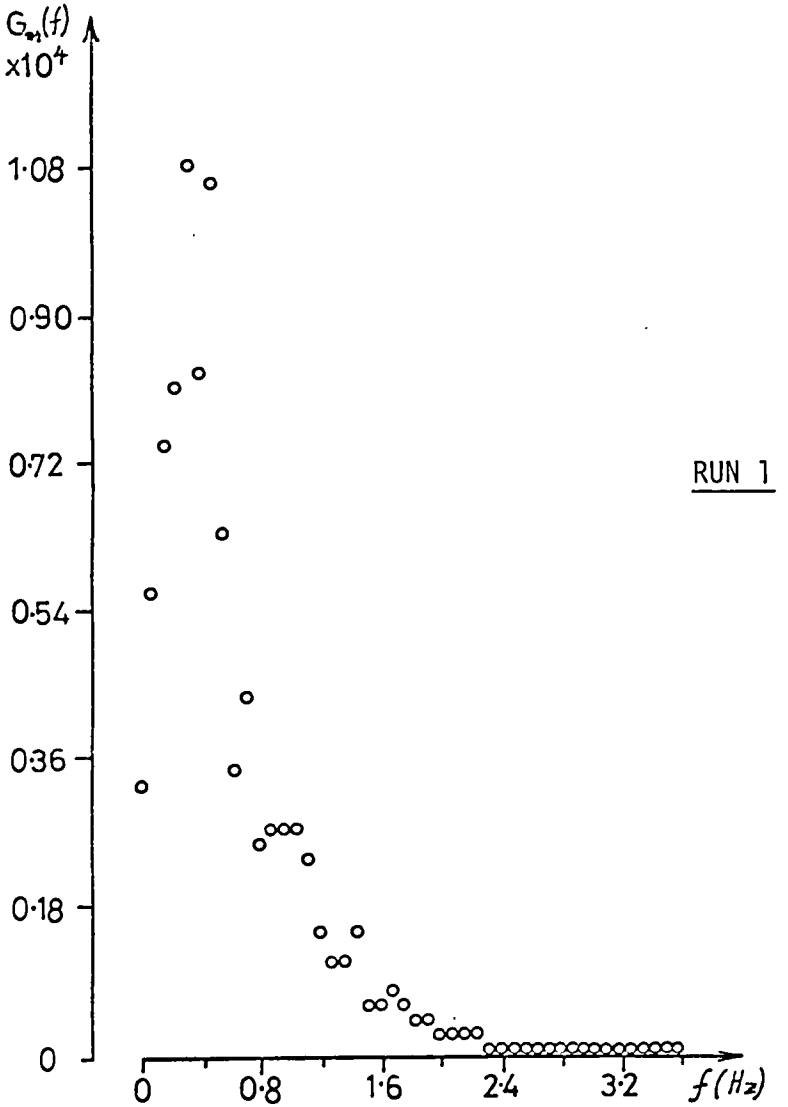

Figure 7.1: Power spectral density function

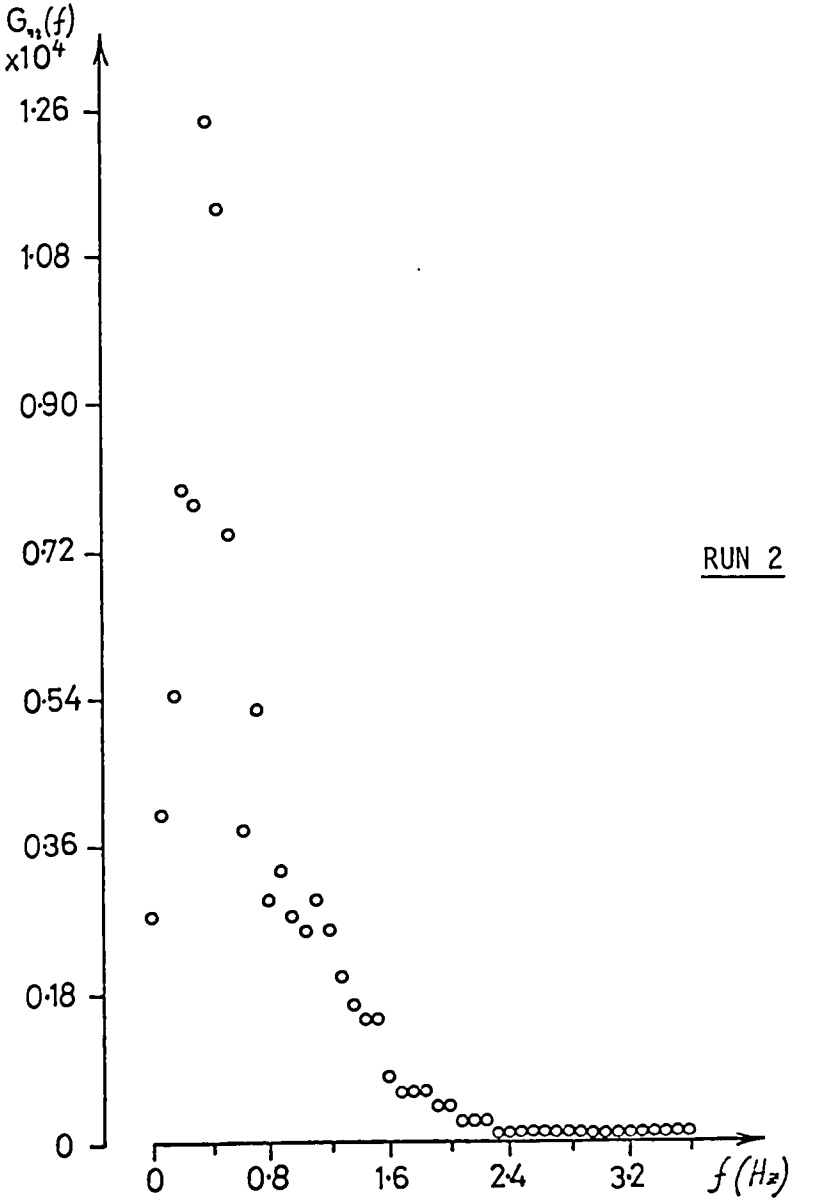

Figure 7.2: Power spectral density function

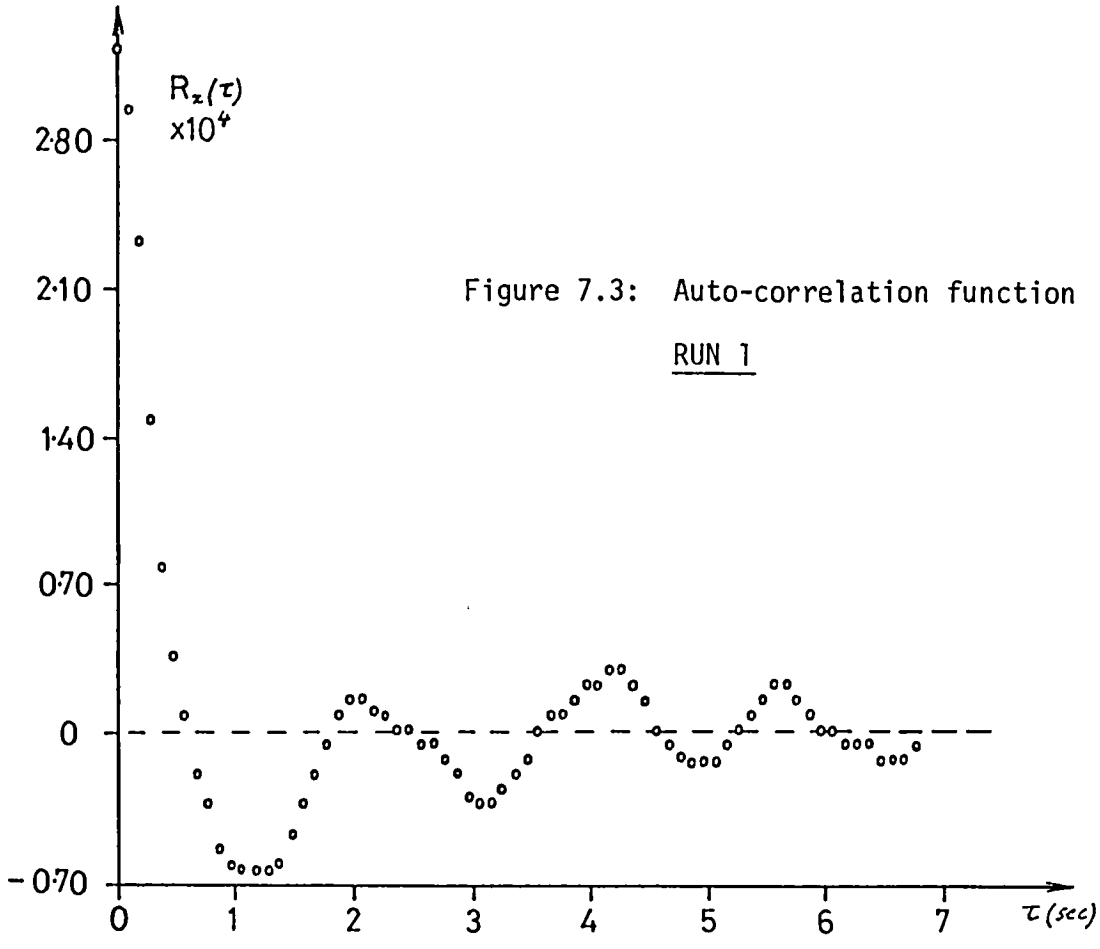

Figure 7.3: Auto-correlation function

RUN 1

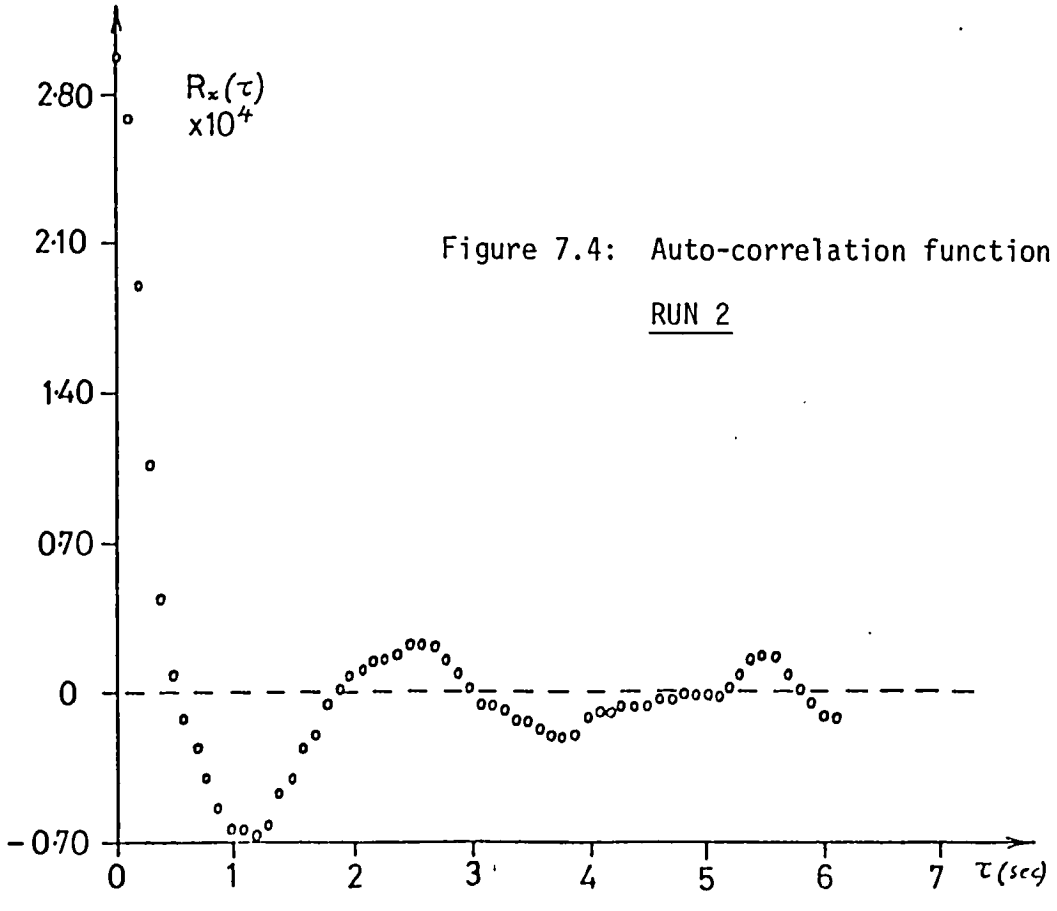

Figure 7.4: Auto-correlation function

RUN 2

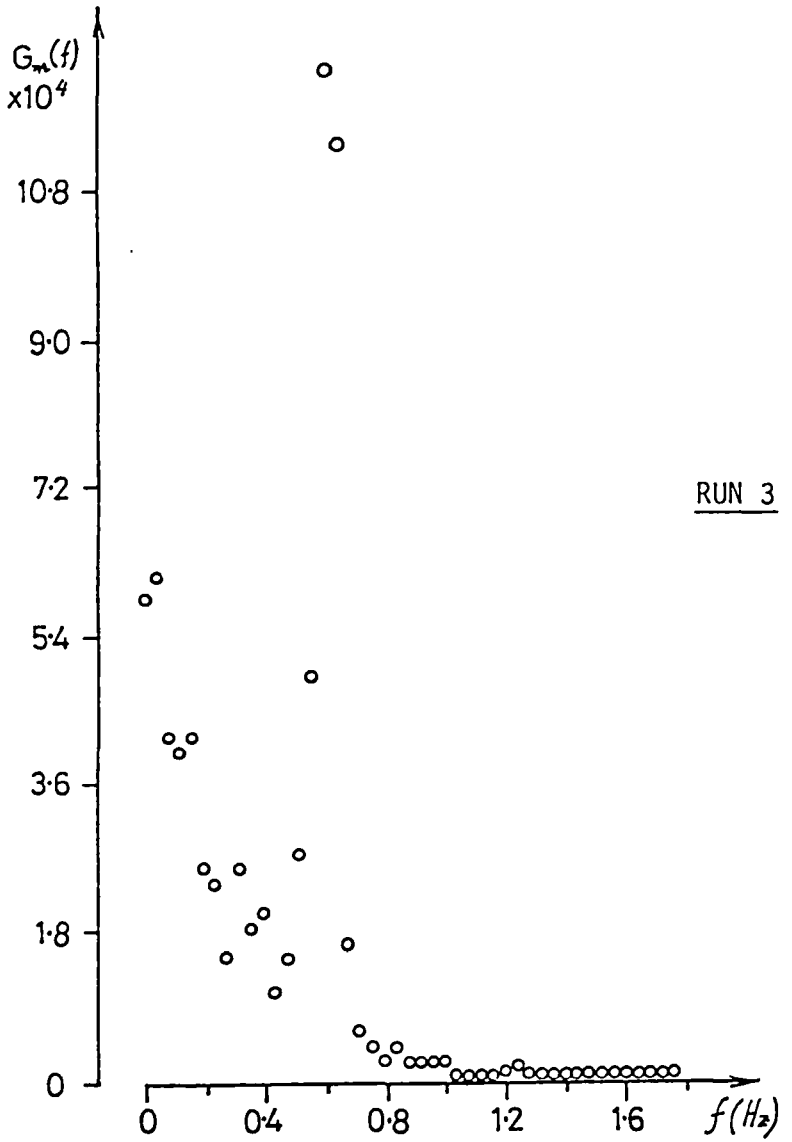

Figure 7.5: Power spectral density function

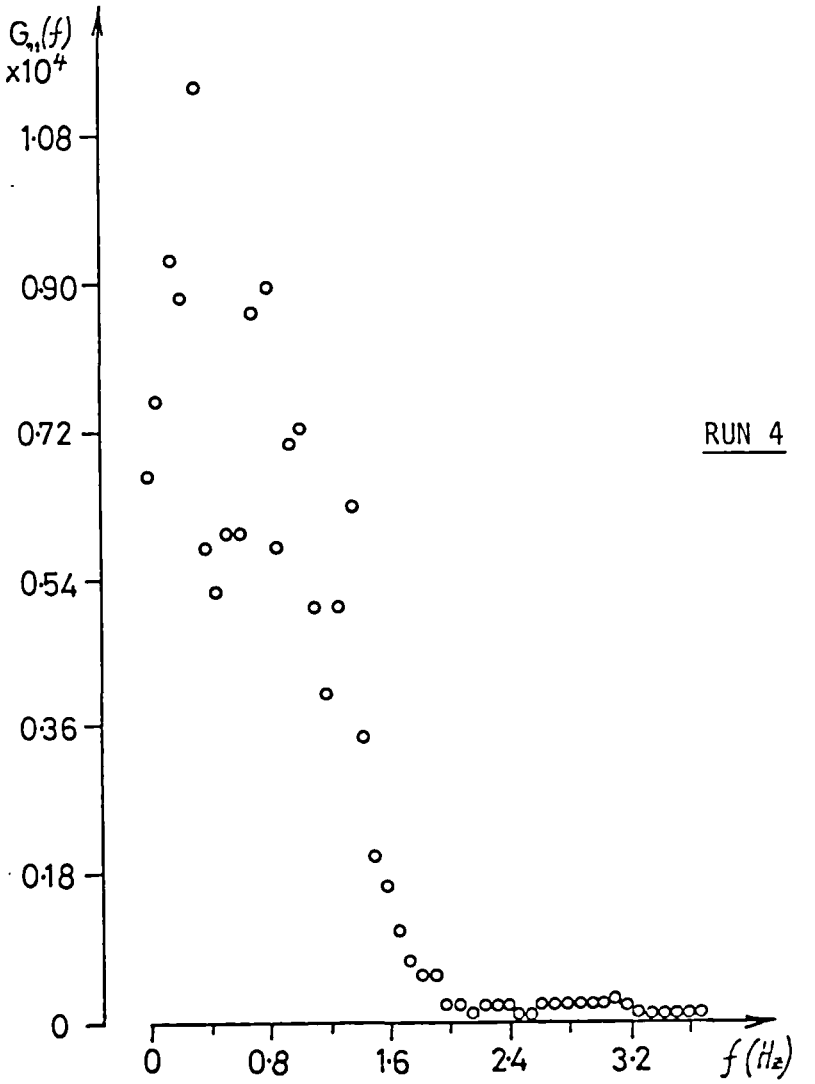

Figure 7.6: Power spectral density function

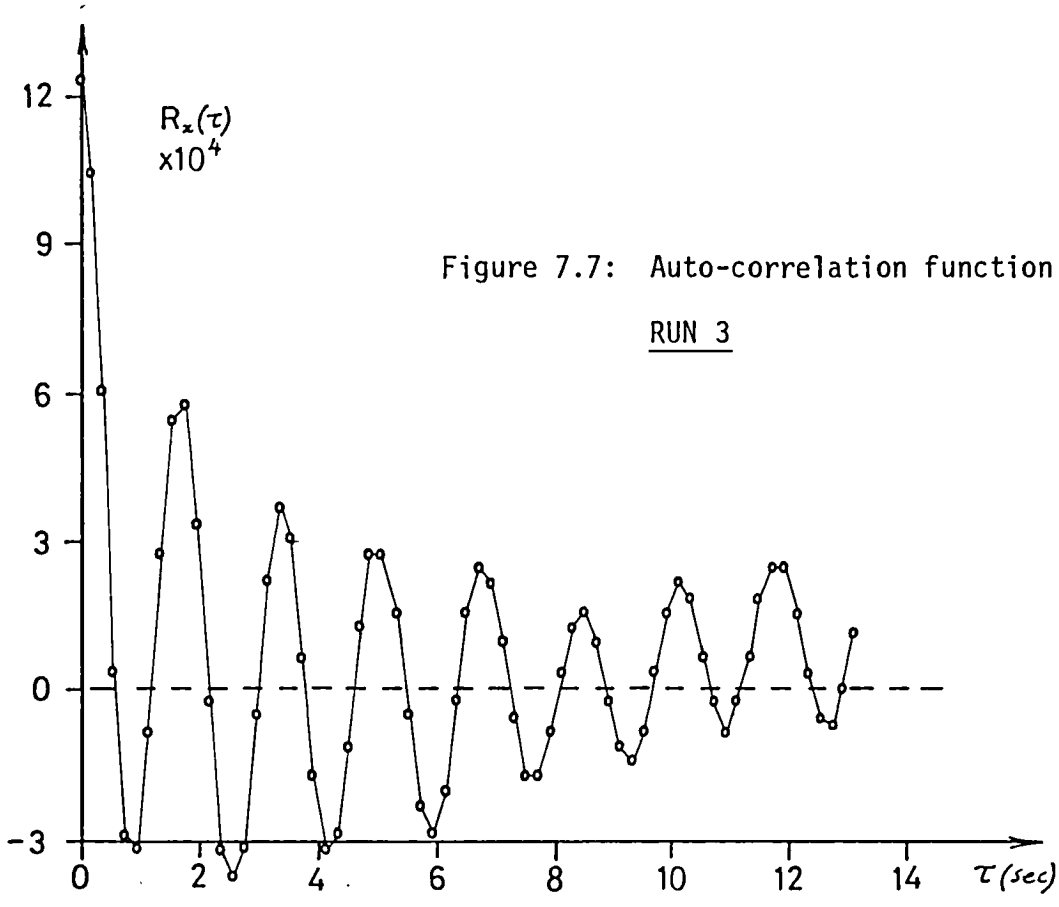

Figure 7.7: Auto-correlation function

RUN 3

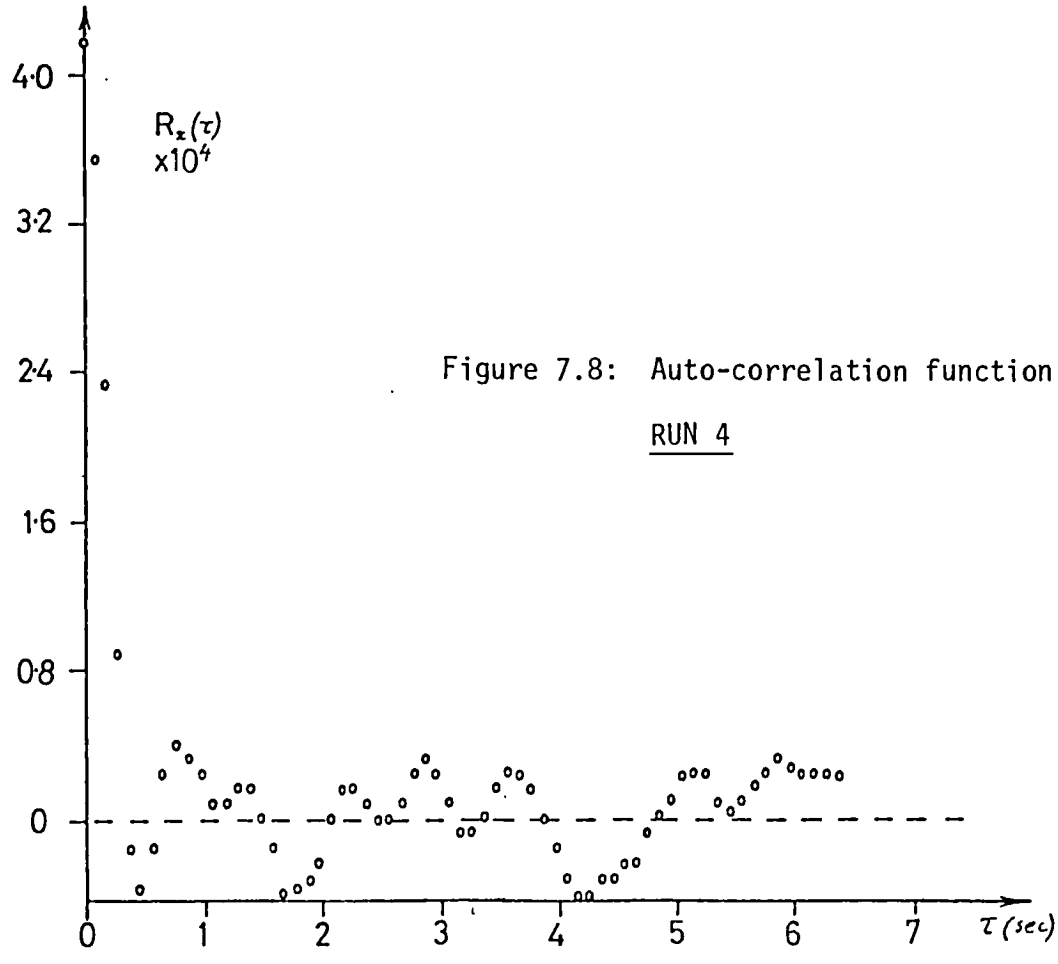

Figure 7.8: Auto-correlation function

RUN 4

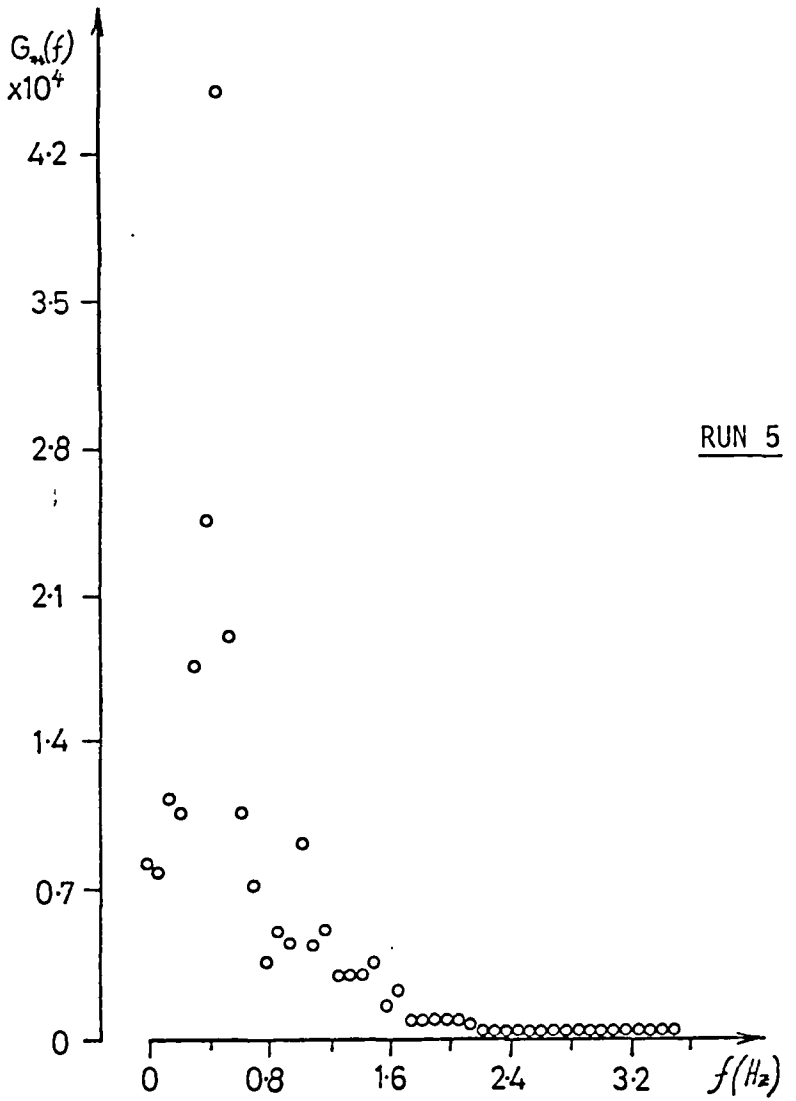

Figure 7.9: Power spectral density function

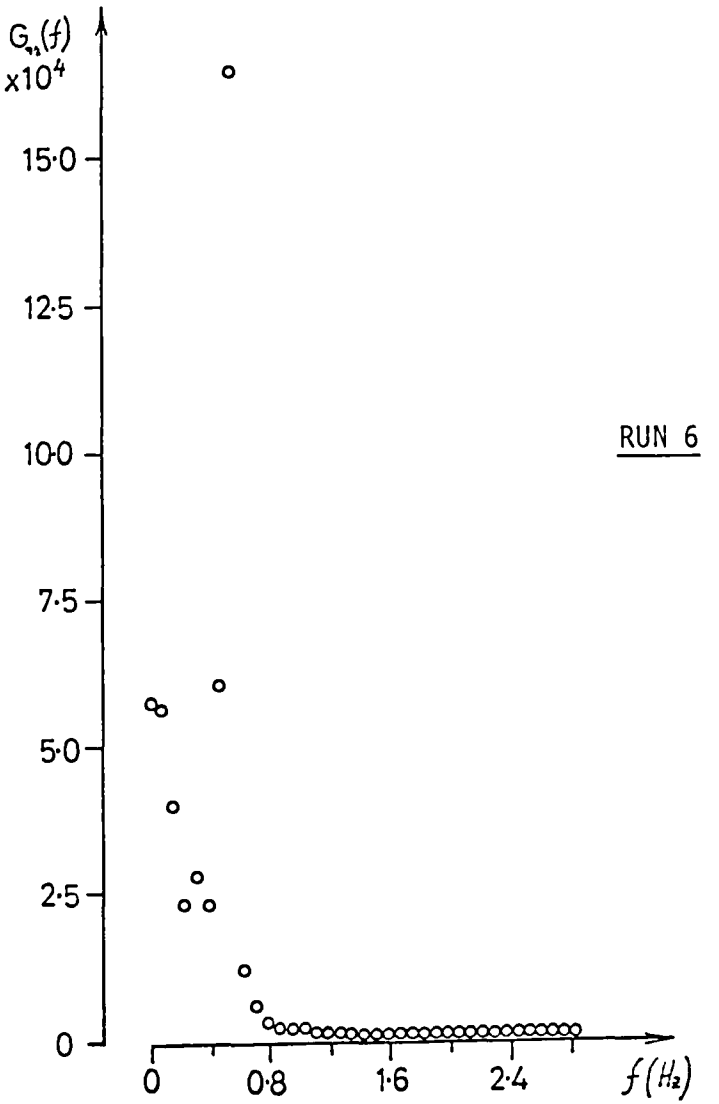

Figure 7.10: Power spectral density function

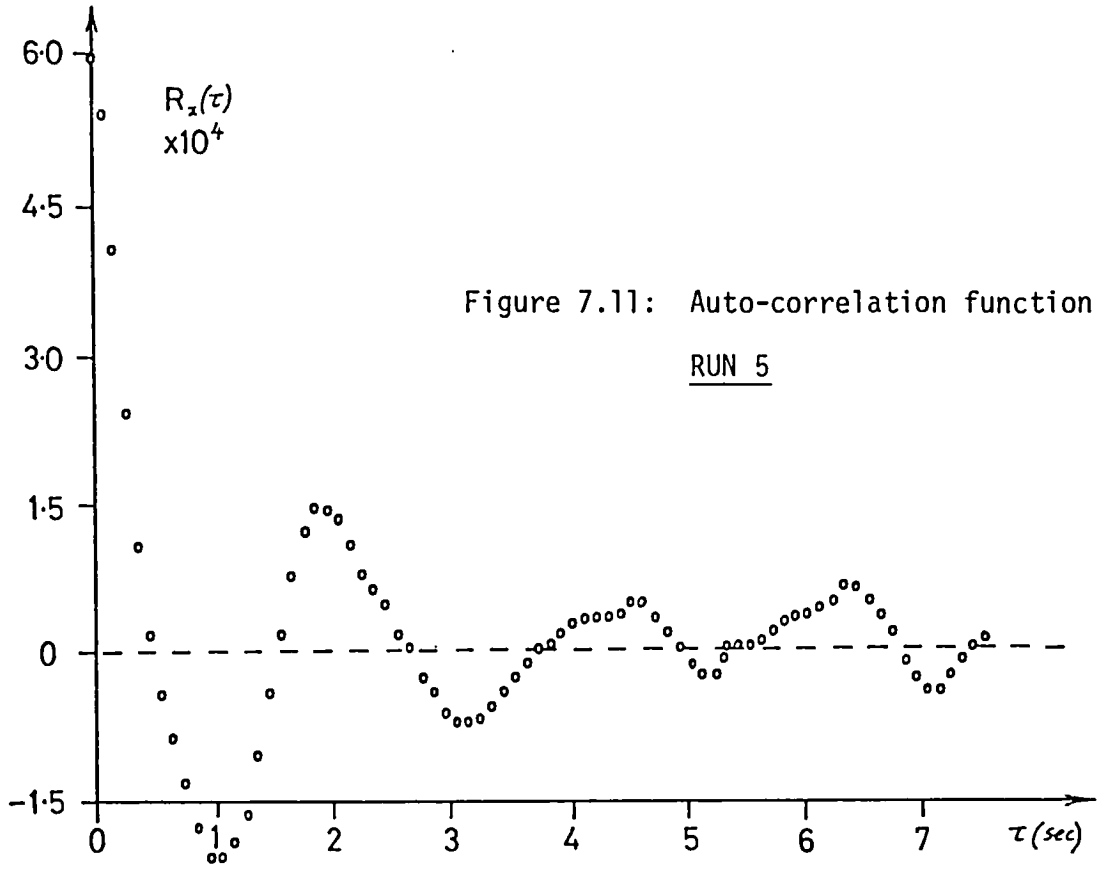

Figure 7.11: Auto-correlation function

RUN 5

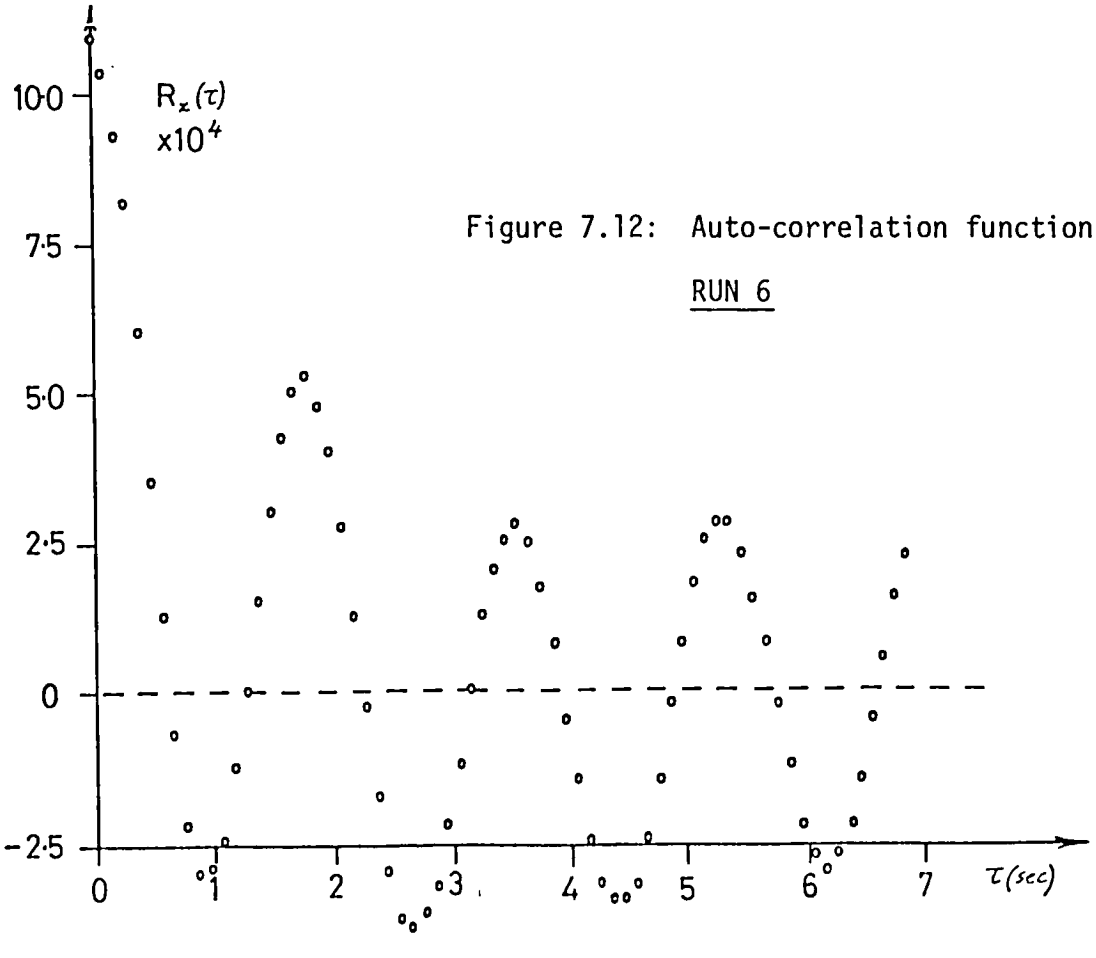

Figure 7.12: Auto-correlation function

RUN 6

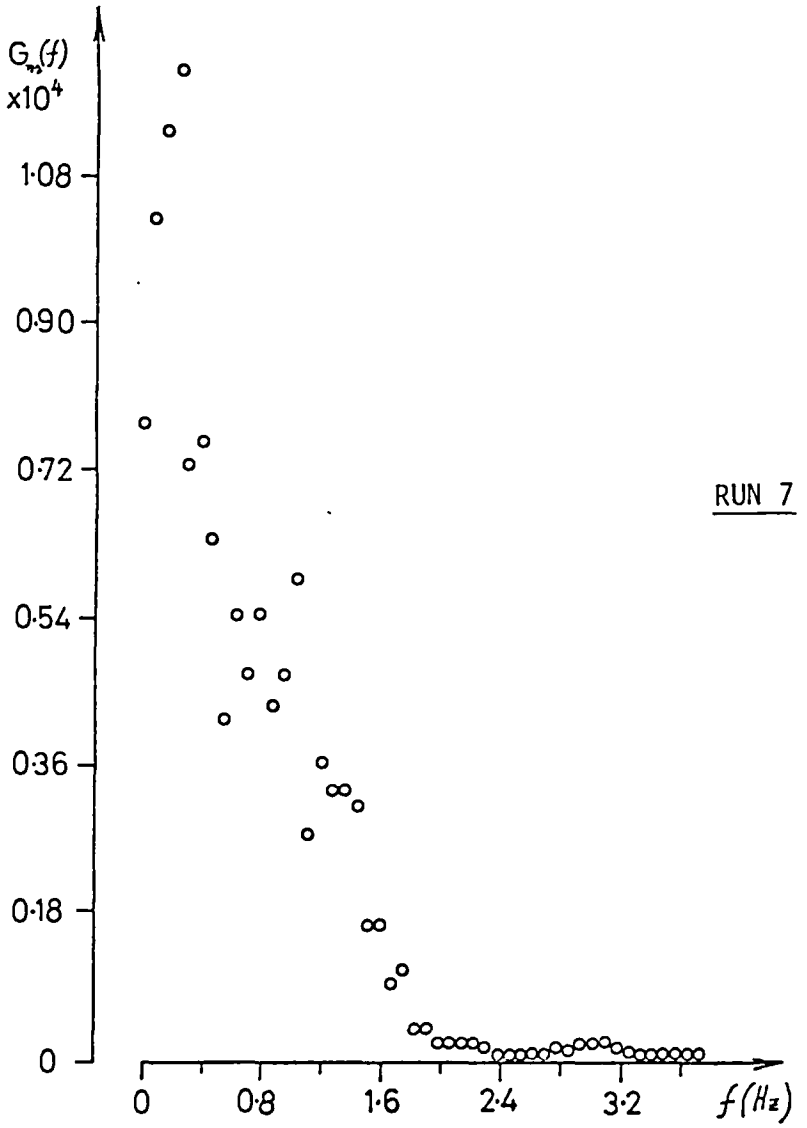

Figure 7.13: Power spectral density function

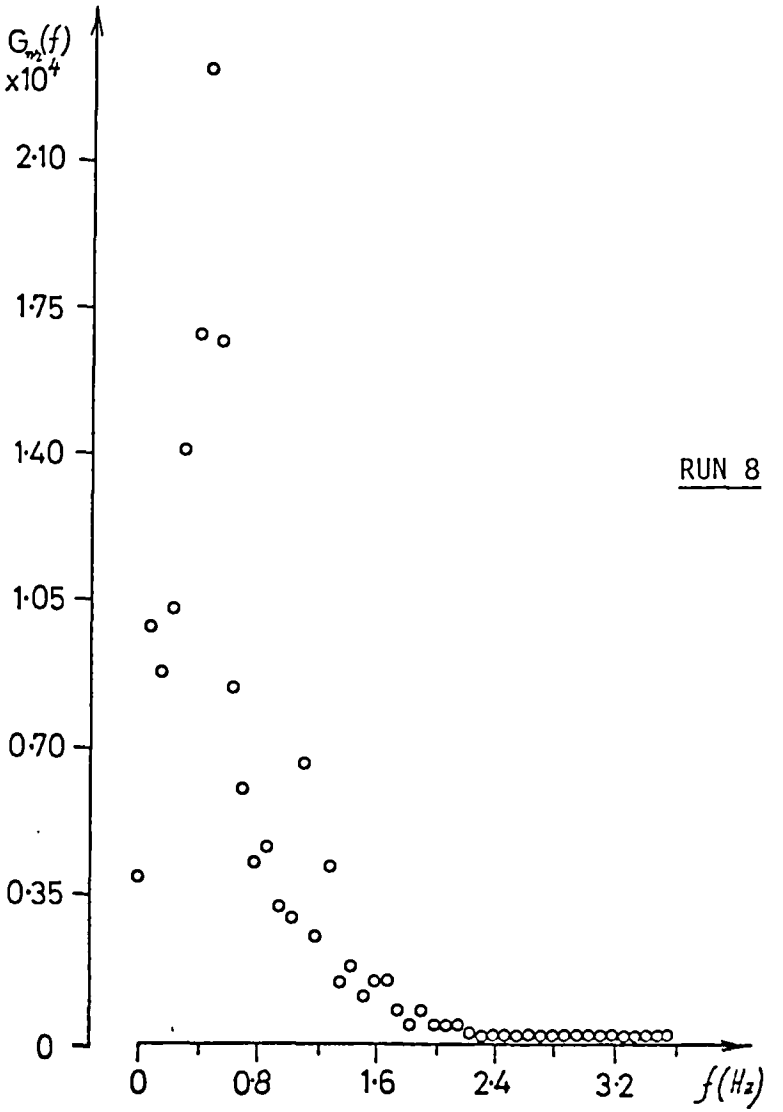

Figure 7.14: Power spectral density function

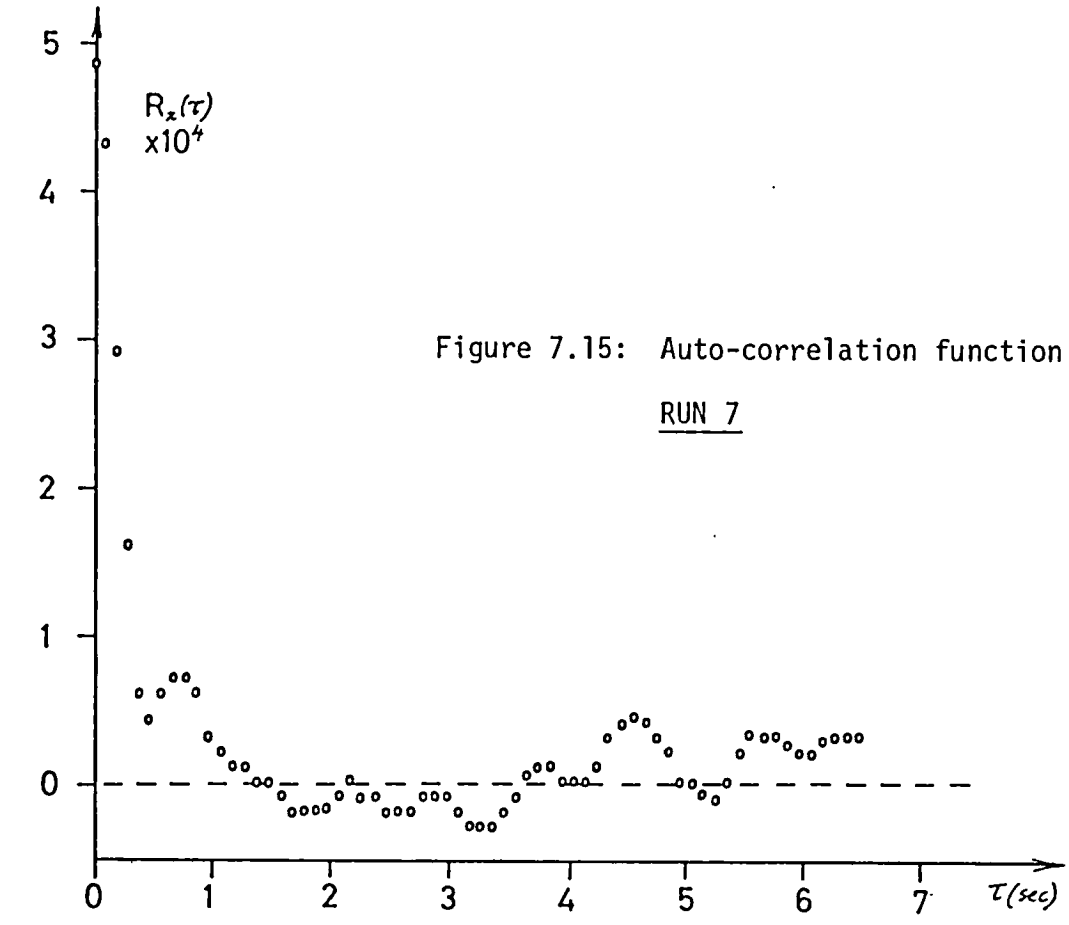

Figure 7.15: Auto-correlation function

RUN 7

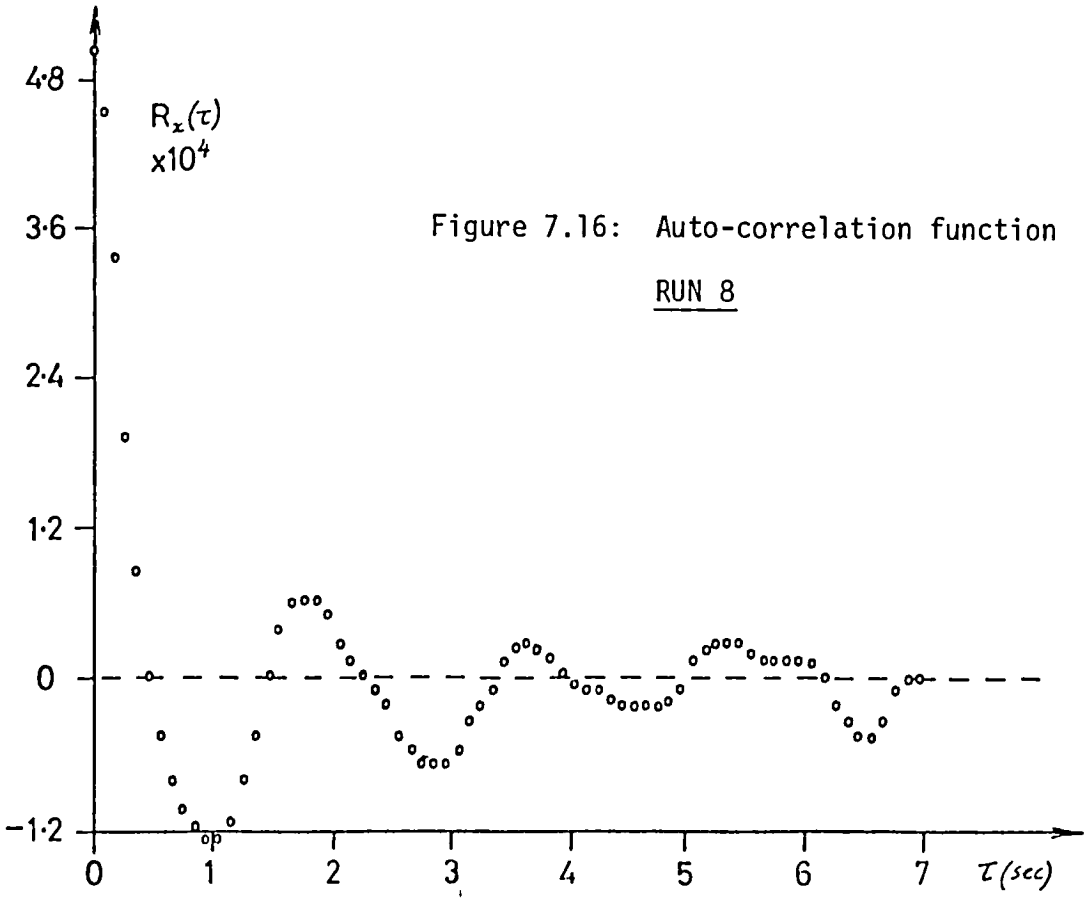

Figure 7.16: Auto-correlation function

RUN 8

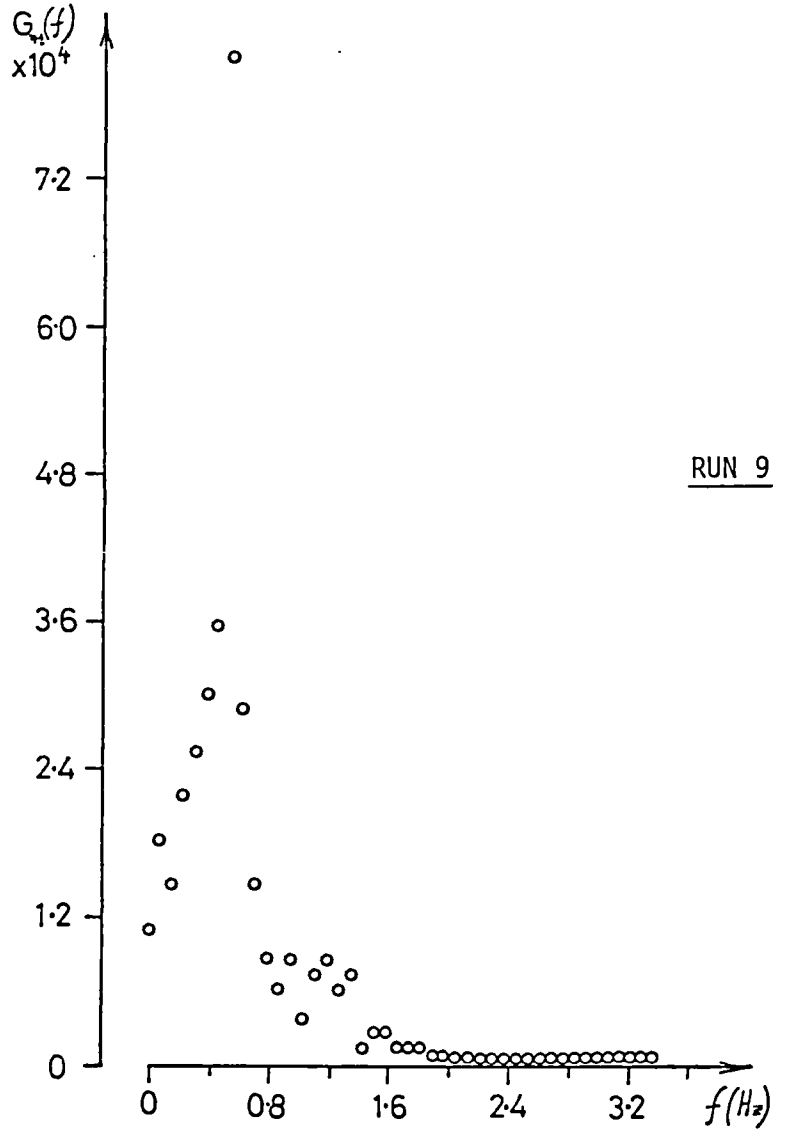

Figure 7.17: Power spectral density function

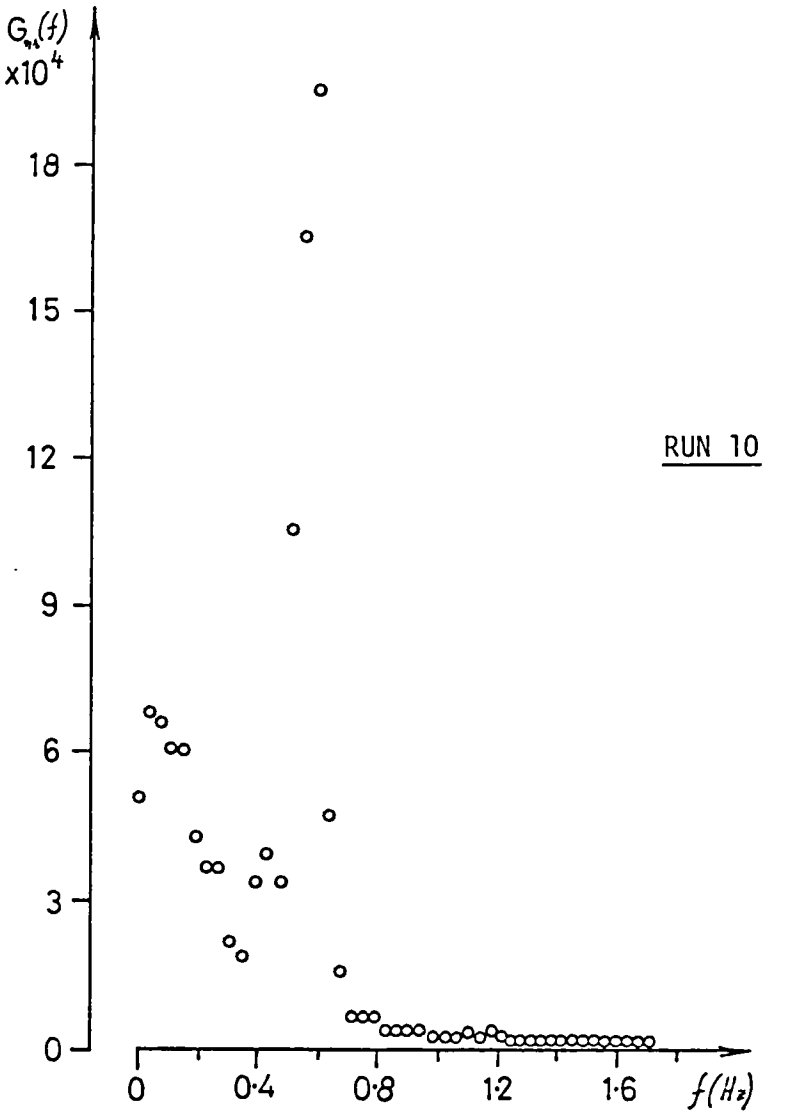

Figure 7.18: Power spectral density function

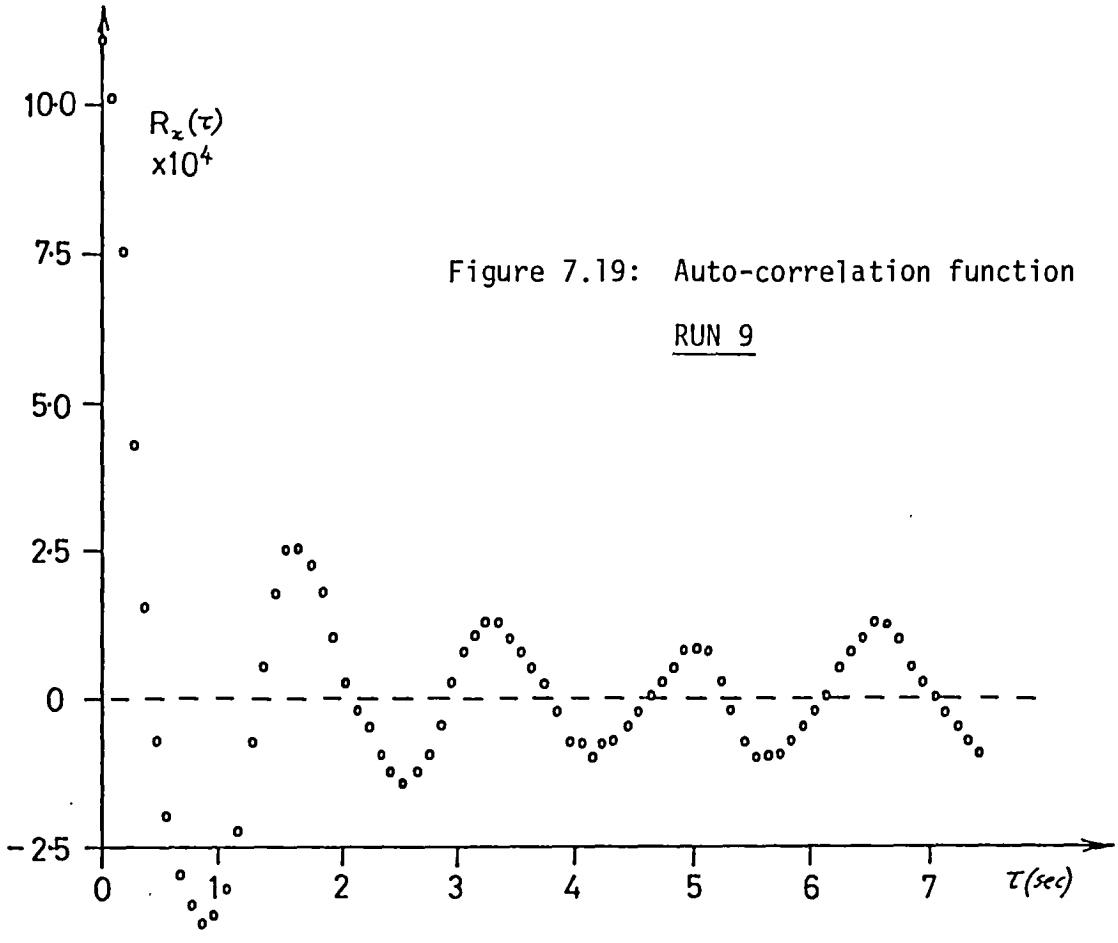

Figure 7.19: Auto-correlation function

RUN 9

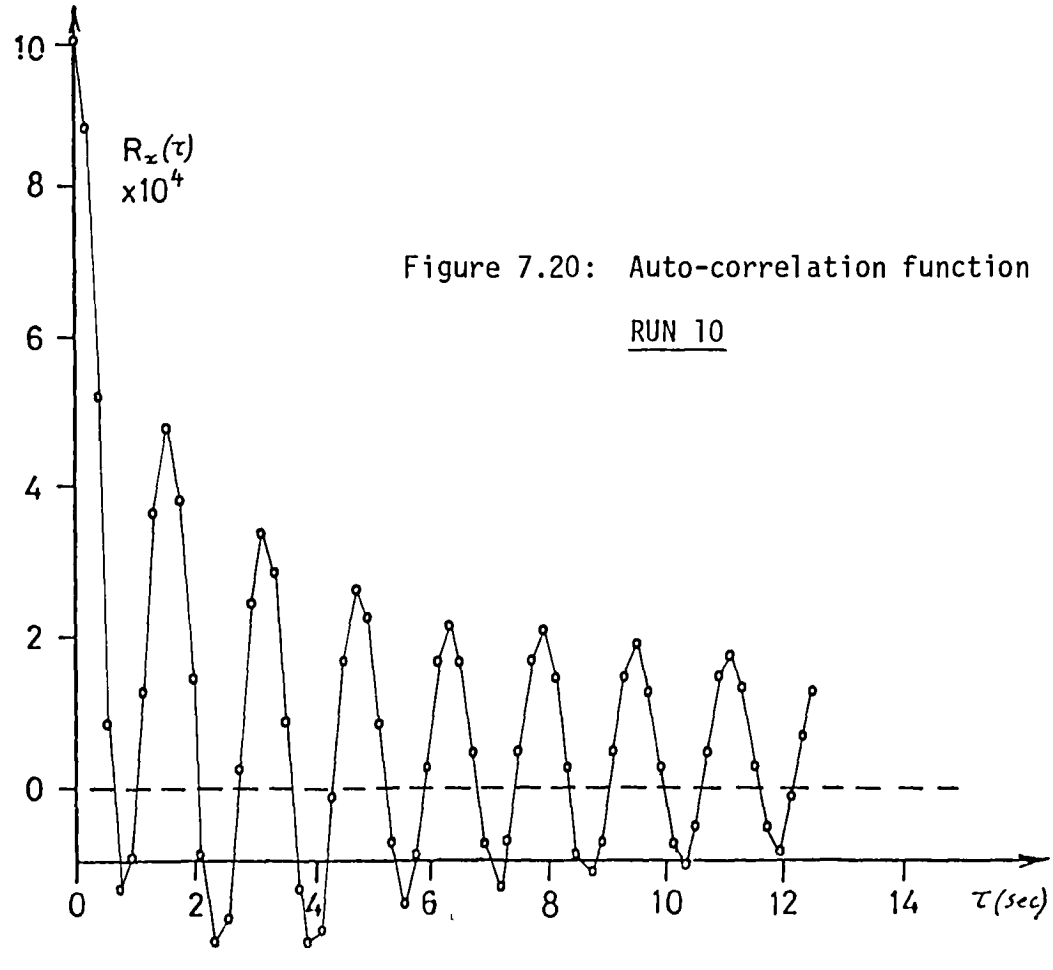

Figure 7.20: Auto-correlation function

RUN 10

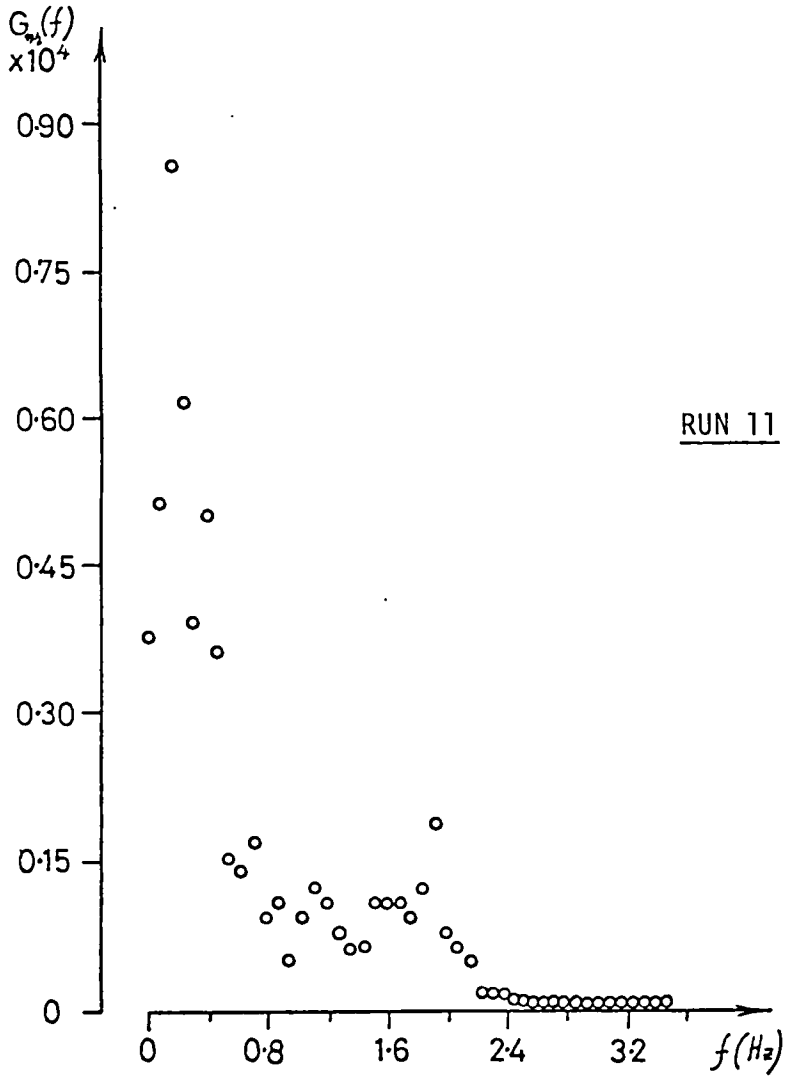

Figure 7.21: Power spectral density function

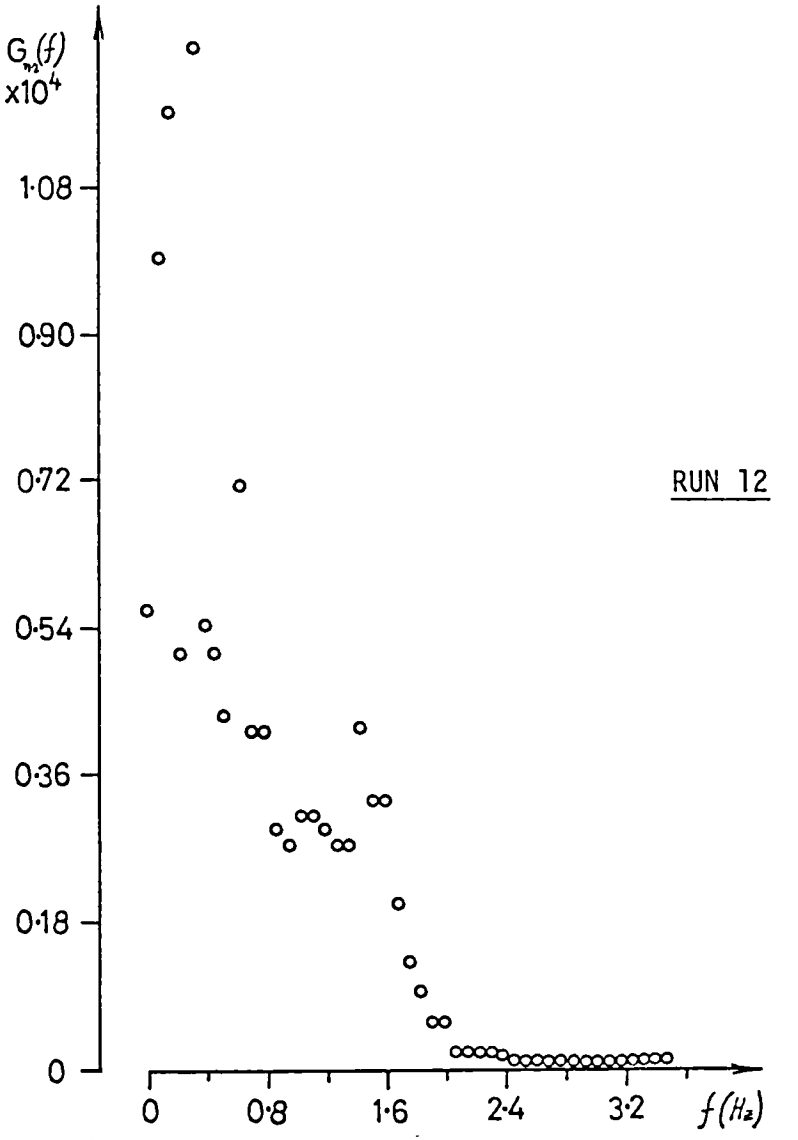

Figure 7.22: Power spectral density function

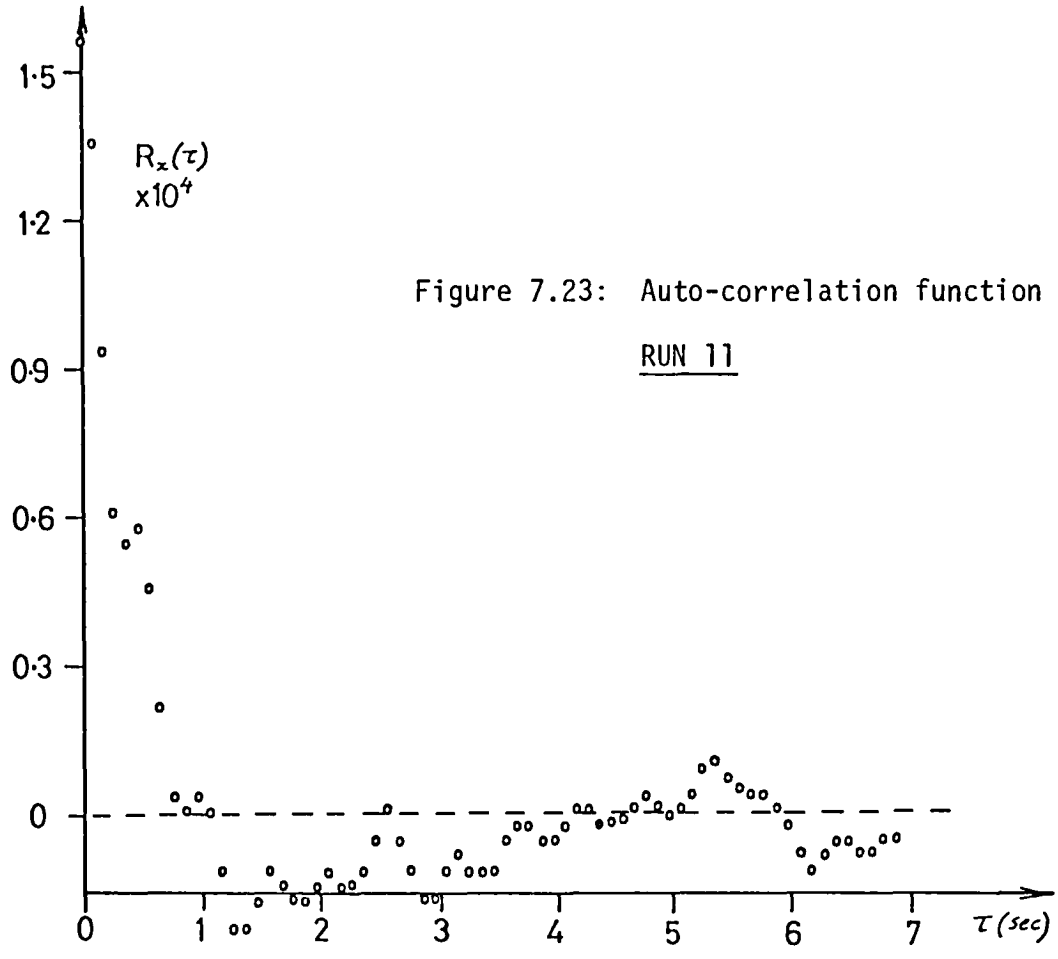

Figure 7.23: Auto-correlation function

RUN 11

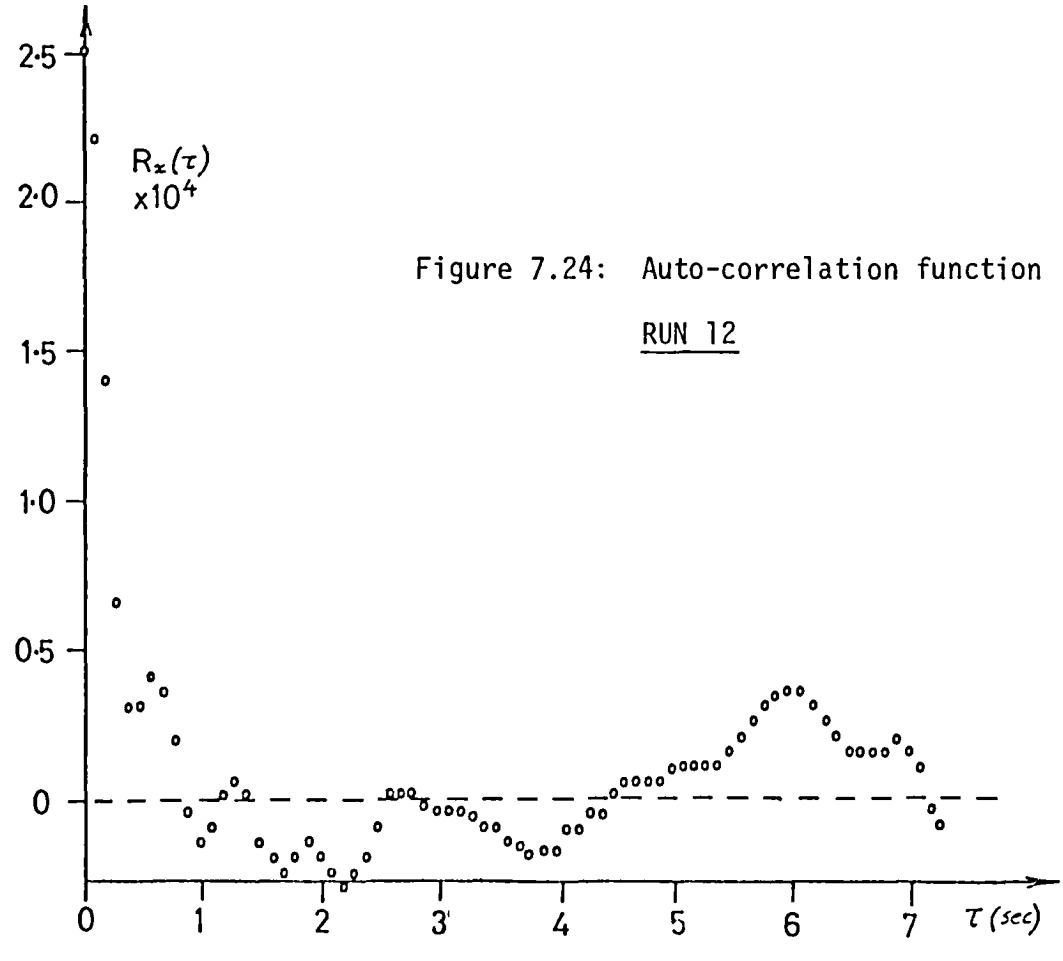

Figure 7.24: Auto-correlation function

RUN 12

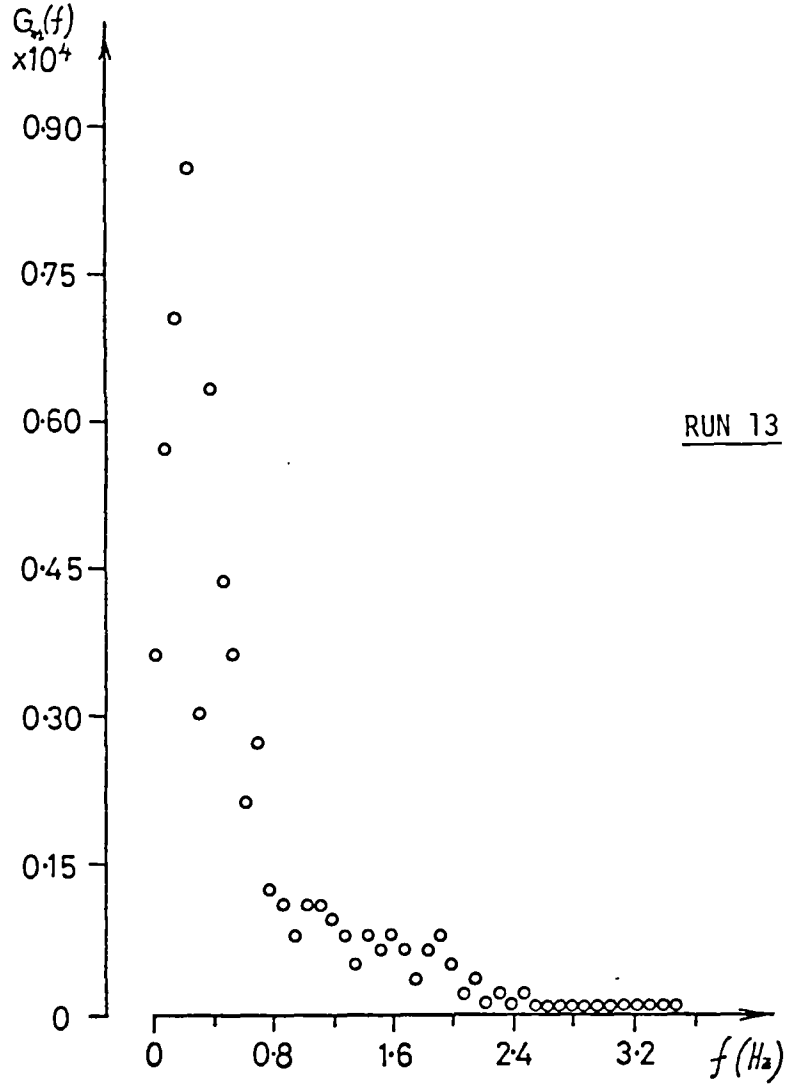

Figure 7.25: Power spectral density function

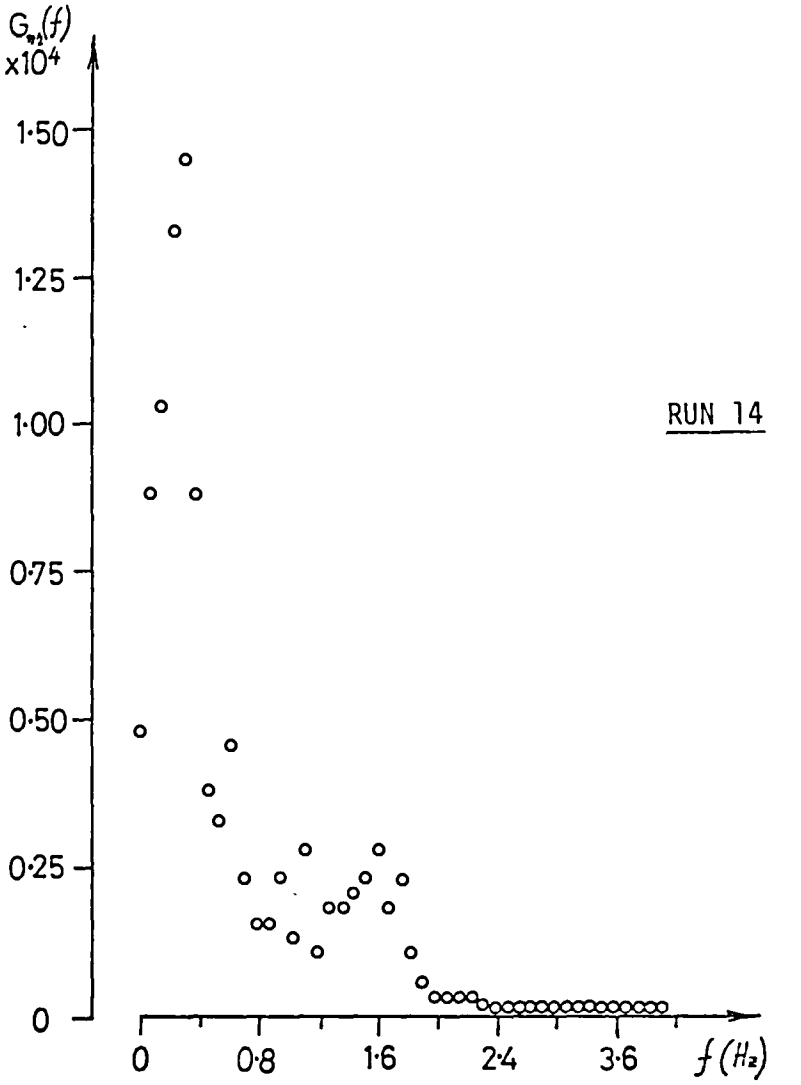

Figure 7.26: Power spectral density function

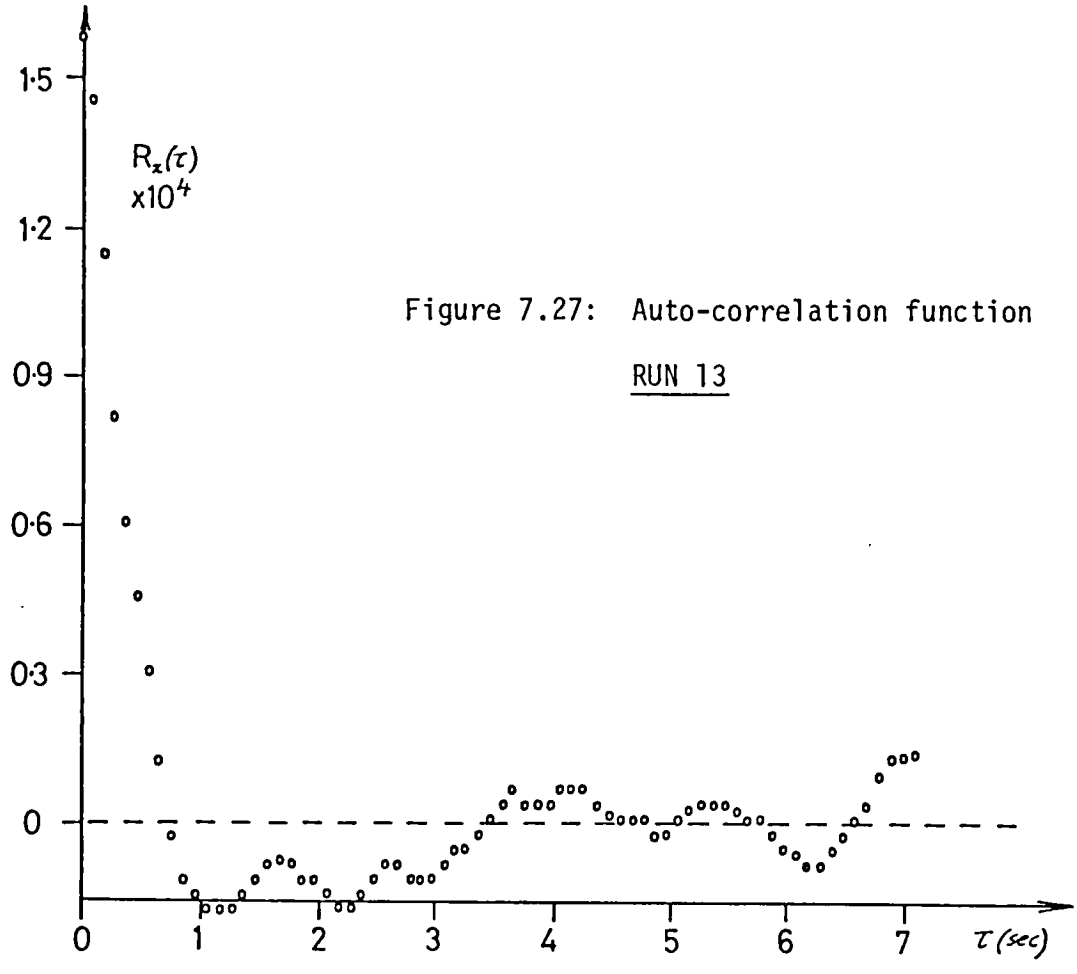

Figure 7.27: Auto-correlation function

RUN 13

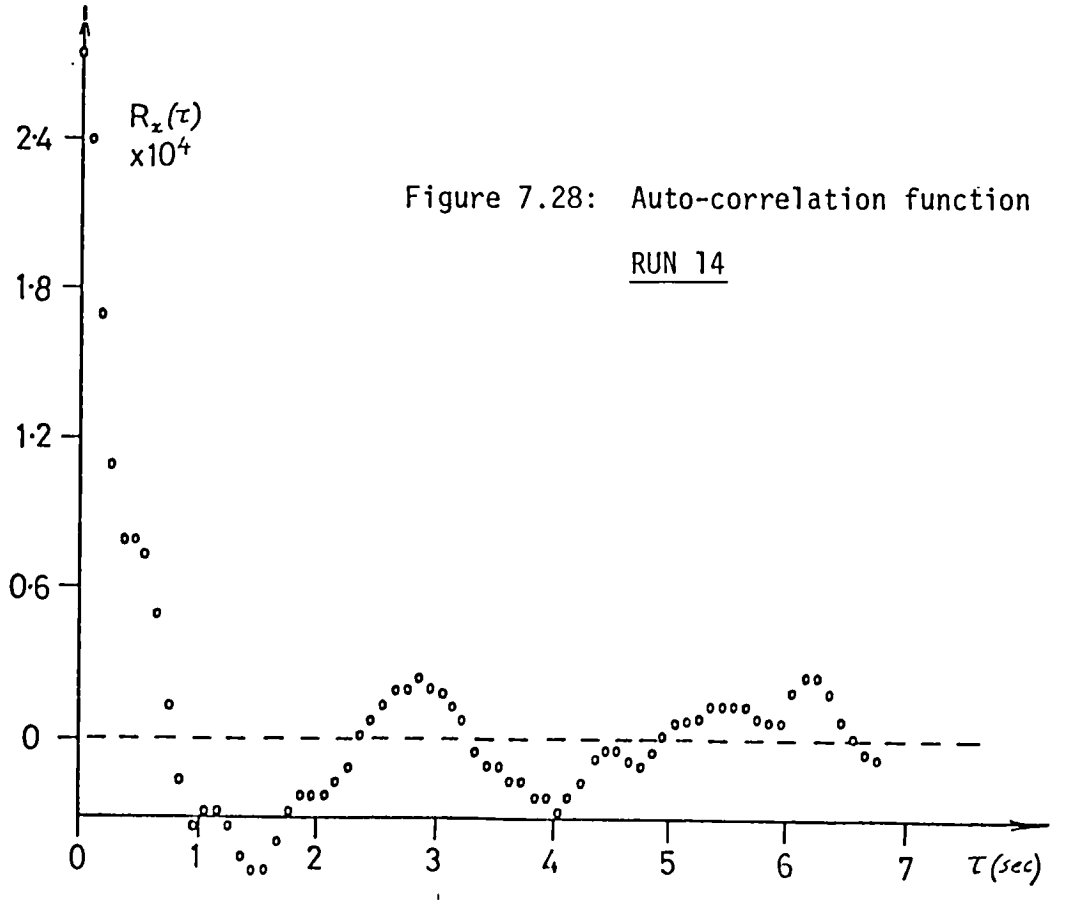

Figure 7.28: Auto-correlation function

RUN 14

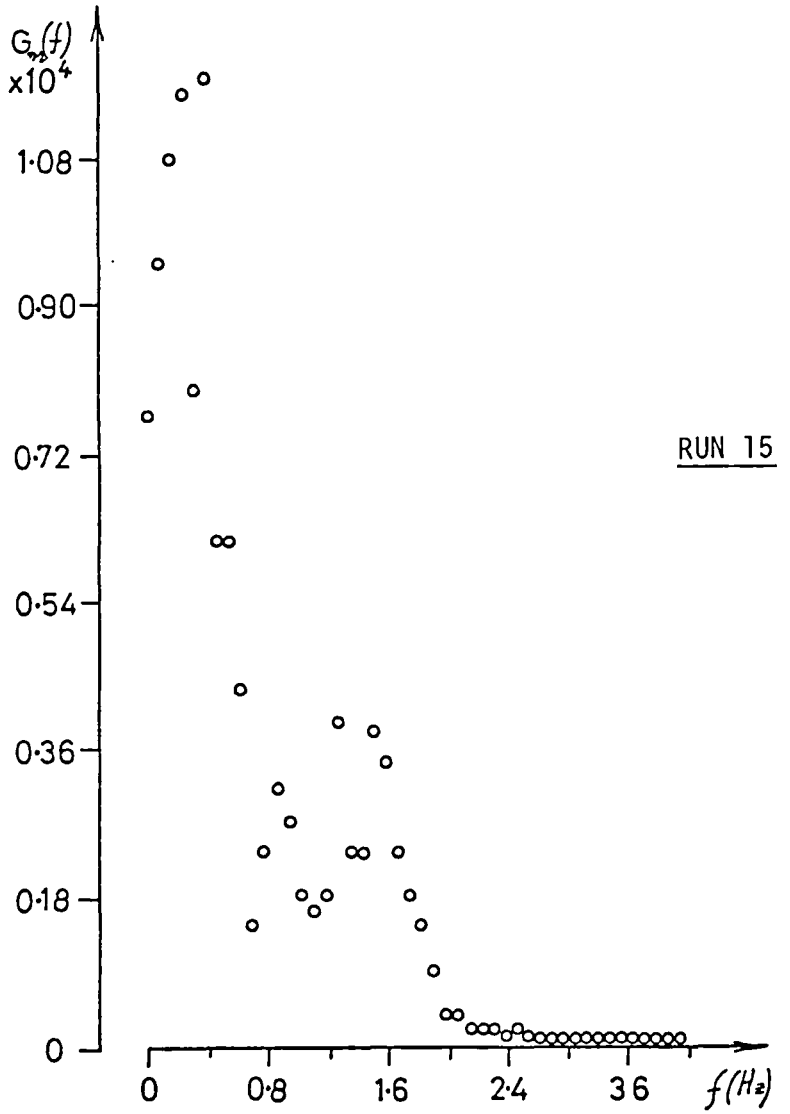

Figure 7.29: Power spectral density function

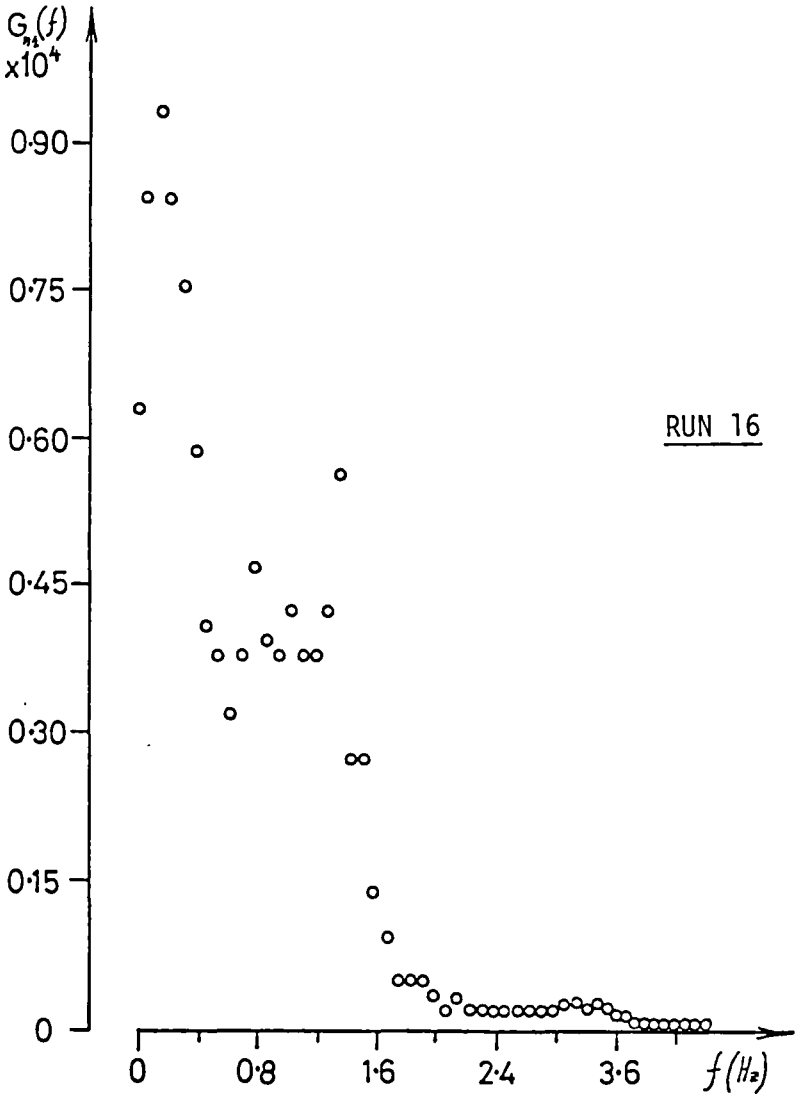

Figure 7.30: Power spectral density function

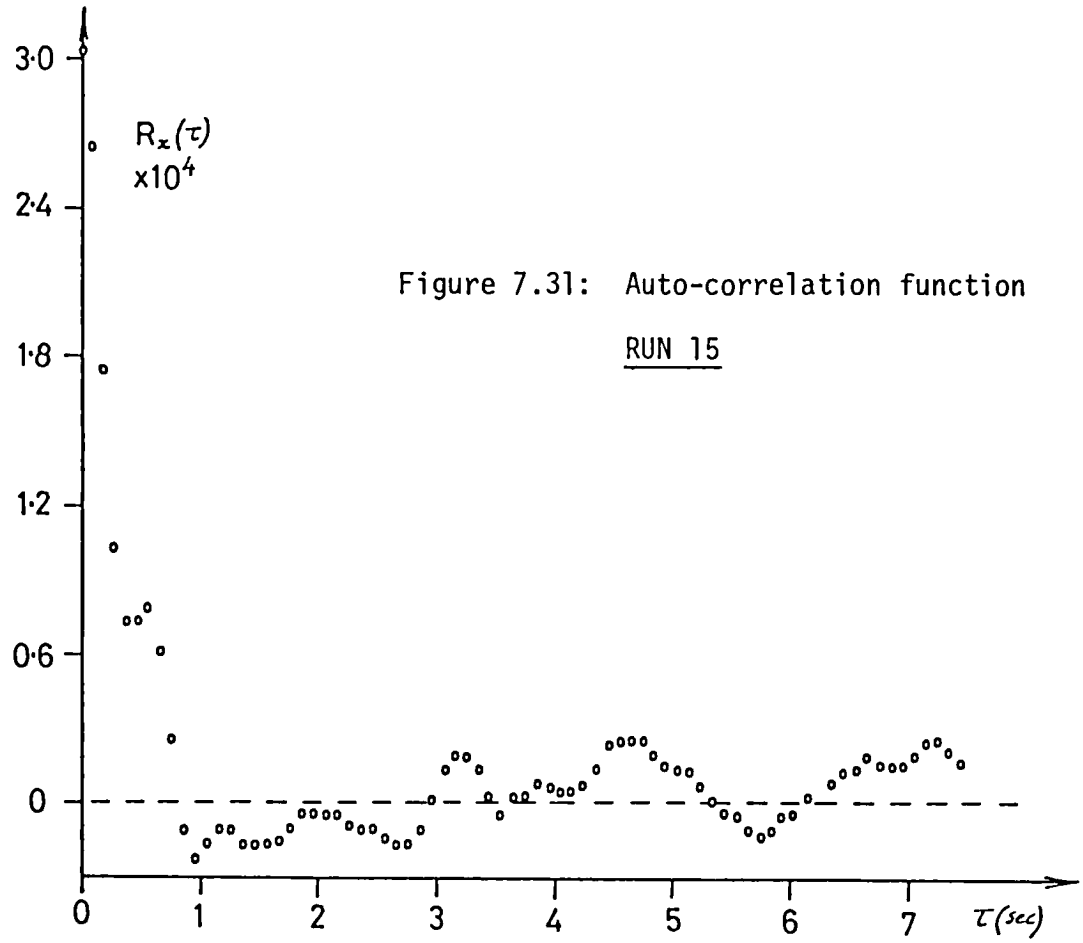

Figure 7.31: Auto-correlation function

RUN 15

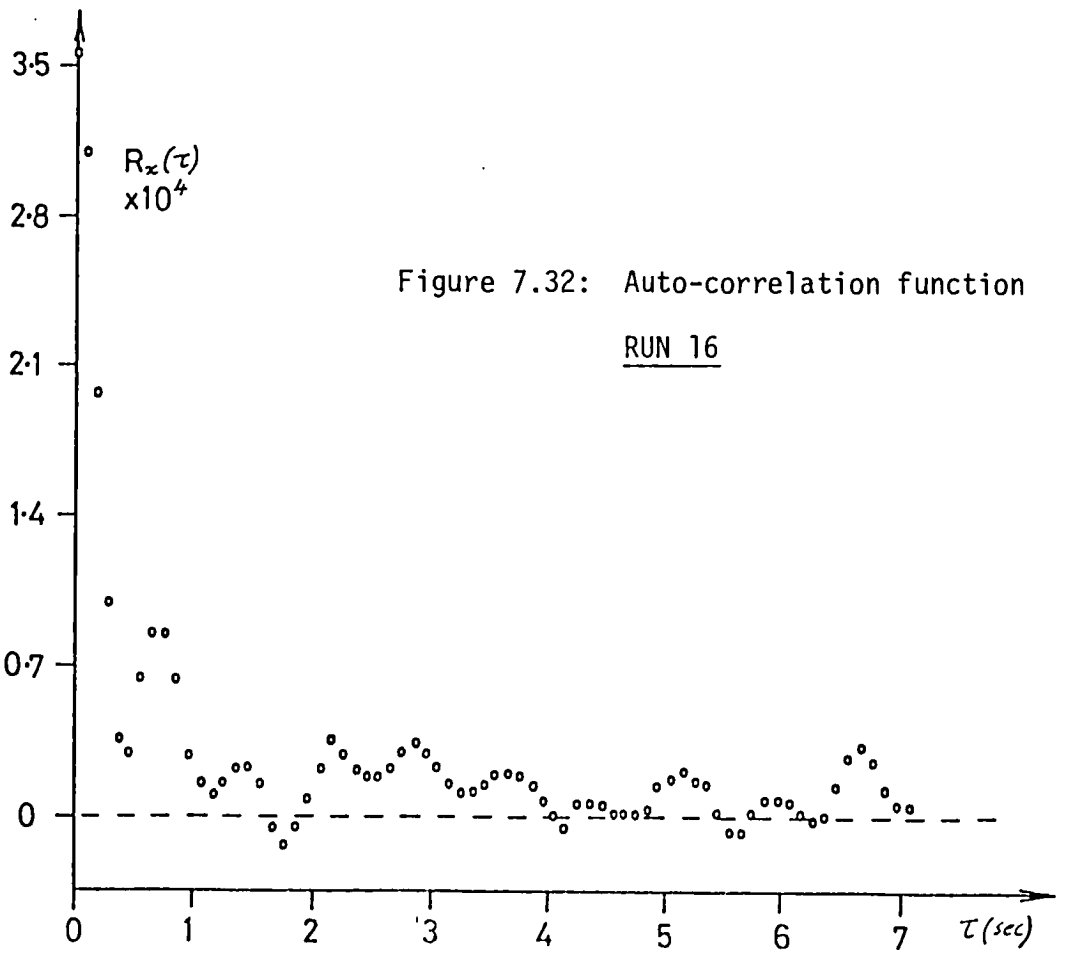

Figure 7.32: Auto-correlation function

RUN 16

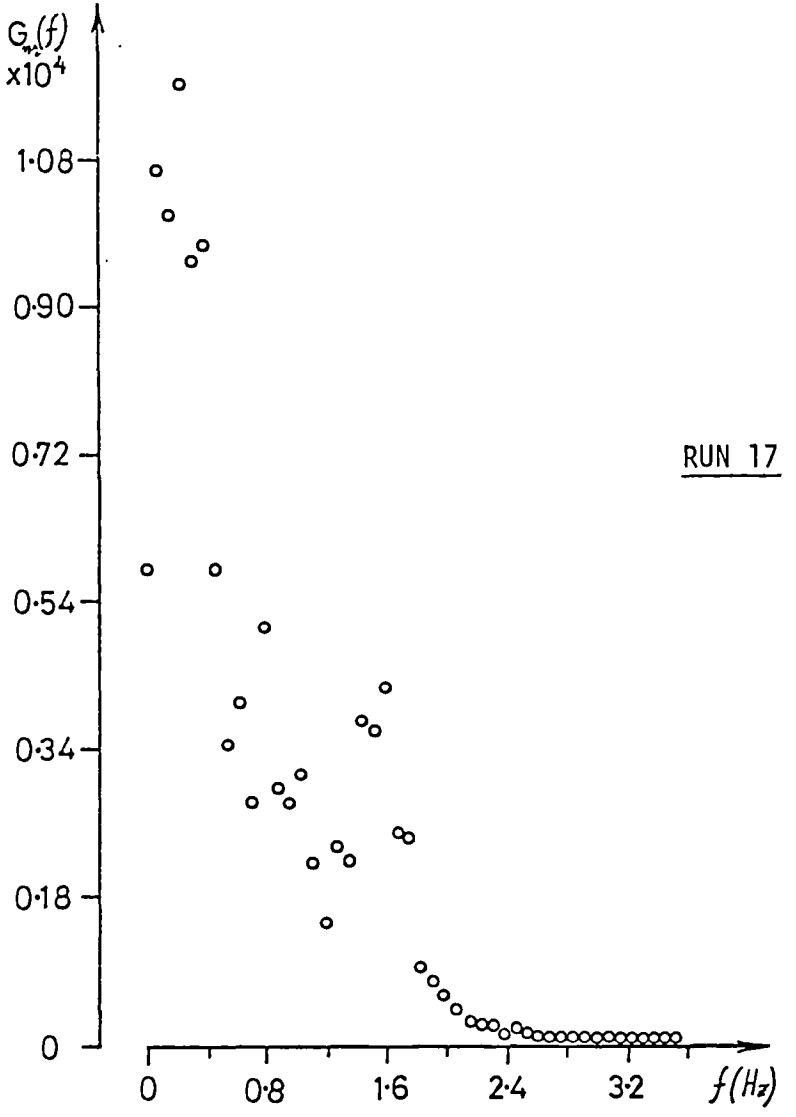

Figure 7.33: Power spectral density function

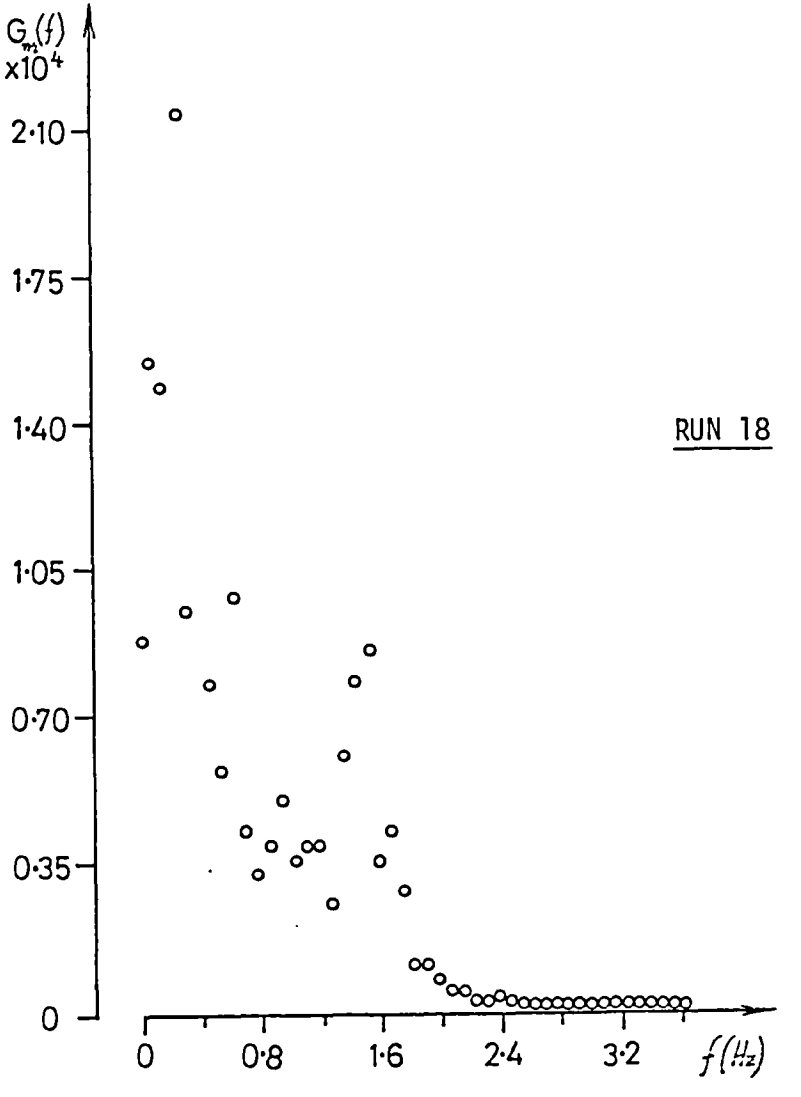

Figure 7.34: Power spectral density function

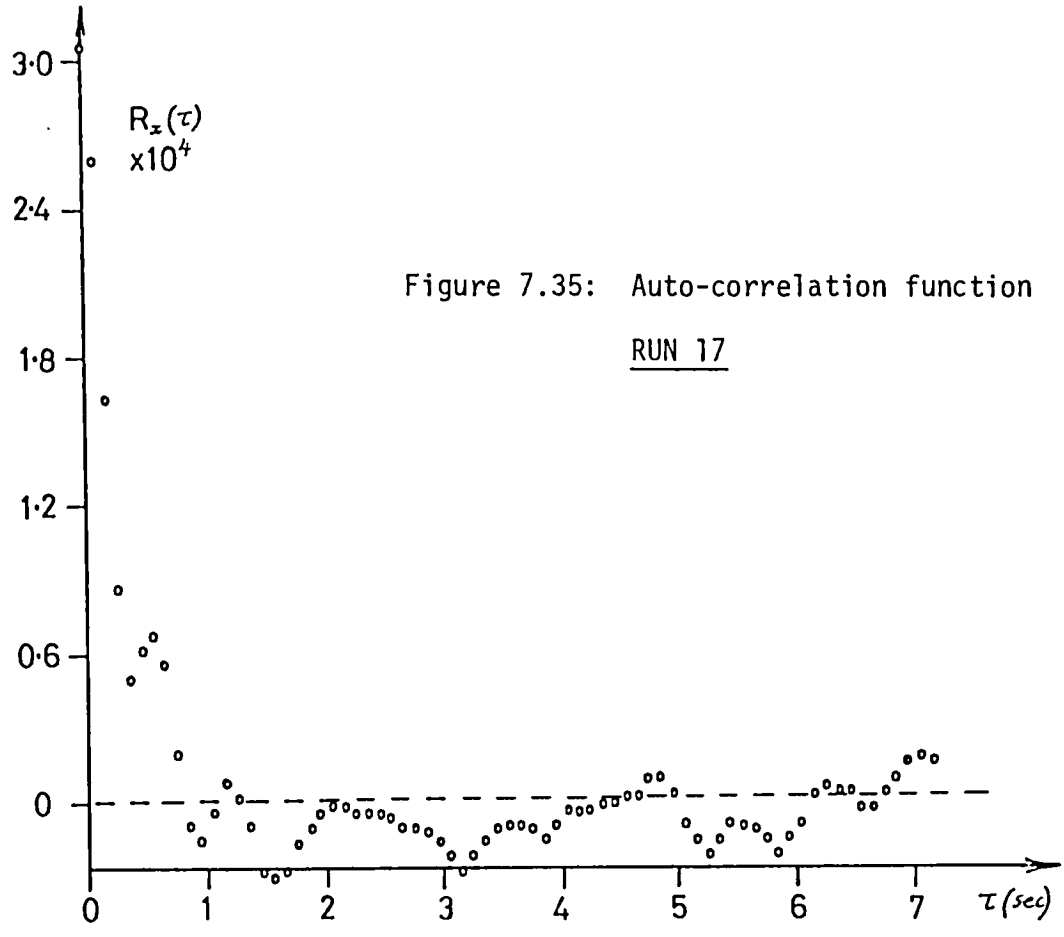

Figure 7.35: Auto-correlation function

RUN 17

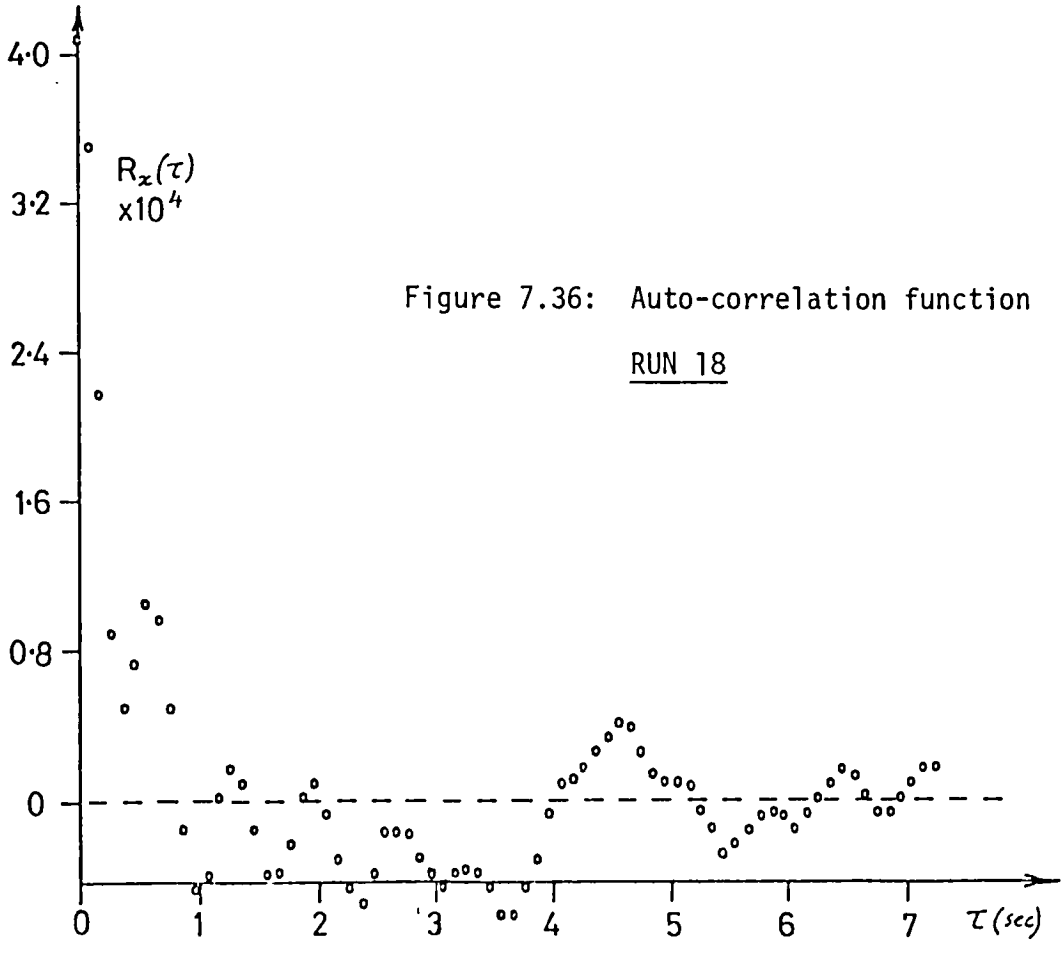

Figure 7.36: Auto-correlation function

RUN 18

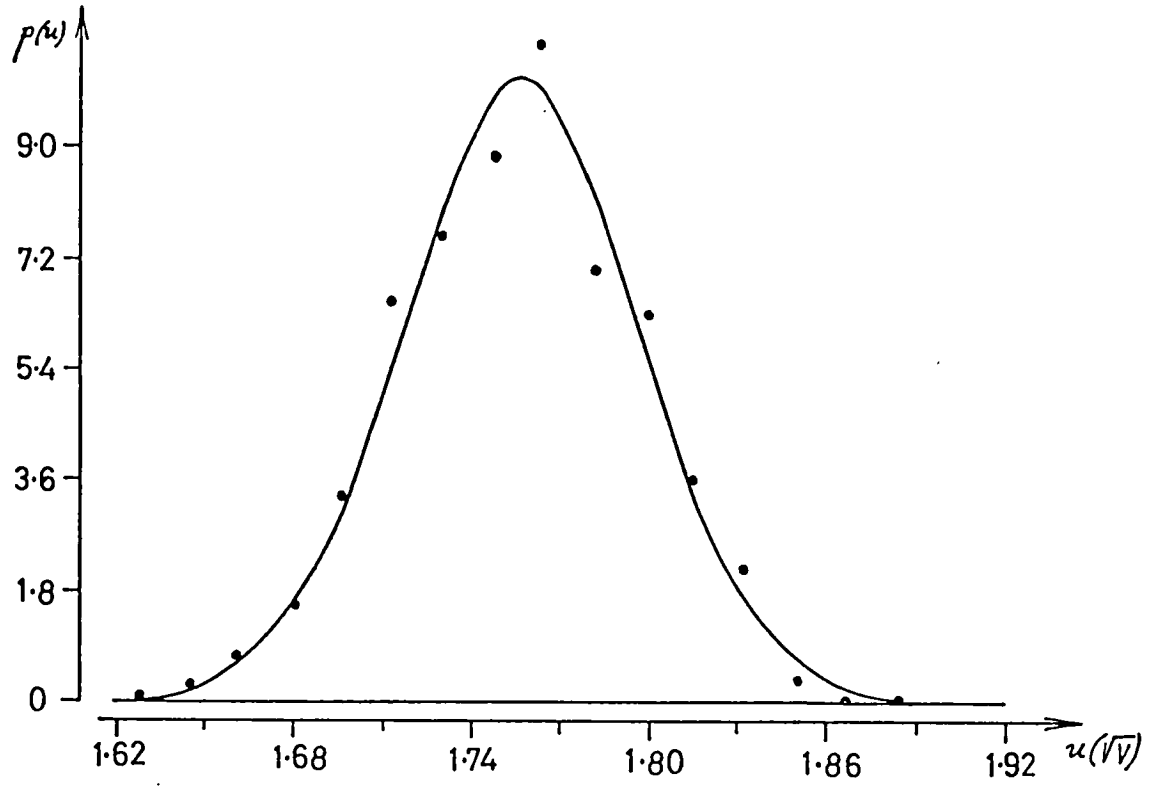

Figure 7.37: Probability density function. RUN 3

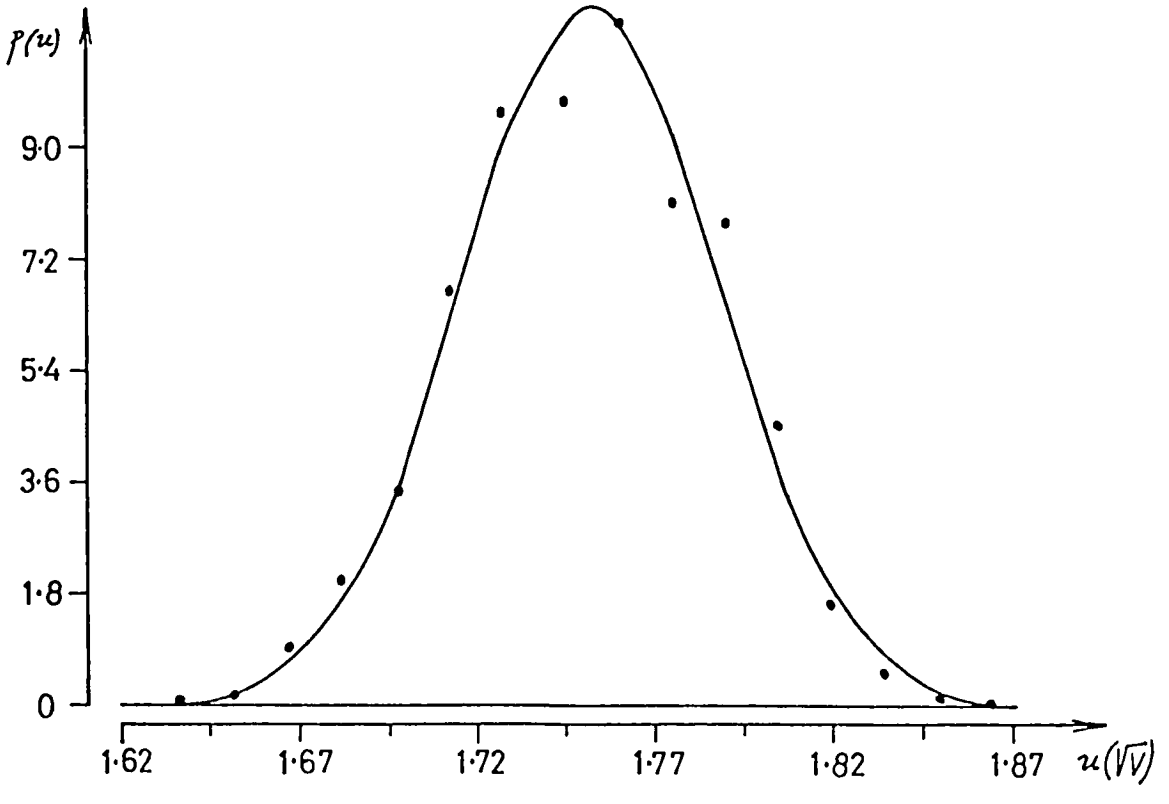

Figure 7.38: Probability density function. RUN 6

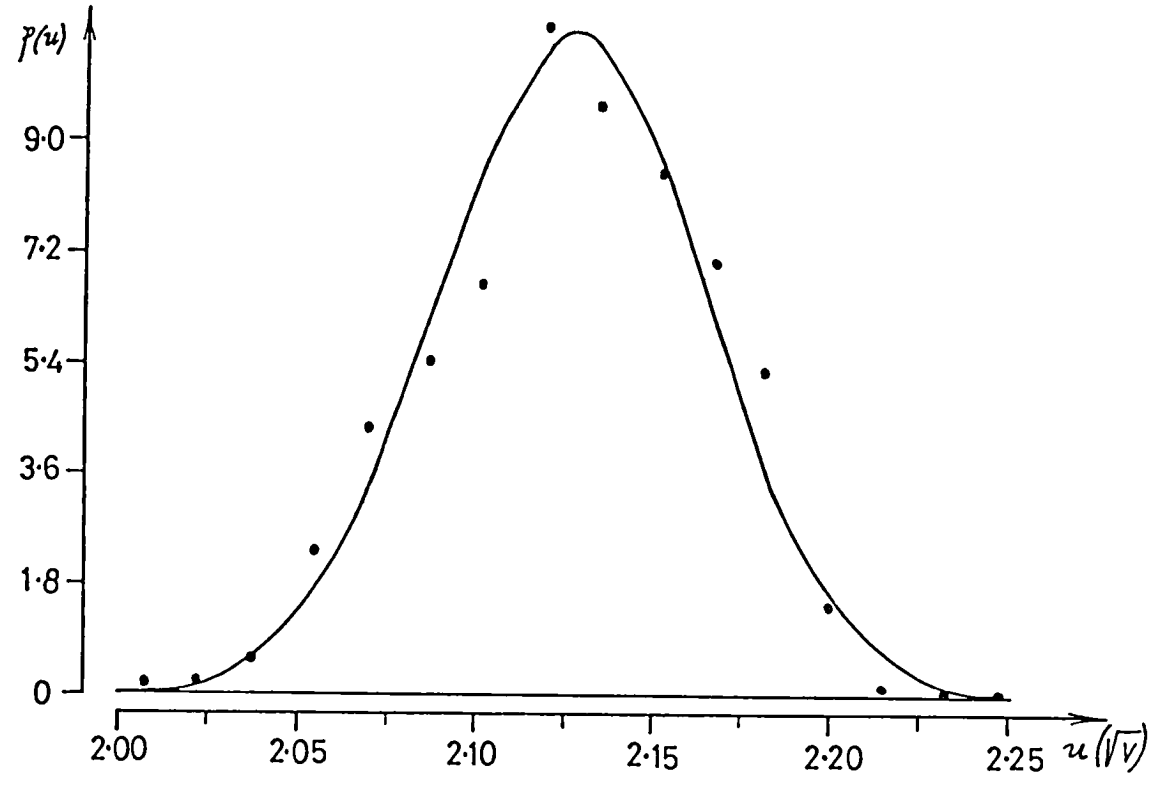

Figure 7.39: Probability density function. RUN 8

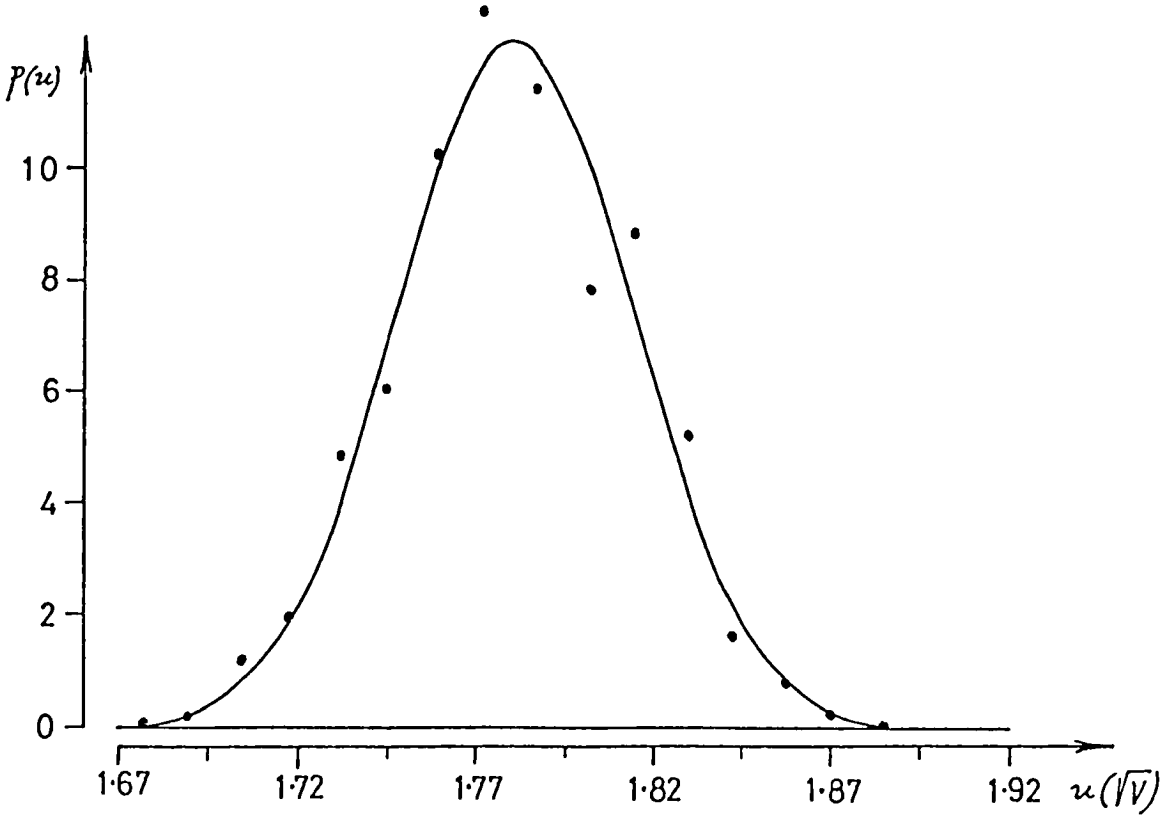

Figure 7.40: Probability density function. RUN 18

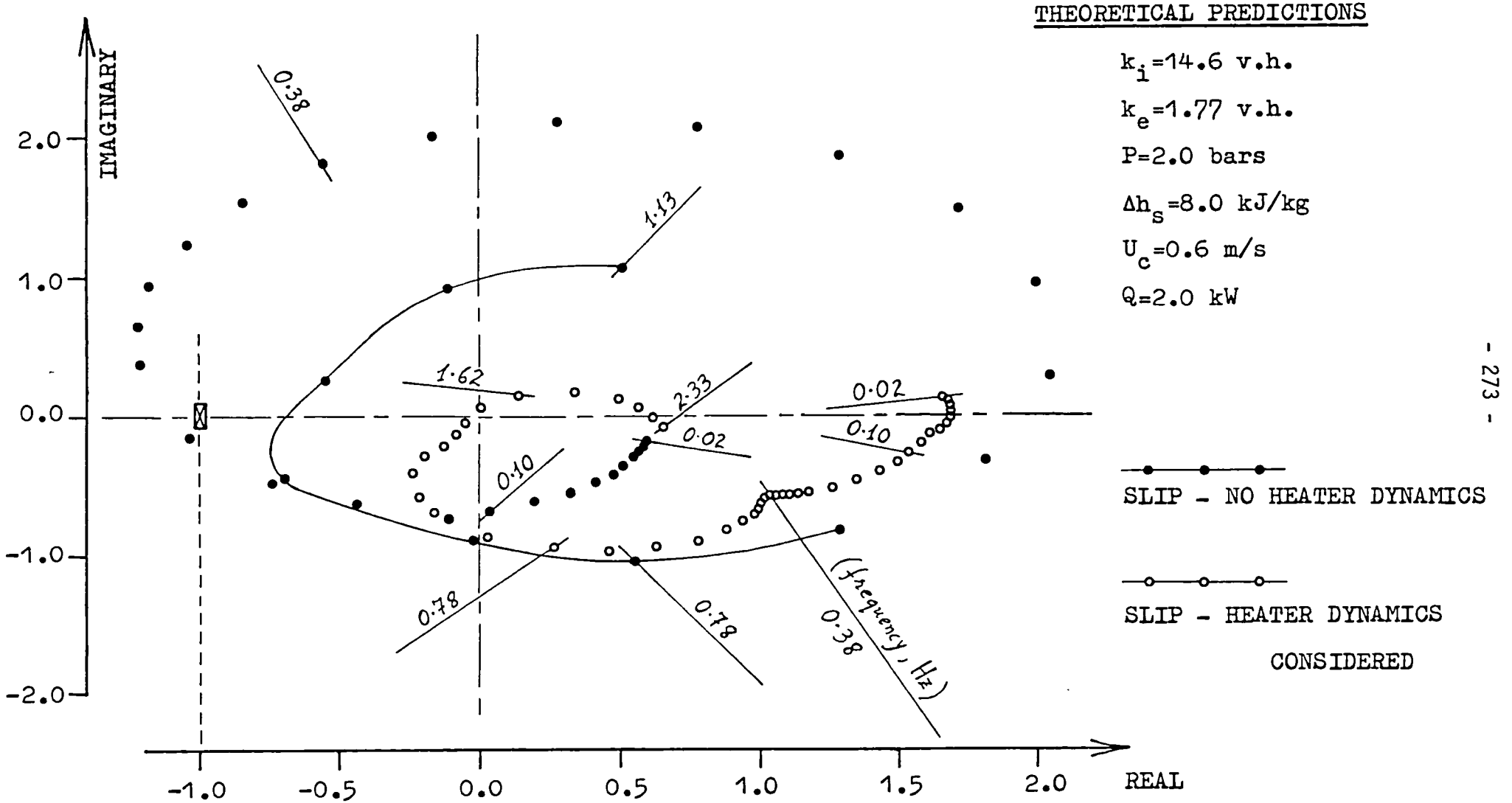

Figure 7.41: Open loop frequency response (present experimental data)

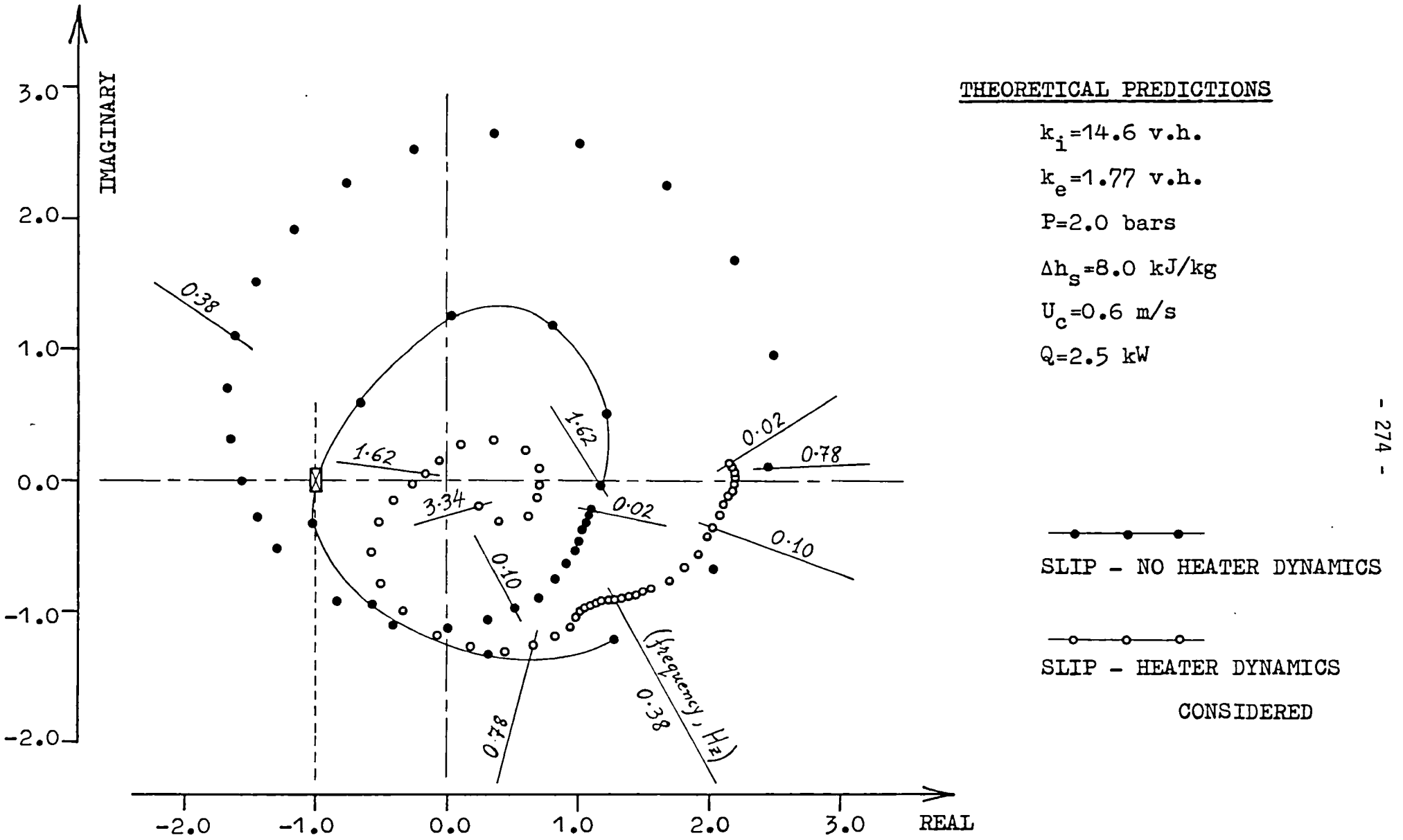

Figure 7.42: Open loop frequency response (present experimental data)

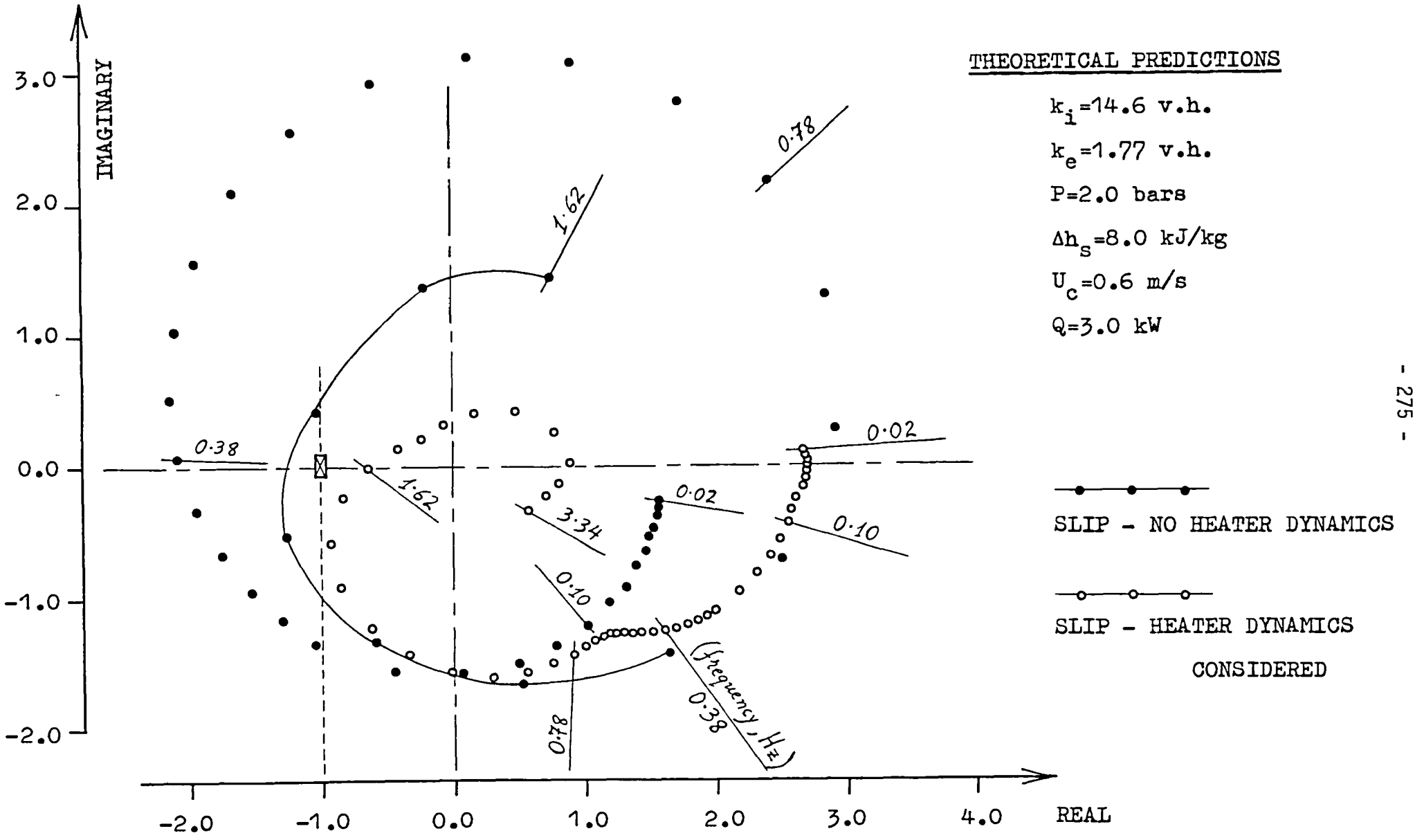

Figure 7.43: Open loop frequency response (present experimental data)

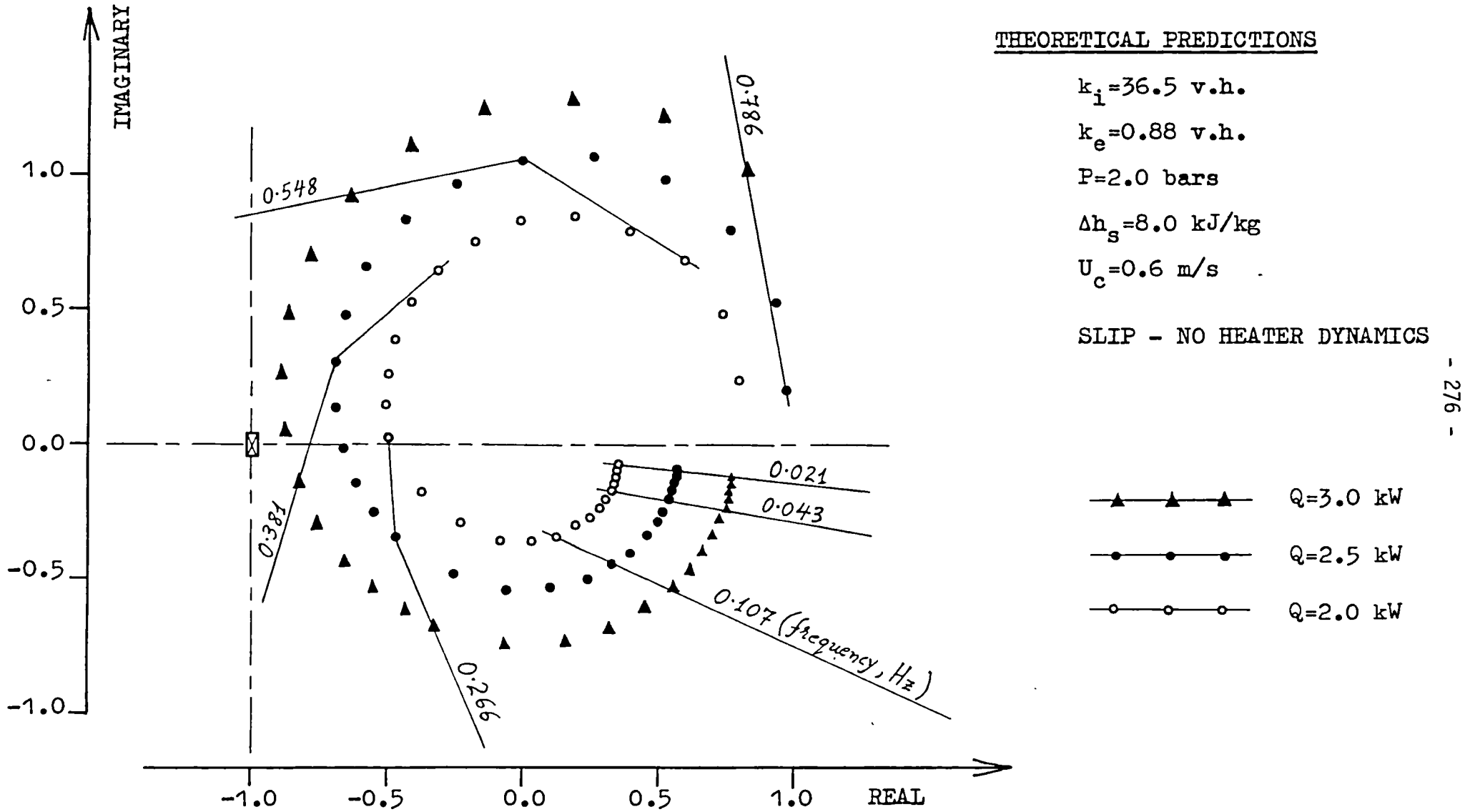

Figure 7.44: Open loop frequency response (present experimental data)

REFERENCES

ABI-ZADEH, D. (1976)

"A non-linear digital simulation of the dynamic behaviour of a steam generator",

Ph.D. Thesis, University of London.

AKAGAWA, K., SAKAGUCHI, T., and UEDA, M. (1971)

"Study on a gas-liquid two-phase flow in helically coiled tubes",

Bulletin, Japan S.M.E., Vol. 14, No. 72, p. 564.

ANDERSON, T.T. (1970)

"Hydraulic impedance: A tool for predicting boiling loop stability",

Nuclear Applications and Technology, Vol. 9, p. 422.

ANGLESEA, W.T., CHAMBERS, D.J.B., and JEFFREY, R.C. (1974)

"Measurement of water/steam pressure drop in helical coils at 179 bars",

Symposium on Multi-Phase Flow Systems, Strathclyde,

I.Mech.E./I.Chem.E., No. I2.

A.S.H.R.A.E. (1965)

Properties of Refrigerants,

Guide and Data Book, C.19.

BANERJEE, S., RHODES, E., and SCOTT, D.S. (1967)

"Film inversion of cocurrent two-phase flow in helical coils",

A.I.Ch.E. Journal, Vol. 13, No. 1, p. 189.

BANERJEE, S., RHODES, E., and SCOTT, D.S. (1969)

"Studies on cocurrent gas-liquid flow in helically coiled tubes: I. Flow patterns, pressure drop and hold-up",

Can. J. Chem. Eng., Vol. 47, p. 445.

BARUA, S.N. (1963)

"On secondary flow in stationary curved pipes",

Quart. J. Mech. and Applied Math., Vol. 16, Pt. I, p. 61.

BELL, K.J., and OWHADI, A. (1969-70)

"Local heat transfer measurements during forced-convection boiling in a helically coiled tube",

Proc. Inst. Mech. Engrs., Vol. 184, Pt. 3C, No. 7, p. 52.

BENDAT, J.S., and PIERSOL, A.G. (1971)

Random Data: Analysis and Measurement Procedures,

Wiley-Interscience, New York.

BERGLES, A.E., GOLDBERG, P., and MAULBETSCH, J.S. (1967)

"Acoustic oscillations in a high pressure single channel boiling system",

Symposium on Two-Phase Flow Dynamics, EUR-4288e, Eindhoven, No. 4.3, p. 525.

BERGLES, A.E., LOPINA, R.F., and FIORI, M.P. (1967)

"Critical heat flux and flow pattern observations for low pressure water flowing in tubes",

J. Heat Transfer, Trans. A.S.M.E., Vol. 89, p. 69.

BIRD, R.B., STEWART, W.E., and LIGHTFOOT, E.N. (1960)

Transport Phenomena,

John Wiley and Sons Incorporated, New York.

BJORLO, T., EUROLA, T., GRUMBACH, R., HANSON, P., OLSEN, A., RASMUSSEN, J., and ROMSLO, K. (1967)

"Comparative studies of mathematical hydrodynamic models applied to selected boiling channels experiments",

Symposium on Two-Phase Flow Dynamics, EUR-4288e, Eindhoven, No. 8.2, p. 981.

BLUMENKRANTZ, A., and TABOREK, J. (1972)

"Application of stability analysis for design of natural circulation boiling systems and comparison with experimental data",

A.I.Ch.E., Symp. Series No. 118, Vol. 68, p. 136.

BOURÉ, J.A. (1966)

"The oscillatory behaviour of heated channels: An analysis of the density effect",

CEA-R 3049, Pts I and II, Grenoble.

BOURÉ, J.A., and MIHAILA, A. (1967)

"The oscillatory behaviour of heated channels",

Symposium on Two-Phase Flow Dynamics, EUR-4288e, Eindhoven, No. 6.1, p. 695.

BOURÉ, J.A., BERGLES, A.E., and TONG, L.S. (1973)

"Review of two-phase flow instability",

Nuclear Eng. and Design, Vol. 25, p. 165.

CARVER, J.R., KAKARALA, C.R., and SLOTNIK, J.S. (1964)

"Heat transfer in coiled tubes with two-phase flow",

TID-20983.

CARVER, M.B. (1969-70)

"Effect of by-pass characteristics on parallel channel flow instabilities",

Proc. Inst. Mech. Engrs., Vol. 184, Pt. 3C, No. 11, p. 84.

CHEXAL, V.K., and BERGLES, A.E. (1973)

"Two-phase instabilities in a low pressure natural circulation loop",

A.I.Ch.E., Symp. Series No. 131, Vol. 69, p. 37.

COLLIER, J.G. (1972)

Convective Boiling and Condensation,

McGraw-Hill Book Company (UK) Limited.

COLLINS, D.B., and GASECA, M. (1969-70)

"Hydrodynamic instability in a full-scale simulated reactor channel", Proc. Inst. Mech. Engrs., Vol. 184, Pt. 3C, No. 15, p. 115.

CROWLEY, J.D., DEAN, Ch., and GOUSE, S.W. Jr. (1967)

"Two-phase flow oscillations in vertical parallel heated channels", Symposium on Two-Phase Flow Dynamics, EUR-4288e, Eindhoven, No. 9.1, p. 1131.

CROWLEY, J.D., and BERGLES, A.E. (1970)

"Fluid-to-fluid modelling of the hydrodynamic stability of flow in boiling channels",

A.S.M.E. Paper No. 70-HT-28.

CORRAN, E.R., and CUMMINS, J.D. (1963)

"Preliminary results of statistical dynamic experiments on a heat exchanger",

U.K.A.E.A., AEEW-R 255.

CRAIN, B. Jr., and BELL, K.J. (1973)

"Forced convection heat transfer to a two-phase mixture of water and steam in a helical coil",

A.I.Ch.E., Symp. Series No. 131, Vol. 69, p. 30.

CUMMINS, J.D. (1968)

"Drift correction of binary cross-correlation measurements",

U.K.A.E.A., AEEW-R 583.

CUMMINS, J.D. (1969)

"Noise spectra measured on the DRAGON reactor primary heat exchangers",

U.K.A.E.A., AEEW-R 641.

D'ARCY, D.F. (1967)

"An experimental investigation of boiling channel flow instability", Symposium on Two-Phase Flow Dynamics, EUR-4288e, Eindhoven, No. 9.2, p. 1173.

DAVIES, A.L., and POTTER, R. (1967)

"Hydraulic stability: An analysis of the causes of unstable flow in parallel channels", Symposium on Two-Phase Flow Dynamics, EUR-4288e, Eindhoven, No. 9.3, p. 1225.

DEAN, W.R. (1927)

"Note on the motion of fluid in a curved pipe", Phil. Mag., Vol. 4, p. 208.

DE LA HARPE, A., LEHONGRE, S., MOLLARD, J., and JOHANNÈS, C. (1968)

"Boiling heat transfer and pressure drop of liquid helium-1 under forced circulation in a helically coiled tube", Advances in Cryogenic Eng., Vol. 14, p. 170.

DIJKMAN, F.J.M. (1969)

"Some hydrodynamic aspects of a boiling water channel", Ph.D. Thesis, Eindhoven University of Technology, The Netherlands.

DiSTEFANO III, J.J., STUBBERUD, A.R., and WILLIAMS, I.J. (1967)

Feedback and Control Systems, Schaum's Outline Series, McGraw-Hill Book Company.

DORSCH, R.G. (1967)

"Frequency response of a forced-flow single-tube boiler", Symposium on Two-Phase Flow Dynamics, EUR-4288e, Eindhoven, No. 2.1, p. 291.

ECKERT, E.R.G., and DRAKE, R.M. Jr. (1959)
Heat and Mass Transfer,
McGraw-Hill Book Company Incorporated.

EDESKUTY, F.J., and THURSTON, R.S. (1967)
"Similarity of flow oscillations induced by heat transfer in cryogenic systems",
Symposium on Two-Phase Flow Dynamics, EUR-4288e, Eindhoven, No. 4.4, p. 551.

FALLOWS, T., HITCHCOCK, J.A., JONES, R.C., LIS, J., and NORTHOVER, E.W. (1973)
"A study of oscillatory instabilities in the parallel channels of a high pressure once-through boiler rig",
Boiler Dynamics and Control in Nuclear Power Stations,
B.N.E.S. (London), No. 14.

FRANCO, G., MÜLLER, H.W., HOSEGOOD, S.B., and PRYTZ, L.H. (1964)
"Review of engineering work for the DRAGON project",
U.N., ICPUAE (Geneva), Vol. 3, No. 549, p. 356.

GALL, C.J. (1973)
"Assessment of system response characteristics from "noise" measurements at a single point with particular application to flow stability",
Journal B.N.E.S., Vol. 12, No. 2, p. 175.

GARDNER, G.C., and NELLER, P.H. (1969-70)
"Phase distributions in flow of an air-water mixture round bends and past obstructions at the wall of a 76 mm bore tube",
Proc. Inst. Mech. Engrs., Vol. 184, Pt. 3C, No. 12, p. 93.

GILLI, P.V. (1965)

"Heat transfer and pressure drop for cross-flow through banks of multistart helical tubes with uniform inclinations and uniform longitudinal pitches",

Nucl. Sci. Eng., Vol. 11, p. 298.

GILLI, P.V. (1967)

"The power density of integral steam generators for high temperature gas-cooled reactors",

Neue Technik, Bl.

HANDS, B.A. (1974)

"A re-examination of the Ledinegg instability criterion and its application to two-phase helium systems",

Symposium on Multi-Phase Flow Systems, Strathclyde,

I.Mech.E./I.Chem.E., No. E.2.

HARVIE, J.D. (1974)

"An experimental investigation of flow instability in Freon-12 and comparison with water data",

Symposium on Two-Phase Flow Systems, Strathclyde,

I.Mech.E./I.Chem.E., No. E.1.

HEWITT, G.F., and HALL-TAYLOR, N.S. (1970)

Annular Two-Phase Flow,

Pergamon Press.

HSU, H.P. (1970)

Fourier Analysis,

Simon and Schuster Tech. Outlines, New York.

IMPERIAL CHEMICAL INDUSTRIES (ICI)

"Thermodynamic properties of Arcton-113 - SI units",

ICI Technical Bulletin, GC/2474.

IMPERIAL CHEMICAL INDUSTRIES (ICI)

"Arcton-113. Properties and uses",

ICI Technical Bulletin, C/2038/2.

ISHII, M., and ZUBER, N. (1970)

"Thermally induced flow instabilities in two-phase mixtures",

4th Int. Heat Transfer Conf., Versailles - Paris, Vol. 5, No. B5.11.

ITÖ, H. (1959)

"Friction factors for turbulent flow in curved pipes",

J. Basic Eng., Trans. A.S.M.E., Vol. 81, p. 123.

KAY, J.M. (1968)

An Introduction to Fluid Mechanics and Heat Transfer,

Cambridge University Press.

LACEY, P.M.C. (1970)

"Two-phase flow in curved ducts",

Annual Meeting of DACHEMA, Frankfurt/Main, June 1970.

LEDINEGG, M. (1938,1954)

"Instability of flow during natural and forced circulation",

Die Wärme, Vol. 61, p. 8, 1938.

AEC-tr.-1861, 1954.

LEE, Y.M. (1960)

Statistical Theory of Communication,

John Wiley and Sons Incorporated, New York.

MARGETTS, R.J. (1972)

"Excursive instability in feed water coils",

A.I.Ch.E., Preprint 16, 13th National Heat Transfer Conf., Denver,

Colorado.

MARTINELLI, R.C., and NELSON, D.B. (1948)

"Prediction of pressure drop during forced-circulation boiling of water",

Trans. A.S.M.E., Vol. 70, p. 695.

MATHISEN, R.P. (1967)

"Out of pile channel instability in the loop SKÄLVAN",

Symposium on Two-Phase Flow Dynamics, EUR-4288e, Eindhoven, No. 1.1, p. 19.

MAULBETSCH, J.S., and GRIFFITH, P. (1967)

"Prediction of the onset of system-induced instabilities in subcooled boiling",

Symposium on Two-Phase Flow Dynamics, EUR-4288e, Eindhoven, No. 7.1, p. 799.

McLACHLAN, N.W. (1961)

Bessel Functions for Engineers,

Oxford University Press.

MEYER, J.E., and ROSE, R.P. (1963)

"Application of a momentum integral model to the study of parallel channel boiling flow oscillations",

J. Heat Transfer, Trans. A.S.M.E., Vol. 85, p. 1.

MIROPOLSKIY, Z.L., PIKUS, V.J., and SHITSMAN, M.E. (1966)

"Regimes of deteriorated heat transfer at forced flow of fluids in curvilinear channels",

3rd Int. Heat Transfer Conf., Chicago, Vol. 2, No. 50.

MIROPOLSKIY, Z.L., and PIKUS, V.J. (1969)

"Critical boiling heat fluxes in curved channels",

Heat Transfer - Soviet Research, Vol. 1, No. 1, p. 74.

MORI, Y., and NAKAYAMA, W. (1965)

"Study on forced convective heat transfer in curved pipes (I. Laminar region)",

Int. J. Heat and Mass Transfer, Vol. 8, p. 67.

MORI, Y., and NAKAYAMA, W. (1967)

"Study on forced convective heat transfer in curved pipes (II. Turbulent region)",

Int. J. Heat and Mass Transfer, Vol. 10, p. 37.

MOXON, D. (1968)

"SLIP. A dynamics program for the hydraulic behaviour of boiling loops",

U.K.A.E.A., AEEW-R 448.

MOXON, D. (1973)

"Stability of once-through steam generators",

A.S.M.E. Paper No. 73-WA/HT-24.

MURPHY, R.W., and BERGLES, A.E. (1972)

"Subcooled flow boiling of fluorocarbons - Hysteresis and dissolved gas effects on heat transfer",

Proc. Heat Transfer and Fluid Mechanics Inst., No. 24, p. 400.

NEAL, L.G., ZIVI, S.M., and WRIGHT, R.W. (1967)

"The mechanisms of hydrodynamic instabilities in boiling systems",

Symposium on Two-Phase Flow Dynamics, EUR-4288e, Eindhoven, No. 8.1, p. 957.

OPPENHEIM, A.V., and SCHAFFER, R.W. (1975)

Digital Signal Processing,

Prentice Hall Incorporated, New Jersey.

OWHADI, A., BELL, K.J., and CRAIN, B. Jr. (1968)

"Forced convection boiling inside helically-coiled tubes",
Int. J. Heat and Mass Transfer, Vol. 11, p. 1779.

PAUL, F.W., and RIEDLE, K.J. (1972)

"Experimental and analytical investigation of the dynamic behaviour of diabatic two-phase flow in a vertical monotube vapour generator - Part I",
A.S.M.E. Paper No. 72-WA/HT-46.

POTTER, R. (1973)

"A review of two-phase flow instability of boiler dynamics",
Boiler Dynamics and Control in Nuclear Power Stations,
B.N.E.S. (London), No. 13.

QUANDT, E.R. (1961)

"Analysis and measurement of flow oscillations",
A.I.Ch.E., Symp. Series No. 32, Vol. 57, p. 111.

QUINN, E.P. (1966)

"Forced flow heat transfer to high pressure water beyond the critical heat flux",
A.S.M.E. Paper No. 66-WA/HT-36.

RAKOPOULOS, C. (1972)

"Electronics and correlation techniques in two-phase bubble flow",
M.Sc. Thesis, Mechanical Engineering Department, Imperial College of Science and Technology, University of London.

REDFIELD, J.A., and MURPHY, J.H. (1971)

"Sectionalised compressible and momentum integral models for channel hydrodynamics",
A.S.M.E. Paper No. 71-HT-14.

RIPPEL, G.R., EIDT, C.M. Jr., and JORDAN, H.B. Jr. (1966)

"Two-phase flow in a coiled tube - Pressure drop, hold-up, and liquid phase mixing",

I & EC Process Design Development and Control, Vol. 5, No. 1, p. 32.

ROGERS, G.F.C., and MAYHEW, Y.R. (1964)

"Heat transfer and pressure loss in helically coiled tubes with turbulent flow",

Int. J. Heat and Mass Transfer, Vol. 7, p. 1207.

SAHA, P., ISHII, M., and ZUBER, N. (1975)

"An experimental investigation of the thermally induced flow oscillations in two-phase systems",

A.S.M.E. Paper No. 75-WA/HT-6.

SEBAN, R.A., and McLAUGHLIN, E.F. (1963)

"Heat transfer in tube coils with laminar and turbulent flow",

Int. J. Heat and Mass Transfer, Vol. 6, p. 387.

SENSINCLE, A. (1968)

Introduction to Control Theory for Engineers,

Blackie and Son Limited.

SHINNERS, S.M. (1972)

Modern Control System Theory and Application,

Addison-Wesley Publishing Company Incorporated.

SHOTKIN, L.M. (1967)

"Stability considerations in two-phase flow",

Nucl. Sci. Eng., Vol. 28, p. 317.

SOLVERG, K.O., and BAKSTAD, P. (1967)

"A model for the dynamics of nuclear reactors with boiling coolant with a new approach to the vapour generation process",

Symposium on Two-Phase Flow Dynamics, EUR-4288e, Eindhoven, No. 7.4, p. 871.

SPIEGEL, M.R. (1968)

Mathematical Handbook of Formulae and Tables,

Schaum's Outline Series,

McGraw-Hill Book Company.

STENNING, A.H., and VEZIROGLU, T.N. (1965)

"Flow oscillation modes in forced-convection boiling",

Proc. Heat Transfer and Fluid Mechanics Inst., No. 18, p. 301.

STENNING, A.H., VEZIROGLU, T.N., and CALLAHAN, G.M. (1967)

""Pressure-drop" oscillations in forced convection flow with boiling",

Symposium on Two-Phase Flow Dynamics, EUR-4288e, Eindhoven, No. 3.1, p. 405.

STEVENS, G.F., and MACBETH, R.V. (1970)

"The use of Freon-12 to model forced convection burn-out in water: The restriction on the size of the model",

Journal B.N.E.S., Vol. 9, No. 4, p. 249.

TAYLOR, P.A., URQUHART, W.M., and JEFFREY, R.C. (1973)

"The development of once-through boilers for gas cooled reactors",

Convention on Steam Plant Operation, Inst. Mech. Engrs., London.

TONG, L.S. (1965)

Boiling Heat Transfer and Two-Phase Flow,

John Wiley and Sons Incorporated, New York.

VERHEUGEN, A.N.J., DIJKMAN, F.J.M., LAMEIN, H.J., and TONG, L.S. (1967)

"The influence of the response characteristics of the heating rod on the stability and burn-out characteristics of a boiling channel",

Symposium on Two-Phase Flow Dynamics, EUR-4288e, Eindhoven, No. 7.3, p. 841.

VEZIROGLU, N.T., and LEE, S.S. (1971)

"Boiling flow instabilities in a cross-connected parallel channel upflow system",

A.S.M.E. Paper No. 71-HT-12.

WALLIS, G.B., and HEASLEY, J.H. (1961)

"Oscillations in two-phase flow systems",

J. Heat Transfer, Trans. A.S.M.E., Vol. 83, p. 363.

WHITE, C.M. (1929)

"Streamline flow through curved pipes",

Proc. R. Soc., A.123, p. 645.

YADIGAROGLU, G., and BERGLES, A.E. (1972)

"Fundamental and higher-mode density wave oscillations in two-phase flow",

J. Heat Transfer, Trans. A.S.M.E., p. 189.

ZUBER, N., and FINDLAY, J. (1965)

"Average volumetric concentration in two-phase flow systems",

J. Heat Transfer, Trans. A.S.M.E., Vol. 87, p. 453.

ZUBER, N. (1967)

"Flow excursions and oscillations in boiling, two-phase flow systems with heat addition",

Symposium on Two-Phase Flow Dynamics, EUR-4288e, Eindhoven, No. 8.4, p. 1071.

APPENDIX A

INTEGRATION OF MOMENTUM EQUATION

According to our assumptions, the conservation of momentum equation can be written as:

$$\frac{\partial}{\partial z}(\rho_i U_i^2) + \frac{\partial}{\partial t}(\rho_i U_i) = -\frac{\partial}{\partial z} P_i - \rho_i g \sin\theta - \lambda_i \rho_i U_i^2 \qquad (A.1)$$

which generally holds for all single-phase regions ($i = f, g$). θ is the inclination of the channel (helix) with respect to the horizontal plane. For horizontal parts $\theta = 0$ and for vertical parts $\theta = 90^{o}$.

The procedure is to linearise by taking small perturbations of each component of pressure drop around a steady-state value and then to Laplace transform and integrate the various pressure drop perturbations through each region separately.

1. SUBCOOLED REGION (index 1)

(a) Gravitational Component

$$\delta(-\Delta P_{1g}) = \int_o^{y_1+\delta y_1} \rho_f . g . \sin\theta . dz - \int_o^{y_1} \rho_f . g . \sin\theta . dz = \int_o^{\delta y_1} \rho_f . g . \sin\theta . dz$$

Therefore:
$$-\overline{\Delta P}_{1g} = \rho_f \cdot g \cdot \bar{y}_1 \cdot \sin\theta \qquad (A.2)$$

(b) Momentum Component

Since $\partial/\partial z . U_1 = 0$, there is only contribution from the temporal component:

$$\delta(-\Delta P_{1m}) = \int_o^{y_1+\delta y_1} \rho_f \frac{\partial}{\partial t}(\delta U_1)\, dz = \int_o^{y_1} \rho_f \frac{\partial}{\partial t}(\delta U_1)\, dz$$

Therefore:

$$-\overline{\Delta P}_{1m} = \int_o^{y_1} \rho_f \, s \, \overline{U}_1 \, dz = \rho_f \, s \, \overline{U}_1 \, y_1 = s \, \tau_1 \frac{\overline{U}_1}{U_1^0} \rho_f \, (U_1^0)^2 \qquad (A.3)$$

(c) Frictional Component

$$\delta \, (-\Delta P_{1f}) = \int_o^{y_1+\delta y_1} (\lambda_f^0 + \delta\lambda_f) \, \rho_f \, (U_1^0 + \delta U_1)^2 \, dz - \int_o^{y_1} \lambda_f^0 \, \rho_f \, (U_1^0)^2 \, dz =$$

$$= \int_o^{\delta y_1} \lambda_f^0 \, \rho_f \, (U_1^0)^2 \, dz + \int_o^{y_1} \left[2 \, \lambda_f^0 \, \rho_f \, U_1^0 \, \delta U_1 + \delta\lambda_f \, \rho_f \, (U_1^0)^2 \right] dz$$

or, according to equations (4.57) and (4.58), therefore:

$$-\overline{\Delta P}_{1f} = \lambda_f^0 \, \rho_f \, (U_1^0)^2 \, \overline{y}_1 + (2 - \beta) \, \lambda_f^0 \, \rho_f \, U_1^0 \, \overline{U}_1 \, y_1 \qquad (A.4)$$

In the steady-state:

$$-\Delta P_{1f}^0 = \lambda_f^0 \, \rho_f \, (U_1^0)^2 \, y_1 \qquad (A.5)$$

Therefore:

$$-\overline{\Delta P}_{1f} = \lambda_f^0 \, \rho_f \, (U_1^0)^2 \, \overline{y}_1 + (2 - \beta) \, (-\Delta P_{1f}^0) \, \frac{\overline{U}_1}{U_1^0} \qquad (A.6)$$

The parameter:

$$\lambda_f^0 = f_f \frac{1}{2d} \qquad (A.7)$$

The value of the friction factor f depends on the Reynolds number, the roughness and the geometry (straight or coiled tube, etc.). The tube has a circular cross-section of internal diameter d (or

hydraulic diameter in general) and it is bent in a coil form of mean diameter D.

For straight tubes, in turbulent flow, the value of f is taken from the Blasius formula (Kay (1968)):

$$f_s = \frac{0.316}{Re_f^{0.25}} \quad , \quad \text{for} \quad 3000 < Re_f < 10^7 \tag{A.8a}$$

For coiled tubes, the value of f_c is taken from Ito (1959), assuming turbulent flow, i.e.

$$f_c = (\frac{d}{D})^{0.5} \frac{0.316}{(Re.(\frac{d}{D})^2)^{0.2}} = f_s \cdot (Re.(\frac{d}{D})^2)^{1/20} \tag{A.8b}$$

if $Re.(d/D) > 6$ and assuming a turbulent flow in the coils, i.e.

$$Re_c > Re_{crit} = 20.000\ (\frac{d}{D})^{0.32} \tag{A.9}$$

Therefore, $\beta_s = 0.25$ for straight parts and $\beta_c = 0.20$ for coiled parts in equation (A.6).

The contribution of the upstream adiabatic length (straight) on the pressure drop perturbation components can now be taken into account.

The upstream adiabatic length is a straight circular channel with inner diameter d_{up} and length y_{up}.

In order to be able to consider the effect of changes in the system geometry (different cross-sectional areas), normalisation will be used with respect to the values in the heated subcooled region.

From the continuity equation for incompressible flow and for small perturbations, we have (see also section 4.4.5):

$$\frac{\overline{U}_1}{\overline{U}_{up}} = \frac{U_1^0}{U_{up}^0} = \frac{A_{up}}{A_1} = \left(\frac{d_{up}}{d_1}\right)^2 = \sigma_{up} \qquad (A.10)$$

and the transit time through the upstream adiabatic length is:

$$\tau_{up} = \frac{y_{up}}{U_{up}^0} = \frac{y_{up}}{U_1^0}\,\sigma_{up} \qquad (A.11)$$

There will not be any contribution on the gravitational component described by equation (A.2).

The momentum component of equation (A.3) will become, in that case, as follows:

$$-\overline{\Delta P}_{mT} = \rho_f\, s\, (\overline{U}_1\, y_1 + \overline{U}_{up}\, y_{up}) = \rho_f\, s \left(\overline{U}_1\, y_1 + \frac{\overline{U}_1}{\sigma_{up}}\, y_{up}\right) =$$

$$= \rho_f\, s\, \overline{U}_1 \left(y_1 + \frac{y_{up}}{\sigma_{up}}\right) = \rho_f\, s\, \overline{U}_1\, U_1^0 \left(\frac{y_1}{U_1^0} + \frac{y_{up}}{U_1^0}\,\frac{1}{\sigma_{up}}\right) = \rho_f\, s\, \overline{U}_1\, U_1^0 \left(\tau_1 + \frac{\tau_{up}}{\sigma_{up}^2}\right)$$

i.e.

$$-\overline{\Delta P}_{mT} = s \left(\tau_1 + \frac{\tau_{up}}{\sigma_{up}^2}\right) \frac{\overline{U}_1}{U_1^0}\, \rho_f\, (U_1^0)^2 \qquad (A.12)$$

The effect of the upstream adiabatic length on the frictional component of equation (A.6) will be only on the second term, which will become as follows:

$$-\overline{\Delta P}_{fT} = (2-\beta_c)\, \lambda_c^0 \rho_f U_1^0 \overline{U}_1 y_1 + (2-\beta_s)\, \lambda_s^0 \rho_f U_{up}^0 \overline{U}_{up} y_{up} + 2\eta_{up} \rho_f U_{up}^0 \overline{U}_{up} =$$

$$= (2 - \beta_c)\, \lambda_c^0\, \rho_f\, U_1^0\, \overline{U}_1\, y_1 + \left((2 - \beta_s)\, \lambda_s^0\, y_{up} + 2\eta_{up}\right) \rho_f\, U_{up}^0\, \overline{U}_{up} =$$

$$= \left\{(2 - \beta_c)\, \lambda_c^0\, y_1 + \left[\frac{(2 - \beta_s)\, \lambda_s^0\, y_{up} + 2\eta_{up}}{\sigma_{up}^2}\right]\right\} \rho_f\, (U_1^0)^2\, \frac{\overline{U}_1}{U_1^0} \qquad (A.13)$$

In the steady-state:

$$-\overline{\Delta P}_{fT}{}^{0} = \lambda_c{}^{0}\,\rho_f\,(U_1{}^{0})^2\,y_1 + \lambda_s{}^{0}\,\rho_f\,(U_{up}{}^{0})^2\,y_{up} + \eta_{up}\,\rho_f\,(U_{up}{}^{0})^2 =$$

$$= \left(\lambda_c{}^{0}\,y_1 + \frac{\lambda_s{}^{0}\,y_{up} + \eta_{up}}{\sigma_{up}{}^{2}}\right)\rho_f\,(U_1{}^{0})^2 \qquad (A.14)$$

Therefore, equation (A.13) becomes:

$$-\overline{\Delta P}_{fT} = \left\{2\,(-\Delta P_{fT}{}^{0}) - \left(\beta_c\,\lambda_c{}^{0}\,y_1 + \frac{\beta_s\,\lambda_s{}^{0}\,y_{up}}{\sigma_{up}{}^{2}}\right)\rho_f\,(U_1{}^{0})^2\right\}\frac{\overline{U}_1}{U_1{}^{0}} \qquad (A.15)$$

2. TWO-PHASE REGION (index 2)

According to our assumptions, the conservation of momentum equation can be written in this region as:

$$\frac{\partial}{\partial z}\left[\rho_f\,(1-\alpha)\,U_f{}^{2} + \rho_g\,\alpha\,U_g{}^{2}\right] + \frac{\partial}{\partial t}\left[\rho_f\,(1-\alpha)\,U_f + \rho_g\,\alpha\,U_g\right] =$$

$$= -\frac{\partial P}{\partial z} - g\,\sin\theta\left[\rho_f\,(1-\alpha) + \rho_g\,\alpha\right] - X\,\lambda_f\,\frac{G^2}{\rho_f} \qquad (A.16)$$

(a) Gravitational Component

It can be observed that the density ρ_2 at any point in the two-phase region is given by:

$$\rho_2 = \rho_f\,(1-\alpha) + \rho_g\,\alpha = \rho_f - \alpha\,\Delta\rho \qquad (A.17)$$

and

$$\delta\rho_2 = -\delta\alpha\,\Delta\rho \qquad (A.18)$$

Therefore:

$$\frac{1}{g \sin\theta}\left(\delta\left(-\Delta P_{2g}\right)\right) = \int_{y_1+\delta y_1}^{y_2+\delta y_2}\left(\rho_f - (\alpha^0 + \delta\alpha)\,\Delta\rho\right) dz - \int_{y_1}^{y_2}\left(\rho_f - \alpha^0\,\Delta\rho\right) dz$$

or

$$\frac{1}{g \sin\theta}\left(-\overline{\Delta P}_{2g}\right) = \int_{\overline{y}_1}^{\overline{y}_2}\left(\rho_f - \alpha^0\,\Delta\rho\right) dz - \int_{y_1}^{y_2}\overline{\alpha}\,\Delta\rho\, dz =$$

$$= \left(\rho_f - \alpha^0_{out}\,\Delta\rho\right)\overline{y}_2 - \left(\rho_f - \alpha^0_{in}\,\Delta\rho\right)\overline{y}_1 - \Delta\rho\int_0^{\tau_{2out}}\overline{\alpha}\,U_g{}^0\, d\tau_2 =$$

$$= \left(\rho_f - \alpha^0_{out}\,\Delta\rho\right)\overline{y}_2 - \rho_f\,\overline{y}_1 - \Delta\rho\int_0^{\tau_{2out}}\overline{\alpha}\,U_g{}^0\, d\tau_2$$

since $\alpha^0_{in} = 0$ according to equation (4.94).

According to equation (4.103), the last term is evaluated as follows:

$$-\Delta\rho\int_0^{\tau_{2out}}\overline{\alpha}\,U_g{}^0\, d\tau_2 = -\Delta\rho\int_0^{\tau_{2out}}\left(-\frac{q\,\rho_f}{\Delta\rho}\,\overline{y}_1\, e^{-s\tau_2} - \frac{\rho_f}{\Delta\rho}\,\overline{J}_{in}\,\frac{e^{-\gamma q\tau_2} - e^{-s\tau_2}}{s/\gamma q - 1}\right) d\tau_2 =$$

$$= q\,\rho_f\,\overline{y}_1\left(\frac{1 - e^{-s\tau_2}}{s}\right) + \frac{\rho_f\,\overline{J}_{in}}{1 - s/\gamma q}\int_0^{\tau_{2out}}\left(e^{-s\tau_2} - e^{-\gamma q\tau_2}\right) d\tau_2 =$$

$$= \rho_f\,\overline{y}_1\left(\frac{e^{-s\tau_2} - 1}{-s/q}\right) + \frac{\rho_f\,\overline{J}_{in}}{q\,(1 - s/\gamma q)}\left(\frac{e^{-s\tau_2} - 1}{-s/q} - \frac{e^{-\gamma q\tau_2} - 1}{-\gamma}\right)$$

For the steady-state:

$$-\Delta P_{2g}{}^0 = g \sin\theta\int_{y_1}^{y_2}\left(\rho_f - \alpha^0\,\Delta\rho\right) dz = g \sin\theta\int_0^{\tau_2}\left(\rho_f - \alpha^0\,\Delta\rho\right) U_g{}^0\, d\tau_2 =$$

$$= g \sin\theta\, U^0_{g_{in}}\int_0^{\tau_2}\left(\rho_f - \alpha^0\,\Delta\rho\right) e^{\gamma q\tau_2}\, d\tau_2$$

Substituting α^0 from equation (4.95), we obtain:

$$-\Delta P_{2g}{}^{0} = g \sin\theta \; U_{g_{in}}^{0} \int_{o}^{\tau_2} \left(\rho_f - \frac{\rho_f}{\gamma}\,(1 - e^{-\gamma q \tau_2})\right) e^{\gamma q \tau_2}\, d\tau_2 =$$

$$= g \sin\theta \; U_{g_{in}}^{0} \; \rho_f \int_{o}^{\tau_2} \left((1 - \frac{1}{\gamma})\, e^{\gamma q \tau_2} + \frac{1}{\gamma}\right) d\tau_2 =$$

$$= g \sin\theta \; U_{g_{in}}^{o} \; \rho_f \left((1 - \frac{1}{\gamma})\, \frac{e^{\gamma q \tau_2} - 1}{\gamma q} + \frac{\tau_2}{\gamma}\right) =$$

$$= g \sin\theta \, \frac{\rho_f \, U_{g_{in}}^{0}}{q} \left((1 - \frac{1}{\gamma})\, \frac{r^* - 1}{\gamma} + \frac{\ln r^*}{\gamma^2}\right) =$$

$$= g \sin\theta \, \frac{\rho_f \, (\gamma \, J_{in}^{0} + V_j)}{q} \left((1 - \frac{1}{\gamma})\, \frac{r^* - 1}{\gamma} + \frac{\ln r^*}{\gamma^2}\right) =$$

$$= g \sin\theta \, \frac{\rho_f \, U_1{}^{0}}{q} \left\{(\gamma + \frac{V_j}{U_1{}^{0}}) \left[(1 - \frac{1}{\gamma})\, \frac{r^* - 1}{\gamma} + \frac{\ln r^*}{\gamma^2}\right]\right\} =$$

$$= g \sin\theta \, \frac{\rho_f \, U_1{}^{0^2}}{q \, U_1{}^{0}} \, R_{2g}{}^{0} \qquad \text{(A.19)}$$

where we have used $J_{in}^{0} = U_1{}^{0}$ as per equation (4.76), and we have given the following definitions:

$$r^* = e^{\gamma q \tau_2} = U_g{}^{0}/U_{g_{in}}^{0} \qquad \text{(A.20a)}$$

$$\varepsilon^* = V_j/U_1{}^{0} \qquad \text{(A.20b)}$$

and
$$R_{2g}{}^{0} = (\gamma + \varepsilon^*) \left[(1 - \frac{1}{\gamma})\, \frac{r^* - 1}{\gamma} + \frac{\ln r^*}{\gamma^2}\right] \qquad \text{(A.21)}$$

Also, by using the value of α^0 from equation (4.95), we get:

$$(\rho_f - \alpha_{out}^{0} \, \Delta\rho) = \rho_f \left[(1 - \frac{1}{\gamma}) + \frac{e^{-\gamma q \tau_2}}{\gamma}\right] = \rho_f \left[(1 - \frac{1}{\gamma}) + \frac{1}{\gamma \, r^*}\right] \qquad \text{(A.22)}$$

Therefore, the perturbed state becomes:

$$-\overline{\Delta P}_{2g} = g \sin\theta \, (\rho_f - \alpha^0_{out}\Delta\rho) \, \bar{y}_2 - g \sin\theta \, \rho_f \bar{y}_1 + g \sin\theta \, \rho_f \bar{y}_1 \left[\frac{e^{-s\tau_2} - 1}{-s/q}\right] +$$

$$+ g \sin\theta \, \frac{\rho_f \, \bar{J}_{in}}{q \, (1 - s/\gamma q)} \left[\frac{e^{-s\tau_2} - 1}{-s/q} - \frac{e^{-\gamma q \tau_2} - 1}{-\gamma}\right] =$$

$$= g \sin\theta \, \rho_f \left[(1 - \frac{1}{\gamma}) + \frac{1}{\gamma r^*}\right] \bar{y}_2 - g \sin\theta \, \rho_f \bar{y}_1 + \frac{(-\Delta P_{2g}{}^0)}{R_{2g}{}^0} \, q \, \tau_1 \, \frac{\bar{y}_1}{y_1} \left[\frac{e^{-s\tau_2} - 1}{-s/q}\right] +$$

$$+ \frac{(-\Delta P_{2g}{}^0)}{R_{2g}{}^0} \, \frac{\bar{J}_{in}}{U_1{}^0} \, \frac{1}{1 - s/\gamma q} \left[\frac{e^{-s\tau_2} - 1}{-s/q} - \frac{r^* - 1}{\gamma \, r^*}\right] \qquad \text{(A.23)}$$

For the non-slip condition, $R_{2g}{}^0 = ln \, r^*$ (since $\gamma = 1$ and $\varepsilon^* = 0$) and $r^* = \rho_f/\rho_g$.

(b) Momentum Component

We consider the acceleration components only (spatial and temporal) in the conservation of momentum equation and we express this in terms of the liquid and vapour mass velocities:

$$-\frac{\partial P_{2m}}{\partial z} = \frac{\partial}{\partial z} \left(\rho_f \, (1-\alpha) \, U_f{}^2 + \rho_g \, \alpha \, U_g{}^2\right) + \frac{\partial}{\partial t} \left(\rho_f \, (1-\alpha) \, U_f + \rho_g \, \alpha \, U_g\right) =$$

$$= \frac{\partial}{\partial z} \left(G_f \, U_f + G_g \, U_g\right) + \frac{\partial}{\partial t} \left(G_f + G_g\right) \qquad \text{(A.24)}$$

For the steady-state:

$$-\Delta P_{2m}{}^0 = (G_f{}^0 \, U_f{}^0 + G_g{}^0 \, U_g{}^0)_{out} - (G_f{}^0 \, U_f{}^0 + G_g{}^0 \, U_g{}^0)_{in} \qquad \text{(A.24a)}$$

For the perturbed state:

$$\delta\,(-\Delta P_{2m}) = \int_{y_1+\delta y_1}^{y_2+\delta y_2}\left(-\frac{\partial P_{2m}}{\partial z}\right) dz - \int_{y_1}^{y_2}\left(-\frac{\partial P_{2m}{}^0}{\partial z}\right) dz =$$

$$= \delta y_2 \left[\frac{d}{dz}\,(G_f{}^0 U_f{}^0 + G_g{}^0 U_g{}^0)\right]_{\alpha=\alpha_{out}} - \delta y_1 \left[\frac{d}{dz}\,(G_f{}^0 U_f{}^0 + G_g{}^0 U_g{}^0)\right]_{\alpha=\alpha_{in}} +$$

$$+ \int_{y_1}^{y_2} \frac{\partial}{\partial z}\,(G_f{}^0\,\delta U_f + \delta G_f\,U_f{}^0 + G_g{}^0\,\delta U_g + \delta G_g\,U_g{}^0)\,dz + \int_{y_1}^{y_2} \frac{\partial\,(\delta G)}{\partial t}\,dz$$

We take the Laplace transform:

$$-\overline{\Delta P}_{2m} = \overline{y}_2 \left[\frac{d}{dz}\,(G_f{}^0 U_f{}^0 + G_g{}^0 U_g{}^0)\right]_{\alpha=\alpha_{out}} - \overline{y}_1 \left[\frac{d}{dz}\,(G_f{}^0 U_f{}^0 + G_g{}^0 U_g{}^0)\right]_{\alpha=\alpha_{in}} +$$

$$+ (G_f{}^0\,\overline{U}_f + \overline{G}_f\,U_f{}^0 + G_g{}^0\,\overline{U}_g + \overline{G}_g\,U_g{}^0)_{\alpha=\alpha_{out}} -$$

$$- (G_f{}^0\,\overline{U}_f + \overline{G}_f\,U_f{}^0 + G_g{}^0\,\overline{U}_g + \overline{G}_g\,U_g{}^0)_{\alpha=\alpha_{in}} + s\int_o^z \overline{G}\,dz \qquad \text{(A.25)}$$

The expressions for $U_f{}^0$, $U_g{}^0$, $\overline{U}_f$, $\overline{U}_g$, $G_f{}^0$, $G_g{}^0$, $\overline{G}_f$ and $\overline{G}_g$ have been found in sections 4.4.3.1 and 4.4.3.2.

We proceed by evaluating the expressions $d/dz\,(G_f{}^0\,U_f{}^0)$ and $d/dz\,(G_g{}^0\,U_g{}^0)$ at the terminal positions $\alpha = \alpha_{in} = 0$ and $\alpha = \alpha_{out}$ and the expression $s\int_o^z \overline{G}\,dz$.

First we consider:

$$\frac{d}{dz}\,(G_f{}^0\,U_f{}^0) = \frac{d}{dz}\left[\rho_f\,(1-\alpha^0)\,U_f{}^0\,U_f{}^0\right] =$$

$$= \rho_f\left\{(1-\alpha^0)\,U_f{}^0\,\frac{dU_f{}^0}{dz} + U_f{}^0\,\frac{d}{dz}\left[(1-\alpha^0)\,U_f{}^0\right]\right\} \qquad \text{(A.26)}$$

But from equation (4.69), we have:

$$\frac{d}{dz}\left[(1-\alpha^0)\,U_f^{\,0}\right] = -\,q\,\frac{\rho_g}{\Delta\rho} \tag{A.27}$$

Furthermore, equation (A.27) becomes:

$$(1-\alpha^0)\,\frac{dU_f^{\,0}}{dz} = U_f^{\,0}\,\frac{d\alpha^0}{dz} - q\,\frac{\rho_g}{\Delta\rho} \tag{A.28}$$

But from equation (4.68), we have:

$$\frac{d}{dz}\,(\alpha^0\,U_g^{\,0}) = q\,\frac{\rho_f}{\Delta\rho} \tag{A.29}$$

or
$$\alpha^0\,\frac{dU_g^{\,0}}{dz} + U_g^{\,0}\,\frac{d\alpha^0}{dz} = q\,\frac{\rho_f}{\Delta\rho}$$

Equation (4.81) gives:

$$\frac{dU_g^{\,0}}{dz} = \gamma\,q \tag{A.30}$$

Therefore:
$$\frac{d\alpha^0}{dz} = \frac{1}{U_g^{\,0}}\left(q\,\frac{\rho_f}{\Delta\rho} - \alpha^0\,\gamma\,q\right)$$

Substituting into equation (A.28), we find:

$$(1-\alpha^0)\,\frac{dU_f^{\,0}}{dz} = \frac{U_f^{\,0}}{U_g^{\,0}}\,q\left[\frac{\rho_f}{\Delta\rho} - \alpha^0\,\gamma\right] - q\,\frac{\rho_g}{\Delta\rho} \tag{A.31}$$

We substitute from equations (A.27) and (A.31) into equation (A.26):

$$\frac{d}{dz}\,(G_f^{\,0}\,U_f^{\,0}) = q\,\frac{\rho_f\,U_f^{\,0}}{\Delta\rho\,U_g^{\,0}}\left[U_f^{\,0}\,(\rho_f - \alpha^0\,\gamma\,\Delta\rho) - 2\,U_g^{\,0}\,\rho_g\right] \tag{A.32}$$

Now we consider:

$$\frac{d}{dz}\left(G_g^0\, U_g^0\right) = \frac{d}{dz}\left(\rho_g\, \alpha^0\, U_g^0\, U_g^0\right) =$$

$$= \rho_g \left[\alpha^0\, U_g^0\, \frac{dU_g^0}{dz} + U_g^0\, \frac{d}{dz}\left(\alpha^0\, U_g^0\right)\right]$$

or, according to equations (A.29) and (A.30):

$$\frac{d}{dz}\left(G_g^0\, U_g^0\right) = q\, \frac{\rho_g}{\Delta\rho}\, U_g^0\, \left(\rho_f + \alpha^0\, \gamma\, \Delta\rho\right) \tag{A.33}$$

Finally, we consider the expression $s \int_o^z \overline{G}\, dz$:

$$s \int_o^z \overline{G}\, dz = s \int_o^{\tau_2} \overline{G}\, U_g^0\, d\tau_2 = s\, U_{g_{in}}^0 \int_o^{\tau_2} \overline{G}\, e^{\gamma q \tau_2}\, d\tau_2$$

Substituting from equation (4.108) for $\overline{G}$, we take:

$$s\int_o^z \overline{G}\, dz = s\, \rho_f U_{g_{in}}^0 \int_o^{\tau_2} \left[\overline{J}_{in}\, \frac{s}{s-\gamma q} - \overline{J}_{in}\, \frac{\gamma q}{s-\gamma q}\, e^{(\gamma q - s)\tau_2} + q\, \overline{y}_1 e^{(\gamma q - s)\tau_2}\right] d\tau_2 =$$

$$= s\, \rho_f U_{g_{in}}^0 \left\{\overline{J}_{in}\, \frac{s}{(s-\gamma q)}\, \tau_2 + \frac{\gamma q \overline{J}_{in}}{(s-\gamma q)}\, \frac{e^{(\gamma q - s)\tau_2} - 1}{(s-\gamma q)} - q\, \overline{y}_1\, \frac{e^{(\gamma q - s)\tau_2} - 1}{(s-\gamma q)}\right\} =$$

$$= \rho_f U_1{}^0{}^2\, \frac{(\gamma + \varepsilon^*)}{U_1^0} \left\{\overline{J}_{in} \left[\gamma q s\, \frac{r^* e^{-s\tau_2} - 1}{(\gamma q - s)^2} - \frac{s^2}{(\gamma q - s)}\, \frac{\ln r^*}{\gamma q}\right] + q\, \overline{y}_1 s\, \frac{r^* e^{-s\tau_2} - 1}{(\gamma q - s)}\right\} \tag{A.34}$$

according to the definition of equation (A.20a).

We evaluate the expression for the steady-state momentum component given by equation (A.24a) by the expression:

$$G_g^0\, U_g^0 + G_f^0\, U_f^0 = \rho_g\, \alpha^0\, U_g^{0\,2} + \rho_f\, (1 - \alpha^0)\, U_f^{0\,2} =$$

$$= U_g^{0\,2}\, \rho_f \left[\frac{\rho_g}{\rho_f}\, \alpha^0 + (1 - \alpha^0)\, \frac{1}{S_{r^*}{}^2}\right] =$$

$$= \rho_f U_{g_{in}}^{0\,2} r^{*2} \left\{ \frac{\rho_g}{\gamma \Delta\rho} \left(1 - \frac{1}{r^*}\right) + \left[1 - \frac{\rho_f}{\gamma \Delta\rho} \left(1 - \frac{1}{r^*}\right)\right] \frac{1}{S_{r^*}^2} \right\} =$$

$$= \rho_f U_1^{0\,2} (\gamma + \varepsilon^*)^2 \left[\frac{1}{\gamma \Delta\rho} \left(\rho_g - \frac{\rho_f}{S_{r^*}^2}\right) r^* (r^* - 1) + \frac{r^{*2}}{S_{r^*}^2} \right] \qquad (A.35)$$

where we have used equations (4.95), (4.91) and the definitions given by equations (A.20a), (A.20b) and (B.1) of Appendix B.

Therefore, equation (A.24a) becomes:

$$-\Delta P_{2m}^{0} = (G_g^0 U_g^0 + G_f^0 U_f^0)_{\substack{out \\ r^*}} - (G_g^0 U_g^0 + G_f^0 U_f^0)_{\substack{in \\ r^*=1}} =$$

$$= \rho_f U_1^{0\,2} \left\{ (\gamma + \varepsilon^*)^2 \left[\frac{1}{\gamma \Delta\rho} \left(\rho_g - \frac{\rho_f}{S_{r^*}^2}\right) r^* (r^* - 1) + \frac{r^{*2}}{S_{r^*}^2} - \frac{1}{S_{r^*=1}^2} \right] \right\} =$$

$$= \rho_f U_1^{0\,2} R_{2m}^{0} \qquad (A.36)$$

For the non-slip case ($\gamma = 1$, $\varepsilon^* = 0$, $S = 1$ and $r^* = \rho_f/\rho_g$):

$$R_{2m}^{0} = r^* - 1$$

We evaluate the first two terms of equation (A.25) using equations (A.32) and (A.33):

$$\bar{y}_2 \left[\frac{d}{dz} (G_g^0 U_g^0 + G_f^0 U_f^0)\right]_{\substack{out \\ r^*}} - \bar{y}_1 \left[\frac{d}{dz} (G_g^0 U_g^0 + G_f^0 U_f^0)\right]_{\substack{in \\ r^*=1}} =$$

$$= \bar{y}_2 \left[q \frac{\rho_g}{\Delta\rho} U_g^0 \rho_f \left(2 - \frac{1}{r^*}\right) + q \frac{\rho_f U_g^0 \rho_g}{\Delta\rho} \frac{1}{S_{r^*}} \left(\frac{1}{S_{r^*}} \frac{\rho_f}{\rho_g} \frac{1}{r^*} - 2\right) \right]_{r^*} -$$

$$- \bar{y}_1 \left[q \frac{\rho_g}{\Delta\rho} U_g^0 \rho_f + q \frac{\rho_f U_g^0 \rho_g}{\Delta\rho} \frac{1}{S_{r^*=1}} \left(\frac{1}{S_{r^*=1}} \frac{\rho_f}{\rho_g} - 2\right) \right]_{r^*=1} =$$

$$= \bar{y}_2 \; q \; \rho_f \; U_{g_{in}}^0 \; r^* \; \frac{\rho_g}{\Delta\rho} \left[\left(2 - \frac{1}{r^*}\right) + \frac{1}{S_{r^*}} \left(\frac{1}{S_{r^*}} \frac{\rho_f}{\rho_g} \frac{1}{r^*} - 2\right) \right] -$$

$$- \bar{y}_1 \; q \; \rho_f \; U_{g_{in}}^0 \; \frac{\rho_g}{\Delta\rho} \left[1 + \frac{1}{S_{r^*=1}} \left(\frac{1}{S_{r^*=1}} \frac{\rho_f}{\rho_g} - 2\right) \right] =$$

$$= \rho_f \; {U_1^0}^2 \; \frac{q}{U_1^0} \left\{ \left[\frac{\rho_g}{\Delta\rho} \left(\gamma + \varepsilon^*\right) \left(2r^* - 1 - \frac{2r^*}{S_{r^*}} + \frac{1}{{S_{r^*}}^2} \frac{\rho_f}{\rho_g} \right) \right] \bar{y}_2 - \right.$$

$$\left. - \left[\frac{\rho_g}{\Delta\rho} \left(\gamma + \varepsilon^*\right) \left(1 - \frac{2}{S_{r^*=1}} + \frac{1}{{S_{r^*=1}}^2} \frac{\rho_f}{\rho_g} \right) \right] \bar{y}_1 \right\} =$$

$$= \rho_f \; {U_1^0}^2 \; \frac{q}{U_1^0} \left(A^*_{r^*} \; \bar{y}_2 - A^*_{r^*=1} \; \bar{y}_1 \right) \qquad \text{(A.37)}$$

where we define:

$$A^*_{r^*} = \frac{\rho_g}{\Delta\rho} \left(\gamma + \varepsilon^*\right) \left(2r^* - 1 - \frac{2r^*}{S_{r^*}} + \frac{1}{{S_{r^*}}^2} \frac{\rho_f}{\rho_g} \right) \qquad \text{(A.38)}$$

For the non-slip case ($S = 1$, $\gamma = 1$, $\varepsilon^* = 0$):

$$A^*_{r^*} = A^*_{r^*=1} = 1 \qquad \text{for any } r^*$$

We evaluate the third and fourth terms of equation (A.25):

$$G_g^0 \; \bar{U}_g + G_f^0 \; \bar{U}_f = \rho_g \; \alpha^0 \; U_g^0 \; \bar{U}_g + \rho_f \left(1 - \alpha^0\right) U_f^0 \; \bar{U}_f =$$

$$= \rho_g \; \frac{\rho_f}{\gamma \; \Delta\rho} \left(1 - \frac{1}{r^*}\right) U_g^0 \; \gamma \; \bar{J}_{in} + \rho_f \left[1 - \frac{\rho_f}{\gamma \; \Delta\rho} \left(1 - \frac{1}{r^*}\right) \right] \frac{1}{S_{r^*}} \; U_g^0 \; \Gamma_{r^*} \; \bar{J}_{in} =$$

$$= \rho_f \; U_{g_{in}}^0 \; r^* \; \bar{J}_{in} \left\{ \frac{\rho_g}{\Delta\rho} \left(1 - \frac{1}{r^*}\right) + \frac{\Gamma_{r^*}}{S_{r^*}} \left[1 - \frac{\rho_f}{\gamma \; \Delta\rho} \left(1 - \frac{1}{r^*}\right) \right] \right\} =$$

$$= \rho_f \; U_1^0 \; \left(\gamma + \varepsilon^*\right) \bar{J}_{in} \left\{ \frac{\rho_g}{\Delta\rho} \left(r^* - 1\right) + \frac{\Gamma_{r^*}}{S_{r^*}} \left[r^* - \frac{\rho_f}{\gamma \; \Delta\rho} \left(r^* - 1\right) \right] \right\}$$

Therefore:

$$(G_g^0\,\overline{U}_g + G_f^0\,\overline{U}_f)_{\substack{out\\ r^*}} - (G_g^0\,\overline{U}_g + G_f^0\,\overline{U}_f)_{\substack{in\\ r^*=1}} =$$

$$= \rho_f\,U_1^{0\,2}\,\frac{\overline{J}_{in}}{U_1^0}\left\{(\gamma+\varepsilon^*)\left[\frac{\rho_g}{\Delta\rho}\,(r^*-1) + \frac{\Gamma_{r^*}}{S_{r^*}}\left[r^* - \frac{\rho_f}{\gamma\,\Delta\rho}\,(r^*-1)\right] - \frac{\Gamma_{r^*=1}}{S_{r^*=1}}\right]\right\} =$$

$$= \rho_f\,U_1^{0\,2}\,\frac{\overline{J}_{in}}{U_1^0}\,E^* \qquad (A.39)$$

where we have used equations (B.2), (B.3), (B.6) and (B.7) of Appendix B.

For the non-slip case ($S = 1$, $\Gamma = 1$, $\gamma = 1$, $\varepsilon^* = 0$, $r^* = \rho_f/\rho_g$):

$$E^* = 0$$

Similarly, we find:

$$\overline{G}_g U_g^0 + \overline{G}_f U_f^0 = \rho_g\,(\alpha^0\overline{U}_g + \overline{\alpha}\,U_g^0)\,U_g^0 + \rho_f\left[(1-\alpha^0)\,\overline{U}_f - \overline{\alpha}\,U_f^0\right]U_f^0 =$$

$$= U_g^0\left[\rho_g\,\alpha^0\,\overline{U}_g + \rho_f\,\frac{1}{S_{r^*}}\,(1-\alpha^0)\,\overline{U}_f + \rho_g\,\overline{\alpha}\,U_g^0 - \rho_f\,\frac{1}{S_{r^*}}\,\overline{\alpha}\,U_f^0\right] =$$

$$= U_{g_{in}}^0\,r^*\left[\rho_g\,\alpha^0\gamma\,\overline{J}_{in} + \rho_f\,(1-\alpha^0)\,\frac{\Gamma_{r^*}}{S_{r^*}}\,\overline{J}_{in} + \rho_g\,\overline{\alpha}\,U_g^0\,\left(1 - \frac{\rho_f}{\rho_g}\,\frac{1}{S_{r^*}^2}\right)\right] =$$

$$= U_1^0\,(\gamma+\varepsilon^*)\,r^*\left\{\frac{\rho_g\rho_f}{\Delta\rho}\,\left(1-\frac{1}{r^*}\right)\overline{J}_{in} + \rho_f\left[1 - \frac{\rho_f}{\gamma\,\Delta\rho}\,\left(1-\frac{1}{r^*}\right)\right]\frac{\Gamma_{r^*}}{S_{r^*}}\,\overline{J}_{in} -\right.$$

$$\left. - \rho_g\,\left(1 - \frac{\rho_f}{\rho_g}\,\frac{1}{S_{r^*}^2}\right)\left(q\,\frac{\rho_f}{\Delta\rho}\,\overline{y}_1\,e^{-s\tau_2} + \frac{\rho_f}{\Delta\rho}\,\overline{J}_{in}\,\frac{(1/r^*) - e^{-s\tau_2}}{(s/\gamma q) - 1}\right)\right\} =$$

$$= \rho_f\,U_1^0\,(\gamma+\varepsilon^*)\left\{\frac{\rho_g}{\Delta\rho}\,(r^*-1)\,\overline{J}_{in} + \left[r^* - \frac{\rho_f}{\gamma\,\Delta\rho}\,(r^*-1)\right]\frac{\Gamma_{r^*}}{S_{r^*}}\,\overline{J}_{in} -\right.$$

$$\left. - \frac{\rho_g}{\Delta\rho}\,\left(1 - \frac{\rho_f}{\rho_g}\,\frac{1}{S_{r^*}^2}\right)\left(q\,r^*\,\overline{y}_1\,e^{-s\tau_2} + \overline{J}_{in}\,\gamma\,q\,\frac{1 - r^*\,e^{-s\tau_2}}{s - \gamma q}\right)\right\} =$$

$$= \rho_f U_1^0 (\gamma + \varepsilon^*) \left\{ \left\{ \frac{\rho_g}{\Delta\rho} (r^* - 1) + \left[r^* - \frac{\rho_f}{\gamma \Delta\rho} (r^* - 1) \right] \frac{\Gamma_{r^*}}{S_{r^*}} - \right.\right.$$

$$\left.\left. - \left(\frac{\rho_g}{\Delta\rho} - \frac{\rho_f}{\Delta\rho} \frac{1}{S_{r^*}^2} \right) \gamma q \frac{r^* e^{-s\tau_2} - 1}{\gamma q - s} \right\} \bar{J}_{in} - \left(\frac{\rho_g}{\Delta\rho} - \frac{\rho_f}{\Delta\rho} \frac{1}{S_{r^*}^2} \right) q\, r^*\, e^{-s\tau_2}\, \bar{y}_1 \right\}$$

where we have used equations (4.103), (B.2), (B.3), (B.6) and (B.7).

Therefore:

$$(\bar{G}_g U_g^0 + \bar{G}_f U_f^0)_{\substack{out \\ r^*}} - (\bar{G}_g U_g^0 + \bar{G}_f U_f^0)_{\substack{in \\ r^*=1}} =$$

$$= \rho_f U_1^{0\,2} \frac{(\gamma + \varepsilon^*)}{U_1^0} \left\{ \left\{ \frac{\rho_g}{\Delta\rho} (r^* - 1) + \left[r^* - \frac{\rho_f}{\gamma \Delta\rho} (r^* - 1) \right] \frac{\Gamma_{r^*}}{S_{r^*}} - \frac{\Gamma_{r^*=1}}{S_{r^*=1}} - \right.\right.$$

$$\left. - \left(\frac{\rho_g}{\Delta\rho} - \frac{\rho_f}{\Delta\rho} \frac{1}{S_{r^*}^2} \right) \gamma q \frac{r^* e^{-s\tau_2} - 1}{(\gamma q - s)} \right\} \bar{J}_{in} -$$

$$\left. - \left[\left(\frac{\rho_g}{\Delta\rho} - \frac{\rho_f}{\Delta\rho} \frac{1}{S_{r^*}^2} \right) q\, r^*\, e^{-s\tau_2} - \left(\frac{\rho_g}{\Delta\rho} - \frac{\rho_f}{\Delta\rho} \frac{1}{S_{r^*=1}} \right) q \right] \bar{y}_1 \right\} \qquad (A.40)$$

Therefore, equation (A.25) is evaluated by adding together equations (A.34), (A.37), (A.39) and (A.40) and noting from equation (A.36) the relation:

$$\rho_f U_1^{0\,2} = \frac{(-\Delta P_{2m}^0)}{R_{2m}^0} \qquad (A.41)$$

For the non-slip case ($S = 1$, $\Gamma = 1$, $\gamma = 1$, $\varepsilon^* = 0$, $r^* = \rho_f/\rho_g$), the addition of equations (A.34) and (A.40) yields:

$$\frac{1}{\rho_f U_1^0} \left[s \int_o^z \bar{G}\, dz + (\bar{G}_g U_g^0 + \bar{G}_f U_f^0)_{out} - (\bar{G}_g U_g^0 + \bar{G}_f U_f^0)_{in} \right] =$$

$$= q\, s \frac{r^* e^{-s\tau_2} - 1}{(q-s)^2} - \frac{s^2}{(q-s)} \frac{\ln r^*}{q} + \left[1 + 0 - 1 + q \frac{r^* e^{-s\tau_2} - 1}{(q-s)} \right] \bar{J}_{in} +$$

$$+ \left[q\ s\ \frac{r^*\ e^{-s\tau_2} - 1}{(q - s)} + q\ r^*\ e^{-s\tau_2} - q \right] \bar{y}_1 =$$

$$= \frac{1}{(1 - \frac{s}{q})} \left[(r^* e^{-s\tau_2} - 1)\ \frac{s}{(q-s)} + (r^* e^{-s\tau_2} - 1) \right] \bar{J}_{in} + \frac{(q-s-q)}{(q-s)} \frac{s\ ln\ r^*}{q} \bar{J}_{in} +$$

$$+ \left[q\ (r^*\ e^{-s\tau_2} - 1)\ (\frac{s}{q - s} + 1) \right] \bar{y}_1 =$$

$$= \frac{1}{(1 - \frac{s}{q})} \frac{r^*\ e^{-s\tau_2} - 1}{(1 - \frac{s}{q})} \bar{J}_{in} + \left[s\ \tau_2 + ln\ r^* - \frac{1}{(1 - \frac{s}{q})}\ ln\ r^* \right] \bar{J}_{in} +$$

$$+ \frac{1}{(1 - \frac{s}{q})} q\ (r^*\ e^{-s\tau_2} - 1)\ \bar{y}_1 \qquad \text{(A.42)}$$

(c) Frictional Component

According to assumption (xiii) of section 4.2, the two-phase flow frictional pressure drop gradient is given by:

$$- \frac{\partial P_{2f}}{\partial z} = X \frac{f_f}{2d} \frac{G^2}{\rho_f} = (1 + B\ x)\ \lambda_f \frac{G^2}{\rho_f} \qquad \text{(A.43)}$$

where λ_f is given by equation (A.7) for the liquid single-phase.

The value of B is determined in such a way that the gradient has the correct value for the vapour single-phase (quality $x = 1$).

Therefore, it can be easily found that:

$$B = \frac{\rho_f}{\rho_g} (\frac{\mu_g}{\mu_f})^{\beta} - 1 \qquad \text{(A.44)}$$

Therefore:
$$X = 1 + \left[\frac{\rho_f}{\rho_g} (\frac{\mu_g}{\mu_f})^{\beta} - 1 \right] x \qquad \text{(A.45)}$$

where $\beta_s = 0.25$ for straight parts and $\beta_c = 0.20$ for coiled parts.

For the homogeneous model assumption (no slip):

$$-\frac{\partial P_{2f}}{\partial z} = \lambda_f \rho_2 U_2^2 = \lambda_f G U_2 = \lambda_f G \left[U_f + (U_g - U_f) x\right] =$$

$$= \lambda_f \frac{G^2}{\rho_f}\left[1 + (\frac{\rho_f}{\rho_g} - 1) x\right] = \lambda_f \frac{G^2}{\rho_f}(1 + \frac{\Delta\rho}{\rho_g} x) \qquad (A.46)$$

From equations (A.43) and (A.46), we have for the non-slip case:

$$B = \frac{\Delta\rho}{\rho_g}$$

In other words, the exponent β in equation (A.44) is taken as zero.

For the steady-state, we find according to equations (4.91), (4.110), (4.76) and (4.83) and noting that $G^0 = \rho_f U_1^0$:

$$-\Delta P_{2f}^0 = \lambda_f^0 \frac{G^{0^2}}{\rho_f}\int_o^z X^0\, dz = \lambda_f^0 \rho_f U_1^{0^2}\int_o^z (1 + B x^0)\, dz =$$

$$= \lambda_f^0 \rho_f U_1^{0^2} U_{g_{in}}^0 \int_o^{\tau_2}\left[1 + B\frac{\rho_g \rho_f U_{g_{in}}^0}{\rho_f U_1^0 \gamma \Delta\rho}(e^{\gamma q \tau_2} - 1)\right] e^{\gamma q \tau_2} d\tau_2 =$$

$$= \lambda_f^0 \rho_f U_1^{0^2} U_1^0 (\gamma+\varepsilon^*)\int_o^{\tau_2}\left[1 + B\frac{\rho_g}{\Delta\rho}(\frac{\gamma+\varepsilon^*}{\gamma})(e^{\gamma q \tau_2} - 1)\right] e^{\gamma q \tau_2} d\tau_2 =$$

$$= \lambda_f^0 \rho_f U_1^{0^3} (\gamma+\varepsilon^*)\left[\frac{e^{\gamma q \tau_2} - 1}{\gamma q} + B\frac{\rho_g}{\Delta\rho}(\frac{\gamma+\varepsilon^*}{\gamma})(\frac{e^{2\gamma q \tau_2} - 1}{2\gamma q} - \frac{e^{\gamma q \tau_2} - 1}{\gamma q})\right] =$$

$$= \frac{\lambda_f^0 \rho_f U_1^{0^3}}{q}\left\{(\gamma+\varepsilon^*)\left\{B\frac{\rho_g}{\Delta\rho}(\frac{\gamma+\varepsilon^*}{\gamma})\frac{r^{*2}-1}{2\gamma} + \left[1 - B\frac{\rho_g}{\Delta\rho}(\frac{\gamma+\varepsilon^*}{\gamma})\right]\frac{r^*-1}{\gamma}\right\}\right\} =$$

$$= \lambda_f^0 \rho_f U_1^{0^3}\frac{R_{2f}^0}{q} \qquad (A.48)$$

For the non-slip case ($\gamma = 1$, $\varepsilon^* = 0$, $B = \Delta\rho/\rho_g$):

$$-\Delta P_{2f}^0 = \lambda_f^0 \rho_f U_1^{0^3}\frac{r^{*2} - 1}{2q}$$

For the perturbed state, we have:

$$\delta\ (-\Delta P_{2f}) = \int_{y_1+\delta y_1}^{y_2+\delta y_2} (-\frac{\partial P_{2f}}{\partial z})\ dz - \int_{y_1}^{y_2} (-\frac{\partial P_{2f}^{0}}{\partial z})\ dz$$

We consider equation (A.43) and take the Laplace transform:

$$-\overline{\Delta P}_{2f} = \frac{\lambda_f^0\ G^{0^2}}{\rho_f} (X^0_{out}\ \overline{y}_2 - X^0_{in}\ \overline{y}_1) +$$

$$+ \frac{1}{\rho_f} \int_o^z (\overline{X}\ \lambda_f^0\ G^{0^2} + X^0\ \overline{\lambda}_f\ G^{0^2} + 2\ X^0\ \lambda_f^0\ G^0\ \overline{G})\ dz \qquad (A.49)$$

We express $\overline{\lambda}_f$ in terms of $\overline{G}$ using equation (4.58) and we note from equation (A.45) that $X^0_{out} = 1 + B$ (quality $x = 1$) and $X^0_{in} = 1$ (quality $x = 0$).

$$-\overline{\Delta P}_{2f} = \frac{\lambda_f^0\ G^{0^2}}{\rho_f} \left((1 + B)\ \overline{y}_2 - \overline{y}_1\right) + \frac{\lambda_f^0\ G^{0^2}}{\rho_f} \int_o^z \overline{X}\ dz +$$

$$+ (2 - \beta)\ \frac{\lambda_f^0\ G^0}{\rho_f} \int_o^z X^0\ \overline{G}\ dz \qquad (A.50)$$

We evaluate the first term of equation (A.50) noting that $G^0 = \rho_f\ U_1^0$ and using equation (A.44):

$$-_1\overline{\Delta P}_{2f} = \lambda_f^0\ \frac{G^{0^2}}{\rho_f} \left(\frac{\rho_f}{\rho_g} (\frac{\mu_g}{\mu_f})^{\beta}\ \overline{y}_2 - \overline{y}_1\right) = \lambda_g^0\ \rho_g\ U_g^{0^2}\ \overline{y}_2 - \lambda_f^0\ \rho_f\ U_f^{0^2}\ \overline{y}_1 \qquad (A.51)$$

For the non-slip case ($B = \Delta\rho/\rho_g$ according to equation (A.47)):

$$-_1\overline{\Delta P}_{2f} = \lambda_f^0\ \frac{G^{0^2}}{\rho_f} (\frac{\rho_f}{\rho_g}\ \overline{y}_2 - \overline{y}_1) = \lambda_f^0\ \rho_g\ U_g^{0^2}\ \overline{y}_2 - \lambda_f^0\ \rho_f\ U_f^{0^2}\ \overline{y}_1$$

We evaluate the third term of equation (A.50). We substitute

for X^0 and $\overline{G}$ from equations (A.45), (4.110) and (4.108):

$$-_3\overline{\Delta P}_{2f} = (2-\beta)\,\frac{\lambda_f^0\,\rho_f\,U_1^0}{\rho_f}\int_o^z (1+B\,x^0)\,\overline{G}\,U_{g_{in}}^0\,e^{\gamma q\tau_2}\,d\tau_2 =$$

$$= (2-\beta)\,\lambda_f^0\,U_1^0\,U_{g_{in}}^0\int_o^z \left\{\left[1+B\,\frac{\rho_g\,\rho_f\,U_{g_{in}}^0}{\rho_f\,U_1^0\,\gamma\,\Delta\rho}\,(e^{\gamma q\tau_2}-1)\right]\rho_f\cdot\right.$$

$$\left.\cdot\left[\overline{J}_{in}\,\frac{s}{s-\gamma q}-\frac{\gamma q}{s-\gamma q}\,\overline{J}_{in}\,e^{(\gamma q-s)\tau_2}+q\,\overline{y}_1\,e^{(\gamma q-s)\tau_2}\right]\right\}d\tau_2 =$$

$$= (2-\beta)\,\lambda_f^0\,\rho_f\,U_1^{0^2}\,(\gamma+\varepsilon^*)\int_o^z \left\{\left[1+B\,\frac{\rho_g}{\Delta\rho}\,(\frac{\gamma+\varepsilon^*}{\gamma})\,(e^{\gamma q\tau_2}-1)\right]\cdot\right.$$

$$\left.\cdot\left[\overline{J}_{in}\,\frac{-s}{\gamma q-s}+\frac{\gamma q}{\gamma q-s}\,\overline{J}_{in}\,e^{(\gamma q-s)\tau_2}+q\,\overline{y}_1\,e^{(\gamma q-s)\tau_2}\right]\right\}d\tau_2 =$$

$$= (2-\beta)\,\lambda_f^0\,\rho_f\,U_1^{0^2}\,(\gamma+\varepsilon^*)\left\{(1-B\,\frac{\rho_g}{\Delta\rho}\,\frac{\gamma+\varepsilon^*}{\gamma})\cdot\right.$$

$$\cdot\left[\overline{J}_{in}\,\frac{-s\tau_2}{\gamma q-s}+\frac{\gamma q}{(\gamma q-s)^2}\,(e^{(\gamma q-s)\tau_2}-1)\,\overline{J}_{in}+\right.$$

$$\left.+\frac{q}{\gamma q-s}\,\overline{y}_1\,(e^{(\gamma q-s)\tau_2}-1)\right]+B\,\frac{\rho_g}{\Delta\rho}\,\frac{\gamma+\varepsilon^*}{\gamma}\cdot$$

$$\cdot\left[\overline{J}_{in}\,\frac{-s}{\gamma q-s}\,\frac{e^{\gamma q\tau_2}-1}{\gamma q}+\frac{\gamma q}{\gamma q-s}\,\overline{J}_{in}\,\frac{e^{(2\gamma q-s)\tau_2}-1}{2\gamma q-s}+\right.$$

$$\left.\left.+\,q\,\overline{y}_1\,\frac{e^{(2\gamma q-s)\tau_2}-1}{2\gamma q-s}\right]\right\} \qquad (A.52)$$

For the non-slip case ($\gamma = 1$, $\varepsilon^* = 0$) for $\beta = 0$, i.e. $\overline{\lambda}_f = 0$ and $B = \Delta\rho/\rho_g$ according to equation (A.47), equation (A.52) becomes:

$$-_3\overline{\Delta P}_{2f} = 2\lambda_f^0\,\rho_f\,U_1^{0^2}\left[\overline{J}_{in}\,\frac{-s}{(q-s)}\,\frac{r^*-1}{q}+\right.$$

$$\left.+\,\frac{q}{(q-s)}\,\overline{J}_{in}\,\frac{r^{*2}\,e^{-s\tau_2}-1}{(2q-s)}+q\,\overline{y}_1\,\frac{r^{*2}\,e^{-s\tau_2}-1}{(2q-s)}\right] \qquad (A.52a)$$

We evaluate the second term of equation (A.50). According to equation (A.45), we obtain:

$$\overline{X} = B\,\overline{x} \tag{A.53}$$

By substituting for $\overline{x}$ from equation (4.112), we have:

$$-_2\overline{\Delta P}_{2f} = \lambda_f^0 \frac{G0^2}{\rho_f} \int_o^z B\,\overline{x}\,dz = \lambda_f^0 \frac{G0^2}{\rho_f} B\,U_{g_{in}}^0 \int_o^{\tau_2} \overline{x}\, e^{\gamma q \tau_2}\, d\tau_2 =$$

$$= \lambda_f^0 \frac{G0^2}{\rho_f} B\,U_1^0\,(\gamma+\varepsilon^*)\,\frac{\rho_g \rho_f}{G0^2}\,\frac{\rho_f U_1^0}{\Delta\rho} \int_o^{\tau_2} \left\{ \overline{J}_{in}\,(e^{\gamma q \tau_2} - 1) - q\,\overline{y}_1\, e^{(\gamma q - s)\tau_2} - \right.$$

$$- \gamma q\,\overline{J}_{in}\,\frac{e^{(\gamma q - s)\tau_2} - 1}{(\gamma q - s)} - \left(\frac{\gamma+\varepsilon^*}{\gamma}\right) \left[\left(\frac{\gamma q}{\gamma q - s}\,\overline{J}_{in} + q\,\overline{y}_1\right)\left(e^{(2\gamma q - s)\tau_2} - e^{(\gamma q - s)\tau_2}\right) - \right.$$

$$\left. \left. - \overline{J}_{in}\,\frac{s}{\gamma q - s}\,(e^{\gamma q \tau_2} - 1) \right] \right\} d\tau_2 =$$

$$= \lambda_f^0\,\rho_f\,U_1^{0^2}\,(\gamma+\varepsilon^*)\,B\,\frac{\rho_g}{\Delta\rho} \left\{ \overline{J}_{in}\left(\frac{e^{\gamma q \tau_2} - 1}{\gamma q} - \tau_2\right) - q\,\overline{y}_1\,\frac{e^{(\gamma q - s)\tau_2} - 1}{\gamma q - s} - \right.$$

$$- \gamma q\,\overline{J}_{in} \left[\frac{e^{(\gamma q - s)\tau_2} - 1}{(\gamma q - s)^2} - \frac{\tau_2}{\gamma q - s} \right] - \left(\frac{\gamma + \varepsilon^*}{\gamma}\right) \left[\left(\frac{\gamma q}{\gamma q - s}\,\overline{J}_{in} + q\,\overline{y}_1\right) \cdot \right.$$

$$\left. \left. \cdot \left(\frac{e^{(2\gamma q - s)\tau_2} - 1}{2\gamma q - s} - \frac{e^{(\gamma q - s)\tau_2} - 1}{\gamma q - s}\right) - \overline{J}_{in}\,\frac{s}{\gamma q - s}\left(\frac{e^{\gamma q \tau_2} - 1}{\gamma q} - \tau_2\right) \right] \right\} =$$

$$= \lambda_f^0\,\rho_f\,U_1^{0^2}\,(\gamma + \varepsilon^*)\,B\,\frac{\rho_g}{\Delta\rho} \left\{ \overline{J}_{in}\left(1 + \frac{\gamma + \varepsilon^*}{\gamma}\,\frac{s}{\gamma q - s}\right)\left(\frac{r^* - 1}{\gamma q} - \tau_2\right) - \right.$$

$$- q\,\overline{y}_1\left(1 - \frac{\gamma + \varepsilon^*}{\gamma}\right)\frac{r^*\, e^{-s\tau_2} - 1}{\gamma q - s} - \gamma q\,\overline{J}_{in}\left(1 - \frac{\gamma + \varepsilon^*}{\gamma}\right)\frac{r^*\, e^{-s\tau_2} - 1}{(\gamma q - s)^2} +$$

$$\left. + \gamma q\,\overline{J}_{in}\,\frac{\tau_2}{\gamma q - s} - \left(\frac{\gamma+\varepsilon^*}{\gamma}\right) \left[\frac{\gamma q}{\gamma q - s}\,\overline{J}_{in}\left(\frac{r^{*2} e^{-s\tau_2} - 1}{2\gamma q - s}\right) + q\,\overline{y}_1\left(\frac{r^{*2} e^{-s\tau_2} - 1}{2\gamma q - s}\right) \right] \right\} \tag{A.54}$$

For the non-slip case ($\gamma = 1$, $\varepsilon^* = 0$, $B = \Delta\rho/\rho_g$), equation (A.54) becomes:

$$-{}_2\overline{\Delta P}_{2f} = \lambda_f{}^0\ \rho_f\ U_1{}^{0\,2}\left[\overline{J}_{in}\frac{q}{(q-s)}\left(\frac{r^*-1}{q}-\tau_2\right)+q\,\overline{J}_{in}\frac{\tau_2}{(q-s)}-\right.$$

$$\left.-\frac{q}{(q-s)}\,\overline{J}_{in}\left(\frac{r^{*2}\,e^{-s\tau_2}-1}{2q-s}\right)-q\,\overline{y}_1\,\frac{r^{*2}\,e^{-s\tau_2}-1}{2q-s}\right]=$$

$$=\lambda_f{}^0\ \rho_f\ U_1{}^{0\,2}\left[\overline{J}_{in}\frac{r^*-1}{(q-s)}-\frac{q}{(q-s)}\,\overline{J}_{in}\left(\frac{r^{*2}e^{-s\tau_2}-1}{2q-s}\right)-q\,\overline{y}_1\left(\frac{r^{*2}e^{-s\tau_2}-1}{2q-s}\right)\right] \qquad \text{(A.54a)}$$

Therefore, equation (A.49) is evaluated by adding together equations (A.51), (A.52) and (A.54) and noting from equation (A.48) the relation:

$$\lambda_f{}^0\ \rho_f\ U_1{}^{0\,2} = \frac{(-\Delta P_{2f}{}^0)}{R_{2f}{}^0\ (U_1{}^0/q)} \qquad \text{(A.55)}$$

For the non-slip case ($\gamma = 1$, $\varepsilon^* = 0$ and $B = \Delta\rho/\rho_g$), the addition of equations (A.52a) and (A.54a) yields:

$$\frac{-{}_3\overline{\Delta P}_{2f}+(-{}_2\overline{\Delta P}_{2f})}{\lambda_f{}^0\ \rho_f\ U_1{}^{0\,2}}=\frac{q}{(q-s)}\,\overline{J}_{in}\left(\frac{r^{*2}e^{-s\tau_2}-1}{2q-s}\right)+q\,\overline{y}_1\left(\frac{r^{*2}e^{-s\tau_2}-1}{2q-s}\right)+$$

$$+\,\overline{J}_{in}\left[\frac{r^*-1}{(q-s)}-\frac{2s}{q}\,\frac{r^*-1}{(q-s)}\right]=$$

$$=\frac{\overline{J}_{in}}{q(1-\frac{s}{q})}\left(\frac{r^*\,e^{-s\tau_2}-1}{2-\frac{s}{q}}\right)+\overline{y}_1\left(\frac{r^*\,e^{-s\tau_2}-1}{2-\frac{s}{q}}\right)-\overline{J}_{in}\,\frac{r^*-1}{q(1-\frac{s}{q})}+2\overline{J}_{in}\,\frac{r^*-1}{q}$$

3. SUPERHEAT REGION (index 3)

(a) Gravitational Component

$$\delta(-\Delta P_{3g}) = \int_{y_2+\delta y_2}^{y_3}\rho_g\ g\ \sin\theta\ dz-\int_{y_2}^{y_3}\rho_g\ g\ \sin\theta\ dz=\int_{\delta y_2}^{o}\rho_g\ g\ \sin\theta\ dz$$

Therefore:
$$-\overline{\Delta P}_{3g} = -\rho_g\ g\ \overline{y}_2\ \sin\theta \qquad \text{(A.56)}$$

(b) Momentum Component

Since $(\partial/\partial z)\ U_3 = 0$, there is only contribution from the temporal component:

$$\delta\ (-\Delta P_{3m}) = \int_{y_2+\delta y_2}^{y_3} \rho_g \frac{\partial}{\partial t}\ (\delta U_3)\ dz = \int_{y_2}^{y_3} \rho_g \frac{\partial}{\partial t}\ (\delta U_3)\ dz$$

Therefore:

$$-\overline{\Delta P}_{3m} = \int_{y_2}^{y_3} \rho_g\ s\ \overline{U}_3\ dz = \rho_g\ s\ \overline{U}_3\ (y_3 - y_2) =$$

$$= \rho_f\ U_1^0\ s\ \overline{U}_3\ \frac{(y_3 - y_2)}{U_3^0} = \rho_f\ (U_1^0)^2\ s\ \tau_3\ \frac{\overline{U}_3}{U_1^0} \qquad \text{(A.57)}$$

where $\tau_3 = (y_3 - y_2)/U_3^0$ is the transit time of the fluid in the superheat region and $\rho_f\ U_1^0 = \rho_g\ U_3^0$ because of continuity.

(c) Frictional Component

$$\delta(-\Delta P_{3f}) = \int_{y_2+\delta y_2}^{y_3} (\lambda_g^0 + \delta\lambda_g)\ \rho_g\ (U_3^0 + \delta U_3^0)^2\ dz - \int_{y_2}^{y_3} \lambda_g^0\ \rho_g\ (U_3^0)^2\ dz =$$

$$= \int_{\delta y_2}^{o} \lambda_g^0\ \rho_g\ (U_3^0)^2\ dz + \int_{y_2}^{y_3} \left[2\lambda_g^0\ \rho_g\ U_3^0\ \delta U_3 + \delta\lambda_g\ \rho_g\ (U_3^0)^2\right] dz$$

or, according to equations (4.57) and (4.58), therefore:

$$-\overline{\Delta P}_{3f} = -\lambda_g\ \rho_g\ (U_3^0)^2\ \overline{y}_2 + (2 - \beta)\ \lambda_g^0\ \rho_f\ U_1^0\ \overline{U}_3\ (y_3 - y_2)$$

In the steady-state:

$$-\Delta P_{3f}^0 = \int_{y_2}^{y_3} \lambda_g^0\ \rho_g\ (U_3^0)^2\ dz = \lambda_g^0\ \rho_g\ (U_3^0)^2\ (y_3 - y_2) =$$

$$= \lambda_g{}^0 \rho_f (U_1{}^0)^2 \frac{\rho_f}{\rho_g} (y_3 - y_2) \qquad (A.58)$$

Therefore:

$$-\overline{\Delta P}_{3f} = \frac{\rho_g}{\rho_f} (2 - \beta) (-\Delta P_{3f}{}^0) \frac{\overline{U}_3}{U_1{}^0} - \lambda_g \rho_g (U_3{}^0)^2 \overline{y}_2 \qquad (A.59)$$

The parameter: $$\lambda_g = f_g \frac{1}{2d} \qquad (A.60)$$

The contribution of the downstream adiabatic length (straight) on the pressure drop perturbation components can be taken into account in a similar analysis as that of the contribution of the upstream adiabatic length on the subcooled region.

The downstream adiabatic length is a straight circular channel with inner diameter d_d and length y_d. Normalisation will be used with respect to the values in the superheat region. It must be mentioned that the diameter of the heated part of the channel is constant, i.e. $d_3 = d_1$.

$$\frac{\overline{U}_3}{\overline{U}_d} = \frac{U_3{}^0}{U_d{}^0} = \frac{A_d}{A_1} = \left(\frac{d_d}{d_1}\right)^2 = \sigma_d \qquad (A.61)$$

and the transit time through the downstream adiabatic length is:

$$\tau_d = \frac{y_d}{U_d{}^0} = \frac{y_d}{U_3{}^0} \sigma_d \qquad \left(= \frac{y_d}{(\rho_f/\rho_g) U_1{}^0} \sigma_d\right) \qquad (A.62)$$

There will not be any contribution on the gravitational component described by equation (A.56).

The momentum component of equation (A.57) will become in that case:

$$-\overline{\Delta p}_{mT} = \rho_g\, s \left[\overline{U}_3\,(y_3 - y_2) + \overline{U}_d\, y_d\right] = \rho_g\, s \left[\overline{U}_3\,(y_3 - y_2) + \frac{\overline{U}_3}{\sigma_d}\, y_d\right] =$$

$$= \rho_g\, s\, \overline{U}_3 \left[(y_3 - y_2) + \frac{y_d}{\sigma_d}\right] = \rho_g\, s\, \overline{U}_3\, U_3^0\, \left(\frac{y_3 - y_2}{U_3^0} + \frac{y_d}{U_3^0}\,\frac{1}{\sigma_d}\right) =$$

$$= \rho_g\, s\, \overline{U}_3\, U_3^0\, \left(\tau_3 + \frac{\tau_d}{\sigma_d^2}\right) = \rho_f\, (U_1^0)^2\, s\, \left(\tau_3 + \frac{\tau_d}{\sigma_d^2}\right) \frac{\overline{U}_3}{U_1^0} \qquad \text{(A.63)}$$

The effect of the downstream adiabatic length on the frictional component of equation (A.59) will be only in the first term, which will become as follows:

$$-\overline{\Delta p}_{fT} = (2 - \beta_c)\, \lambda_c^0\, \rho_g\, U_3^0\, \overline{U}_3\, (y_3 - y_2) +$$

$$+ (2 - \beta_s)\, \lambda_s^0\, \rho_g\, U_d^0\, \overline{U}_d\, y_d + 2\eta_d\, \rho_g\, U_d^0\, \overline{U}_d =$$

$$= (2 - \beta_c)\, \lambda_c^0\, \rho_g\, U_3^0\, \overline{U}_3\, (y_3 - y_2) +$$

$$+ \left[(2 - \beta_s)\, \lambda_s^0\, y_d + 2\eta_d\right] \rho_g\, U_d^0\, \overline{U}_d =$$

$$= \left\{(2 - \beta_c)\, \lambda_c^0\, (y_3 - y_2) + \left[\frac{(2 - \beta_s)\, \lambda_s^0\, y_d + 2\eta_d}{\sigma_d^2}\right]\right\} \rho_f\, (U_1^0)^2\, \frac{\overline{U}_3}{U_1^0} \qquad \text{(A.64)}$$

In the steady-state:

$$-\Delta P_{fT}^0 = \lambda_c^0\, \rho_g\, (U_3^0)^2\, (y_3 - y_2) + \lambda_s^0\, \rho_g\, (U_d^0)^2\, y_d + \eta_d\, \rho_g\, (U_d^0)^2 =$$

$$= \left[\lambda_c^0\, (y_3 - y_2) + \frac{\lambda_s^0\, y_d + \eta_d}{\sigma_d^2}\right] \rho_g\, (U_3^0)^2 =$$

$$= \left[\lambda_c^0\, (y_3 - y_2) + \frac{\lambda_s^0\, y_d + \eta_d}{\sigma_d^2}\right] \frac{\rho_f}{\rho_g}\, \rho_f\, (U_1^0)^2 \qquad \text{(A.65)}$$

Therefore, equation (A.64) becomes:

$$-\overline{\Delta P}_{fT} = \left\{ 2 \frac{\rho_g}{\rho_f} (-\Delta P_{fT}{}^0) - \left[\beta_c \lambda_c{}^0 (y_3 - y_2) + \frac{\beta_s \lambda_s{}^0 y_d}{\sigma_d{}^2} \right] \rho_f (U_1{}^0)^2 \right\} \frac{\overline{U}_3}{U_1{}^0} \quad \text{(A.66)}$$

It must be noticed that the gravity and friction terms in the short length of the channel over which the boiling and superheat boundary move, cancel out in adjacent regions and are therefore omitted when the overall pressure drop perturbation needs to be calculated (the term of equation (A.2), the first term of equation (A.6), the first two terms of equation (A.23), the terms of equation (A.51), the term of equation (A.56), and the second term of equation (A.59), where the assumption has been made that the departure of the value of void fraction from unity at the exit (x = 1) is very small, so that the first term of equation (A.23) can be evaluated as $g \sin \theta \rho_g \overline{y}_2$ for $\alpha_{out} \simeq 1$).

APPENDIX B

EXPRESSIONS FOR THE SLIP RATIO AND PHASE VELOCITIES PERTURBATIONS

Dividing equation (4.85) by equation (4.81), we obtain the expression for the reciprocal of slip ratio, i.e.

$$\frac{1}{S} = \frac{U_f^0}{U_g^0} = \frac{(J_{in}^0 + q\ z)\ (1 - \alpha^0\ \gamma) - \alpha^0\ V_j}{(1 - \alpha^0)\ (\gamma\ J_{in}^0 + V_j + \gamma\ q\ z)} \qquad (B.1)$$

However, a more appropriate form of equation (B.1), to be used in the context of the present analysis, can be obtained starting from equation (4.71), i.e.

$$(1 - \alpha^0)\ U_f^0 = J - \alpha^0\ U_g^0$$

or, according to equation (4.79):

$$(1 - \alpha^0)\ U_f^0 = \frac{U_g^0 - V_j}{\gamma} - \alpha^0\ U_g^0$$

Therefore:

$$\frac{1}{S} = \frac{U_f^0}{U_g^0} = \frac{1 - (V_j/U_g^0)}{\gamma\ (1 - \alpha^0)} - \frac{\alpha^0}{1 - \alpha^0}$$

or, using equations (4.91) and (4.95) and the definition $r^* = e^{\gamma q \tau_2} = U_g^0/U_{g_{in}}^0$ (see equation (A.20a)):

$$\frac{1}{S_{r^*}} = \frac{U_f^0}{U_g^0} = \frac{(1 - \dfrac{V_j}{U_{g_{in}}^0\ r^*})}{\gamma - \dfrac{\rho_f}{\Delta\rho}\ (1 - \dfrac{1}{r^*})} - \frac{\dfrac{\rho_f}{\Delta\rho}\ (1 - \dfrac{1}{r^*})}{\gamma - \dfrac{\rho_f}{\Delta\rho}\ (1 - \dfrac{1}{r^*})}$$

or, using equations (4.83) and (4.76):

$$\frac{1}{S_{r^*}} = \frac{U_f^0}{U_g^0} = \frac{\left[1 - \frac{V_j}{U_1^0\,(\gamma + (V_j/U_1^0))}\,\frac{1}{r^*}\right] - \frac{\rho_f}{\Delta\rho}\,(1 - \frac{1}{r^*})}{\gamma - \frac{\rho_f}{\Delta\rho}\,(1 - \frac{1}{r^*})} \qquad \text{(B.2a)}$$

By using the definition $\varepsilon^* = V_j/U_1^0$ (see equation (A.20b)):

$$\frac{1}{S_{r^*}} = \frac{U_f^0}{U_g^0} = \frac{1 - (\frac{\varepsilon^*}{\gamma + \varepsilon^*})\,\frac{1}{r^*} - \frac{\rho_f}{\Delta\rho}\,(1 - \frac{1}{r^*})}{\gamma - \frac{\rho_f}{\Delta\rho}\,(1 - \frac{1}{r^*})} \qquad \text{(B.2b)}$$

Therefore: $S_{r^*} = S(r^*) = S(\alpha) = S(z)$

For $\alpha = 0$ ($\tau_2 = 0$, therefore $r^* = 1$), we find from equation (B.2a):

$$\frac{1}{S_{r^*=1}} = \frac{1 - \frac{V_j}{\gamma\,U_1^0 + V_j}}{\gamma} = \frac{U_1^0}{\gamma\,U_1^0 + V_j} = \frac{1}{\gamma + \varepsilon^*} \qquad \text{(B.3)}$$

For the homogeneous flow assumption (no slip) $S = 1$ for any $\alpha(r^*)$ (any axial position z).

From equation (4.82) therefore:

$$\overline{U}_g = \gamma\,\overline{J}_{in} \qquad \text{(B.4)}$$

According to equations (4.86), (B.1), (4.95) and (4.103), we have:

$$\overline{U}_f = \frac{\overline{J}_{in}\,(1 - \gamma\,\alpha^0) + \overline{\alpha}\,U_g^{\,0}\,(\frac{1}{S_{r^*}} - 1)}{1 - \alpha^0} =$$

$$= \frac{\overline{J}_{in}\left[1 - \frac{\rho_f}{\Delta\rho}\,(1 - \frac{1}{r^*})\right] - (\frac{1}{S_{r^*}} - 1)\left[\frac{q\rho_f}{\Delta\rho}\,\overline{y}_b\,e^{-s\tau_2} + \frac{\rho_f}{\Delta\rho}\,\overline{J}_{in}\,\frac{\frac{1}{r^*} - e^{-s\tau_2}}{s/\gamma q - 1}\right]}{1 - \frac{\rho_f}{\gamma\,\Delta\rho}\,(1 - \frac{1}{r^*})}$$

But from equations (4.54) and (4.78), we take:

$$q\,\frac{\overline{y}_b}{\overline{J}_{in}} = q\,\frac{\overline{y}_b}{\overline{U}_1 - q\,\overline{y}_b} = q\,\frac{\frac{1 - e^{-s\tau_1}}{s}}{1 - q\,\frac{1 - e^{-s\tau_1}}{s}} = \frac{1 - e^{-s\tau_1}}{\frac{s}{q} - (1 - e^{-s\tau_1})} \qquad (B.5)$$

Therefore:

$$\frac{\overline{U}_f}{\overline{J}_{in}} = \frac{\left[1 - \frac{\rho_f}{\Delta\rho}\,(1 - \frac{1}{r^*})\right] - (\frac{1}{S_{r^*}} - 1)\,\frac{\rho_f}{\Delta\rho}\left[\frac{(1 - e^{-s\tau_1})\,e^{-s\tau_2}}{\frac{s}{q} - (1 - e^{-s\tau_1})} + \frac{\frac{1}{r^*} - e^{-s\tau_2}}{(\frac{s}{\gamma q} - 1)}\right]}{1 - \frac{\rho_f}{\gamma\,\Delta\rho}\,(1 - \frac{1}{r^*})}$$

and we define:

$$\frac{\overline{U}_f}{\overline{J}_{in}} = \Gamma_{r^*} = \Gamma(r^*, \tau_2, \tau_1) \qquad (B.6)$$

For $r^* = e^{\gamma q \tau_2} = 1$, i.e. $\tau_2 = 0$, equation (B.6) gives:

$$\Gamma_{r^*=1} = 1 + (1 - \frac{1}{S_{r^*=1}})\,\frac{\rho_f}{\Delta\rho}\,\frac{1 - e^{-s\tau_1}}{\frac{s}{q} - (1 - e^{-s\tau_1})} \qquad (B.7)$$

For the non-slip case ($S = 1$, $\gamma = 1$), we find from equations (B.4) and (B.6):

$$\frac{\overline{U}_g}{\overline{J}_{in}} = 1 = \frac{\overline{U}_f}{\overline{J}_{in}} = \Gamma_{r^*} \qquad \text{for any } r^*(\tau_2) \tag{B.8}$$

APPENDIX C

MODIFIED BESSEL FUNCTIONS WITH COMPLEX ARGUMENT OF THE FORM $x\sqrt{j}$

The modified Bessel functions of the first and second kind, of zero and first order (I_o, K_o, I_1, K_1) with a complex argument of the form $x\sqrt{j}$, where x is real, take the following form (McLachlan (1961)):

$$ber_o(x) = \sum_{K=0}^{\infty} \frac{(\frac{x}{2})^{2K}}{(K!)^2} \cos\frac{K\pi}{2} = 1 - \frac{(\frac{x}{2})^4}{(2!)^2} + \frac{(\frac{x}{2})^8}{(4!)^2} - \ldots \qquad (C.1)$$

$$bei_o(x) = \sum_{K=0}^{\infty} \frac{(\frac{x}{2})^{2K}}{(K!)^2} \sin\frac{K\pi}{2} = (\frac{x}{2})^2 - \frac{(\frac{x}{2})^6}{(3!)^2} + \frac{(\frac{x}{2})^{10}}{(5!)^2} - \ldots \qquad (C.2)$$

where $ber_o(x)$ and $bei_o(x)$ denote the real and imaginary parts of $I_o(x\sqrt{j})$. Similarly, the real and imaginary parts of $K_o(x\sqrt{j})$ are denoted by $Ker_o(x)$ and $Kei_o(x)$, where:

$$Ker_o(x) = -\{ln(\tfrac{x}{2}) + \gamma\} ber_o(x) + \tfrac{\pi}{4} bei_o(x) +$$

$$+ \sum_{K=0}^{\infty} \frac{(\frac{x}{2})^{2K}}{(K!)^2} \phi(K) \cos\frac{K\pi}{2} =$$

$$= -\{ln(\tfrac{x}{2}) + \gamma\} ber_o(x) + \tfrac{\pi}{4} bei_o(x) -$$

$$- \frac{(\frac{x}{2})^4}{(2!)^2}(1 + \frac{1}{2}) + \frac{(\frac{x}{2})^8}{(4!)^2}(1 + \frac{1}{2} + \frac{1}{3} + \frac{1}{4}) - \ldots \qquad (C.3)$$

$$Kei_o(x) = -\{ln(\tfrac{x}{2}) + \gamma\} bei_o(x) - \tfrac{\pi}{4} ber_o(x) +$$

$$+ \sum_{K=0}^{\infty} \frac{(\frac{x}{2})^{2K}}{(K!)^2} \phi(K) \sin\frac{K\pi}{2} =$$

$$= -\left\{ln\left(\frac{x}{2}\right) + \gamma\right\} bei_o(x) - \frac{\pi}{4} ber_o(x) +$$

$$+ \left(\frac{x}{2}\right)^2 - \frac{\left(\frac{x}{2}\right)^6}{(3!)^2}\left(1 + \frac{1}{2} + \frac{1}{3}\right) + \ldots \qquad (C.4)$$

where:

$\gamma = 0.5772156...$ is the Euler's constant

and:

$$p! = 1.2.3...p \quad , \quad 0! = 1$$

and:

$$\phi(p) = 1 + \frac{1}{2} + \frac{1}{3} + \ldots + \frac{1}{p} \quad , \quad \phi(0) = 0$$

We now evaluate the modified Bessel functions of the first order:

$$I_1(x\sqrt{j}) = \frac{d}{d(x\sqrt{j})} I_o(x\sqrt{j}) = \frac{1}{\sqrt{j}} \frac{d}{dx}\left[ber_o(x) + j\, bei_o(x)\right] =$$

$$= \sqrt{-j}\left[ber_o'(x) + j\, bei_o'(x)\right] \qquad (C.5)$$

$$K_1(x\sqrt{j}) = \frac{-d}{d(x\sqrt{j})} K_o(x\sqrt{j}) = \frac{-1}{\sqrt{j}} \frac{d}{dx}\left[Ker_o(x) + j\, Kei_o(x)\right] =$$

$$= -\sqrt{-j}\left[Ker_o'(x) + j\, Kei_o'(x)\right] \qquad (C.6)$$

The forms of $ber_o'(x)$, $bei_o'(x)$, $Ker_o'(x)$ and $Kei_o'(x)$ are found by differentiation of equations (C.1), (C.2), (C.3) and (C.4), respectively, with respect to the real argument x.

$$2\, ber_o'(x) = \sum_{K=0}^{\infty} 2K \frac{\left(\frac{x}{2}\right)^{2K-1}}{(K!)^2} \cos\frac{K\pi}{2} = -4\frac{\left(\frac{x}{2}\right)^3}{(2!)^2} + 8\frac{\left(\frac{x}{2}\right)^7}{(4!)^2} - \ldots \qquad (C.7)$$

$$2\,bei_o'(x) = \sum_{K=0}^{\infty} 2K \frac{(\frac{x}{2})^{2K-1}}{(K!)^2} \sin\frac{K\pi}{2} = 2(\frac{x}{2}) - 6\frac{(\frac{x}{2})^5}{(3!)^2} + \ldots \qquad (C.8)$$

$$Ker_o'(x) = -\{ln(\frac{x}{2}) + \gamma\}\,ber_o'(x) - \frac{1}{x}ber_o(x) + \frac{\pi}{4}bei_o'(x) +$$

$$+ \frac{1}{2}\sum_{K=0}^{\infty} 2K \frac{(\frac{x}{2})^{2K-1}}{(K!)^2}\phi(K)\cos\frac{K\pi}{2} =$$

$$= -\{ln(\frac{x}{2}) + \gamma\}\,ber_o'(x) - \frac{1}{x}ber_o(x) + \frac{\pi}{4}bei_o'(x) +$$

$$+ \frac{1}{2}\{-4\frac{(\frac{x}{2})^3}{(2!)^2}(1+\frac{1}{2}) + 8\frac{(\frac{x}{2})^7}{(4!)^2}(1+\frac{1}{2}+\frac{1}{3}+\frac{1}{4}) - \ldots\} \qquad (C.9)$$

$$Kei_o'(x) = -\{ln(\frac{x}{2}) + \gamma\}\,bei_o'(x) - \frac{1}{x}bei_o(x) - \frac{\pi}{4}ber_o'(x) +$$

$$+ \frac{1}{2}\sum_{K=0}^{\infty} 2K \frac{(\frac{x}{2})^{2K-1}}{(K!)^2}\phi(K)\sin\frac{K\pi}{2} =$$

$$= -\{ln(\frac{x}{2}) + \gamma\}\,bei_o'(x) - \frac{1}{x}bei_o(x) - \frac{\pi}{4}ber_o'(x) +$$

$$+ \frac{1}{2}\{2(\frac{x}{2}) - 6\frac{(\frac{x}{2})^5}{(3!)^2}(1+\frac{1}{2}+\frac{1}{3}) + \ldots\} \qquad (C.10)$$

According to the previous analysis, the expressions for $M(x)$, $M'(x)$ and $F(s)$ encountered in equations (4.27), (4.28) and (4.33) can be evaluated easily for the case where $s = j\omega$ (ω = real). In that case, $x = \sqrt{T_K\omega}$ and $x\sqrt{j} = \sqrt{jT_K\omega} = \sqrt{T_K S}$.

A subroutine (BESIMG) has been constructed to calculate the values of $ber_o(x)$, $bei_o(x)$, $Ker_o(x)$, $Kei_o(x)$, $ber_o'(x)$, $bei_o'(x)$, $Ker_o'(x)$ and $Kei_o'(x)$, for the various values of x (real).

The values of these Bessel functions exist in tabular form in McLachlan's book (1961) for values of the argument x in the range 0 to 10 (every 0.1).

APPENDIX D

COMPUTER PROGRAM FOR DATA TRANSLATION

```
      PROGRAM CHEK1 (TAPE9,INPUT,OUTPUT,TAPE5=INPUT,TAPE6=OUTPUT)
      DIMENSION  KDAT(410)
      COMMON  X(2048), Y(2048), Z(2048)
      MASKA=00000000000000001777B
      NCHAN=3
      NCHAN=1
      NDATRC=205
      NOREC=2
      NKDAT=NOREC*NDATRC
      IF  (NOREC.NE.1)    GO  TO  2
      STOP
    2 DO  3  I=1, NOREC
      INDEX1=I*NDATRC-NDATRC+1
      INDEX2=I*NDATRC
      READ (9)  (KDAT(J),  J=INDEX1, INDEX2)
    3 CONTINUE
      ICAUNT=1
      NEO=1
      DO  1  K=1, NOREC
      IND1=K*NDATRC-NDATRC+1
      IND2=K*NDATRC
      DO  1  J=IND1, IND2
      IND3=5*J-4-K+1
      IND4=IND3+4
      IF  (IND4.EQ.(IND2*5-K+1))    IND4=IND4-1
      LDISPL=12
      DO  1  I=IND3, IND4
      LDAT=LRSHFT(KDAT(J), LDISPL).AND.MASKA
      GO  TO (11, 12, 13),  ICAUNT
   11 X(NEO)=FLOAT(LDAT)*10./1024.
      GO  TO  6
   12 Y(NEO)=FLOAT(LDAT)*10./1024.
      GO  TO  6
   13 Z(NEO)=FLOAT(LDAT)*10./1024.
    6 LDISPL=LDISPL+12
      ICAUNT=ICAUNT+1
      IF (NCHAN.EQ.1)    ICAUNT=1
      IF (NCHAN.EQ.1)    NEO=NEO+1
      IF  (ICAUNT.LE.3)   GO  TO  1
      ICAUNT=1
      NEO=NEO+1
    1 CONTINUE
      WRITE (6, 7)  X, Y, Z
    7 FORMAT (2X,  16F7.2)
      STOP
      END
```

APPENDIX E

FAST FOURIER TRANSFORM CALCULATION PROCEDURES

1. FAST FOURIER TRANSFORMS

The infinite-range Fourier transform of a real or complex-valued record $x(t)$ is defined by the complex-valued quantity:

$$X(f) = \int_{-\infty}^{\infty} x(t)\, e^{-j2\pi ft}\, dt \qquad \text{(E.1)}$$

In a practical case, the limits are restricted to a finite time interval of $x(t)$, say in the range 0 - T. Then the finite-range Fourier transform exists and is defined by:

$$X(f,T) = \int_{0}^{T} x(t)\, e^{-j2\pi ft}\, dt \qquad \text{(E.2)}$$

If the time record $x(t)$ is sampled at N equally spaced points with a sampling interval h (sec) according to the considerations of section 7.4.3.1, then:

$$x(t) \hat{=} x_n = x(nh) \qquad n = 0, 1, 2, \ldots, N-1 \qquad \text{(E.3)}$$

and for an arbitrary frequency f, the discrete version of equation (E.2) becomes:

$$X(f,T) = h \sum_{n=0}^{N-1} x_n \exp\left(-j\, 2\pi\, f\, n\, h\right) \qquad \text{(E.4)}$$

The discrete frequency values for the computation of $X(f,T)$ are usually selected as:

$$f_k = k f = \frac{k}{T} = \frac{k}{N h} \qquad k = 0, 1, 2, \ldots, N-1 \qquad \text{(E.5)}$$

At these frequencies, the transformed values give the Fourier components defined by:

$$X_k = \frac{X(f_k, T)}{h} = \sum_{n=0}^{N-1} x_n \exp\left(-j \frac{2\pi k n}{N}\right)$$

for $$k = 0, 1, 2, \ldots, N-1 \qquad \text{(E.6)}$$

The results are unique only up to $k = N/2$ since the Nyquist cut-off frequency occurs at this point.

Fast Fourier transform (FFT) methods are designed to compute these quantities X_k.

We set:

$$W(u) = \exp\left(-j \frac{2\pi u}{N}\right) \qquad \text{(E.7)}$$

$$X(k) = X_k \quad \text{and} \quad x(n) = x_n \qquad \text{(E.8)}$$

We observe that:

$$W(N) = 1 \qquad \text{for any } u, v$$

and

$$W(u + v) = W(u)\, W(v) \qquad \text{(E.9)}$$

Then equation (E.6) becomes:

$$X(k) = \sum_{n=0}^{N-1} x(n)\, W(kn) \qquad k = 0, 1, 2, \ldots, N-1 \qquad \text{(E.10)}$$

This equation requires a total of approximately N^2 complex multiply-add operations (1 complex multiply-add = 4 real multiply-adds) to compute all of the $X(k)$ terms.

2. BASIS FOR FFT PROCEDURES

The fast Fourier transform procedures are now based upon decomposing N into its composite (non-unity) factors, and carrying out Fourier transforms over the smaller number of terms in each of the composite factors. In particular, if:

$$N = \prod_{i=1}^{p} r_i = r_1 \, r_2 \, \ldots \, r_p \tag{E.11}$$

where all r_i are integers higher than unity, then it can be proved that the $X(k)$ in equation (E.10) can be found by computing in an iterative fashion the sum of p terms, where for each term r_i, (N/r_i) Fourier transforms must be executed requiring $4r_i^2$ real operations each.

Henceforth, the total number of real operations becomes:

$$\sum_{i=1}^{p} 4r_i^2 \frac{N}{r_i} = 4N \sum_{i=1}^{p} r_i \tag{E.12}$$

The resulting speed ratio of these FFT procedures to the standard method is then:

$$\text{Speed ratio} = N^2/4N \sum_{i=1}^{p} r_i = N/4 \sum_{i=1}^{p} r_i \tag{E.13}$$

For the particular case of $N = 2^p$ (p = positive integer):

$$\sum_{i=1}^{p} r_i = 2p = 2 \log_2 N \tag{E.14}$$

Therefore, the speed ratio of equation (E.14) gives:

$$\text{Speed ratio} = \frac{N^2}{4N\ 2p} = \frac{N}{8p} \tag{E.15}$$

A further doubling of the speed can be achieved in practice by noting that:

$$W(kn) = +1 \text{ or } -1 \qquad \text{if } N = 2^p \tag{E.16}$$

Therefore:

$$\text{Speed ratio} = \frac{N}{4p} \tag{E.17}$$

For the present work, the Cooley-Tukey procedure was used, which is a special case of the general fast Fourier transform algorithm and appropriate for binary digital computers. The number of data samples must be a power of 2, namely $N = 2^p$. If this is not so, zeros must be added to the data sequence to satisfy this requirement.

A further doubling of computational speed can also be achieved (over that of equation (E.17)) by dividing a single record into two parts and computing as indicated in the next section.

Therefore, the final speed ratio is:

$$\text{Speed ratio} = \frac{N}{2p} \tag{E.18}$$

3. FOURIER TRANSFORM OF A COMPLEX RECORD

The Fourier transforms of two real-valued records may be computed simultaneously by inserting one record $x(n)$ as the real part and one record $y(n)$ as the imaginary part of a complex record $z(n)$:

Let:

$$z(n) = x(n) + j\, y(n) \qquad n = 0, 1, \ldots, N-1 \tag{E.19}$$

The Fourier transform of $z(n)$, as given by equation (E.6), is:

$$Z(k) = \sum_{n\ 0}^{N-1} \left(x(n) + j\, y(n)\right) \exp\left[-j\, \frac{2\pi\, k\, n}{N}\right]$$

for $$k = 0, 1, 2, \ldots, N-1 \tag{E.20}$$

This is computed by fast Fourier transform procedures. The N data points in $x(n)$ and $y(n)$ are transformed into N frequency points which are spaced $1/T$ apart. The Nyquist cut-off frequency occurs when $k = N/2$ (N is even), so that unique results occur only for $k = 0, 1, 2, \ldots, (N/2) - 1$.

We observe that:

$$\exp\left[j\, \frac{2\pi\, n\, (N-k)}{N}\right] = \exp\left[-j\, \frac{2\pi\, n\, k}{N}\right] \tag{E.21}$$

since $\exp\left(j\, 2\pi\, n\right) = 1$ for any n. Hence, if $Z^*(k)$ is the complex conjugate of $Z(k)$, then:

$$Z^*(N-k) = \sum_{n=0}^{N-1} \left(x(n) - j\, y(n)\right) \exp\left[-j\, \frac{2\pi\, n\, k}{N}\right] \tag{E.22}$$

From equations (E.20) and (E.22), it follows that:

$$Z(k) + Z^*(N-k) = 2 \sum_{n=0}^{N-1} x(n) \exp\left[-j\, \frac{2\pi\, n\, k}{N}\right] = 2\, X(k) \tag{E.23}$$

$$Z(k) + Z^*(N-k) = 2j \sum_{n=0}^{N-1} y(n) \exp\left[-j\, \frac{2\pi\, n\, k}{N}\right] = 2j\, Y(k) \tag{E.24}$$

Therefore, the Fourier transforms $X(k)$, $Y(k)$ of the two real-valued records $x(n)$ and $y(n)$ are given by:

$$X(k) = \frac{Z(k) + Z^*(N - k)}{2}$$

$$Y(k) = \frac{Z(k) - Z^*(N - k)}{2j} \qquad k = 0, 1, 2, \ldots, N - 1 \qquad \text{(E.25)}$$

The inverse Fourier transform of the $X(f)$ in equation (E.1) is:

$$x(t) = \int_{-\infty}^{\infty} X(f)\, e^{j2\pi ft}\, df \qquad \text{(E.26)}$$

This leads to the discrete inverse Fourier transform formula:

$$x_n = \frac{1}{N} \sum_{k=0}^{N-1} X_k \exp\left(j \frac{2\pi\, k\, n}{N}\right) \qquad n = 0, 1, \ldots, N - 1 \qquad \text{(E.27)}$$

This inverse Fourier transform can be computed by the same FFT procedures by merely interchanging k and n, and replacing x_n by X_k and $W(kn)$ by $W(-kn)$.